







## TESIS DOCTORAL

*Ex-situ catalytic fast pyrolysis of wheat straw  
over acid-base catalysts for the production of  
high-added value bio-based chemicals*

Autor:

**Luis Miguel López Renau**

Directores:

**Juan Ángel Botas Echevarría**

**David Pedro Serrano Granados**

Programa de Doctorado en Tecnologías Industriales: Química,  
Ambiental, Energética, Electrónica, Mecánica y de los Materiales

Escuela Internacional de Doctorado

Septiembre, 2022



**D. Juan Ángel Botas Echevarría**, Catedrático de Universidad del área de Ingeniería Química del Departamento de Tecnología Química, Energética y Mecánica de la Universidad Rey Juan Carlos,

y

**D. David P. Serrano Granados**, Catedrático de Ingeniería Química del Departamento de Tecnología Química, Energética y Mecánica de la Universidad Rey Juan Carlos, y Director del Instituto IMDEA Energía y Jefe de la Unidad de Procesos Termoquímicos,

**CERTIFICAN:**

Que el presente trabajo de investigación titulado “*Ex-situ catalytic fast pyrolysis of wheat straw over acid-base catalysts for the production of high-added value bio-based chemicals*” constituye la memoria que presenta el Ingeniero Químico **D. Luis Miguel López Renau** para aspirar al grado de Doctor en Tecnologías Industriales: Química, Ambiental, Energética, Electrónica, Mecánica y de los Materiales por la Universidad Rey Juan Carlos, y ha sido realizada en los laboratorios del Grupo de Ingeniería Química y Ambiental de la Universidad Rey Juan Carlos y de la Unidad de Procesos Termoquímicos del Instituto IMDEA Energía bajo nuestra dirección.

Y para que conste, firmamos el presente certificado en Móstoles a 30 de septiembre de 2022.

Fdo: Juan Ángel Botas Echevarría

Fdo: David P. Serrano Granados



*Después de tanto tiempo me he dado cuenta de que  
las cosas que me asustan me hacen más feliz.*

*Miss Caffaina – Lisboa*





## Agradecimientos – Acknowledgements

*En primer lugar, me gustaría agradecer a mis directores Gotzon y David por su inestimable ayuda durante la realización de la presente Tesis Doctoral. Con Gotzon he podido tener un trato más personal y ha sabido transmitirme su buen hacer tanto en lo que refiere a la tesis y como a lo que no, mientras que David con su esfuerzo y dedicación me ha enseñado a hacer investigación de calidad. En segundo lugar, pero no menos importante, me gustaría agradecer a mis compañeros doctores Gema y Héctor, sin cuya implicación no habría podido sacar todo este trabajo de laboratorio y de redacción adelante. Cada uno ha sabido aportarme lo que a ambos se les daba mejor hacer y me gustaría hacerles saber que para mí son dos de los mejores ejemplos de personas que hacen bien su trabajo. No quisiera olvidarme de mi compañera Almu, que ha sido como una hermana pequeña para mí, y sin duda la persona con la que más horas he pasado en el laboratorio.*

*I would also like to show my gratitude to Prof. Weihong Yang for giving me the opportunity to do my international stay at the KTH Royal Institute of Technology in Stockholm, Sweden. I would also like to thank Katarzyna, who was my mentor while conducting my experiments in the laboratory, and José Juan, who became a close friend.*

*Esta tesis me ha enseñado que lo importante no solo es llegar, sino también lo que te encuentras por el camino. He hecho muchos amigos durante estos cinco años. A algunas de estas personas ya las conocía antes de empezar, como a Javi y Bea. Javi ha demostrado ser mi amigo más fiel desde que lo conocí en el grado. Aunque conocí a Bea durante el máster, me hice su amigo al empezar el doctorado y ha sido la mejor compañera de despacho que me hubiera podido tocar. Mara y Sara, junto a Bea, se han convertido en uno de mis pilares mientras he estado realizando esta tesis. Mara ha sido como una hermana mayor para mí y es una de las personas que más admiro tanto personal como profesionalmente, mientras que Sara es una de las personas más afines a mí que he conocido durante mi paso por esta universidad y fue cuando llegó ella que empecé a sentirme de verdad a gusto aquí. Los abrazos de mis amigos Fran y Maia me han ayudado a mantenerme cargado de energía durante el duro periodo de escritura. Me reconforta saber que a Fran siempre lo tendré cerca porque nuestros pueblos son vecinos, mientras que el espíritu aventurero de Maia hará que cualquier*

## Agradecimientos – Acknowledgements

*distancia sea corta sea donde sea que acabemos viviendo. Los jueves de cervezas con Anabel, Eva, María, Mónica, Paloma y Samuel, y los viernes de sushi con José Manuel, Miriam y Jorge han hecho los finales de semana de los últimos años mucho más llevaderos. Finalmente, quisiera agradecer a mis compañeros de promoción Miriam, Igor, los Danis, Luis y Gabi, todos los momentos compartidos, tanto los buenos como los malos.*

*Para terminar, me gustaría dar las gracias a esas personas que forman parte de mi día a día:*

*A mis amigos de siempre, Héctor, Miguel, Jorge, Sol, Ana, Fer, Irina, Ignacio, Espe, Ulises, Marta, Kevin, Poly y Kelly, que le han dado un toque de color a mi vida y me han ayudado a convertirme en la persona que soy hoy.*

*A mis padres, Luis Miguel y Marisa, y a mi hermano Dani, que siempre me han apoyado en todas mis decisiones y son mis ejemplos de superación.*

*A mi novio Álvaro, que es sin ninguna duda la persona con la que mejor me he sentido acompañado durante los últimos cuatro años.*

*Septiembre, 2022*

# Scientific production during the Doctoral Thesis

## Scientific publications

**L. M. López-Renau**, H. Hernando, G. Gómez-Pozuelo, J. A. Botas, D. P. Serrano, “Utilisation of a basic K-grafted USY zeolite in catalytic pyrolysis of wheat straw to produce valuable oxygenated compounds”, *Catalysis Today*, vol. 390–391, pp. 198–209, 2021, doi: 10.1016/j.cattod.2021.11.034

**L. M. López-Renau**, L. García-Pina, H. Hernando, G. Gómez-Pozuelo, J. A. Botas, D. P. Serrano, “Enhanced bio-oil upgrading in biomass catalytic pyrolysis using KH-ZSM-5 zeolite with acid-base properties”, *Biomass Conversion and Biorefinery*, vol. 11, pp. 2311–2323, 2021, doi: 10.1007/s13399-019-00455-9

## Contribution to congresses

G. Gómez-Pozuelo, **L. M. López-Renau**, H. Hernando, J. A. Botas, D. P. Serrano, “Combining nano and layered materials with acid-basic features for the upgrading of bio-oil vapours produced by wheat straw catalytic pyrolysis,” 8th International Workshop of Layered & Nanostructured Materials 2022, 10<sup>th</sup>-13<sup>th</sup> July 2022, Toledo (Spain). (Poster)

**L. M. López-Renau**, H. Hernando, G. Gómez-Pozuelo, J. A. Botas, D. P. Serrano, “Staged catalytic fast pyrolysis of wheat straw coupling acid H-ZSM-5 zeolite with basic MgO to produce valuable bio-based chemicals,” IZC-2022, 20th International Zeolite Conference, 3<sup>rd</sup>-8<sup>th</sup> July 2022, Valencia (Spain). (Poster)

**L. M. López-Renau**, H. Hernando, G. Gómez-Pozuelo, J. A. Botas, D. P. Serrano, “Utilisation of a basic K-grafted USY zeolite in catalytic pyrolysis of wheat straw to produce valuable oxygenated compounds,” Young Researchers CIS 2021, 6<sup>th</sup>-8<sup>th</sup> September 2021, online conference. (Short oral presentation)

**L. M. López-Renau**, H. Hernando, G. Gómez-Pozuelo, J. A. Botas, D. P. Serrano, “Obtención de compuestos fenólicos por pirólisis catalítica de biomasa lignocelulósica sobre zeolita K-USY”, IV Encuentro de Jóvenes Investigadores de la SECAT, 21<sup>st</sup>-23<sup>th</sup> september 2020, Bilbao (Spain). (Flash oral presentation + Poster)

## Scientific production during the Doctoral Thesis

**L. M. López-Renau**, L. García-Pina, H. Hernando, G. Gómez-Pozuelo, J.A. Botas, D.P. Serrano, “Empleo de una zeolita KH-ZSM-5 con propiedades ácido-base en la pirólisis rápida de biomasa lignocelulósica,” II Congreso de la Escuela Internacional de Doctorado, 27<sup>th</sup>-28<sup>th</sup> November 2019, Móstoles (Madrid, Spain). (Oral presentation)

**L. M. López-Renau**, L. García-Pina, H. Hernando, G. Gómez-Pozuelo, J. A. Botas, D. P. Serrano, “Pirólisis catalítica de residuos lignocelulósicos sobre zeolita KH-ZSM-5 con propiedades ácido-base,” SECAT '19, Catálisis para el futuro: Avances en Estructuras, Procesos y Aplicaciones, 24<sup>th</sup>-26<sup>th</sup> June 2019, Córdoba (Spain). (Oral presentation)

**G. Gómez-Pozuelo**, **L. M. López-Renau**, L. García-Pina, H. Hernando, J. A. Botas, D. P. Serrano, “Catalytic biomass pyrolysis over KH-ZSM-5 zeolite with acid-base properties,” 8th Czech-Italian-Spanish Conference on Molecular Sieves and Catalysis, 11<sup>th</sup>-14<sup>th</sup> June 2019, Amantea (Italy). (Oral presentation)

**L. M. López-Renau**, H. Hernando, G. Gómez-Pozuelo, J. A. Botas, D. P. Serrano, Performance of K-ZSM-5 zeolites in lignocellulose catalytic pyrolysis. EFCATS School on Catalysis; 25<sup>th</sup>-29<sup>th</sup> June 2018, Prague (Czech Republic). (Poster)

# Index

<b>Summary.....</b>	<b>1</b>
<b>Resumen.....</b>	<b>11</b>
<b>1. Introduction.....</b>	<b>21</b>
1.1. Lignocellulosic biomass .....	23
1.2. Biomass conversion technologies .....	24
1.3. Bio-oil production via pyrolysis of biomass .....	26
1.4. Biomass pyrolysis chemistry.....	28
1.5. Pyrolysis reactor types .....	29
1.6. Catalytic fast pyrolysis.....	31
1.7. Ex-situ CFP over heterogeneous acid-base catalysts .....	32
1.7.1. Clay minerals.....	33
1.7.2. Single and mixed metal oxides.....	35
1.7.3. Zeolites .....	38
1.8. Catalytic fast pyrolysis chemistry .....	40
1.8.1. Acid-catalysed reactions.....	41
1.8.2. Base-catalysed reactions.....	44
1.9. Valorisation of bio-oil to bio-based chemicals .....	45
<b>2. Motivation and objectives .....</b>	<b>49</b>
<b>3. Materials and methods .....</b>	<b>53</b>
3.1. Catalysts preparation .....	55
3.1.1. Stabilisation of clay materials .....	55
3.1.2. Synthesis of Mg and Zr single and mixed oxides.....	55
3.1.3. Potassium incorporation to zeolitic materials.....	55
3.1.4. Pelletisation of catalysts .....	56
3.2. Catalyst characterisation .....	56
3.2.1. Thermogravimetric and chemical analyses of the catalyst samples .....	56
3.2.2. Crystallinity, textural properties and morphology of the catalyst samples .....	57
3.2.3. Acid-base properties of the catalyst samples.....	59
3.3. Pre-treatment of raw biomass.....	60
3.4. Fast pyrolysis tests .....	61

## Index

3.5. Characterisation of raw materials and products.....	63
3.5.1. Solid fractions: raw biomass, char and coke .....	63
3.5.2. Liquid fractions: bio-oil* (water-free bio-oil) and water .....	66
3.5.3. Gas fractions: permanent gases .....	67
3.5.4. Mass and energy balances and catalytic deoxygenation selectivities .....	68
<b>4. Results and discussion .....</b>	<b>71</b>
4.1. Catalytic fast pyrolysis of wheat straw and cellulose over clay catalysts.....	73
4.1.1. Characterisation of lignocellulosic feedstocks .....	73
4.1.2. Characterisation of the catalysts.....	74
4.1.3. Catalytic pyrolysis tests.....	78
4.2. Catalytic fast pyrolysis of wheat straw over metal oxides.....	91
4.2.1. Characterisation of the catalysts.....	91
4.2.2. Wheat straw catalytic tests .....	96
4.3. Catalytic fast pyrolysis of wheat straw over K-incorporated zeolites .....	105
4.3.1. K-exchanged and parent H-ZSM-5 zeolites.....	105
4.3.2. K-grafted and parent USY zeolites .....	115
4.4. Fast pyrolysis of wheat straw by dual-catalyst tandem system .....	135
4.4.1. Characterisation of the catalysts.....	135
4.4.2. Wheat straw catalytic tests .....	138
4.5. Comparison of studied catalysts and coupling configurations .....	155
<b>5. General conclusions.....</b>	<b>159</b>
<b>6. Recommendations for future work .....</b>	<b>165</b>
<b>7. References.....</b>	<b>169</b>
<b>List of tables .....</b>	<b>187</b>
<b>List of figures .....</b>	<b>189</b>
<b>Appendix .....</b>	<b>195</b>

# List of abbreviations

75MgZr	Mg and Zr mixed metal oxide with a Mg/(Mg+Zr) ratio of 0.75
A+B	Acid+Basic coupling configuration
AAEMs	Alkali and Alkaline Earth Metals
AC	Carboxylic acids
ACS	American Chemical Society
AR	Aromatic hydrocarbons
ASA	Amorphous Silica-Alumina
ATP	Attapulgite
B+A	Basic+Acid coupling configuration
BBOT	2,5-bis(5-t-butylbenzoxazol-2-yl)thiophene
BEA	Beta-type zeolites
BET	Brunauer-Emmet-Teller
Bio-oil*	Bio-oil in a water free basis
BJH	Barret-Joyner-Halenda
BNT	Bentonite
BTEX	Benzene, Toluene, Ethylbenzene and Xylene
C/B	Catalyst to Biomass ratio
C <sub>B</sub>	Concentration of Brønsted acid sites
Cell	Cellulose
CFP	Catalytic Fast Pyrolysis
CHNS-O	Elemental analysis
C <sub>L</sub>	Concentration of Lewis acid sites
DTG	Derivative Thermogravimetry
EDX	Energy-Dispersive X-ray spectroscopy
FAU	Faujasite-type zeolites
FC	Fixed Carbon
FT-IR	Fourier-Transform Infrared spectroscopy
FUR	Furans
GC-MS	Gas Chromatography coupled to Mass Spectrometry
H/C <sub>eff</sub>	Effective H/C ratio
Hemicell	Hemicellulose

## List of abbreviations

HHV	Higher Heating Value
HMF	5-hydroxymethylfurfural
HTL	Hydrothermal Liquefaction
H-ZSM-5	Protonated form of Zeolite Socony Mobil-5
ICP-OES	Inductively Coupled Plasma-Optical Emission Spectroscopy
ID	Inside Diameter
IUPAC	International Union of Pure and Applied Chemistry
KF	Karl-Fischer titration
KH-ZSM-5	Partially potassium-exchanged H-ZSM-5 zeolite
K-USY	Potassium-grafted USY zeolite
LDHs	Layered Double Hydroxides
LDOs	Layered Double Oxides
LG	Levoglucosan
LGO	Levoglucosenone
Lign	Lignin
LO	Light oxygenates
MAHs	Monocyclic aromatic hydrocarbons
MFC	Mass Flow Controller
MFI	Mobil-type five zeolites
MS	Mass Spectrometry
N-C	Non-catalytic test
NL-DFT	Non-Local Density Functional Theory
O-AR	Oxygenated aromatics
P/P <sub>0</sub>	Relative pressure
PAHs	Polycyclic aromatic hydrocarbons
Py/GC-MS	Pyrolyser coupled with Gas Chromatography-Mass Spectrometry
S <sub>BET</sub>	BET Surface Area
SEM	Scanning Electron Microscopy
S <sub>MIC</sub>	Micropore Surface Area
S <sub>MZ+EXT</sub>	Mesopore and External Surface Area
SUG	Anhydrosugars
T <sub>catalysis</sub>	Temperature of catalytic zone
TCD	Thermal Conductivity Detector



## List of abbreviations

TEM	Transmission Electron Microscopy
TG	Thermogravimetric analysis
THF	Tetrahydrofuran
TPD	Temperature Programmed Desorption
USY	Ultrastable Y zeolite
VM	Volatile Matter
$V_{\text{MIC}}$	Micropore Volume
$V_{\text{MZ+EXT}}$	Mesopore + External Volume
$V_{\text{T}}$	Total Pore Volume
WHSV	Weight Hourly Space Velocity
ws	Wheat straw
ws-ac	Acid-washed wheat straw
XRD	X-Ray Diffraction
$\mu$ -GC	Micro-Gas Chromatography



## **Summary**



The present Doctoral Thesis has been developed in the laboratories of the School of Experimental Sciences and Technology of the Rey Juan Carlos University, and of the IMDEA Energy Institute. Specifically, it is included in the research lines: *Biomass and Bioenergy* of the Chemical and Environmental Engineering Group of the Rey Juan Carlos University; and *Sustainable Fuels* of the Thermochemical Processes Unit of the IMDEA Energy Institute.

Funding for this research has been provided through the *BIOCASCHEM* project: *Valorisation of Lignocellulosic Waste through the Integration of Cascade Thermo-catalytic Processes* (reference: CTQ2017-87001-R), led by Rey Juan Carlos University and IMDEA Energy Institute, and funded by the Spanish Ministry of Economy, Industry and Competitiveness.

Lignocellulosic biomass is one of the most abundant and least cost renewable resources, considered as a source of great potential for obtaining fuels and/or chemical products. Lignocellulosic biomass is mainly composed of macromolecules (cellulose, hemicellulose and lignin), extractives and inorganic matter, in varying proportions depending on their origin. In the present Doctoral Thesis, pyrolysis has been chosen as the thermochemical conversion technology for the valorisation of lignocellulosic biomass from agroforestry residues, specifically wheat straw, due to its high availability and abundance. Pyrolysis of biomass is a thermal treatment in an inert atmosphere at moderate temperatures (300 – 700 °C), normally at atmospheric pressure, which causes its decomposition, giving rise to three fractions: non-condensable gases, a carbonaceous residue or char, and bio-oil, in variable proportions depending on the nature of the raw biomass and pyrolysis conditions. The liquid fraction or bio-oil is the main product of biomass pyrolysis, which consists of a complex mixture of oxygenated organic compounds of different nature (carboxylic acids, sugars, alcohols, aldehydes, ketones, phenols, furans, guaiacols, etc.) and water in different proportions, as a consequence of the great number of simultaneous reactions that occur during the pyrolysis process: cracking and depolymerisation, decarbonylation, decarboxylation, dehydration, carbonisation, etc. Bio-oil has undesirable properties for its use as a fuel: high oxygen content (40 – 45 wt.%, dry basis), low higher heating value (16 – 19 MJ/kg), acidic pH (2 – 4), high viscosity and low stability.

## Summary

When the objective of thermal pyrolysis is to maximise bio-oil production, the optimal operating conditions are: biomass with particle size of 2 – 3 mm to favour heat transfer, temperatures in the range of 500 – 600 °C, high heating rates (*fast pyrolysis*) and short residence times (2 – 3 s). Fluidised bed reactors are therefore one of the most commonly used systems in this research area. Under these conditions, bio-oil yields in the order of 70 – 75 wt.% can be achieved.

In recent years, a great research effort has been put into the development of catalytic processes to improve bio-oil properties, by removing most of the water and oxygen present and increasing the molecular weight of its components in order to produce mainly hydrocarbons. However, this route has shown to have many limitations, due to the very complex nature of bio-oil and the relatively low economic value of the products finally obtained. In this context, the general objective of the present Doctoral Thesis is to study new routes for the valorisation of lignocellulosic biomass from agroforestry residues by means of a combination of cascade thermo-catalytic treatments, in order to maximise the production not only of aromatic hydrocarbons but also of oxygenated compounds of commercial interest. The aim is to maximise bio-oil production by means of a catalytic pyrolysis process that includes basic and multifunctional catalysts, and their selectivity towards oxygenated products of different nature with application as raw materials.

In catalytic pyrolysis, *pyrovapours* are normally brought into contact with acid catalysts, mainly protonic zeolites such as H-ZSM-5, which allows the oxygen to be removed from the bio-oil by converting it into CO, CO<sub>2</sub> and H<sub>2</sub>O, obtaining aromatic hydrocarbons and light olefins as the main end products. It can be carried out *in-situ*, by adding the catalyst to the biomass pyrolysis reactor itself, or *ex-situ*, by passing the gases and vapours from the thermal pyrolysis through a second reactor, in this case a catalytic one. This second option allows the two stages (thermal and catalytic) of lignocellulosic biomass conversion to be operated and optimised separately and prevents the char from being in direct contact with the catalyst, thus mitigating its deactivation. Catalytic pyrolysis of biomass takes place at atmospheric pressure and intermediate temperatures (400 – 500 °C). However, it has important limitations such as low yields of liquid hydrocarbons, the development of severe cracking reactions and the extensive deactivation of the catalyst due to the deposition of great amounts of coke.

Conversely, basic catalysts used to enhance the formation of oxygenates from biomass pyrolysis include clay minerals, alkaline earth and transition metal oxides, and zeolites with basic properties. Most of the catalysts used in the present Doctoral Thesis were derived from commercial samples, but in a few cases, they were synthesised. Previous work in the literature as well as results from the research groups themselves were used as references. The basic catalysts prepared are the following: cationic clays (bentonite and attapulgite), single and mixed metal oxides of Mg and Zr, and commercial H-ZSM-5 nanocrystalline and USY zeolites modified with K to provide them with basicity.

To prevent the inorganic matter in the raw biomass from acting as an in-situ catalyst, a washing pre-treatment with a dilute solution of nitric acid (1 wt.%) was proposed in order to reduce its content in alkali and alkaline earth metals (K, Na, Ca, Mg, etc.), since it is known that their presence favours the development of carbonisation reactions, increasing char production and decreasing bio-oil yields.

On the one hand, the characterisation of the different catalysts has been carried out by means of the following experimental techniques: thermal stability (TG), chemical composition (ICP-OES and EDX), crystallinity (XRD), textural properties ( $N_2$  and Ar physisorption), morphology and crystal size (SEM and TEM), acidity ( $NH_3$ -TPD and pyridine FT-IR) and basicity ( $CO_2$ -TPD). On the other hand, the characterisation of the different raw materials and reaction products has been carried out using the following experimental techniques: chemical composition (ICP-OES and CHNS-O), water content (Karl-Fischer titration), ash, coke and volatile matter content (TG) and composition of liquid (GC-MS) and gaseous ( $\mu$ -GC) products.

An ex-situ reaction system has been used in the biomass catalytic tests, in which vapours and gases from the thermal pyrolysis stage are passed through a catalytic fixed bed. The reaction system consists of a single downflow vertical fixed bed reactor heated by two independent electric furnaces at different temperatures, the first one at higher temperature being the thermal pyrolysis furnace, and the second one at lower temperature being the catalytic pyrolysis furnace. In this way, the behaviour of the different types of catalysts prepared has been investigated and the following tests have been carried out:

## Summary

- Coupling of thermal pyrolysis with basic or multifunctional catalysts for the production of oxygenated compounds from biomass.
- Coupling of thermal pyrolysis with acid and basic catalysts in cascade for the production of aromatic hydrocarbons from biomass.

The most relevant results obtained during this Doctoral Thesis are summarised below:

### **1) Catalytic pyrolysis of lignocellulosic biomass over bentonite and attapulgite**

The cationic clays bentonite and attapulgite previously calcined in air have been used in the catalytic fast pyrolysis of pre-treated wheat straw in order to obtain high-added value bio-based chemicals. Both clay catalysts present mainly mesoporous structures with relatively low specific surface area, acidity and basicity values, those of attapulgite being slightly higher than those of bentonite in all cases. The use of bentonite as a catalyst in catalytic pyrolysis of biomass has been observed to be more appropriate due to its higher bio-oil yields and lower formation of undesirable by-products, since attapulgite shows higher activity towards cracking and deoxygenation reactions. Anhydrosugars are the most abundant compounds in the bio-oil produced using bentonite as catalyst and the synergistic effect of its textural properties and high weak-mild basicity seem to improve the yield towards this type of compounds. The catalytic pyrolysis of cellulose over bentonite has been shown to yield a bio-oil rich in anhydrosugars, mainly levoglucosan, a compound with potential interest in the chemical, food and pharmaceutical industries. The most widely accepted route of formation of levoglucosan is the hydrolysis of glucose, which is the monomer unit of cellulose. It is concluded that a low catalyst/biomass ratio results in a higher levoglucosan yield in both catalytic pyrolysis of cellulose and pre-treated wheat straw, thus avoiding reduction in bio-oil yield and saving on catalyst costs.

### **2) Catalytic pyrolysis of wheat straw over Mg and Zr metal oxides**

Single and mixed Mg and Zr metal oxides prepared by precipitation exhibit mesoporous structures with very similar specific surface areas. The basic sites of alkaline earth metal oxides, such as MgO, and of certain transition metals, such as ZrO<sub>2</sub>, catalyse C–C bond formation reactions, such as aldol condensation and ketonisation reactions. In addition, ZrO<sub>2</sub> shows acidic sites that make it active in cracking and deoxygenation reactions. It has been confirmed by NH<sub>3</sub>-TPD that ZrO<sub>2</sub> exhibits the highest concentration of weak acidic sites among the three materials,



whereas a Mg-Zr mixed oxide with a Mg/(Mg+Zr) ratio of 0.71 shows the highest proportion of medium and strong acid sites, confirming the synergistic effect of the two single oxides when coprecipitated. In contrast, MgO exhibits the highest basicity with a high contribution of medium basicity, with such basic centres being responsible for catalysing the aldol condensation reactions. Magnesium oxide and Mg-Zr mixed oxide showed the most promising results in terms of bio-oil deoxygenation and production of potential high-added value bio-based chemicals. However, unlike ZrO<sub>2</sub>, their bio-oil yields are considerably reduced. MgO resulted in a bio-oil with the lowest oxygen content and a high proportion of light oxygenates, such as cyclic ketones, and especially, aromatic oxygenates, such as acetophenones and guaiacols. Conversely, the Mg-Zr mixed oxide produced a bio-oil with a lower oxygen content, but richer in light oxygenates, including acetals and both linear and cyclic ketones.

### **3) Catalytic pyrolysis of wheat straw over K-incorporated zeolites**

K-incorporated zeolites prepared by different methods have been used in the catalytic fast pyrolysis of pre-treated wheat straw. The incorporation of alkali metals such as potassium into protonic zeolites is an interesting way to increase their basicity and, at the same time, to reduce their cracking activity because of their high acidity, leading to a considerable decrease in bio-oil yield and increased deactivation due to the formation of coke deposits. Two different zeolites have been studied: a nanocrystalline H-ZSM-5 zeolite ion-exchanged with an aqueous KCl solution, and an USY zeolite modified by potassium grafted with KOH in alcoholic medium. The partial ion-exchange with K<sup>+</sup> cations hardly affects the crystallinity and properties of the KH-ZSM-5 zeolite. This material presents a good balance between its acidic and basic properties, since this treatment notably decreases the acidity of the parent zeolite, reducing the concentration of strong acidic sites while generating basic sites of weak-medium basicity. On the other hand, treatment of a commercial USY zeolite with a methanol solution of KOH results in a zeolitic material with a high concentration of active centres of weak-medium basicity. However, contact with a strong base causes some desilication/amorphisation of the parent zeolite, accompanied by a reduction in its textural properties.

Increasing the catalyst/biomass ratio in the catalytic pyrolysis of pre-treated wheat straw with K-modified zeolites causes a progressive reduction in the bio-oil yield,

## Summary

followed by an enhancement in the production of water, gases and coke, and accompanied by a decrease in the oxygen content of the bio-oil. The KH-ZSM-5 catalyst has proven to be less active than the parent H-ZSM-5 zeolite for the same catalyst/biomass ratio, due to a lower contribution in deoxygenation and cracking reactions, in line with the lower acidity of the K-exchanged zeolite. However, the KH-ZSM-5 catalyst shows a more efficient behaviour, as its bio-oil oxygen contents in the bio-oil are close to or even lower than those of the parent material, which is related to the lower concentration of strong acidic sites in this material. Moreover, the basicity generated plays an important role in the deoxygenation selectivity, since it promotes ketonisation and aldol condensation reactions between the components of bio-oil, releasing oxygen in the form of water and/or CO<sub>2</sub> more effectively. Conversely, this catalyst produces oxygenated and light oxygenated aromatics, with the greatest variation observed for the latter family, which has a large proportion of ketones that could be assigned to the ketonisation activity of the basic sites of KH-ZSM-5. This enhanced production of oxygenated aromatics and light oxygenates is also observed over the K-USY catalyst with high weak-mild basicity and negligible acidity. By studying the synergistic effect on both catalytic temperature and catalyst/biomass ratio for this zeolite, the bio-oil composition was further optimised. Thus, when operating at 500 °C in the catalytic zone of the reaction system and with a catalyst/biomass ratio of 0.6 g/g, the formation of both ketones (with a high proportion of cyclic ketones) derived from the pyrolysis of cellulose and hemicellulose, and phenols from the transformation of lignin oligomers and their derivatives was favoured. Both types of products are of great commercial interest, as they have a wide variety of applications as fine chemicals.

### **4) Catalytic pyrolysis of wheat straw in a three-stage cascade thermo-catalytic process combining acidic and basic catalysts**

Dual-catalytic staged-pyrolysis is an innovative way to produce aromatic hydrocarbons while deoxygenating bio-oil by sequentially using catalysts with different pore sizes and acid-base properties. The nanocrystalline zeolite H-ZSM-5 with mainly microporous structure and high acidity has been chosen as the sole acid catalyst (A), whereas bentonite clay and magnesium oxide have been chosen as basic catalysts (B), having different mesoporous structures and concentrations of basic sites. Two different configurations have been studied depending on whether the pyrolysis

vapours passed first through the acid catalyst bed (A+B) or the basic catalyst bed (B+A). The combination of acidic and basic catalysts in the sequential pyrolysis of pre-treated wheat straw resulted in a bio-oil with a lower oxygen content at the cost of a decrease in mass yield. In particular, the combination of bentonite/MgO and H-ZSM-5 favours the transformation of oligomers into smaller species that are precursors of furans and light olefins when passing through the first basic catalyst bed, and their subsequent conversion into aromatic hydrocarbons when passing through the second acid catalyst bed. Thus, the bio-oil from the B+A configurations showed higher aromatic hydrocarbon concentrations than that of the sole H-ZSM-5 zeolite, especially in combination with MgO. The highest concentration of aromatic hydrocarbons in bio-oil with the highest ratio of monoaromatic/polycyclic aromatic hydrocarbons was achieved in this test. In addition, this bio-oil showed the lowest oxygen content of all the catalysts and configurations studied.



## **Resumen**



La presente Tesis Doctoral ha sido llevada a cabo en los laboratorios de la Escuela Superior de Ciencias Experimentales y Tecnología de la Universidad Rey Juan Carlos, y del Instituto IMDEA Energía. Concretamente, se engloba en las líneas de investigación: *Biomasa y Bioenergía* del Grupo de Ingeniería Química y Ambiental de la Universidad Rey Juan Carlos; y *Combustibles Sostenibles* de la Unidad de Procesos Termoquímicos del Instituto IMDEA Energía.

La financiación de esta investigación se ha realizado a través del proyecto *BIOCASCHEM: Valorización de Residuos Lignocelulósicos mediante la Integración de Procesos Termo-catalíticos en Cascada* (referencia: CTQ2017-87001-R), liderado por la Universidad Rey Juan Carlos y el Instituto IMDEA Energía, y financiado por el Ministerio de Economía, Industria y Competitividad.

La biomasa lignocelulósica es uno de los recursos renovables más abundante y de menor coste, considerándose como una fuente de gran potencial para la obtención de combustibles y/o productos químicos de interés. La biomasa lignocelulósica está formada por macromoléculas (celulosa, hemicelulosa y lignina), extractivos y materia inorgánica, en proporción variable según su origen. En la presente Tesis Doctoral, se ha escogido la pirólisis como tecnología de conversión termoquímica para la valorización de biomasa lignocelulósica procedente de residuos agroforestales, en concreto, de paja de trigo, debido a su alta disponibilidad y abundancia. La pirólisis de biomasa es un tratamiento térmico en atmósfera inerte a temperaturas moderadas (300 – 700 °C) y, normalmente a presión atmosférica, lo que provoca su descomposición, dando lugar a tres fracciones: gases incondensables, un residuo carbonoso o char, y bio-oil, en proporciones variables dependiendo de la naturaleza de la biomasa de partida y las condiciones en las que se realiza la pirólisis. La fracción líquida o bio-oil es el producto principal de la reacción de pirólisis. Consiste en una mezcla compleja de compuestos orgánicos oxigenados de distinta naturaleza (ácidos carboxílicos, azúcares, alcoholes, aldehídos, cetonas, fenoles, furanos, guaiacoles, etc.) y agua en diferente proporción, como consecuencia del elevado número de reacciones simultáneas que se producen durante el proceso de pirólisis: craqueo y despolimerización, descarbonilación, descarboxilación, deshidratación, carbonización, etc. El bio-oil cuenta con propiedades poco aptas para su utilización como combustible: elevado contenido en oxígeno (40 – 45 % en peso, base seca), bajo

## Resumen

poder calorífico superior (16 – 19 MJ/kg), pH ácido (2 – 4), elevada viscosidad y baja estabilidad.

Cuando el objetivo es maximizar la producción de bio-oil, las condiciones óptimas son las siguientes: biomasa en forma de partículas de 0,5 – 1,0 mm para favorecer la transmisión de calor, temperaturas en el rango de 500 – 600 °C, elevadas velocidades de calefacción (pirólisis rápida) y cortos tiempos de residencia (2 – 3 s). Por ello, uno de los sistemas más utilizados en este campo son los reactores de lecho fluidizado. En estas condiciones se pueden alcanzar rendimientos de bio-oil del orden del 70 – 75 %.

Durante los últimos años se ha realizado un gran esfuerzo investigador en el desarrollo de procesos catalíticos que permitan mejorar las propiedades del bio-oil, eliminando la mayor parte del agua y del oxígeno presentes e incrementando el peso molecular de algunos de los componentes con el fin de producir principalmente hidrocarburos. Sin embargo, esta vía ha demostrado poseer numerosas limitaciones, como consecuencia de la propia naturaleza del bio-oil y del relativamente bajo valor económico de los productos finalmente obtenidos. En este contexto, la presente Tesis Doctoral tiene como objetivo general el estudio de nuevas rutas de valorización de biomasa lignocelulósica procedente de residuos agroforestales mediante la combinación de tratamientos termo-catalíticos en cascada, a fin de maximizar la producción no sólo de hidrocarburos aromáticos sino también de otros compuestos oxigenados de interés comercial. Se pretende maximizar la producción de bio-oil mediante un proceso de pirólisis catalítica que incluya catalizadores básicos y multifuncionales, y su selectividad hacia productos oxigenados de diferente naturaleza con aplicaciones como materias primas químicas.

En la pirólisis catalítica, los vapores de pirólisis se ponen en contacto con catalizadores normalmente ácidos, fundamentalmente zeolitas protónicas como la H-ZSM-5, lo que permite eliminar el oxígeno del bio-oil mediante su conversión en CO, CO<sub>2</sub> y H<sub>2</sub>O, y obteniéndose como productos finales mayoritarios hidrocarburos aromáticos y olefinas ligeras. Se puede llevar a cabo *in-situ*, añadiendo el catalizador al propio reactor de pirólisis de biomasa, o *ex-situ*, haciendo pasar los gases y vapores de la pirólisis térmica por un segundo reactor, en este caso catalítico. Esta segunda opción permite operar y optimizar de forma separada las dos etapas (térmica y catalítica) de conversión de la biomasa lignocelulósica y evita que el char entre en contacto directo



con el catalizador, atenuando su desactivación. La pirólisis catalítica de biomasa transcurre a presión atmosférica y temperaturas intermedias (400 – 500 °C). Sin embargo, ésta presenta importantes limitaciones como son el bajo rendimiento en hidrocarburos líquidos, el desarrollo de reacciones de craqueo severo y la extensiva desactivación que experimenta el catalizador por la deposición de grandes cantidades de coque.

Por otro lado, entre los catalizadores básicos utilizados para incrementar la formación de compuestos oxigenados a partir de la pirólisis de biomasa, cabe mencionar los siguientes: arcillas, óxidos de metales alcalino-térreos y de transición, y zeolitas con propiedades básicas. La mayor parte de los catalizadores utilizados en la presente Tesis Doctoral se obtuvieron mediante la modificación de muestras comerciales, pero en algunos casos se sintetizaron en nuestros laboratorios con este fin. Se tomaron como referencia trabajos previos de la bibliografía, así como resultados del propio grupo de investigación. Los catalizadores básicos preparados son los siguientes: arcillas catiónicas (bentonita y atapulgita), óxidos metálicos simples y mixtos de Mg y Zr, y zeolitas H-ZSM-5 nanocrystalina y USY comerciales modificadas con K para dotarles de basicidad.

Para evitar que la materia inorgánica de la biomasa de partida actúe de por sí como un catalizador in-situ, se ha realizado un lavado con una disolución diluida de ácido nítrico (1 % en peso) con objeto de disminuir su contenido en metales alcalinos y alcalinotérreos (K, Na, Ca, Mg, etc.), ya que su presencia favorece el desarrollo de reacciones de carbonización, aumentando la producción de char y disminuyendo el rendimiento en bio-oil.

La caracterización de los diferentes catalizadores se ha llevado a cabo mediante las siguientes técnicas experimentales: estabilidad térmica (TG), composición química (ICP-OES y EDX), cristalinidad (DRX), propiedades texturales (fisisorción de N<sub>2</sub> y Ar), morfología y tamaño de cristal (SEM y TEM), acidez (TPD de amoníaco y FT-IR de muestras tratadas con piridina) y basicidad (TPD de dióxido de carbono). Por otro lado, la caracterización de las diferentes materias primas y productos de reacción se ha llevado a cabo mediante las siguientes técnicas experimentales: composición química (ICP-OES y CHNS-O), contenido en agua (valoración Karl-Fischer),

## Resumen

contenido en cenizas, coque y materia volátil (TG) y distribución de productos líquidos (GC-MS) y gaseosos ( $\mu$ -GC).

Para llevar a cabo los experimentos de valorización catalítica del bio-oil, se ha utilizado un sistema de reacción ex-situ, en el que los vapores y gases procedentes de la etapa de pirólisis térmica se hacen pasar por un lecho fijo catalítico. El sistema de reacción consiste en un único reactor de lecho fijo vertical de flujo descendente calentado con dos zonas de calefacción por dos hornos eléctricos independientes a distinta temperatura, siendo el primero y de mayor temperatura el de pirólisis térmica, y el segundo y de menor temperatura el de pirólisis catalítica. De esta forma, se ha investigado el comportamiento de los diferentes tipos de catalizadores preparados llevándose a cabo los siguientes ensayos:

- Acoplamiento de pirólisis térmica con catalizadores básicos o multifuncionales para la producción de compuestos oxigenados a partir de biomasa.
- Acoplamiento de pirólisis térmica con catalizadores ácidos y básicos en cascada para la producción de hidrocarburos aromáticos a partir de biomasa.

A continuación, se resumen los resultados más relevantes que se han obtenido a lo largo de esta Tesis Doctoral:

### **1) Pirólisis catalítica de biomasa lignocelulósica sobre bentonita y atapulgita**

Se han utilizado las arcillas catiónicas bentonita y atapulgita previamente calcinadas en aire en la pirólisis rápida catalítica de paja de trigo pretratada con el objetivo de obtener potenciales productos químicos de interés. Ambos catalizadores de arcilla presentan estructuras principalmente mesoporosas con valores de superficie específica, acidez y basicidad relativamente bajos, siendo los de la atapulgita ligeramente superiores a los de la bentonita en todos los casos. El uso de bentonita como catalizador en la pirólisis catalítica de biomasa parece ser más apropiado debido a sus mayores rendimientos en bio-oil y su menor formación de subproductos, ya que la atapulgita muestra una actividad más elevada hacia las reacciones de craqueo y desoxigenación. Los azúcares anhidros son los compuestos más abundantes en el bio-oil producido utilizando bentonita como catalizador y el efecto sinérgico entre sus propiedades texturales y elevada basicidad de fuerza débil-media parecen mejorar el rendimiento hacia este tipo de compuestos. Se ha comprobado que la pirólisis catalítica de la celulosa sobre bentonita da lugar a un bio-oil rico en azúcares anhidros,

principalmente levoglucosano, un compuesto con potencial interés en la industria química, alimentaria y farmacéutica. La vía de formación más aceptada del levoglucosano es la hidrólisis de la glucosa, que es el monómero de la celulosa. Se concluye que una baja relación catalizador/biomasa da lugar a un mayor rendimiento de levoglucosano tanto en la pirólisis catalítica de la celulosa como de la paja de trigo pretratada, evitando así la reducción del rendimiento en bio-oil y ahorrando en costes asociados al catalizador.

## **2) Pirólisis catalítica de paja de trigo sobre óxidos metálicos de Mg y Zr**

Se han utilizado óxidos metálicos simples y mixtos de Mg y Zr preparados por precipitación en la pirólisis rápida catalítica de paja de trigo pretratada. Estos catalizadores presentan estructuras mesoporosas con superficies específicas muy similares. Los centros básicos de los óxidos de metales alcalinotérreos, como el MgO, y de algunos metales de transición, como el ZrO<sub>2</sub>, catalizan las reacciones de formación de enlaces C–C, como las reacciones de condensación aldólica y cetonización. Además, el ZrO<sub>2</sub>, en concreto, cuenta con centros ácidos que lo hacen activo en reacciones de craqueo y desoxigenación. Se ha confirmado mediante TPD de amoníaco que el ZrO<sub>2</sub> presenta la mayor concentración de centros ácidos débiles entre los tres materiales, mientras que un óxido mixto Mg-Zr con una relación de Mg/(Mg+Zr) de 0.71 muestra la mayor proporción de centros ácidos medios y fuertes, lo que confirma el efecto sinérgico de los dos óxidos simples cuando co-precipitan. En cambio, el MgO presenta la mayor basicidad con una elevada contribución de basicidad de fuerza media, siendo este tipo de centros básicos los responsables de catalizar las reacciones de condensación aldólica. El óxido de magnesio y el óxido mixto Mg-Zr mostraron los resultados más prometedores en términos de desoxigenación del bio-oil y de producción de productos químicos de alto valor añadido. Sin embargo, a diferencia del ZrO<sub>2</sub>, el rendimiento a bio-oil se ve considerablemente reducido. El MgO dio lugar a un bio-oil con el menor contenido en oxígeno y con una gran proporción de compuestos oxigenados ligeros, como cetonas cíclicas, y, sobre todo, de aromáticos oxigenados, como acetofenonas y guaiacoles. Por otro lado, el óxido mixto Mg-Zr produjo un bio-oil con un contenido en oxígeno no tan bajo, pero más rico en oxigenados ligeros, entre los que destacan acetales y cetonas tanto lineales como cíclicas.

### 3) Pirólisis catalítica de paja de trigo sobre zeolitas protónicas modificadas con potasio

Se han utilizado zeolitas modificadas mediante diferentes métodos de incorporación de potasio en la pirólisis rápida catalítica de paja de trigo pretratada. La incorporación de metales alcalinos como el potasio a las zeolitas protónicas es una forma interesante de aumentar su basicidad y, al mismo tiempo, de reducir su actividad de craqueo debido a su elevada acidez, lo que conlleva una disminución considerable del rendimiento del bio-oil y una mayor desactivación, ya que esta da lugar a la formación de depósitos de coque. Las dos zeolitas estudiadas son: una zeolita nanocristalina H-ZSM-5 intercambiada con potasio de una solución acuosa de KCl, y una zeolita USY modificada por grafting de potasio con KOH en medio alcohólico. El intercambio iónico parcial con cationes  $K^+$  apenas afecta a la cristalinidad y propiedades de la zeolita H-ZSM-5. El material presenta un buen equilibrio entre sus propiedades ácidas y básicas, ya que este tratamiento disminuye notablemente la acidez de la zeolita de partida, reduciendo la concentración de los centros ácidos fuertes a la vez que genera centros básicos de fuerza débil-media. Por otro lado, el tratamiento de una zeolita USY comercial con una solución de KOH en metanol da lugar a un material zeolítico con una elevada concentración de centros básicos de fuerza débil-media. Sin embargo, el contacto con una base fuerte provoca una cierta desilicación/amorfización de la zeolita de partida, acompañada de una reducción en sus propiedades texturales.

El aumento de la relación catalizador/biomasa en la pirólisis catalítica de paja de trigo pretratada con zeolitas modificadas con K provoca una reducción progresiva del rendimiento de bio-oil y acompañado de una disminución de su contenido en oxígeno, debido a una mejora en la producción de agua, gases y coque. El catalizador KH-ZSM-5 resulta ser menos activo que la zeolita H-ZSM-5 de partida para una misma relación catalizador/biomasa, ya que presenta una menor contribución de las reacciones de desoxigenación y craqueo, en línea con la menor acidez de la zeolita intercambiada. Sin embargo, el catalizador KH-ZSM-5 muestra un comportamiento más eficiente ya que se obtienen contenidos de oxígeno iguales o incluso inferiores en el bio-oil a los obtenidos con la zeolita de partida, relacionado con la menor concentración de centros ácidos fuertes de este material. Además, la basicidad generada tiene un papel importante en la selectividad de desoxigenación, ya que promueve reacciones de cetonización y condensación aldólica entre los componentes del bio-oil, liberando

oxígeno en forma de agua y/o CO<sub>2</sub> de manera más efectiva. Por otro lado, este catalizador produce compuestos aromáticos oxigenados y oxigenados ligeros, observándose la mayor variación para esta última familia, con una gran proporción de cetonas, que podría asignarse a la actividad de cetonización por parte los centros básicos de KH-ZSM-5. Esta producción mejorada de aromáticos oxigenados y oxigenados ligeros también se observa sobre el catalizador de K-USY con elevada basicidad de fuerza débil-media y acidez despreciable. Al estudiar el efecto sinérgico de la temperatura de la etapa catalítica y la relación catalizador/biomasa para esta zeolita, se optimizó aún más la composición del bio-oil. Así, cuando se trabajó a 500 °C en la zona catalítica del sistema de reacción y con una relación catalizador/biomasa de 0,6 g/g, se vio favorecida la formación tanto de cetonas (con una alta proporción de cetonas cíclicas) derivadas de la pirólisis de celulosa y hemicelulosa, como de fenoles provenientes de la transformación de los oligómeros de lignina y sus derivados. Ambos tipos de productos son de gran interés comercial, ya que tienen una amplia variedad de aplicaciones en Química Fina.

#### **4) Pirólisis catalítica de paja de trigo en un proceso termo-catalítico en cascada de tres etapas que combina catalizadores ácidos y básicos**

La pirólisis catalítica por etapas con dos catalizadores es una forma innovadora de producir hidrocarburos aromáticos a la vez que se desoxigena el bio-oil utilizando secuencialmente catalizadores con diferentes tamaños de poro y propiedades ácido-base. Se eligió la zeolita nanocrystalina H-ZSM-5 con estructura principalmente microporosa y elevada acidez como catalizador ácido (A), mientras que la bentonita y el óxido de magnesio fueron elegidos como catalizadores básicos (B), teniendo diferentes estructuras mesoporosas y concentraciones de centros básicos. Se estudiaron dos configuraciones diferentes en función de si los vapores de pirólisis pasaban primero por el lecho de catalizador ácido (A+B) o por el básico (B+A). La combinación de catalizadores ácidos y básicos en la pirólisis secuencial de paja de trigo pretratada dio lugar a un bio-oil con un menor contenido en oxígeno a costa de una disminución de su rendimiento másico. En concreto, la combinación de bentonita/MgO y H-ZSM-5 favorece la transformación de oligómeros en especies de menor tamaño que son precursoras de furanos y olefinas ligeras al pasar por el primer lecho de catalizador básico, y su posterior conversión en hidrocarburos aromáticos en su paso por el segundo lecho de catalizador ácido. Así, el bio-oil obtenido con las

## Resumen

configuraciones B+A mostró mayores concentraciones de hidrocarburos aromáticos que el de una única zeolita H-ZSM-5, especialmente en combinación con MgO. La mayor concentración de hidrocarburos aromáticos en el bio-oil, con la mayor proporción de compuestos monoaromáticos frente a los poliaromáticos, se alcanzó para este experimento. Además, este bio-oil resultó tener el menor contenido de oxígeno de entre todos los ensayos con los catalizadores y configuraciones estudiados.

## **1. Introduction**





### 1.1. Lignocellulosic biomass

Generally, *biomass* is defined as renewable organic material that comes from plants and animals [1]. However, the term *biomass* is commonly used to refer to plant biomass. Biomass resources can be classified as agricultural residues, forestry residues, energy crops, algal biomass, and urban waste [2]. Concretely, lignocellulosic biomass is mainly derived from agricultural and forestry residues and can be valorised as biofuels and/or bio-based chemicals via thermochemical conversion technologies [3]. The lignocellulosic feedstocks stand out for their abundance (10 GT/year) and low cost [4]. However, lignocellulosic biomass has a very complex composition, consisting of macromolecules (**Figure 1.1**), extractives, and some inorganic materials. The content of these components depends on the nature of the biomass, whether woody or not. Among macromolecules, three major biopolymers can be distinguished: cellulose and hemicellulose (*holocellulose*, considered together), and lignin. Lignocellulosic biomass components and contents are described below [5]:

- Cellulose (30 – 50 %): It is a linear homopolysaccharide with a long chain of glucose units that are connected by  $\beta$ -(1-4)-glycosidic bonds, and inter- and intramolecular H-bonds. Its chain length, crystallinity, and degree of polymerisation (300 – 15,000) may vary depending on the type of lignocellulosic biomass [5–7].
- Hemicellulose (15 – 30 %): It is a heteropolysaccharide composed by pentoses, hexoses and sugar acids. It has a shorter chain length and lower degree of polymerisation than cellulose (80 – 100), but it also depends on the type of lignocellulosic biomass [5,6,8].
- Lignin (20 – 40 %): It is a three-dimensional polymer composed of three monomeric units (coniferyl alcohol, coumaryl alcohol and sinapyl alcohol) which are linked through C–C and C–O bonds. Simultaneously, holocellulose and lignin are crosslinked by ether and ester bonds [7]. Several functional groups, such as carbonyl (CO-), carboxylic (CO<sub>2</sub>-), hydroxyl (HO-), and methoxyl (CH<sub>3</sub>O-) groups, can be found as part of lignin structure [8].
- Extractives (2 – 10 %): The nature of the components which are considered as extractives is very variable. Components, such as flavonoids, lignans, lipids,

## 1.2. Biomass conversion technologies

essential oils, proteins, resins, simple sugars, starch, tanins, terpenes, stilbenes, and water, can be found in lignocellulosic biomass [3,5].

- Inorganic matter (0.5 – 20 %): Alkali and Alkaline Earth Metals (AAEMs) are present in the lignocellulosic biomass as cations ( $K^+$ ,  $Na^+$ ,  $Ca^{2+}$  and  $Mg^{2+}$ , among others) [4] and have variable composition depending on whether biomass is woody (<4 %) or not (>4 %) [7].

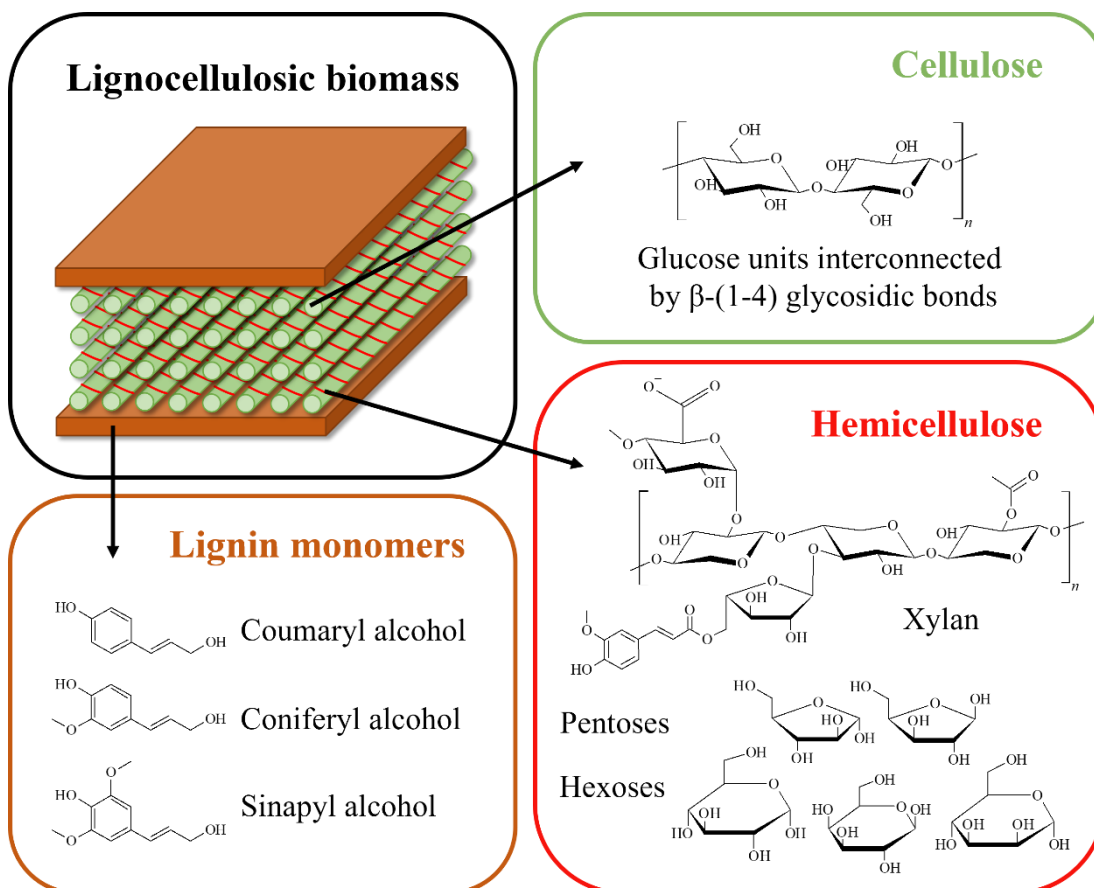


**Figure 1.1.** Chemical structure of lignocellulosic biomass [9].

## 1.2. Biomass conversion technologies

Valorisation of biomass is commonly oriented to energy production. Biomass can be burnt to produce heat via direct combustion or transformed into fuels of any state of aggregation, either solid, liquid, or gaseous [1]. Modern bioenergy, i.e. renewable energy produced from biomass, accounts for 10 % of the world's primary energy according to the International Energy Agency [10], and it is expected that up to 27 % of world's transportation fuel could be replaced by biofuels by 2050 [11,12].

Typically, biomass is transformed into bioenergy via four different routes [2,7,13]. A summary of conversion technologies, products and utilisation of lignocellulosic biomass is depicted in **Figure 1.2**.

- i) Physical conversion: Biomass is compacted into pellets or briquettes for its use as a solid fuel in direct combustion.
- ii) Chemical conversion: Biodiesel is produced via transesterification of a vegetable oil or animal fat with an alcohol.
- iii) Biological conversion: Fermentation and anaerobic digestion are used to produce liquid and gaseous biofuels and/or bio-based chemicals.
- iv) Thermochemical conversion technologies: Biomass thermally degrades to give rise to solid (*biochar*), liquid (*bio-oil*) or gaseous (*syngas*) biofuels under moderate/severe temperature conditions.

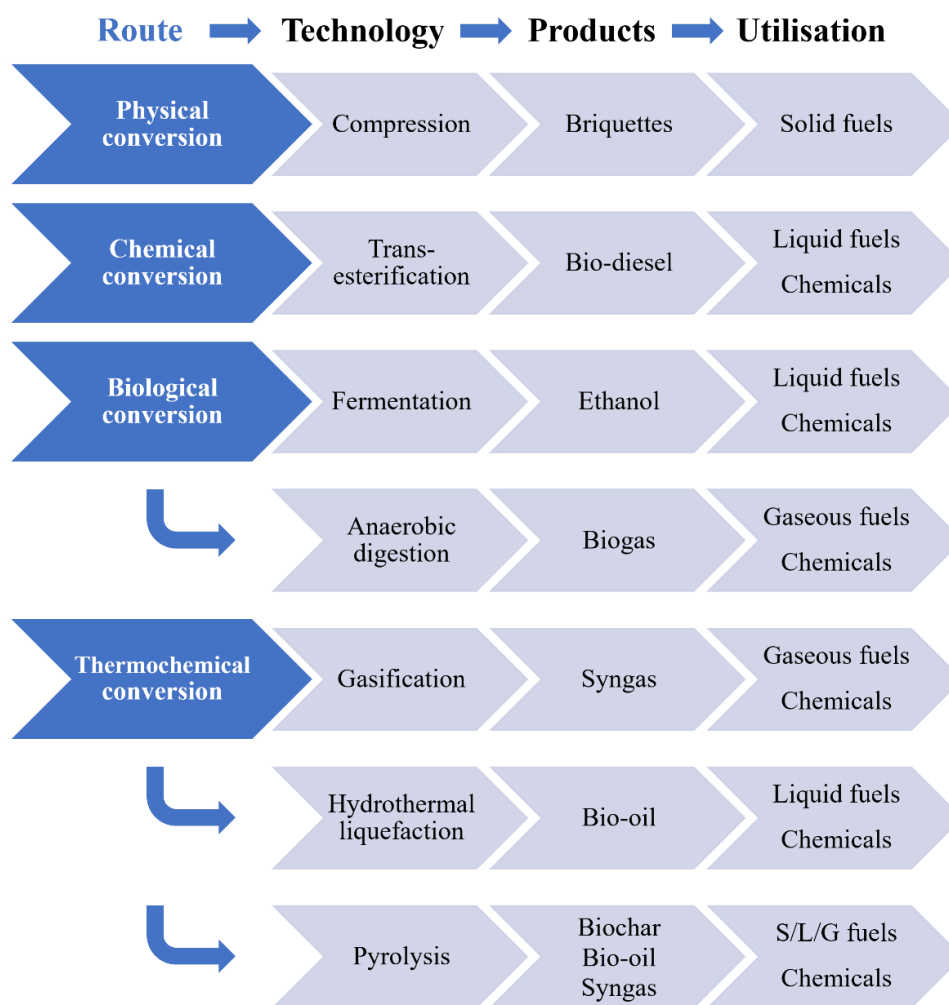


**Figure 1.2.** Conversion technologies, products and utilisation of lignocellulosic biomass [14]. S: solid; L: liquid; G: gaseous.

### 1.3. Bio-oil production via pyrolysis of biomass

The present Doctoral Thesis focuses on the *commoditisation* of lignocellulosic biomass, and, among these valorisation routes, thermochemical conversion technologies are the most developed [15]. These thermal processes are carried out at moderate-high temperatures, variable pressure and absence/presence of oxygen [2]. Three technologies are mainly used to obtain high-added value bio-based chemicals from lignocellulosic biomass:

- Gasification: Biomass is partially oxidised in the presence of gasifying agents, such as air, CO<sub>2</sub>, oxygen, steam, or a mixture of these. The main product of the reaction is syngas, which is a mixture of gaseous CO and H<sub>2</sub> in variable concentrations. A carbonaceous residue or biochar, ash and oil/tar are obtained as by-products to a lesser extent [16]. Syngas can be a platform for alkenes and short-chain oxygenated hydrocarbons production after secondary processing, such as Fischer-Tropsch technology [8].
- Hydrothermal liquefaction (HTL): Generally, biomass decomposes into liquid *bio-oil* in a pressurised hot water atmosphere [2]. Bio-oil has two phases: a heavy and an aqueous fraction, both of which contain a wide variety of organic compounds. The heavy fraction can be upgraded by several processes to obtain bio-based chemicals, whereas the aqueous fraction can be digested by microorganisms to produce biogas. Biochar obtained from HTL is also an interesting by-product due to its potential as adsorbent or solid biofuel [17].
- Pyrolysis: This process consists of the thermal degradation of biomass in oxygen-free conditions to produce either biochar, bio-oil or syngas depending on the operating temperature, heating rate and vapours residence time [18,19]. Bio-oil is the most desired product when it comes to producing bio-based chemicals. As this liquid product is rich in a wide variety of organic compounds, numerous high-added value chemicals can be obtained from *bio-oil* after proper upgrading and separation [4].

### 1.3. Bio-oil production via pyrolysis of biomass

The term *pyrolysis* refers to the irreversible thermal decomposition of materials in inert conditions. During the pyrolysis process, biomass is heated up in absence of oxygen and transformed into char and *pyrovapours*. These pyrolytic vapours are condensed into bio-oil after reaction and remaining gases are released. Resulting solid fraction is

called biochar. Hence, pyrolysis involves simultaneous solid, liquid and vapor phase reactions [8]. Products of the three states of aggregation are described in more detail below:

- *Biochar*: It is a solid carbonaceous residue which consists of unconverted inert organic matter and ash remains. It has a variable carbon content of 65 to 90 wt.% [3,15].
- *Bio-oil*: It is a dark brown liquid rich in numerous oxygenated compounds (>300) and water, which is obtained from the condensation of pyrovapours after proper biomass pyrolysis. It has undesired properties, such as high oxygen content (40–45 wt.%, dry basis) and acidic pH (2 – 4), which cause the bio-oil to have low stability, high viscosity and low higher heating value (16 – 19 MJ/kg) [20]. Thus, further bio-oil upgrading is necessary.
- *Pyrolytic gases*: It is a mixture of non-condensable gases which is separated from pyrovapours after their condensation into bio-oil. They contain variable concentrations of H<sub>2</sub>, CO, CO<sub>2</sub> and C<sub>1</sub>-C<sub>4</sub> hydrocarbons [3].

Among thermochemical conversion technologies, pyrolysis has the highest maximum yield of bio-oil at the adequate conditions of temperature, heating rate and vapours residence time [13,18]. Pyrolysis can be categorised as slow, fast or flash depending on these parameters (see **Table 1.1**). Other factors, which are related to the nature of the biomass, such as, particle size, moisture and impurities contents, can affect maximum bio-oil yield [3,19].

**Table 1.1.** Maximum bio-oil yields according to pyrolysis types [7,13,18,19,21].

Pyrolysis type	Temperature (°C)	Heating rate (°C/min)	Pyrovapours residence time (s)	Maximum bio-oil yield (wt. %)
Slow	300-700	<10	>600	<30
Fast	400-600	10-200	0.5-10	50-75
Flash	650-900	10 <sup>3</sup> -10 <sup>4</sup>	<0.5	75-80

Lignocellulosic biomass is generally pretreated to maximise bio-oil yield. Several pretreatment technologies are used to improve the efficiency of biomass pyrolysis [20]. Among pretreatment technologies, the following stand out:

## 1.4. Biomass pyrolysis chemistry

- i) Chemical pretreatment: Water and acid washing are extensively employed to remove impurities from raw biomass. AAEMs are reactive during biomass pyrolysis and can affect the quality and yield of bio-oil [22].
- ii) Physical pretreatment: Milling and grinding are employed to obtain a specific biomass particle size. It is necessary to select the correct particle size to have a good mass and heat transfer during biomass pyrolysis, since greater particles tend to transform into char and finer ones into permanent gases [3].
- iii) Thermal pretreatment: Drying is commonly employed to reduce the moisture content of the biomass. If wet biomass undergoes pyrolysis, it results in poorer quality bio-oil [3]. Additionally, torrefaction is included as thermal pretreatment. During this *mild pyrolysis* process (200 – 300 °C), not only is water removed from biomass, but also light oxygenated compounds are released in the form of CO and CO<sub>2</sub>. In this way, the quality of the bio-oil is improved, despite the reduction in its yield [7].

## 1.4. Biomass pyrolysis chemistry

As discussed in **Section 1.1**, lignocellulosic biomass is composed of three major components: cellulose, hemicellulose, and lignin. It is interesting to analyse the pyrolysis mechanisms of these three individual biopolymers to understand better how lignocellulosic biomass pyrolysis works [3,5,13]:

- Cellulose pyrolysis: This homopolysaccharide starts to degrade at about 300 °C with the cleavage of its more unstable glycosidic bonds, which leads to the formation of low molecular weight compounds, like formic acid, furan, glycolaldehyde, CO, CO<sub>2</sub>, and H<sub>2</sub>O. On the other hand, anhydrosugars and levoglucosenone are formed by cracking and dehydration reactions at moderate temperatures (< 450 °C). When temperature rises slightly (> 450 °C), multiple competing reactions give rise to more stable compounds, such as furfural, 5-hydroxymethylfurfural (HMF) and pyran. Light oxygenates, such as hydroxyacetaldehyde and acetone, are favoured at higher temperatures (550-600 °C) and their oligomerisation provokes the formation of *biochar*.
- Hemicellulose pyrolysis: Xylan is the most abundant unit of this heteropolysaccharide, and the cleavage of its glycosidic bonds induces xylose production. Simultaneously, multiple decomposition reactions take place leading

to similar low molecular weight compounds to cellulose pyrolysis at low temperatures ( $< 300\text{ }^{\circ}\text{C}$ ). On the other hand, acetic acid and furfural are the main products of xylose degradation, which occurs at higher temperatures ( $> 425\text{ }^{\circ}\text{C}$ ). A low yield of HMF is also obtained since it is a precursor of furfural. Additionally, biochar is also formed from oligomerisation of light oxygenates.

- Lignin pyrolysis: C–O bonds start to cleave at  $200\text{ }^{\circ}\text{C}$ , whereas C–C bonds do so at  $300\text{ }^{\circ}\text{C}$ . The formation of methoxyphenols begins at  $400\text{ }^{\circ}\text{C}$ . Depending on the biomass origin, lignin pyrolysis results into syringol (both softwood and hardwood biomass) and/or guaiacol derivatives (softwood biomass). Dealkylation and demethoxylation reactions give rise to  $\text{CH}_4$ , CO and  $\text{CO}_2$  in the temperature range of  $350 - 500\text{ }^{\circ}\text{C}$ , whereas catechols are more predominant below  $550\text{ }^{\circ}\text{C}$ , above this temperature formation of phenols and aliphatics, including methanol, is favoured. When it comes to catalytic fast pyrolysis, methyl- and methoxy- groups are central structural elements for coke production.

### 1.5. Pyrolysis reactor types

The reactor design is one of the key parts of the pyrolysis process. Changing from batch or semi-batch to continuous operation mode and selecting the correct reactor size and configuration are crucial for good scalability. The most relevant technologies in this research area are described below (**Figure 1.3**), from the smallest to the largest scale:

- Pyrolyser coupled with Gas Chromatography-Mass Spectrometry (Py/GC-MS): It consists of a micro-scale reactor which performs direct online analysis of the pyrovapours by GC-MS. Condensation of these vapours into bio-oil is not required for the analysis. This reactor operates with high heating rates ( $>100\text{ }^{\circ}\text{C/s}$ ) and short residence times ( $15 - 20\text{ ms}$ ) [7]. Py/GC-MS technology is useful for catalyst screening and reaction pathway studies, among other research purposes [20].
- Fixed-bed reactor: It consists of a bench-scale tubular reactor and operates in batch or semi-batch mode [20]. In this configuration, pyrovapours pass through the catalytic bed and are then condensed into bio-oil for their separation from permanent gases and subsequent analysis. Despite its simple design, mass and heat transfer coefficients are generally low and numerous modifications must be done to take fixed-bed reactors to larger scales [7].

## 1.5. Pyrolysis reactor types

- Fluidised bed reactor: It consists of a pilot- or commercial-scale reaction system which operates in continuous mode. There are two possible configurations: bubbling and circulating fluidised bed reactors [23]. The difference between both is whether char is obtained as by-product or burned to heat the sand inside the fluidised bed [24]. Pyrovolapours upgrading is usually carried out in a secondary reactor [25]. Fluidised bed reactors have effective mass and heat transfer due to the turbulence and provide high bio-oil yields (70 – 75 wt.%), being easily scalable due to their simplicity in design and medium operational complexity [7].

Other reactor types that are also found in literature are the following: TG-FTIR and TG-MS (micro-scale) [7]; microwave-assisted and grinding pyrolysis [5]; and spouted bed [13], rotating cone, auger and ablative reactors [23].

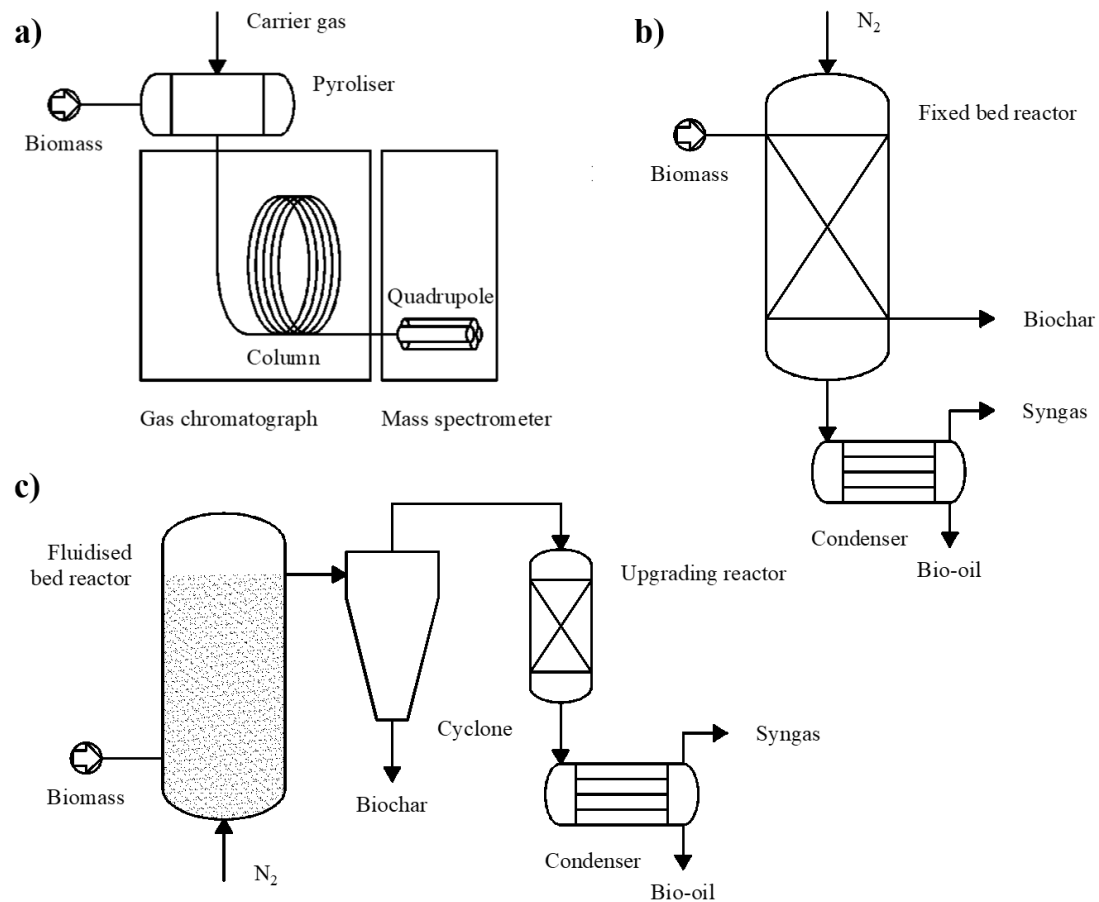


**Figure 1.3.** Types of biomass pyrolysis reactors from the smallest to the largest scale: a) Py/GC-MS (micro-scale) [26]; b) fixed-bed reactor (bench-scale) [27]; c) fluidised bed reactor (pilot- or commercial-scale) [3].



## 1.6. Catalytic fast pyrolysis

Catalytic fast pyrolysis (CFP) integrates biomass thermal decomposition and catalytic upgrading with the aim of improving bio-oil quality. A correct selection of catalysts and configuration are necessary to obtain desirable products from specific chemical reactions [6,7]. Depending on how the catalyst is introduced in the reaction system (**Figure 1.4**), different configurations can be found [13,19,20]:

- **In-situ:** Catalyst is directly mixed with biomass, either pre-absorbed or physically mixed. Biomass and catalyst are heated up under fast pyrolysis conditions (450-550 °C and atmospheric pressure). Pyrovapours are released from biomass, and subsequently, react with the surrounding catalyst.
- **Ex-situ:** Catalyst is deposited in a fixed bed in the same reactor or in a separate one. Degradable components of biomass are transformed into vapours in the pyrolytic zone, which then pass through the catalytic bed. Reaction conditions can be varied from pyrolytic to catalytic zones.
- **Staged:** Several ex-situ catalysts with different properties can be located in the catalytic zone as a downstream cascade reaction system. In addition, in-situ and ex-situ catalysts can also be combined for pyrovapours upgrading.

Numerous catalysts of different nature, such as mesoporous silica [6], zeolites, metal oxides and carbon-based catalysts [13], are used in ex-situ configurations, whereas inorganic salt additives and red mud are used as in-situ catalysts [19,20].

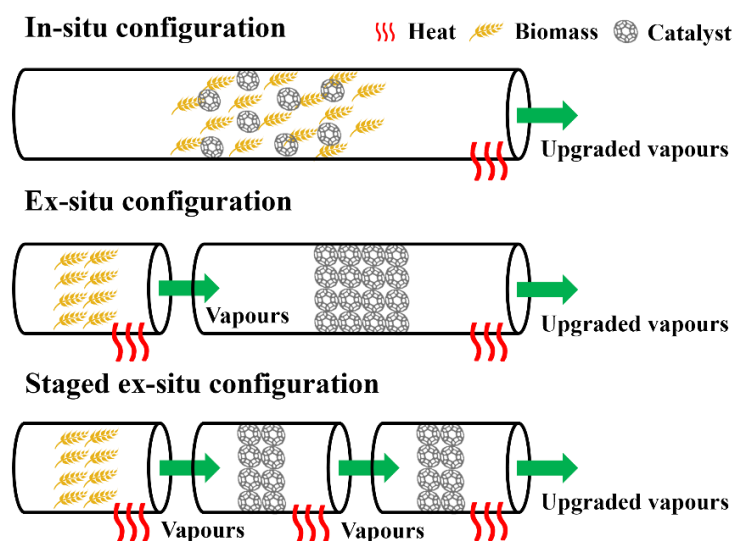


**Figure 1.4.** Configuration of in-situ, ex-situ and staged ex-situ CFP [13].

### 1.7. Ex-situ CFP over heterogeneous acid-base catalysts

When catalysts are included, additional parameters must be considered, such as temperature of the catalytic zone, catalyst to biomass (C/B) ratio and weight hourly space velocity (WHSV) [20]. Temperature and C/B ratio affect deoxygenation reactions during CFP [28], whereas WHSV influences coke deposition [29].

Coke is a by-product of CFP that is mainly produced by the polymerisation of furans and/or aromatic hydrocarbons over the surface of the catalyst [19,29]. Coke formation involves the physical deactivation of the catalyst due to the blocking of its active sites [6].

### 1.7. Ex-situ CFP over heterogeneous acid-base catalysts

In-situ catalysts can be homogenous or heterogeneous, whereas ex-situ catalysts are only heterogeneous. Ex-situ catalysts are preferred over in-situ catalysts since they can be easily separated from the other solid fractions, i.e., char, and regenerated by burning the residues deposited on their surfaces. In addition, another advantage of using heterogeneous ex-situ catalysts is the possibility of conducting thermal and catalytic pyrolysis at different temperatures in the same reaction system.

Catalysts for acid-base reactions can be categorised as acid, basic, or multifunctional based on the nature of their active sites. On the one hand, catalysts with acidic centres can be Brønsted or Lewis, either donating a proton or accepting an electron pair, respectively. On the other hand, catalysts with Brønsted basic active sites are proton acceptors, whereas the ones with Lewis basic centres are electron pair donors [30]. Finally, multifunctional catalysts present more than one of these functionalities.

Acid-base properties depend on the nature of the catalysts. In the present Doctoral Thesis, three families of catalysts will be used and described in depth: clay minerals, metal oxides and zeolites (**Figure 1.5**); but there are still numerous materials with such properties.

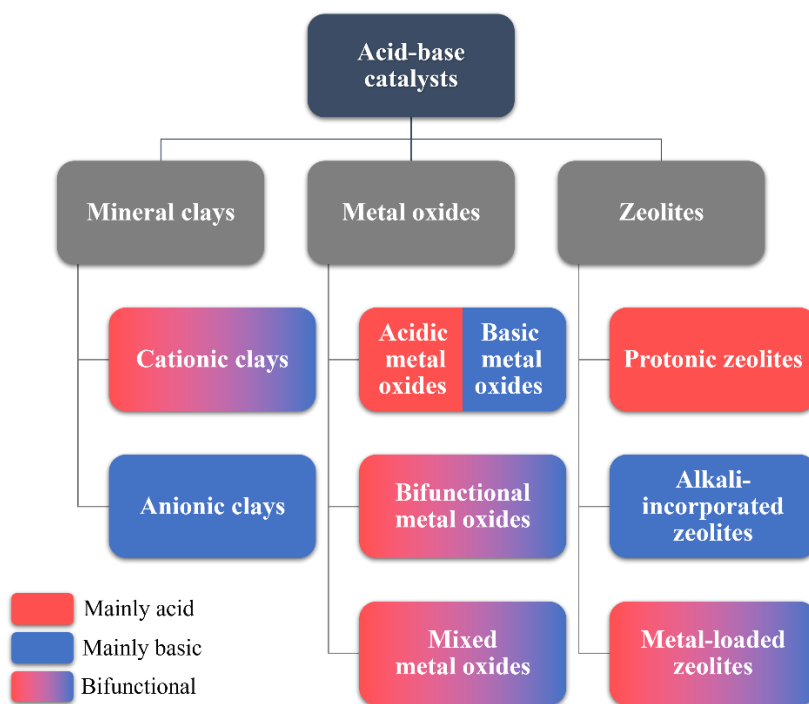


**Figure 1.5.** Classification of mineral clays, metal oxides and zeolites according to their acid-base properties [13,27,30–33].

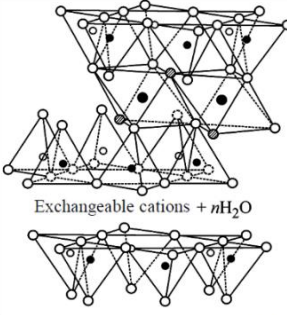
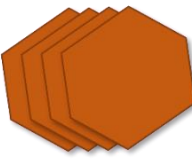
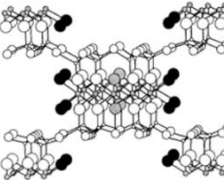

### 1.7.1. Clay minerals

Clay minerals are one of the most abundant materials on the surface of Earth and present a great number of applications, among which their use as adsorbents, catalysts or catalyst supports stand out. Depending on the charge of the layers or fibres of clay minerals, they can be grouped as cationic or anionic. Cationic clays are more abundant in nature than anionic clays, but the latter can be easily synthesised in the laboratory and are relatively inexpensive to manufacture industrially.

Phyllosilicates are the most studied cationic clays in catalysis due to their particular physicochemical properties. They show layered or fibrous aluminosilicate structures formed by the combination of connected tetrahedral and octahedral sheets. The partial substitution of  $\text{Si}^{4+}$  by  $\text{Al}^{3+}$  in tetrahedral sheets and  $\text{Al}^{3+}$  by  $\text{Mg}^{2+}$  in the octahedral ones give rise to a negative charge that is compensated by alkali or alkaline earth metal cations in the interlayer space. Both Brønsted and Lewis acidities are present in cationic clays: Brønsted acidity arises from the partial substitution of  $\text{Si}^{4+}$  by  $\text{Al}^{3+}$ , whereas Lewis acidity resides in the external hydroxyl groups. However, accessibility to active acidic sites is very limited due to the narrow interlayer space between

## 1.7. Ex-situ CFP over heterogeneous acid-base catalysts

layers/fibres, so only external acidic centres are available [34]. On the one hand, montmorillonites of the smectite family present 2:1 dioctahedral structures (**Figure 1.6**), in which each layer is composed by an octahedral sheet sandwiched between two tetrahedral ones and the interlayer space is expandable according to the size of the counterbalancing cations [35]. Sodium bentonite [36] and K10 montmorillonite [37], belonging to this group, have been evaluated in the CFP of cellulose, resulting in bio-oils rich in levoglucosan and/or their derivatives. On the other hand, palygorskite (attapulgite) is a chain phyllosilicate with fibrous structure. It contains continuous two-dimensional tetrahedral sheets, but lacks continuous octahedral sheets, giving rise to fibres of interconnected 2:1 ribbon-like units (**Figure 1.6**). Protons, exchangeable cations and zeolitic water are responsible for compensating the negative charge along the channels [38]. Attapulgite, along with other clay catalysts, including bentonite and red mud, were tested at different catalyst to biomass (C/B) ratios in an auger reactor for the CFP of forest pinewood chips [39]. The use of attapulgite was highlighted due to its cracking and deoxygenation activity, since the resulting bio-oil showed the lowest oxygen content among the materials studied.

	Crystalline structure	Particle morphology
Montmorillonite (e.g. bentonite)	 <p>Exchangeable cations + <math>n\text{H}_2\text{O}</math></p> <p>○ ○ ● OH ● Al, Fe, Mg ● Si, partially Al</p> <p>2:1 type layer silicate</p>	 <p>Layers</p>
Palygorskite (attapulgite)	 <p>○ = O ● = OH ● = H<sub>2</sub>O = Si = Al &amp; Mg</p> <p>2:1 type chain silicate</p>	 <p>Fibres</p>

**Figure 1.6.** Crystalline structure and particle morphology of montmorillonite [40] and attapulgite [41].

Natural hydrotalcite ( $\text{Mg}_6\text{Al}_2(\text{OH})_{16}\text{CO}_3 \cdot 4\text{H}_2\text{O}$ ) is the most representative material among anionic clays. Magnesium cations are octahedrally surrounded by hydroxyl groups forming infinite brucite-like sheets. The partial substitution of  $\text{Mg}^{2+}$  by  $\text{Al}^{3+}$  give rise to a positive charge that is compensated by  $\text{CO}_3^{2-}$  anions in the interlayer space. Other hydrotalcite-like materials are also called layered double hydroxides (LDHs).  $\text{Mg}^{2+}$  and  $\text{Al}^{3+}$  cations can be replaced by any other two metal cations with the same valences ( $\text{M}^{2+}$  and  $\text{M}^{3+}$ , respectively) during their preparation by co-precipitation or sol-gel methods. The properties of resulting LDHs vary depending on the  $\text{M}^{2+}/\text{M}^{3+}$  molar ratio and the compensating anions introduced into the interlayer space during their synthesis. Hydrotalcite-like materials are used in organic chemistry as solid base catalysts of weak strength [30]. However, LDHs are unstable under CFP temperature conditions and prior calcination is required to form their respective layered double oxides (LDO).

### 1.7.2. Single and mixed metal oxides

Alumina ( $\text{Al}_2\text{O}_3$ ) and silica ( $\text{SiO}_2$ ) are acidic metal oxides that have been extensively studied as catalysts and catalyst supports and both present Lewis active sites of weak acidity [13]. Whereas  $\text{Al}_2\text{O}_3$  acts as promoter of dehydration and decarbonylation reactions during CFP of lignocellulosic biomass [42,43],  $\text{SiO}_2$  contributes to the reduction of the amount of oxygenated compounds in bio-oil and inhibits the formation of coke [44].

Alkaline earth metal oxides are typical solid base catalysts. Alkaline earth metals are usually found in the form of hydroxides (Mg, Ca) and carbonates (Sr, Ba) [30]. When thermally stabilised in the temperature range of 500 – 600 °C, adsorbed acidic molecules, such as  $\text{H}_2\text{O}$  or  $\text{CO}_2$ , are removed and give rise to their respective oxides revealing their generated basic sites. The basic strength of these active sites depends on the coordination number of the  $\text{M}^{2+}\text{--O}^{2-}$  ion pairs, M being an alkaline earth metal [45]. Conversely, the overall basicity of alkaline earth metal oxides is ordered by cation size (in other words,  $\text{MgO} < \text{CaO} < \text{SrO} < \text{BaO}$ ), whereas surface area is in the reverse order. Surface areas of MgO, CaO, SrO and BaO are approximately on the order of  $10^2$ ,  $10^1$ ,  $10^0$  and  $10^{-1}$   $\text{m}^2/\text{g}$ , respectively, if no special methods are employed during thermal treatment. Concretely, MgO and CaO have been more frequently studied because of their higher surface areas [30].

### 1.7. Ex-situ CFP over heterogeneous acid-base catalysts

Basic alkaline earth metal oxides are mainly used to catalyse C–C bond-forming reactions, e.g., ketonisation of carboxylic acids and aldol condensation reactions of carbonyl groups. The addition of CaO in the catalytic pyrolysis of woody biomass gives rise to a better-quality bio-oil with lower acidity and oxygen content [13]. Ketonisation reactions avoid the formation of carboxylic acids, whereas dehydration reactions contribute to the deoxygenation of bio-oil. In addition, the concentration of anhydrosugars and phenolic compounds is reduced, whereas the production of hydrocarbons is enhanced compared to non-catalytic pyrolysis [7]. Similarly, the addition of MgO decreases oxygen content of bio-oil at the expense of its overall mass yield and organic content. Resulting bio-oil presents higher high heating value due to formation of diesel-range hydrocarbons and the removal of oxygenated functional groups [7,13]. When comparing the performance of natural MgO catalysts in CFP of biomass with that of H-ZSM-5 zeolite, these base metal oxides showed either similar bio-oil organic fraction yield with lower oxygen content or similar oxygen content with higher organics yield. In this way, MgO catalysts remove oxygen from bio-oil more effectively due to their basic features that promote CO<sub>2</sub> formation as a by-product of ketonisation reactions. However, dehydration and decarbonylation pathways are more predominant in the deoxygenation of bio-oil when employing H-ZSM-5 zeolite. Not only that, but MgO can also be regenerated more easily since its calcination temperature does not need to be as high as in the case of the protonic zeolite [46].

In addition to alkaline earth metal oxides, transition and rare earth metal oxides, such as, ZnO, TiO<sub>2</sub>, ZrO<sub>2</sub> and CeO<sub>2</sub>, show high selectivity towards ketonisation of carboxylic acids and aldol condensation reactions [47]. Concretely, zirconia is well known among metal oxides due to its amphoteric catalytic properties, or what it is the same, it possesses both acidic and basic active sites. However, this oxide presents weak-medium strength that depends on the crystalline phase of ZrO<sub>2</sub>. There are three different crystalline structures of zirconium oxide: monoclinic, tetragonal, and cubic. Monoclinic phase shows the acid-basic active sites of higher strength, in addition to a higher surface area, followed by tetragonal and cubic phases. Nevertheless, selectivity towards different products can be obtained for the same reaction depending on whether zirconia is used in one or another crystalline phase [32]. A similar phenomenon occurs in the case of TiO<sub>2</sub>, which also presents three different crystalline phases: rutile, anatase and brookite. In the work of Lu et al. [48], rutile and anatase phases of titania,

as well as a solid solution of 60-40 wt.% monoclinic/tetragonal zirconia and anatase ( $\text{ZrO}_2\text{-TiO}_2$ ), were compared in the ex-situ CFP of poplar wood. Rutile produced a bio-oil richer in monoaromatic phenolic compounds derived from the pyrolysis of lignin, whereas that of  $\text{ZrO}_2\text{-TiO}_2$  showed a lower content in phenolics, carboxylic acids and anhydrosugars, but a higher concentration of aromatic hydrocarbons, cyclopentanones and other ketones.

The interest in mixed metal oxides, like  $\text{ZrO}_2\text{-TiO}_2$ , lies in their activity for ketonisation and aldol condensation reactions that improve bio-oil quality by reducing oxygen content and acidic pH [7]. In this line, by combining two or more different metal oxides, mixed metal oxides with multifunctional properties are obtained (**Figure 1.7**). There are several preparation methods of mixed metal oxides, among which co-precipitation, sol-gel and impregnation methods stand out. Regarding acid-base properties of mixed metal oxides, overall acidity can be increased by a synergistic effect of mixing different metal oxides with acid properties, but basic strength is limited to those of the base metal oxides that form the mixed oxide [49].

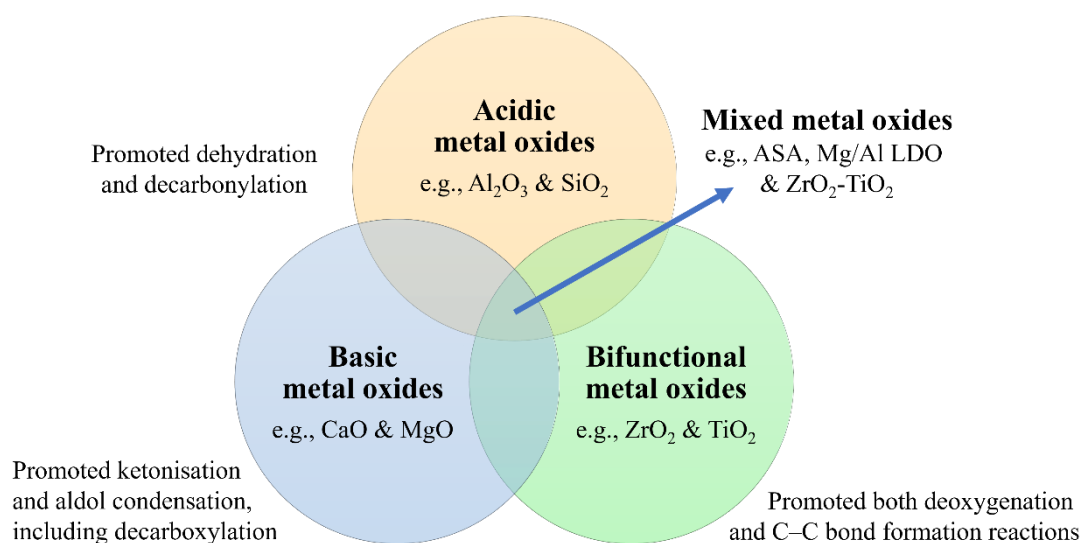


**Figure 1.7.** Catalytic effects of metal oxides on fast pyrolysis of lignocellulosic biomass [13].

To give another example, amorphous silica-alumina (ASA) is synthesised by co-precipitation or sol-gel methods from mixed Si and Al precursors. ASA presents both Brønsted and Lewis active centres, but their concentration depends on the preparation method and the  $\text{SiO}_2/\text{Al}_2\text{O}_3$  molar ratio. However, overall acidity of ASA is not

### 1.7. Ex-situ CFP over heterogeneous acid-base catalysts

comparable to that of zeolites despite of similarities in composition [30]. Zabeti et al. [50] compared non-supported ASA with alkali or alkaline earth metal-loaded ASAs in the CFP of pinewood and observed that non-supported ASA produced a higher yield of less deoxygenated bio-oil than the impregnated samples and Cs/ASA showed the lowest oxygen content and highest yield of aromatic hydrocarbons.

Moreover, calcination of layered double hydroxides give rise to their respective mixed oxides. Among LDOs, Mg/Al layered double oxide obtained by calcination of natural hydrotalcite is the most extensively studied. The strength of basic active sites can be altered by varying Mg/Al ratio of synthetic hydrotalcite-like materials [30]. Navarro et al. [51] probed Mg/Al layered double oxides with different Mg/Al ratio in ex-situ CFP of wheat straw and concluded that those LDOs with lower Al content contributed to a more effective deoxygenation of bio-oil. The increasing concentration of basic sites with Mg content promotes ketonisation and aldol condensation reactions removing oxygen in the form of H<sub>2</sub>O and CO<sub>2</sub>.

#### 1.7.3. Zeolites

Zeolites are crystalline aluminosilicates with ordered tetrahedral structure showing a dense network of micropores and tuneable acidity [6]. Silicon and aluminium atoms are covalently bonded in the zeolite framework, and the substitution of aluminium for silicon generates a negative charge that must be compensated by extra-framework cations, which can be interchangeable. In the case of protonic zeolites, the compensating cations are protons that come from the decomposition of exchanged ammonium ions. Protonic zeolites stand out over other acid catalysts due to the strong Brønsted acidity of their Si-OH-Al hydroxyl groups generated by the presence of Al atoms and balancing protons, and their crystalline and microporous structures [52]. In addition to Brønsted acidity, Lewis acidity caused by the presence of tricoordinate silicon defects can also be observed in protonic zeolites. Numerous zeolite catalysts (e.g., BEA-, FAU- and MFI-type protonic zeolites) have been evaluated in catalytic fast pyrolysis of lignocellulosic biomass due to their deoxygenation capacities giving rise to bio-oils rich in aromatic hydrocarbons. Zeolite H-ZSM-5 (MFI-type) is the most effective catalyst in the CFP of biomass for aromatic hydrocarbons production due to its strong acidity, medium pore size, shape selectivity, and chemical and thermal stability [19]. This zeolite catalyst produces monoaromatic hydrocarbons (MAHs)



more selectively than others with larger pores, such as H-Beta (BEA-type) or H-USY (Ultrastable Y, FAU-type), which instead give rise to more polycyclic aromatic hydrocarbons (PAHs) and coke deposits [6].

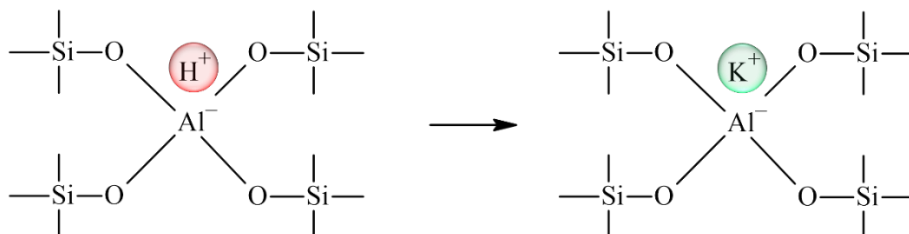
The use of alkali-incorporated zeolites has not been extensively studied in ex-situ CFP of lignocellulosic biomass, but they present an interesting alternative to obtain high-added value bio-based chemicals due to their already known textural and acid properties, but their not so explored basicity. Alkali-incorporated zeolites are divided into alkali ion-exchanged and alkali-grafted zeolites. On the one hand, the basicity of alkali ion-exchanged zeolites depends on their type of structure and chemical composition. Superficial oxygen atoms are the basic active sites of the zeolite. Their negative charge increases when more aluminium atoms are present in the zeolite framework due to its lower electronegativity compared to silicon. A good accessibility to more electronegative oxygen atoms is crucial for a better performance of zeolites in base-catalysed reactions [49]. Thus, faujasites (FAU) are typical base zeolites due to their more open structures (7.4 Å). It has been confirmed that X-zeolites are more efficient than Y-zeolites in typical base-catalysed test reactions. Overall basicity of zeolites can also be increased by exchanging charge compensation ions with higher radius alkali metal cations (**Scheme 1.1.a**). The less electronegative the alkali metal cation ( $\text{Li}^+ < \text{Na}^+ < \text{K}^+ < \text{Rb}^+ < \text{Cs}^+$ ), the more basic the resulting zeolite will be [32]. The basic sites generated by alkali cation-exchanged are considered as weak to medium in strength [49]. On the other hand, grafting consists of the deprotonation of Si-OH-Al hydroxyl groups at high pH in order to coordinate alkali metal cations generating basic active sites of medium strength (**Scheme 1.1.b**). As in the case of alkali-ion added zeolites, less electronegative alkali metal cations give rise to more basic alkali-grafted zeolites [33].

Loading metals on zeolite catalysts in the form of metal cations or metal oxides provide them bifunctional properties [27]. Numerous alkaline earth and transition metals, such as Mg, Zn [53,54], Fe, Co, Ni, Ga [6,7] or Zr [55,56], have been evaluated in CFP of lignocellulosic biomass with the aim of obtaining high bio-oil yields with low oxygen content and rich in aromatic hydrocarbons. In most cases, deposition of metals causes a reduction in Brønsted acidity, which is responsible of excessive cracking and oligomerisation reactions resulting in high gas and coke yields, respectively [6]. Conversely, the generation of weak Lewis acid and/or basic sites on zeolite catalysts

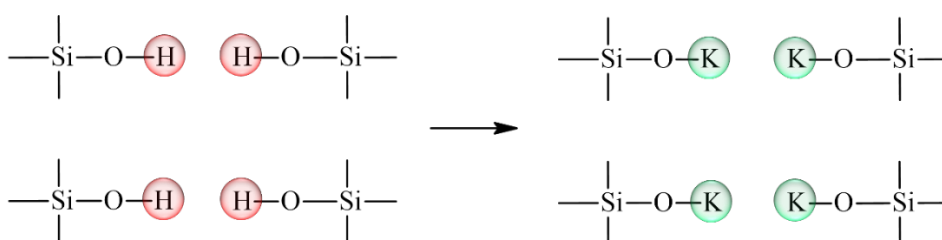
## 1.8. Catalytic fast pyrolysis chemistry

offers new possibilities for the production of high-added value bio-based chemicals from pyrolytic bio-oil.

### a) Ion-exchange with alkali metal cations



### b) Grafting with alkali metal cations



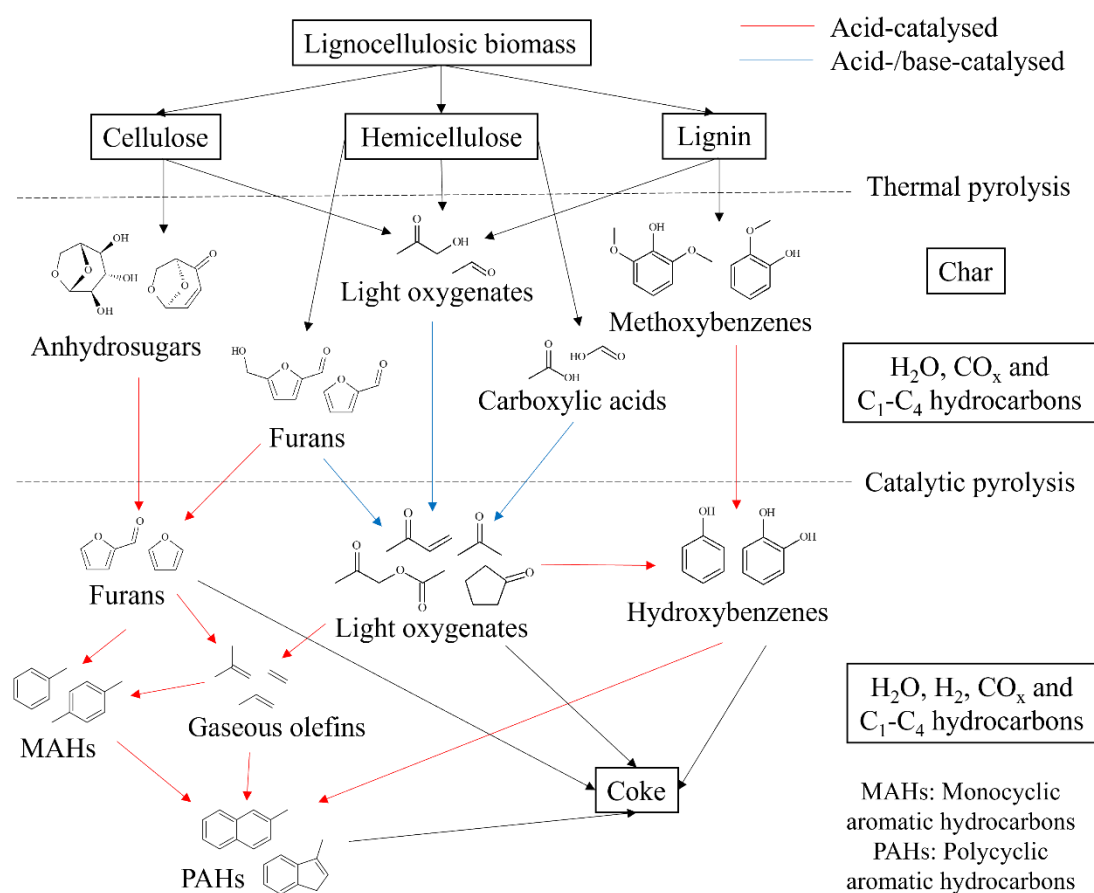
**Scheme 1.1.** Methods of alkali metal incorporation into protonated zeolites: a) ion-exchange [49]; b) grafting [33].

## 1.8. Catalytic fast pyrolysis chemistry

Numerous reactions occur simultaneously during catalytic upgrading of pyrovapours. Depending on the nature of catalysts employed the resulting bio-oil will present different properties and composition. The selectivity towards certain families of compounds is affected by the type of active centres of the catalysts used in CFP and their accessibility [5]. Acid-catalysed reactions over heterogeneous catalysts have been more extensively studied than base-catalysed ones in CFP of lignocellulosic biomass. Acid catalysis mainly affects the oxygen content and high heating value of bio-oils, since catalysts with such properties promote cracking and deoxygenation reactions, as well as the production of aromatic hydrocarbons. Conversely, the use of basic catalysts reduces acidic character of bio-oil through the production of longer-chain compounds with lower oxygen content [14].

Several reaction mechanisms have been proposed for the fast catalytic pyrolysis of lignocellulosic biomass over acid catalysts, with zeolite H-ZSM-5 as a model catalyst.

However, no reaction mechanisms have been proposed for CFP of biomass over basic catalysts. MgO and CaO are typical base catalysts that have been studied in CFP of biomass giving rise to more deoxygenated bio-oils with enhanced properties compared to those obtained by thermal pyrolysis. **Scheme 1.2** depicts a reaction mechanism that summarises both acid- and base-catalysed reactions that occur during the pyrolysis upgrading. These reactions will be described below according to the type of active centres that catalyse them.

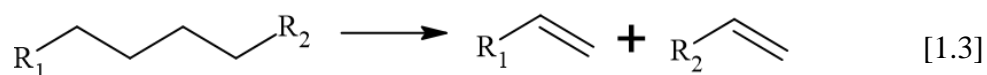


**Scheme 1.2.** Reaction mechanism for catalytic pyrolysis of biomass over acid-base catalysts [14,28,57–61].

### 1.8.1. Acid-catalysed reactions

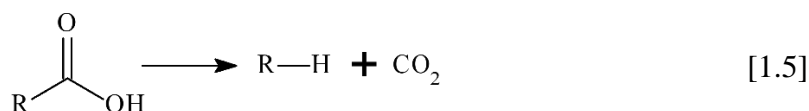
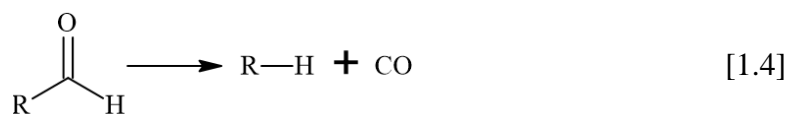
Cracking of  $C_{6+}$  hydrocarbons proceeds by  $\beta$ -scission of carbenium ion intermediates, which are protonated olefins with a trivalent carbon atom. This kind of reaction provokes the cleavage of C–C bonds of hydrocarbons giving rise to lower molecular weight alkenes (**Scheme 1.3**) [62].  $\beta$ -scission is carried out at the  $\beta$ -position of carbenium ion intermediates and is followed by hydrogen transfer reactions [30].

## 1.8. Catalytic fast pyrolysis chemistry

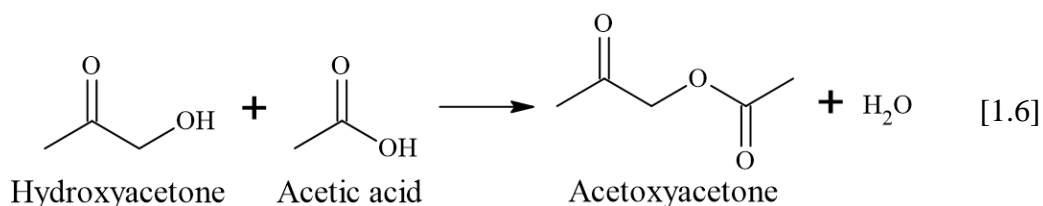


In CFP of lignocellulosic biomass, cracking of low-molecular weight oxygenated compounds produces C<sub>1</sub>-C<sub>4</sub> hydrocarbons [63], whereas that of lignin-derived aromatic oxygenates can contribute to the successive cleavage of C<sub>aromatic</sub>-O bonds giving rise to guaiacols and phenols [64].

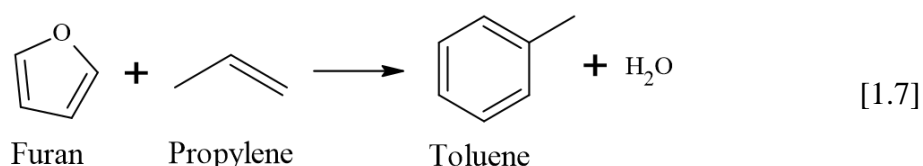
Deoxygenation implies decreasing oxygen content of pyrolytic bio-oil, which enhances its properties. There are three main reaction pathways: dehydration, decarbonylation and decarboxylation. Dehydration reactions release oxygen in the form of water, whereas decarbonylation and decarboxylation reactions do so in the form of CO and CO<sub>2</sub>, respectively (**Schemes 1.4** and **1.5**) [62]. A great number of dehydration reactions are carried out simultaneously during CFP of lignocellulosic biomass, e.g. dehydration of glucose from hollocelulose into levoglucosan or that of anhydrosugars into furans, but both involve several transformations.



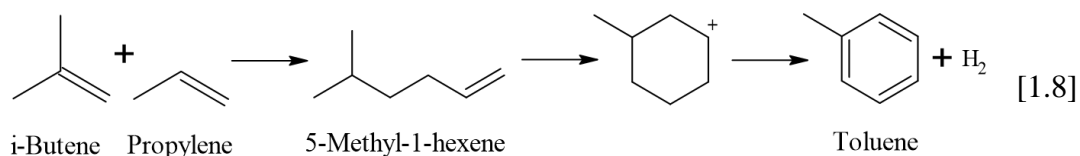
A simple model reaction of dehydration would be the esterification of alcohols and carboxylic acids (**Scheme 1.6**). Acetic acid is an abundant compound in bio-oil that reduces its pH and makes it highly unstable [20]. In addition, a great share of compounds with hydroxy functional groups can be found in pyrovapours that can react with acetic acid. The use of a solid catalyst with Brønsted acidity, such as zirconia or zeolites Y and ZSM-5 [30], is convenient since it promotes the removal of both oxygen and acetic acid, but not very effectively.



Lignocellulosic biomass is a possible source of aromatic hydrocarbons. However, the use of acidic catalysts is required to transform oxygenated compounds found in pyrovapours into this kind of compounds. Aromatic hydrocarbons can be obtained through different reaction pathways, but the optimal route is Diels-Alder condensation of furans and gaseous olefins followed by dehydration (**Scheme 1.7**). It has been confirmed that BEA [65] and ZSM-5 zeolites [66] selectively produce aromatic hydrocarbons via Diels-Alder condensation and dehydration reactions.



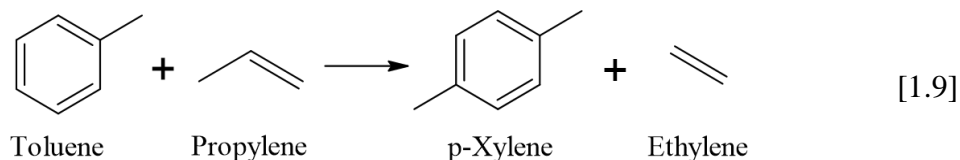
An alternative route to produce aromatic hydrocarbons is the oligomerisation-cyclisation-aromatisation reaction mechanism (**Scheme 1.8**). Gaseous  $C_2$ - $C_4$  olefins oligomerise to form  $C_{6+}$  linear alkenes that tend to cyclise into carbenium ion intermediates and ultimately aromatised by releasing hydrogen [67]. It was found that aromatisation reactions are catalysed by Brønsted acid sites of modified H-ZSM-5 zeolites in vacuum pyrolysis of rape straw [68].



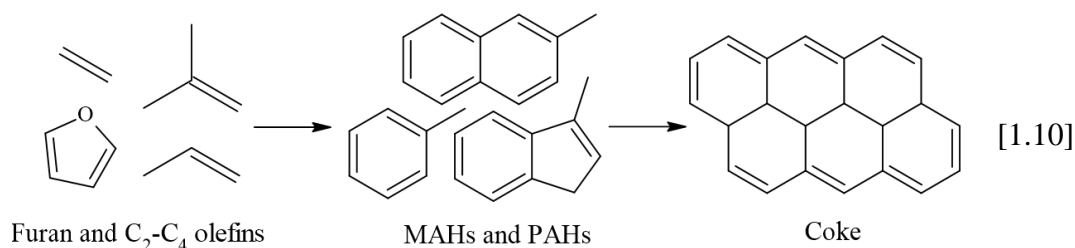
Aromatic hydrocarbons react with gaseous olefins in the presence of acidic catalysts to produce alkylated aromatics. Olefins are first protonated by the action of the acidic active centres of the catalyst and then included in the aromatic system by electrophilic substitution (**Scheme 1.9**) [30]. It has been evaluated the performance of ZSM-5 and Ga/ZSM-5 zeolites in CFP of pinewood and it was found that alkylation reactions are limited by their overall acidity and pore diffusion of the catalysts. Thus, selectivity

## 1.8. Catalytic fast pyrolysis chemistry

towards p-xylene formation is increased concerning other xylene isomers due to zeolite pore features in the reaction between toluene and propylene with an ethylene leaving group [69].

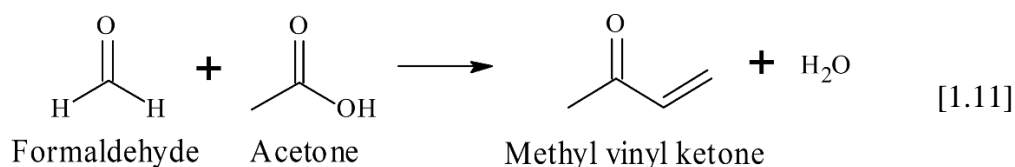


Polycyclic aromatic compounds (PAHs) are formed by polymerisation of monocyclic aromatic compounds (MAHs) (**Scheme 1.10**). Polymerisation into PAHs mainly occur on wide-pore catalysts with strong Brønsted acidity, such as protonic  $\beta$  or Y zeolites [70], and include successive dehydrogenation, hydrogen transfer, and isomerisation reactions [71]. In this way, excessive cracking of original biomass oligomers gives rise to high yields of gaseous olefins that tend to polymerise into coke within the catalyst pores, poisoning its active sites [56].

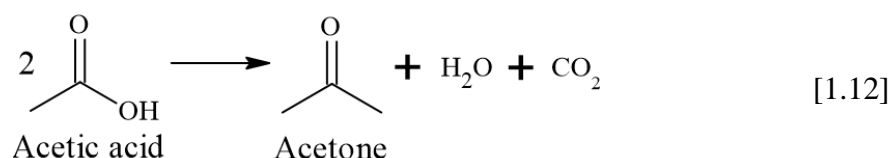


### 1.8.2. Base-catalysed reactions

Two molecules with carbonyl groups can generate C–C bonds by aldol condensation reactions. Self-condensation is called when two molecules of the same compound react with each other, whereas cross-condensation is called to the interaction between two molecules of a different nature, e.g. aldehydes with ketones, both present in significant concentrations in pyrolytic bio-oils. Base-catalysed aldol condensation followed by dehydration of the aldol intermediates yields unsaturated ketones and water (**Scheme 1.11**) [72].



The ketonisation reaction consists of the formation of longer chain ketones from two carboxylic acid molecules, such as acetic acid. Interestingly, oxygen is effectively removed in the form of water and carbon dioxide (**Scheme 1.12**), whereas acidic pH of bio-oil is slightly neutralised [73].



As commented in **Section 1.7.2**, C–C bond-forming reactions are mainly catalysed by alkaline earth, transition, rare earth metal oxides and their combinations when it comes to CFP of lignocellulosic biomass [7,13,47].

## 1.9. Valorisation of bio-oil to bio-based chemicals

Catalytic fast pyrolysis is a promising process to produce high-added value chemicals from lignocellulosic biomass. Specific bio-based chemicals can be selectively produced by using catalysts with certain acid-base properties [5]. The families of compounds found in catalytic bio-oils are classified according to their main functional groups. The catalytic reaction pathways and possible applications of each family of compounds are briefly explained below (**Figure 1.8**).

**Anhydrosugars (SUG):** The most accepted formation pathway of levoglucosan (LG) is the hydrolysis of glucose, which is the monomer unit of cellulose. LG is the most abundant product of thermal bio-oil and its separation and recovery are relatively easy, but somewhat expensive in commercial applications [4]. LG is a potential building block for the synthesis of additives, agrochemicals, natural chemical fuels, platform chemicals, pharmaceuticals, polymers, surfactants, resins and solvents [74]. In the manufacture of platform chemicals, levoglucosenone (LGO) stands out. LGO is usually obtained by pyrolysis of cellulose over Brønsted acid catalysts with

## 1.9. Valorisation of bio-oil to bio-based chemicals

levoglucosan as an intermediate [36]. LGO is used in asymmetric and enantiopure syntheses and as precursor of commodity and fine chemicals, polyols, polymers and solvents [75].

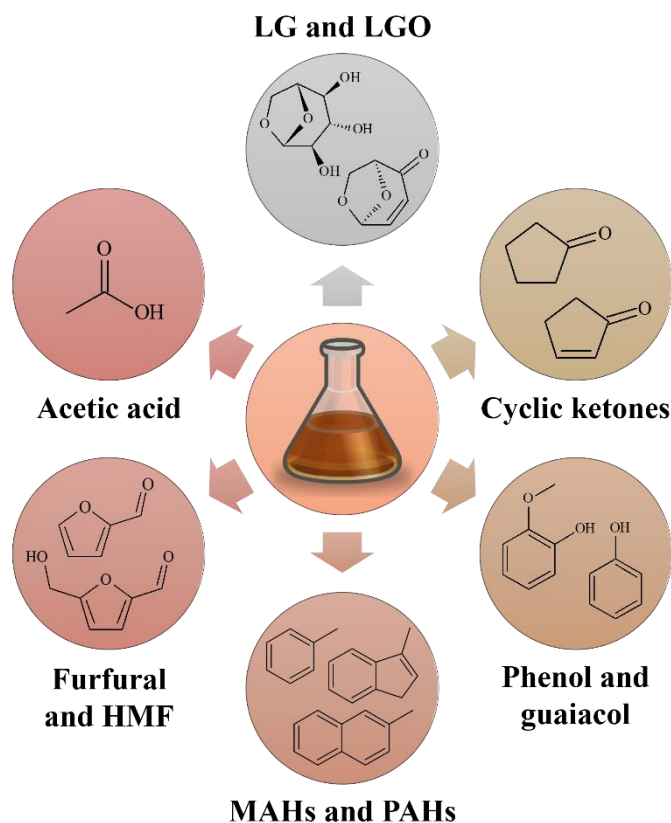


**Figure 1.8.** Obtainable high-added value bio-based chemicals from bio-oil classified by compound family. LG: levoglucosan; LGO: levoglucosenone; HMF: 5-hydroxymethyl-furfural; MAHs: monocyclic aromatic hydrocarbons; PAHs: polycyclic aromatic hydrocarbons.

Carboxylic acids (AC): Acetic acid is the most abundant compound in the pyrolysis of hemicellulose [76], especially in presence of AAEMs if biomass is not previously treated. Although acetic acid could rather be considered as a by-product, as its presence in bio-oil is deleterious, its yield can be maximised by catalytic pyrolysis of lignocellulose. However, there is not an optimal separation technique to obtain pure acetic acid from pyrolytic bio-oil. Conversely, acetic acid has several applications in the manufacture of dyes, foods, pharmaceuticals and polymers, since it is precursor of ethyl and propyl acetates, vinegar, acetic anhydride, vinyl acetate monomer and terephthalic acid, among others [77].



Furans (FUR): Furfural is the furan model compound found in bio-oil. It is obtained in the thermal pyrolysis of hollocelulose [3] and/or the dehydration of levoglucosan during CFP of lignocellulosic biomass [75] and serve as precursor of additives of biofuels and numerous high-added value C<sub>4</sub>-C<sub>5</sub> bio-based chemicals. Furan and tetrahydrofuran (THF) stand out among other C<sub>4</sub> bio-based chemicals. Furan is obtained from decarbonylation and THF from the successive hydrogenation of furan. Furan has relevant applications as a solvent and as a building block in the production of several agrochemicals and pharmaceuticals, whereas THF is a precursor for anionic polymerisation of urethane elastomer and fibre manufacture, as well as a solvent for many chromatographic techniques. There are numerous C<sub>5</sub> bio-based chemicals of different nature that come from the catalytic transformation of furfural: furans, such as methyl furan; alcohols, such as furfuryl alcohol, tetrahydrofurfuryl alcohol and pentanediol; esters, such as  $\gamma$ -valerolactone; ketones, such as cyclopentanone; and ketoacids, such as levulinic acid [8]. Moreover, 5-hydroxy methyl furfural (HMF) can also be found in bio-oil in low concentrations, but it mainly serves as precursor of furfural through cracking reactions [3]. Among the HMF derivatives, C<sub>6</sub> bio-based chemicals stand out, such as dimethylfuran, hexanediol or furandicarboxylic acid [75].

Light oxygenates (LO): This category gathers several families of compounds, including alcohols, aldehydes, esters, ethers, ketones, etc. Ketones stand out over other subfamilies in catalytic bio-oils since they are formed in both acid- and base-catalysed upgrading reactions. Concretely, C<sub>5+</sub> cyclic ketones, such as cyclopentanones and cyclopentenones, are of great interest due to their potential use in industrial applications. They can be employed as precursors of flavours, fragrances, jet fuels, pesticides, pharmaceuticals and polymers [61,78]. Cyclopentenone, in particular, acts as an intermediate in the synthesis of dicyclopentadiene, which is of great importance in the manufacture of hydrocarbon resins [79]. Moreover, methyl cyclopentenone is considered the most remarkable intermediate in the phenol production via Diels-Alder condensation reactions when it comes to upgrading of pyrovapours over activated carbons with acid properties [58].

Oxygenated aromatics (O-AR): Pyrolysis of lignin gives rise to a bio-oil rich in phenolic compounds, including methoxybenzenes (guaiacols and syringols) and hydroxybenzenes (phenols and cathecols). On the one hand, guaiacol is derived from creosol and is precursor of other methoxybenzenes, such as eugenol or vanillin. On the

## 1.9. Valorisation of bio-oil to bio-based chemicals

other hand, hydroxybenzenes are obtained by the degradation of methoxybenzenes, with phenol being the most representative compound of this family due to its widespread use in petrochemistry [5]. Both methoxy- and hydroxybenzenes have a wide variety of applications, since they can be used as intermediates of adhesives [80], flavourings [81], fuel additives [82], pesticides [83] and phenolic resins [84], among others.

Aromatic hydrocarbons (AR): Catalytic fast pyrolysis over acid zeolite catalysts gives rise to bio-oils rich in mono- and polycyclic aromatic hydrocarbons (MAHs and PAHs, respectively) with variable concentrations depending on the acid strength and porosity of the catalysts employed [70]. Benzene, toluene, ethylbenzene and xylene (BTEX) are typical MAHs found in conventional liquid fuels. In addition to their use in combustion engines, MAHs are of great importance in petrochemistry with various applications as dyes, pharmaceuticals, plastics, surfactants, resins and solvents [85]. Conversely, the presence of PAHs in bio-oil increases its octane number, but also its toxicity. The most widespread use of naphthalenes is as pesticides, although applications such as dyes, resins and plasticisers are also highlighted [86]. In contrast, indenenes and their derivatives arouse great interest in the pharmaceutical industry and organometallic chemistry [87].

## **2. Motivation and objectives**



As mentioned in the previous chapter, lignocellulosic biomass derived from agricultural and forestry residues can be valorised as both biofuels and bio-based chemicals via thermochemical conversion technologies. The present Doctoral Thesis explores ex-situ catalytic fast pyrolysis as a thermochemical conversion technology for the transformation of wheat straw into a bio-oil rich in bio-based chemicals with interest in industry. Due to the high content of impurities found in lignocellulosic biomass, an acid pre-treatment of wheat straw is required. The main objective of this work is the evaluation of catalysts of different nature with diverse textural and acid-base properties in the fast pyrolysis of acid-washed wheat straw. Acid catalysts have been more extensively studied in the catalytic fast pyrolysis of lignocellulosic biomass into biofuels; however, the novelty of this research lies in the use of basic catalysts to obtain bio-based chemicals from bio-oil. In order to achieve the main objective, this work has been divided into different specific objectives that are detailed below.

**I. Performance of clay catalysts in pyrolysis vapours upgrading in a two-stage thermocatalytic reaction system.** The main objectives of this section are to study of the effect of bentonite and attapulgite clays on the composition of upgraded bio-oil and other by-products and to optimise the operating conditions:

- Evaluation of the composition of pre-treated wheat straw by acid-washing.
- Evaluation of physicochemical properties of stabilised clays by calcination.
- Study of the influence of the catalyst to biomass ratio in the ex-situ catalytic fast pyrolysis of wheat straw over bentonite and attapulgite clays.
- Study of the influence of the catalyst to biomass ratio in the ex-situ catalytic fast pyrolysis of cellulose over bentonite clay.

**II. Performance of Mg and Zr single and mixed oxides in pyrolysis vapours upgrading in a two-stage thermocatalytic reaction system.** The main objective of this section is to study the effect of Mg and Zr single and mixed oxides on the composition of upgraded bio-oil and other by-products:

- Evaluation of physicochemical properties of Mg and Zr single and mixed oxides synthesised by precipitation.
- Study of the effect of the acidity and basicity of Mg and Zr single and mixed oxides on the catalytic fast pyrolysis of wheat straw.

**III. Performance of K-incorporated zeolites in pyrolysis vapours upgrading in a two-stage thermocatalytic reaction system.** The main objectives of this section

## 2. Motivation and objectives

are to study the effect of K-incorporated zeolites on the composition of upgraded bio-oil and other by-products and to optimise the operating conditions:

- Evaluation of physicochemical properties of K-incorporated zeolites by ion-exchange and grafting.
- Study of the influence of the catalyst to biomass ratio in the ex-situ catalytic fast pyrolysis of wheat straw over K-exchanged and parent H-ZSM-5 zeolites.
- Study of the influence of the catalyst to biomass ratio and catalytic zone temperature in the ex-situ catalytic fast pyrolysis of wheat straw over K-grafted and parent USY zeolites.

**IV. Performance of tandem acid-base catalysts in pyrolysis vapours upgrading in a three-stage thermocatalytic reaction system.** Starting from H-ZSM-5 zeolite as selected acid catalyst (A), and bentonite and magnesium oxide as selected basic catalysts (B), the main objectives of this section are to study the effect of tandem acid-base catalysts on the composition of the upgraded bio-oil and other by-products and to optimise the operating conditions. The influence of the coupling configuration (A+B or B+A) in the ex-situ dual-catalyst catalytic fast pyrolysis of wheat straw over H-ZSM-5 zeolite and bentonite and magnesium oxide is also investigated.

### **3. Materials and methods**





#### 3.1. Catalysts preparation

##### 3.1.1. Stabilisation of clay materials

Bentonil A (standard sodium bentonite) and PFI-1 palygorskite (attapulgite) were provided by Clariant and Clay Minerals Society, respectively. Both clay materials were directly calcined in static air in a muffle furnace at 550 °C for 5 h (heating rate: 1.8 °C/min).

##### 3.1.2. Synthesis of Mg and Zr single and mixed oxides

The syntheses of Mg and Zr single and mixed oxides were based on the works of Faba et al. [72] and Sádaba et al. [88]. Concretely, magnesium nitrate hexahydrate (99 wt.%, Sigma Aldrich) and zirconyl nitrate hydrate (99 wt.%, Sigma Aldrich) were dissolved in 1 L of Milli-Q water (resistivity: 18.2 MΩ·cm) in variable concentrations depending on Mg/(Mg+Zr) nominal values (0.00, 0.75 and 1.00). The solution was stirred at 500 rpm and room temperature, and an aqueous NaOH solution (25 wt.%, Sigma Aldrich) was added until the pH value was between 9-10. When pH was adjusted, whitish gels began to form. The resulting gels were aged at room temperature for 72 h. Solids were recovered by centrifugation due to their small particle size and washed three times with Milli-Q water. Samples were dried in a stove at 120 °C for 24 h and then calcined under flowing air in a tubular muffle furnace at 600 °C for 3 h (heating rate: 5 °C/min; air flow: 100 mL/min).

##### 3.1.3. Potassium incorporation to zeolitic materials

###### 3.1.3.1 K-exchanged H-ZSM-5 zeolite

Nanocrystalline H-ZSM-5 zeolite (Si/Al = 39.5) was provided by Clariant (ref. HCZP-90). The preparation of ion-exchanged KH-ZSM-5 sample was based on the procedure described by Nicolaides et al. [89]. Typically, the commercial H-ZSM-5 was ion-exchanged three times with a fresh 0.4 M KCl (99.5 wt.%, Fluka) aqueous solution at 25 °C (10 mL·g<sub>zeolite</sub><sup>-1</sup>). The ion-exchange consisted of stirring at 500 rpm for at least 20 h. After each exchange, the sample was recovered by centrifugation due to its small particle size and washed once with Milli-Q water. Finally, the solid material was washed with Milli-Q water three times to remove unexchanged potassium and chloride

## 3.2. Catalyst characterisation

ions, dried overnight (>16 h) at 110 °C in a stove and calcined in static air in a muffle furnace at 550 °C for 5 h (heating rate: 1.8 °C/min).

### 3.1.3.2 K-grafted USY zeolite

The high-silica USY zeolite in protonic form was provided by Tosoh Corporation (ref. HSZ-390HUA). The preparation of the grafted K-USY sample was based on the procedure described by Keller et al. [33]. Typically, 2 g of the as-received commercial USY zeolite was introduced into a solution (60 cm<sup>3</sup>) of 0.1 M of potassium hydroxide (Scharlau, 85 wt.%) in methanol (Scharlau, 99.9 wt.%) at room temperature (30 ml·g<sub>zeolite</sub><sup>-1</sup>). The mixture was stirred at 500 rpm for 10 min, filtered under vacuum, washed with 100 ml of methanol, and dried in an oven at 60 °C for 6 h. Afterwards, the solid was crushed using an agate mortar and, subsequently, it was calcined in static air (550 °C, 5 h, heating rate of 1.8 °C/min) in a muffle furnace.

### 3.1.4. Pelletisation of catalysts

All catalysts were pelletised to a particle size of 180 – 250 µm in order to avoid internal diffusional limitations and excessive pressure drop during their use as catalysts in biomass pyrolysis reactions. A hydraulic press was used to fabricate tablets with variable heights and weights, depending on the density of the catalyst samples. The press die exhibits a diameter of 25 mm, and the force applied by the hydraulic press was 10,000 kgF, which was maintained for 1 – 2 min to obtain the catalyst tablets. The tablets were crushed with a porcelain mortar and then sieved to the desired particle size. Finally, catalysts were dried overnight at 110 °C in a stove before fast pyrolysis tests.

## 3.2. Catalyst characterisation

### 3.2.1. Thermogravimetric and chemical analyses of the catalyst samples

Thermogravimetric analyses (TG) of clay catalysts were performed on a Mettler Toledo TGA/DSC 1 instrument in order to study their stability in fast pyrolysis conditions. Representative amounts of raw bentonite and attapulgite (10 – 20 mg) were deposited in 70 µL alumina capsules and subjected to TG analysis in flowing nitrogen (heating rate: 10 °C/min up to 550 °C; N<sub>2</sub> flow: 100 mL/min). TG curves illustrate the evolution of the catalyst weight loss with temperature. Likewise, derivative

thermogravimetry (DTG) curves indicate the temperature ranges at which the different compounds are released.

Inductively Coupled Plasma – Optical Emission Spectrometry (ICP-OES) was used to determine the metal contents of the Mg-Zr mixed metal oxide, as well as the K/Al and Si/Al ratios of the K-incorporated zeolites.

- Mg-Zr mixed metal oxide: ICP-OES technique was used to determine Mg and Zr contents. The equipment used was a Perkin Elmer Optima 3300 DV. A representative amount of Mg-Zr mixed metal oxide ( $\approx 0.1$  g) was digested by treatment with an  $\text{HNO}_3/\text{HF}$  solution (3 mL : 1 mL per 0.025 g) in an Anton Paar Multiwave 3000 microwave oven and then diluted with Milli-Q water.
- K-incorporated zeolites: ICP-OES technique was used to determine Al and K contents. The equipment used was a Varian Vista AX spectrometer. Representative amounts of parent and K-incorporated H-ZSM-5 and USY zeolites ( $\approx 0.1$  g) were digested in an  $\text{HF}/\text{H}_2\text{SO}_4$  solution (5 mL : 1 mL per 0.05 g) and then diluted with Milli-Q water.

Quantification of elements was carried out from a previous calibration, using standards prepared with certified solutions for ICP analysis (Scharlau) with concentrations of 1,000 mg/L in water (K), 2 wt.% nitric acid (Mg and Al), and 5 wt.% nitric acid + 0.5 wt.% hydrofluoric acid (Zr). The metal contents of the catalyst samples is determined according to **Equation 1**:

$$\text{Metal content (wt. \%)} = \frac{\text{Conc. (mg/L)} \cdot \text{vol. solution (L)}}{\text{sample mass (mg)}} \cdot 100 \quad (1)$$

#### 3.2.2. Crystallinity, textural properties and morphology of the catalyst samples

X-ray diffraction (XRD) was employed to determine the crystallinity of all catalyst samples. The equipment used was a PHILIPS X'PERT diffractometer with  $\text{Cu K}\alpha$  radiation ( $\lambda = 1.5406 \text{ \AA}$ ), operated at 45 kV and 40 mA. The step size, scanning step time and  $2\theta$  angle range of the X-ray diffractograms were varied according to the catalyst samples studied (**Table 3.1**).

### 3.2. Catalyst characterisation

**Table 3.1.** X-ray diffraction parameters as a function of the type of catalyst studied.

Catalyst type	Step size (°)	Scanning step time (s)	2 $\theta$ angle range (°)
Clays	0.02	1	2 – 70
Metal oxides	0.02	1	10 – 80
Zeolites	0.04	2	5 – 50

For comparison purposes, X-ray diffractograms of the catalyst samples discussed in **Section 4.2.1** were obtained with a step size of 0.04°, a scanning step time of 2 s and a 2 $\theta$  angle range of 5 – 70°.

Gas physisorption was used to determine the textural properties of all catalyst samples. The analyses were carried out employing two different adsorbates depending on the type of porosity of the samples:

- N<sub>2</sub> physisorption at 77 K. The equipment used was a Micromeritics TriStar 3000 analyser. Representative amounts of the Mg-Zr single and double metal oxides and K-grafted and parent USY zeolites ( $\approx$  0.1 g) were first outgassed at 300 °C under vacuum for 5 h in a Micromeritics VacPrep 061 instrument.
- Ar physisorption at 87 K. The equipment employed was an AUTOSORB iQ analyser of Quantachrome Instruments. Representative amounts of the clay catalysts, K-exchanged and parent H-ZSM-5 zeolites ( $\approx$  0.1 g), were first outgassed at 300 °C under vacuum for 3 h.

Adsorption-desorption isotherms were obtained by measuring the amount of gas adsorbed/desorbed over a wide range of relative pressures at a constant temperature. The range of relative pressures selected for each test depended on the nature, expected surface area and porosity type of the catalyst samples, as well as the adsorbate used. The specific surface area of all the catalysts was determined by applying the Brunauer-Emmet-Teller (BET) equation in the range of  $P/P_0 = 0.05 - 0.20$ . The application of the t-plot method estimated the micro- and mesopore contributions to the overall surface area. The total pore volume was calculated from the amount of gas adsorbed at a relative pressure of 0.98. The pore size distribution was obtained by applying the Barret-Joyner-Halenda (BJH) model in the case of K-grafted and parent USY zeolites and the NL-DFT (Non-Local Density Functional Theory) equilibrium model, assuming cylindrical pore geometry, in the case of the K-exchanged and parent H-ZSM-5 zeolites.

Electron microscopy was employed to study the crystal sizes and morphologies at high resolution of the zeolite samples. Two different techniques were used, depending on whether it is desired to examine the external (SEM-EDX) or internal features (TEM) of the catalyst samples:

- Scanning Electron Microscopy – Energy-Dispersive X-ray spectroscopy (SEM-EDX): The equipment used was a JEOL JSM-7900 F microscope, operated at 1 kV. No pre-treatment of the catalyst samples was required. Micrographs were taken at magnification from x50,000 to x250,000 by SEM. The most representative elements of the surface of the K-USY sample were determined by EDX.
- Transmission electron microscopy (TEM): The equipment used was a JEOL JEM-2100 microscope, operated at 200 kV. Representative amounts of catalyst samples were dispersed in acetone and sonicated in an ultrasonic bath for 5 min prior to analysis. Micrographs were taken at magnifications from x25,000 to x500,000.

#### 3.2.3. Acid-base properties of the catalyst samples

Temperature-Programmed Desorption (TPD) of probe molecules was used to quantify the concentrations and strength of acidic and basic sites in all catalyst samples. The equipment employed was a Micromeritics Autochem 2910 (TPD/TPR) apparatus provided with a thermal conductivity detector (TCD).

- NH<sub>3</sub>-TPD: Ammonia was used as probe molecule to determine the acidity of the catalyst samples. Typically, a representative amount of catalyst ( $\approx 0.1$  g) was degassed under He flow at 550 °C for 2 h followed by saturation at 120 °C using a NH<sub>3</sub>-He mixture (10 vol.% of NH<sub>3</sub>). After that, the sample was purged for 30 min under He flow to remove the weakly physisorbed ammonia. NH<sub>3</sub>-TPD profiles were subsequently recorded increasing the temperature from 120 to 550 °C using a ramp rate of 10 °C/min with isothermal step during 30 min.
- CO<sub>2</sub>-TPD: Carbon dioxide was used as probe molecule to quantify the basicity of the catalyst samples. A similar procedure was used for the CO<sub>2</sub>-TPD analyses, but the saturation temperature was changed to 50 °C, and the flowing gas mixture was replaced with a CO<sub>2</sub>-He mixture (5 vol.% of CO<sub>2</sub>). The maximum desorption temperature was varied from 350 to 550 °C depending on the catalyst evaluated.

### 3.3. Pre-treatment of raw biomass

For the calibration of the TPD apparatus, 1 mL pulses of NH<sub>3</sub> and CO<sub>2</sub> at 50 and 120 °C, respectively, were introduced directly to the TCD detector to determine the response factors for the estimation of the concentration (conc.) of acidic and basic active sites in the catalyst samples. Overall acidities and basicities were expressed in mmol/g of respective probe molecules and calculated according to **Equation 2**:

$$\text{Conc. active sites (mmol/g)} = \frac{\text{response factor (mmol)} \cdot \text{TPD curve area}}{\text{sample mass (g)}} \quad (2)$$

Pyridine adsorption/desorption followed by Fourier transform infrared spectroscopy (FT-IR) was employed to determine the nature and strength of acidic sites of the K-grafted and parent USY zeolites. The equipment used was a Jasco FT/IR-4600 spectrometer provided with a triglycine sulphate detector (TGS). The sample was prepared as self-supporting wafers ( $\varnothing = 13$  mm, 8 – 15 mg/cm<sup>2</sup>), mounted into a 316SS cell provided with CaF<sub>2</sub> windows. Wafers were dried overnight at 110 °C and activated at 500 °C for 2 h under vacuum prior to the adsorption of the pyridine at 150 °C and a pressure of 4 mbar. All spectra were recorded with a resolution of 4 cm<sup>-1</sup> in the 4000 – 1000 cm<sup>-1</sup> region (background: 64 scans; samples: 32 scans). The strength of the acidic sites was studied by recording the FT-IR spectra after treating the sample at different desorption temperatures (150, 250, 350, and 450 °C). The quantification of the acidic sites was performed using the following bands (vibration mode of pyridine) and absorption coefficients: pyridinium PyH<sup>+</sup> band at 1545 cm<sup>-1</sup> ( $\epsilon = 1.67$  cm/mol) and pyridine PyL band at 1455 cm<sup>-1</sup> ( $\epsilon = 2.2$  cm/mol) [90].

### 3.3. Pre-treatment of raw biomass

Wheat straw (ws) obtained from agricultural residues (Segovia, Spain) was the lignocellulosic biomass feedstock chosen for the fast pyrolysis tests. Softwood lignocellulosic biomass, like wheat straw, presents a noticeable ash content (around 5 wt.% in the case of ws), composed mostly by silica and Alkali and Alkaline Earth Metals (AAEMs), that can act as indigenous catalysts during fast pyrolysis reducing bio-oil\* (water-free bio-oil) yield [91]. In order to remove these interferences, wheat straw is subjected to acid washing. Before that, raw biomass is ground with a cutter mill and sieved to the desired particle size of 0.5 – 1.0 mm to favour mass and heat transfer during fast pyrolysis.

Acid washing of wheat straw was described in the work of Hernando et al. [28]. A 1 wt.%  $\text{HNO}_3$  solution is prepared from a 70 wt.%  $\text{HNO}_3$  solution (Sigma-Aldrich) and diluted with Milli-Q water. The acid solution to biomass ratio was 20 mL per gram of wheat straw.  $\text{HNO}_3$  solution is introduced in an Erlenmeyer flask and heated up to 40 °C in a thermal bath. When the target temperature is reached, biomass is added to the solution to form a suspension, and it is vigorously stirred for 2 h. The resulting biomass is filtered under vacuum and repeatedly washed with Milli-Q water until the filtrate reaches a pH value of 5 – 6. Wet biomass is subjected to drying in a stove at 110 °C for 48 h and then stored in a sealed container at room temperature for its later use.

#### 3.4. Fast pyrolysis tests

The schematic diagram of the lab-scale experimental set-up used for the lignocellulosic biomass fast-pyrolysis tests is shown in **Figure 3.1**. This set-up consists of a down-flow stainless steel fixed-bed reactor (ID: 16 mm; length: 400 mm) with an ex-situ configuration. The reaction system operates at atmospheric pressure and is separated into two zones: a thermal non-catalytic section and a catalytic one, being heated with independent electric furnaces. The thermal zone operates at 550 °C, whereas the effect of the temperature of the catalytic zone was studied by varying it in the range 400 – 500 °C. The reaction temperatures are measured by two type-K thermocouples placed on the char and catalyst beds, respectively. In a typical experiment, a representative amount of lignocellulosic biomass (4 g) is introduced in the purged feeding tank located above the thermal zone of the reactor and kept at room temperature. The catalyst sample is placed inside the reactor over a bed consisting of quartz wool and metallic grids. In case of using two different catalysts, both materials are physically separated by another metallic grid. The system is purged by passing a nitrogen flow of 100 cm<sup>3</sup>/min. Two pierced stainless steel inner cylinders allow the char to be retained in the thermal part. The tests were carried out using catalyst to biomass (C/B) ratios in the range 0.2 – 0.8 g/g by varying the catalyst load. Once the target temperatures are reached, and the oxygen concentration levels in the reaction system are lower than 0.1 vol.%, the biomass is discharged as once, being subjected to thermal fast pyrolysis to produce a carbonaceous residue (char), gases and vapours. The char is accumulated in the thermal zone of the reactor, avoiding its contact with

### 3.4. Fast pyrolysis tests

the catalyst. The gases and vapours coming from biomass pyrolysis are swept by the nitrogen stream and passed through the catalytic zone.

Once the reaction is completed, char and the spent catalyst are recovered from pyrolytic and catalytic reaction zones, respectively, for further characterisation. The liquid bio-oil fraction is recovered employing a condensation system comprised of refrigerating flasks connected in series and cooled by an ice-water bath (0 – 4 °C). Two different condensation systems were used in the fast pyrolysis tests, depending on the procedure employed for the bio-oil recovery and the collection of non-condensable gases:

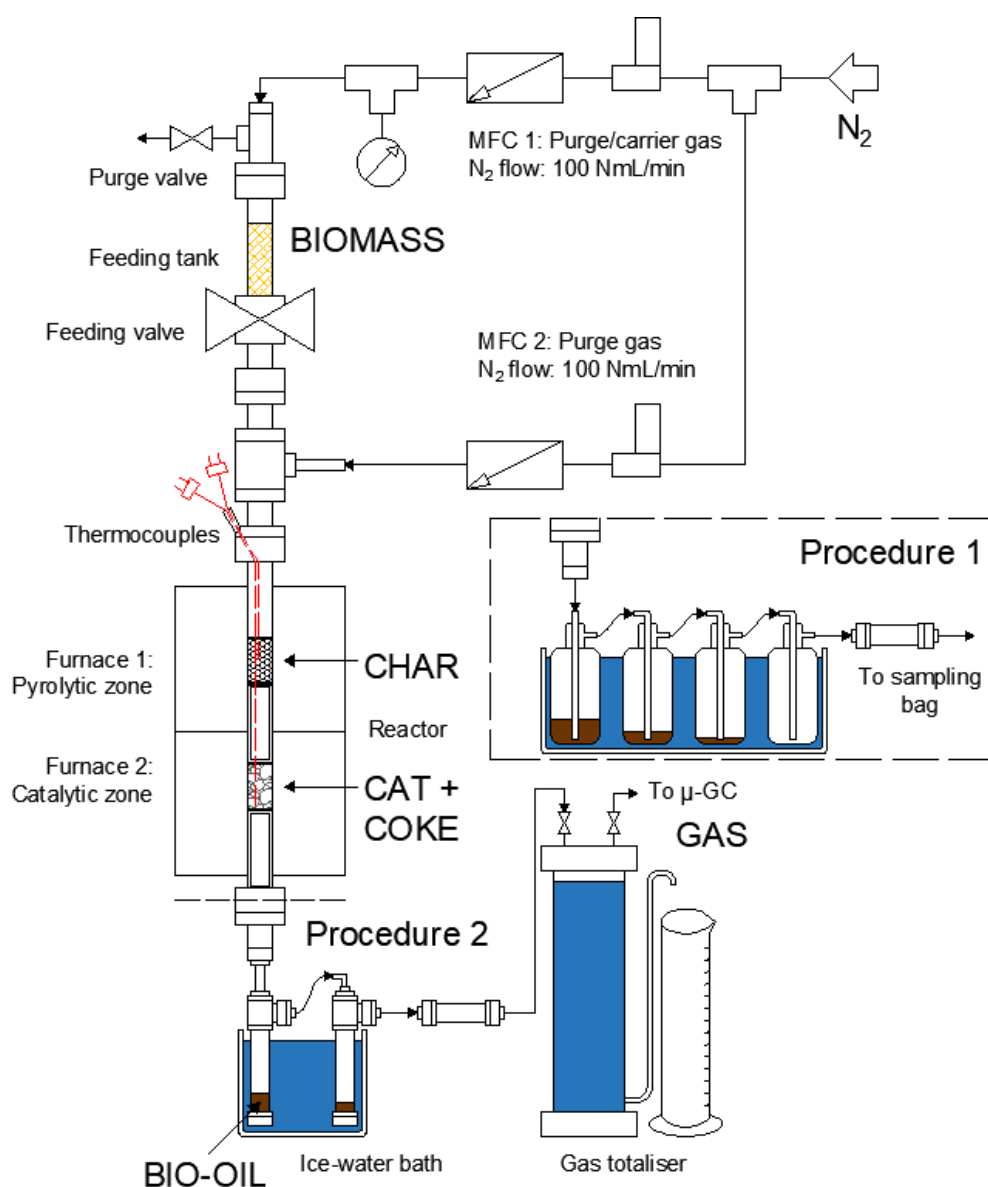


**Figure 3.1.** Schematic diagram of the experimental set-up used for the fast pyrolysis tests.



- **Procedure 1:** The condensation system is composed of four 125 cm<sup>3</sup> glass flasks. The bio-oil is recovered directly from the bottom of the flasks and stored in a separate closed vial. Traces of bio-oil from the condenser walls and the lower part of the reactor are recovered with acetone and kept in another air-open vial. When the acetone is evaporated, the contents of the two vials are mixed in a single closed vial. When two phases are formed, as in the case of the catalytic tests with a C/B ratio > 0.4, aqueous and organic phases are divided into different vials and analysed separately. Permanent gases are collected in a Tedlar sampling bag for their further analysis. A handcrafted stainless steel filter filled with magnesium perchlorate (ACS reagent, Sigma Aldrich) is placed before the sampling bag to remove moisture from the permanent gases and prevent malfunction of the gas analyser. This procedure was followed in the fast pyrolysis tests of acid-washed wheat straw over K-exchanged and parent H-ZSM-5 zeolites.
- **Procedure 2:** The condensation system is composed of two 50 cm<sup>3</sup> cylindrical stainless steel vessels. Bio-oil is recovered directly from the bottom of the flasks and stored in a closed vial. Traces of bio-oil from the condenser walls and the lower part of the reactor are recovered with acetone for subsequent weighing but are not mixed with the rest of the bio-oil. Aqueous and organic phases are separated when needed. Permanent gases are first collected in a totaliser, which measures the gas volume by water displacement and is subsequently connected to the gas chromatograph for further analysis. This procedure was followed in the fast pyrolysis tests of acid-washed wheat straw (and cellulose) over clay catalysts, Mg-Zr single and mixed metal oxides, K-grafted and parent USY zeolites, and staged CFP tests of ws-ac over acid-base catalysts.

## 3.5. Characterisation of raw materials and products

### 3.5.1. Solid fractions: raw biomass, char and coke

In order to obtain representative amounts of ash samples, 10 g of the different lignocellulosic feedstocks were calcined in static air in a muffle furnace at 900 °C (heating rate: 1.8 °C/min).

Inductively Coupled Plasma – Optical Emission Spectrometry (ICP-OES) was employed to determine the composition of the ash samples from calcination of raw (ws) and acid-washed (ws-ac) wheat straw. The equipment used was a Perkin Elmer

### 3.5. Characterisation of raw materials and products

Optima 3300 DV. Representative amounts of ash samples ( $\approx 0.1$  g) were digested by treatment with an  $\text{HNO}_3/\text{HF}$  solution (3 mL : 1 mL per 0.025 g) in an Anton Paar Multiwave 3000 microwave oven and then diluted with Milli-Q water.

Thermogravimetric analysis (TG) was employed to determine the ash and volatile matter contents of the different lignocellulosic feedstocks, as well as the coke deposited on the catalysts after the fast pyrolysis tests (proximate analyses):

- TG analyses of the different lignocellulosic feedstocks and pyrolytic chars were performed on a NETZSCH STA 449 instrument. Representative amounts of raw and acid-washed wheat straw, cellulose and pyrolytic chars (3 – 5 mg) were deposited in 70  $\mu\text{L}$  alumina crucibles and subjected to TG analysis in flowing air or nitrogen depending on whether it is desired to determine ash and volatile matter, respectively (heating rate: 10  $^\circ\text{C}/\text{min}$  up to 800  $^\circ\text{C}$ ; gas flow: 100 mL/min).
- TG analyses of the spent catalysts were performed on a Mettler Toledo TGA/DSC 1 instrument. Representative amounts of spent catalyst samples (5 – 35 mg) were deposited in 70  $\mu\text{L}$  alumina crucibles and subjected to TG analysis in flowing air to determine the coke deposited on the spent catalyst samples after fast pyrolysis tests (heating rate: 10  $^\circ\text{C}/\text{min}$  up to 850  $^\circ\text{C}$ ; air flow: 100 mL/min).

When the final temperature of the TG analysis was reached, the ash and volatile matter contents of biomass and char, and that of coke of the spent catalysts were calculated as total weight losses expressed in wt.% according to **Equation 3**:

$$\begin{aligned} & \text{Weight loss (wt. \%)} \\ &= \frac{(\text{sample mass})_{T_0} (g) - (\text{sample mass})_{T_t} (g)}{(\text{sample mass})_{T_0} (g)} \cdot 100 \end{aligned} \quad (3)$$

where  $T_0$  and  $T_t$  refer to the start and final temperatures of the TG analyses, respectively.

Elemental analysis (CHNS-O) was employed to determine the C, H, N, S and O (by difference) contents of the different lignocellulosic feedstocks, pyrolytic chars and coke deposited on the spent catalysts after the fast pyrolysis tests (ultimate analyses). The equipment used was a Thermo Fisher Scientific Flash 2000 micro-elemental analyser provided with a thermal conductivity detector (TCD). Representative

amounts of the solid samples (1 – 2 mg) were deposited in 157  $\mu\text{L}$  sealed tin capsules and were fully oxidised at 900  $^{\circ}\text{C}$  under an atmosphere of pure  $\text{O}_2$ . The resulting  $\text{CO}_2$ ,  $\text{H}_2\text{O}$ ,  $\text{N}_2$  and  $\text{SO}_2$  were carried by 140 mL/min of flowing helium and separated in a packed column CHNS/NCS (PTFE; 2 m; 6x5 mm). When desorbed, these gases were quantified separately by TCD. Sulphanilic acid (Thermo Scientific, 99 wt.%) and 2,5-bis(5-t-butylbenzoxazol-2-yl)thiophene (BBOT; Thermo Scientific, 99 wt.%) were applied as standards for the CHNS-O analysis. Sulphanilic acid was employed for the samples with a carbon content lower than 50 wt.% (i.e. coke and lignocellulosic feedstocks), whereas BBOT was used for the samples with a carbon content higher than 50 wt.% (i.e. char).

#### 3.5.1.1. Characterisation of lignocellulosic feedstocks

In this thesis work, acid-washed wheat straw (ws-ac) was the lignocellulosic biomass feedstock chosen for the fast pyrolysis tests. On the other hand, cellulose medium fibres (quality level: 200, Sigma Aldrich) were employed as raw material for the fast pyrolysis over bentonite.

Proximate analyses of the different lignocellulosic feedstocks were carried out according to European standards for the determination of ash (UNE-EN 14775:2010), volatile matter (UNE-EN 15148:2010) and fixed carbon (determined by difference), using **Equation 4**:

$$\text{Fixed Carbon (wt. \%)} = 100 - \text{Volatile Matter (dry basis)} - \text{Ash (dry basis)} \quad (4)$$

Ultimate analyses were carried out in a micro-elemental analyser to determine C, H, N, S and O (by difference), as explained in the previous section. In addition, the higher heating values (HHV) of the different lignocellulosic feedstocks were calculated according to the following empirical correlation (**Equation 5**) [92]:

$$\text{HHV} \left( \frac{\text{MJ}}{\text{kg}} \right) = 0.3491 \cdot C + 1.1783 \cdot H + 0.1005 \cdot S - 0.1034 \cdot O - 0.0151 \cdot N - 0.2110 \cdot A \quad (5)$$

where C, H, S, O, N and A stand for carbon, hydrogen, sulphur, oxygen, nitrogen and ash contents expressed in wt.% on dry basis.

### 3.5. Characterisation of raw materials and products

Proximate and ultimate analyses of raw wheat straw and biopolymers distribution and chemical composition of both raw and acid-washed wheat straw were extracted from the work of Hernando et al. [28].

#### 3.5.2. Liquid fractions: bio-oil\* (water-free bio-oil) and water

Karl-Fischer titrations (KF) were carried out in order to determine the water content of the bio-oil samples. The equipment used was a Metrohm Titrando 801 instrument. The procedure followed was described in the ASTM E203-08 method. Representative amounts of bio-oil samples (0.03 – 0.06 g) were dissolved in HYDRANAL™ Medium K (Honeywell Fluka™) under constant stirring. HYDRANAL™ Composite 5K (Honeywell Fluka™) was then added to the solution until the equivalence point was reached and detected by voltammetry. HYDRANAL™ Water Standard 10.0, containing 1.0 wt.% water, was used for the calibration of the Karl Fischer titrator. Prior to analysis, the titre was verified to have an average value of 4.5 – 5.5 mg water per mL reagent by measuring 1 mL aliquots of water standard three times. The water content of the bio-oil samples was expressed in mg/g and calculated according to **Equation 6**:

$$\text{Water content (mg/g)} = 0.5 \cdot \frac{\text{burette volume (mL)} \cdot \text{titre (mg/mL)}}{\text{sample size (g)}} \quad (6)$$

Elemental analysis (CHNS-O) was employed to determine the C, H, N, S and O (by difference) contents of the bio-oil samples. The equipment used was a Thermo Fisher Scientific Flash 2000 micro-elemental analyser provided with a thermal conductivity detector (TCD). Representative amounts of the liquid samples (1 – 2 mg) were adsorbed on Chromosorb® W/AW (Thermo Scientific) and sealed in 87 µL tin capsules. The same procedure followed for the solid samples was carried out for the liquid ones. Sulphanilic acid was applied as the standard for the CHNS-O analyses of the bio-oil samples.

Gas Chromatography – Mass Spectrometry (GC-MS) was employed to identify the major components present in the bio-oil samples. The equipment used was a gas chromatograph coupled to a triple quadrupole mass spectrometer, Bruker® SCION 436-GC (Electron Energy: 70 eV; Emission: 300 V), provided with WCOT fused silica column (30 m x 0.25 mm ID x 0.25 µm), operating helium as the carrier gas (flow rate:

1 cm<sup>3</sup>/min). Representative amounts of bio-oil samples (0.03 – 0.10 g) were diluted in ethanol (1:11 in mass) and then filtered through 0.22 µm nylon syringe filters to remove char, glass wool and/or spent catalyst traces. The products were identified through comparison with the NIST EI-MS spectral library (v2.0), applying a minimum match score of 700 as identification criteria. The bio-oil compounds were grouped into different families according to their main functional groups: carboxylic acids (AC), light oxygenates (LO: including aldehydes, ketones and ethers, among others), furans (FUR), anhydrosugars (SUG), oxygenated aromatics (O-AR) and aromatic hydrocarbons (AR). A total of 20 compounds, typically present in either thermal and catalytic bio-oils as major components, were calibrated (including AC: acetic acid, propanoic acid; LO: hydroxyacetone, diethoxypropane, cyclopentenone; FUR: furfural; O-AR: phenol, guaiacol, cresol, creosol, syringol, trimethoxytoluene, eugenol, methoxycathecol, vanillin; AR: toluene, xylene, styrene, trimethylbenzene, naphthalene, and SUG: levoglucosan). As the response factors were found to vary within 15 % for each family, an average response factor was assigned to the rest of the components detected in the different families to estimate their concentration. The concentration of any individual compound detected by GC-MS expressed in wt.% is computed according to **Equation 7**:

$$Concentration\ (wt.\ \%) = \frac{response\ factor\ (g/g) \cdot peak\ area}{\frac{1}{11} \cdot \frac{(100 - water\ content\ (wt.\ \%))}{100}} \cdot 100 \quad (7)$$

#### 3.5.3. Gas fractions: permanent gases

Gas Chromatography was employed to identify the molecular composition of the permanent gases. The equipment used was an Agilent CP-4900 Micro Gas Chromatograph (µ-GC), provided with a molecular sieve (Molsieve 5 Å) and PPQ columns and a thermal conductivity detector (TCD), operating argon and helium as carrier gases, respectively. The equipment was periodically calibrated with standard gas mixtures of different gas concentrations containing N<sub>2</sub>, O<sub>2</sub>, H<sub>2</sub>, CO, CO<sub>2</sub>, CH<sub>4</sub>, C<sub>2</sub>H<sub>4</sub>, C<sub>2</sub>H<sub>6</sub>, C<sub>3</sub>H<sub>6</sub>, C<sub>3</sub>H<sub>8</sub>, C<sub>4</sub>H<sub>8</sub> and C<sub>4</sub>H<sub>10</sub>.

### 3.5. Characterisation of raw materials and products

#### 3.5.4. Mass and energy balances and catalytic deoxygenation selectivities

Global mass balances were closed to the amount of the biomass fed in the reaction system with an experimental error lower than 5 wt.% in all trials. According to the procedure followed for bio-oil recovery and gas collection, the weights of the different product fractions are calculated differently.

- Procedure 1: Bio-oil and char fractions are weighted directly; coke fraction data is obtained by TG analysis of the spent catalyst under air flow; and the gas fraction is calculated by difference.
- Procedure 2: Char fraction is weighted directly; coke fraction data is obtained by TG analysis of the spent catalyst under air flow; gas fraction is quantified from the volume stored in the totaliser; and bio-oil fraction is calculated by difference.

Mass yields of the different product fractions were determined according to **Equation 8**:

$$Mass\ yield_i\ (wt.\ \%) = \frac{mass_i\ (g)}{biomass\ (g)} \cdot 100 \quad (8)$$

where  $i$  = char, coke, bio-oil\* (water-free bio-oil), water, or gas.

Concretely, mass yields of the different components of the gas fraction were computed according to **Equation 9**:

$$Mass\ yield_j\ (wt.\ \%) = \frac{mass_j\ (g)}{biomass\ (g)} \cdot 100 \quad (9)$$

where  $j$  = H<sub>2</sub>, CH<sub>4</sub>, (C<sub>2</sub>-C<sub>4</sub>)<sub>paraffins</sub>, (C<sub>2</sub>-C<sub>4</sub>)<sub>olefins</sub>, CO and CO<sub>2</sub>.

Elemental (C, H and O) mass balances were also closed to the ultimate analysis of the biomass fed in the reaction system with an experimental error lower than 10 wt.% in all trials. Nitrogen mass balance was normalised to the N content of the biomass fed due to the experimental error associated with the CHNS-O analysis of bio-oil.

The oxygen distribution in the different product fractions was computed according to **Equation 10**:

$$O_i \text{ (wt. \%)} = \frac{O_i \text{ (g)}}{O_{biomass} \text{ (g)}} \cdot 100 \quad (10)$$

where  $i$  = char, bio-oil\* (water-free bio-oil), water, coke and gas.

The overall deoxygenation selectivities corresponding to the three main deoxygenation pathways (decarbonylation, decarboxylation and dehydration) were calculated from the oxygen contained in the produced CO, CO<sub>2</sub> and H<sub>2</sub>O, respectively, by means of **Equation 11**:

$$S_k \text{ (\%)} = \frac{O_k \text{ (g)}}{O_{biomass} \text{ (g)}} \cdot 100 \quad (11)$$

where  $k$  represents the respective deoxygenation route.

The deoxygenation selectivity corresponding to the catalytic step in each test was determined with a similar equation, but subtracting to the overall production of CO, CO<sub>2</sub> and H<sub>2</sub>O the amounts obtained in a pure thermal test performed in the same conditions as the catalytic ones but with no catalyst in the reaction system.

The energy yield of any  $i$  fraction was determined according to **Equation 12**:

$$\text{Energy yield}_i \text{ (\%)} = \frac{\text{mass yield}_i \text{ (wt. \%)} \cdot \text{HHV}_i \text{ (MJ/kg)}}{\text{HHV}_{biomass} \text{ (MJ/kg)}} \cdot 100 \quad (12)$$

The quality of bio-oil is evaluated representing atomic O/C ratios vs. atomic H/C and effective H/C ratios (H/C<sub>eff</sub>) in Van Krevelen diagrams. The latter accounts only for the hydrogen that could be finally available if all the oxygen present in the bio-oil is removed in the form of water as it has been defined in the work of Chen et al. [93] as **Equation 13**:

$$H/C_{eff} = (H - 2O - 3N - 2S)/C \quad (13)$$

where H, O, N, S and C represent the mole percentages of hydrogen, oxygen, nitrogen, sulphur and carbon in bio-oil, respectively.





## **4. Results and discussion**



### 4.1. Catalytic fast pyrolysis of wheat straw and cellulose over clay catalysts

Clay minerals have many applications, including catalysis, due to their low cost and availability. Bentonite is a phyllosilicate that belongs to the montmorillonite subfamily and therefore has a layered structure. In contrast, attapulgite has a fibrous structure as it is a chain phyllosilicate. Both clay catalysts tend to have relatively low surface areas and acid-base properties without further modification.

In this section, bentonite and attapulgite clays have been used in the catalytic fast pyrolysis of wheat straw with the aim of obtaining high-added value bio-based chemicals. Wheat straw has been previously washed with a 1 wt.% aqueous solution of  $\text{HNO}_3$  in order to remove interferences and maximise bio-oil yields. In addition to catalyst type, variation of catalyst to biomass ratio has been also studied. These clay catalysts were previously stabilised by calcination in air. In the case of bentonite, it has also been employed in the catalytic pyrolysis of cellulose to better understand the reaction mechanism of this biopolymer, since cellulose is one of the predominant components in lignocellulosic biomass.

#### 4.1.1. Characterisation of lignocellulosic feedstocks

Acid-washed wheat straw (ws-ac) was the lignocellulosic biomass feedstock chosen for the fast pyrolysis tests. Cellulose was employed as feedstock for the fast pyrolysis over bentonite. Their characterisation results, as well as those of raw wheat straw, were listed in Table 4.1.1.

When comparing wheat straw before and after de-ashing, it is observed that their proximal analyses differ in their contents of volatile matter and fixed carbon. Acid washing has a negative effect on the lignin content in the treated biomass, since the holocellulose/lignin ratio increases from 1.9 to 2.6 after ash removal. Fixed carbon is reduced until half of its value after acid pretreatment, suggesting that lignin contributes to a greater extent to char formation. This fact is consistent with the low content of fixed carbon in cellulose. In contrast, cellulose presents the highest volatile matter content, in line with that of acid-washed wheat straw, which shows a higher concentration of cellulose than raw biomass.

#### 4.1. Catalytic fast pyrolysis of wheat straw and cellulose over clay catalysts

**Table 4.1.1.** Proximate, ultimate and biopolymers analyses of the raw (ws), acid-washed (ws-ac) wheat straw and cellulose samples [28].

Sample	Proximate analysis (wt.%)			Ultimate analysis (wt.%)				HHV (MJ/kg)	Biopolymers distribution (wt.%)		
	VM <sup>a</sup>	Ash <sup>a</sup>	FC <sup>a,b</sup>	C	H	N	O <sup>b</sup>		Cell	Hemicell	Lign
ws	75.3	4.7	20.0	45.6	5.6	0.5	43.7	17.9	37.8	27.5	34.7
ws-ac	88.2	1.3	10.5	47.8	5.9	0.2	44.8	19.0	42.3	29.9	27.8
cell	94.8	0.8	4.4	43.9	6.3	–	49.1	17.6	100.0	–	–

Sample	Ash elements (wt.%·10 <sup>2</sup> )													
	Al	Ba	Ca	Fe	K	Mg	Mn	Na	P	Si	Sn	Sr	Ti	Zn
ws	1.01	0.34	17.28	0.55	28.03	5.02	0.27	4.42	4.69	89.06	0.56	0.25	0.06	0.06
ws-ac	0.62	0.05	0.19	0.30	0.59	0.08	0.01	0.12	0.55	87.20	0.29	0.01	0.04	0.01

VM: volatile matter; FC: fixed carbon; Cell: cellulose; Hemicell: hemicellulose; Lign: lignin

<sup>a</sup>Dry basis; <sup>b</sup>Determined by difference

In addition, one of the advantages of ash removal (with an effectiveness of 72 wt.%) is the increase of the higher heating value of treated biomass. Not only did the ash content decrease, but also the carbon and hydrogen contents increased compared to raw wheat straw. Coming back to **Equation 5**, these increments have a more positive impact on HHV than the detriment due to the higher oxygen content.

Alkali and Alkaline Earth Metals (AAEMs) can act as indigenous catalysts during fast pyrolysis. Acid-washing had an effectiveness of 96 – 99 % in removing Ca, K, Mg, Na and Sr (except Ba, which is only 85 % effective), which would favour the production of bio-oil from biomass. Phosphorus is other element that is found in notable concentration (around 0.05 wt.%) in the raw biomass. In this case, de-ashing had an effectiveness of 88 %. Finally, elements with negligible catalytic activity, such as Si, were scarcely removed (2 %).

#### 4.1.2. Characterisation of the catalysts

Raw bentonite (BNT) and attapulgite (ATP) were previously calcined at 550 °C for their stabilisation. Thermo-gravimetric analysis in air was performed in order to study their stability in CFP conditions. Maximum temperature of 550 °C was chosen because thermal step is heated up until this value, despite the fact that catalyst bed is only heated

up until 450 °C. Thermogravimetry (TG) and derivative thermogravimetry (DTG) curves are shown in **Figure 4.1.1**.

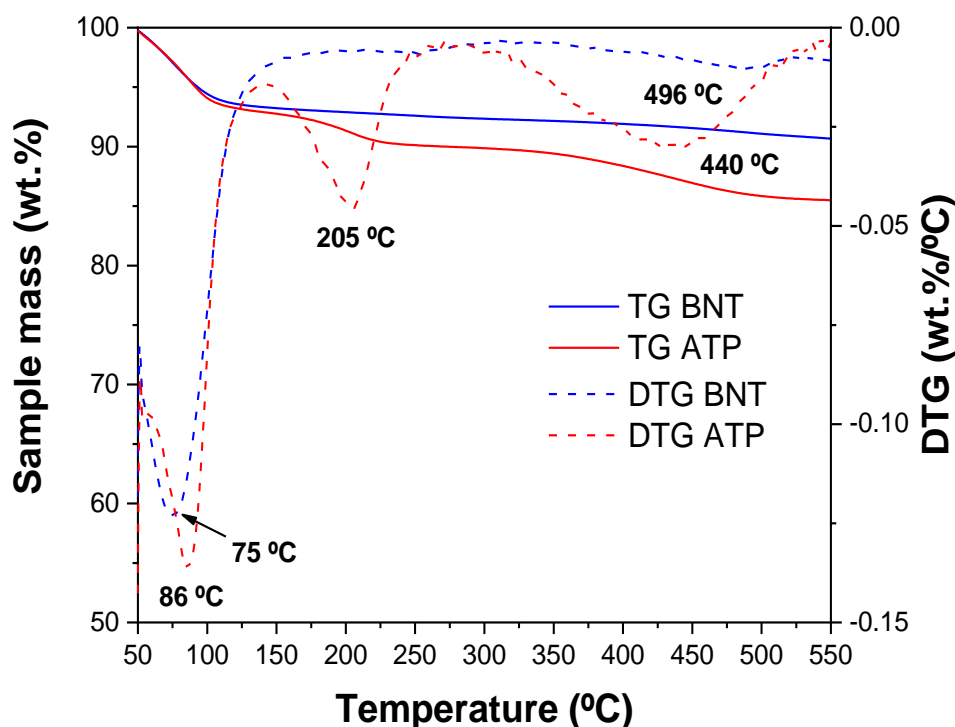


**Figure 4.1.1.** TG/DTG curves in nitrogen of parent bentonite and attapulgite.

It is observed that the total weight loss of bentonite is lower than that of attapulgite (9.3 vs. 14.5 wt.%). When comparing DTG curves, it is noticed that BNT shows a more intense peak in the range of 50 – 125 °C, which is mainly attributed to the desorption of adsorbed and exchangeable-cation coordinated H<sub>2</sub>O (recorded weight loss of 6.5 wt.%), and a less intense and broader peak in the range of 400 – 550 °C, which is associated to the dehydroxylation of amorphous smectites [94,95]. However, ATP shows three distinct peaks: i) the first one at 86 °C coincides with the desorption of superficial H<sub>2</sub>O and less strongly bonded zeolitic H<sub>2</sub>O, but its maximum is slightly displaced compared to that of BNT; ii) the second one is in the range of 150 – 250 °C and corresponds to the desorption of residual zeolitic H<sub>2</sub>O and a first dehydroxylation step of structural H<sub>2</sub>O; and iii) the third one is broader in the range of 325 – 550 °C and is attributed to the dehydroxylation of residual structural H<sub>2</sub>O [96]. Moreover, it should be noted that stabilisation of both clay materials is reached at approximately 550 °C, as both TG and DTG curves begin to flatten at that temperature value, indicating no further weight loss for either material.

#### 4.1. Catalytic fast pyrolysis of wheat straw and cellulose over clay catalysts

XRD patterns of the clay catalysts are given in **Figure 4.1.2.a**. The reflections of sodium bentonite (Na-Al-Si-OH), quartz ( $\text{SiO}_2$ ) and attapulgite (Mg-Al-Si-OH) are indicated in the diffractograms matching with the those found in literature [97,98]. Quartz, which is a frequent impurity in clay minerals, has a common peak with high intensity at  $26.5^\circ$ , in addition to the rest of the quartz peaks found in both diffractograms [99].

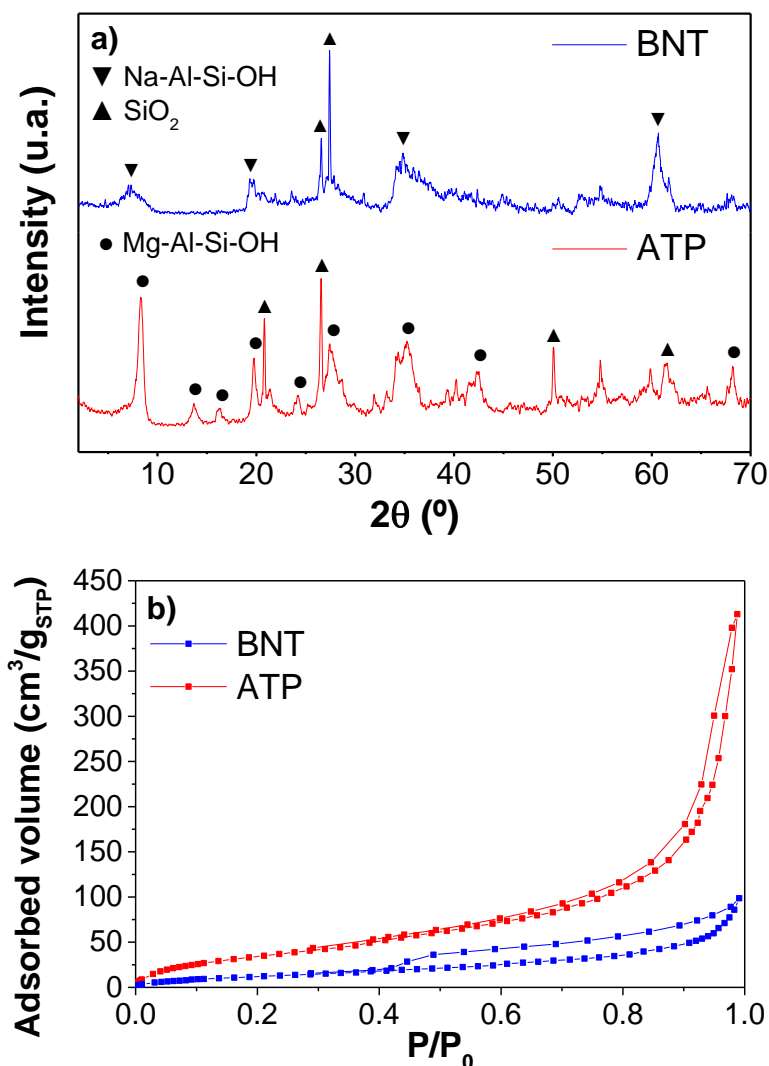


**Figure 4.1.2.** a) XRD patterns; b)  $\text{N}_2$  adsorption-desorption isotherms at 77 K; of the clay catalysts.

Textural properties of the catalysts were studied by  $\text{N}_2$  adsorption-desorption isotherms at 77 K. Both samples exhibit type IV isotherms and H3 hysteresis loops according to IUPAC classification (**Figure 4.1.2.b**), which are typical of particles with slit-like mesopores [100,101]. Both clays have low BET surface areas, which coincide

with their external surface areas due to the absence of micropores. Attapulgite particles are needle-shaped, whereas bentonite particles have a lamellar structure [99]. When comparing the textural properties of both catalysts, attapulgite presents a higher BET surface area and total pore volume than bentonite (**Table 4.1.2**). Bentonite shows typical values of BET surface area ( $9 - 70 \text{ m}^2/\text{g}$ ) of Na-montmorillonites, but presents slightly higher values of total pore volume ( $0.04 - 0.11 \text{ cm}^3/\text{g}$ ), whereas attapulgite exhibits slightly lower values of BET surface area and higher values of total pore volume than those found in literature ( $125 - 140 \text{ m}^2/\text{g}$  and  $0.32 - 0.37 \text{ cm}^3/\text{g}$ , respectively) [102].

**Table 4.1.2.** Physicochemical properties of the clay catalysts.

Catalyst	<sup>a</sup> S <sub>BET</sub> (m <sup>2</sup> /g)	<sup>b</sup> V <sub>T</sub> (cm <sup>3</sup> /g)	Acidity (mmol <sub>NH3</sub> /g)	Basicity (mmol <sub>CO2</sub> /g)
BNT	43	0.126	0.080	0.592
ATP	117	0.526	0.200	0.689

<sup>a</sup>BET surface area; <sup>b</sup>Total pore volume ( $P/P_0 \approx 0.98$ )

Acid-base properties of the clay catalysts are studied by NH<sub>3</sub>- and CO<sub>2</sub>-TPD, respectively. On the one hand, attapulgite shows a higher overall acidity than bentonite (**Table 4.1.2**). Ammonia-TPD of attapulgite shows a broader and more intense signal than bentonite with a maximum peak at 191 °C, whereas that of bentonite is centred at 180 °C (**Figure 4.1.3.a**). On the other hand, basicity was probed by CO<sub>2</sub>-TPD. Bentonite exhibits high weak-mild basicity through an intense and asymmetrical peak centred at 96 °C (**Figure 4.1.3.b**). Attapulgite shows an intense peak with similar shape, but centred at 89 °C and with slightly higher overall basicity (0.689 vs. 0.596 mmol<sub>CO2</sub>/g) (**Table 4.1.2**).

L. Novikova et al. studied the effect of acid-base properties of natural clays in the catalytic conversion of methylbutynol. Their study concluded that attapulgite showed higher yields of methylbutyne (55.8 vs. 33.9 mol%) and acetone (18.0 vs. 15.2 mol%) than bentonite. These reactions are catalysed by acidic and basic active sites, respectively; which is in line with the characterisation data [103].

## 4.1. Catalytic fast pyrolysis of wheat straw and cellulose over clay catalysts

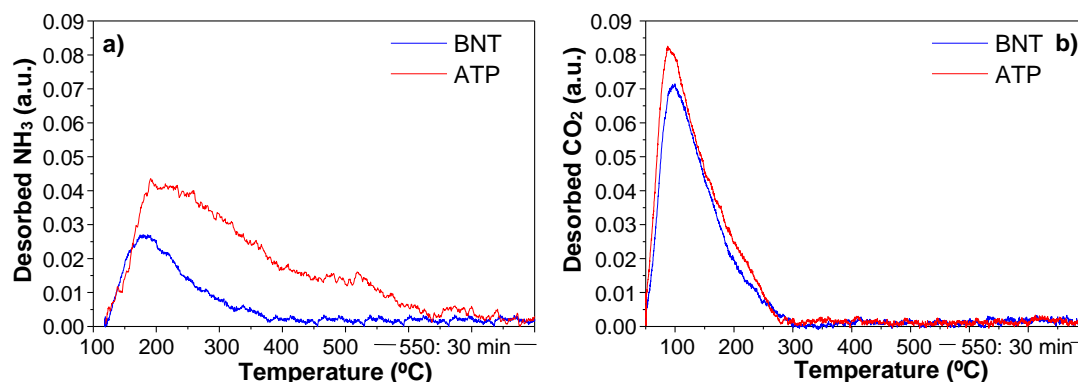


**Figure 4.1.3.** Acid-base properties of the clay catalysts: a) NH<sub>3</sub>-TPD; b) CO<sub>2</sub>-TPD.

### 4.1.3. Catalytic pyrolysis tests

Clay catalysts were evaluated in catalytic fast pyrolysis (CFP) of acid-washed wheat straw (ws-ac) and cellulose (cell). Catalyst to biomass (C/B) ratio was varied from 0.2 to 0.6 g/g in the catalytic pyrolysis tests. Reference non-catalytic (N-C) experiments with both acid-washed wheat straw and cellulose are also included in the study (**Tables A.1 – A.8** in the Appendix). Temperatures of thermal and catalytic zones were set at 550 and 450 °C in all trials, respectively.

#### 4.1.3.1 Wheat straw pyrolysis over clay catalysts

The following products were obtained from CFP of ws-ac over bentonite and attapulgite: i) Char and coke, which are solid; ii) bio-oil\* (water-free bio-oil) and water, which are liquid; and iii) permanent gases. **Figure 4.1.4.a** shows fraction yields when both clay catalysts are employed in CFP of ws-ac. The char mass yield has been omitted because an average value of 17.8 wt.% was calculated for all experiments. The activity tests were performed without catalyst (designed as N-C) and with C/B ratios of 0.2 and 0.6 g/g.

The non-catalytic test exhibited the highest bio-oil\* yield, and it was reduced as a higher amount of catalyst was used, since the presence of catalysts in CFP favours its conversion into other fractions. Bentonite showed higher bio-oil\* yields compared to attapulgite at the same C/B ratios. Improved textural and acid-base properties of attapulgite lead to the transformation of pyrolytic vapours into other fractions. Otherwise, the experiment without catalyst presented the lowest values of water and permanent gases and no coke was formed because of the lack of catalyst, which is the main responsible for deoxygenation reactions. Mass yields of water, permanent gases,



and coke increased with the catalyst to biomass ratio, especially in the case of using attapulgite as catalyst. These results can be attributed to attapulgite being more active in cracking and deoxygenation reactions, which are promoted by both acidic [104] and basic sites [105,106], which are more abundant than in bentonite, as was observed in TPD results. This fact also explains the lowest oxygen concentrations of bio-oil\* obtained when using attapulgite at the same catalyst to biomass ratios (**Figure 4.1.4.b**).

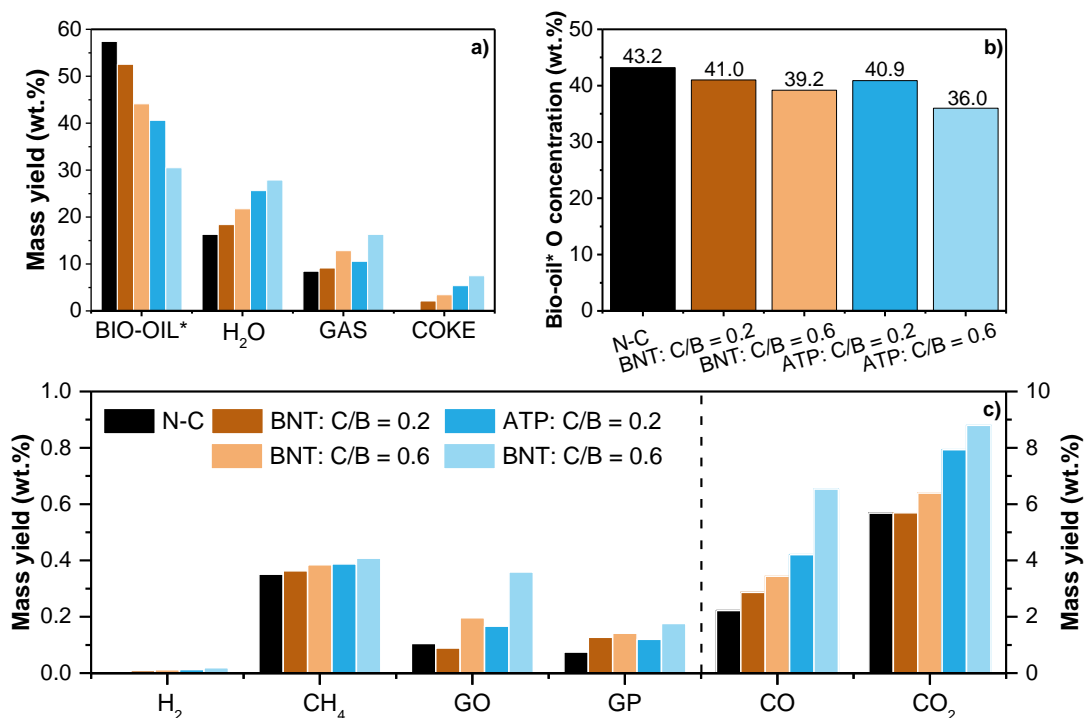


**Figure 4.1.4.** Fast pyrolysis of ws-ac over BNT and ATP at different C/B ratios, including reference thermal test: a) fraction yields; b) bio-oil\* oxygen concentration; c) gaseous components yields (GO: gaseous olefins, GP: gaseous paraffins).

Considering that oxygen is mainly removed from bio-oil\* in the form of water (dehydration), CO (decarbonylation) and CO<sub>2</sub> (decarboxylation) [107], mass yields of CO<sub>x</sub>, as well as hydrogen and C<sub>1</sub>-C<sub>4</sub> hydrocarbons yields, are depicted in **Figure 4.1.4.c**. It can be observed that the production of permanent gases when using a low C/B ratio of bentonite (0.2) is close to that of the non-catalytic experiment due to the low acidity of the catalyst, which is responsible for the cracking reactions. In contrast, CO and CO<sub>2</sub> yields, which are the main components in the permanent gases, start to differ with the non-catalytic experiment at a catalyst to biomass ratio of 0.6. On the other hand, a greater difference is observed when using attapulgite as catalyst. Concretely, CO and CO<sub>2</sub> yields are significantly enhanced at both catalysts to biomass

#### 4.1. Catalytic fast pyrolysis of wheat straw and cellulose over clay catalysts

ratios. The synergetic effect of acidity and basicity favours their production, especially that of CO<sub>2</sub>, since several reactions promoted by basic sites give rise to CO<sub>2</sub> [105,106]. Additionally, mass yields of C<sub>2</sub>-C<sub>4</sub> olefins are doubled compared to the experiments performed with bentonite since cracking reactions are promoted due to the higher concentration of acidic active sites in attapulgite [99].

The catalytic deoxygenation selectivities have been calculated from the incremental production of H<sub>2</sub>O and CO and CO<sub>2</sub> with respect to the thermal test, being represented in **Figure 4.1.5**. In the case of bentonite, oxygen is mainly removed from bio-oil\* via dehydration and with a low contribution of decarbonylation and decarboxylation. The latter one is more significant only for the highest C/B ratio. Conversely, attapulgite shows a higher catalytic activity than bentonite due to its needle-like morphology, which provides it with higher surface area and accessibility to its both acidic and basic sites [103]. Deoxygenation is more efficient when attapulgite is employed as catalyst because oxygen elimination is balanced among all deoxygenation routes. Concretely, decarboxylation has a greater influence on deoxygenation, which can be attributed to two atoms of oxygen being removed in the same molecule. Due to this fact, lower values of bio-oil\* oxygen concentrations have been observed in the fast pyrolysis tests using attapulgite as catalyst (**Figure 4.1.4.b**).

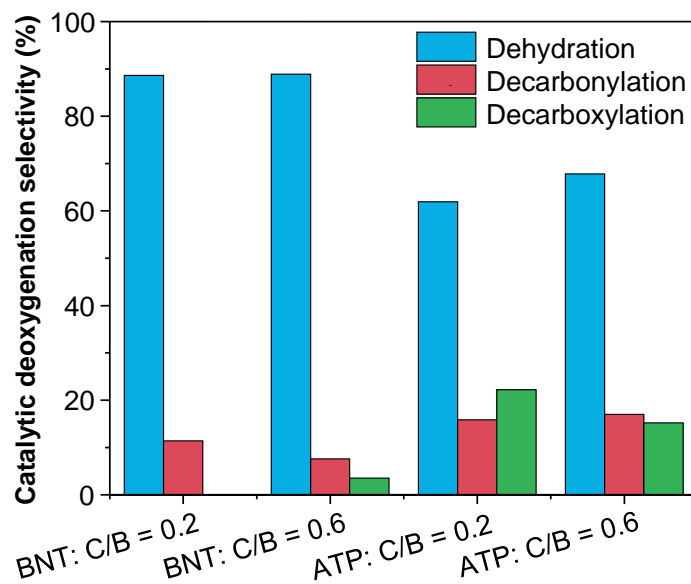


**Figure 4.1.5.** Catalytic deoxygenation selectivity obtained in the fast pyrolysis of ws-ac over BNT and ATP at different C/B ratios.

Compositions and HHVs of char and coke are shown in **Table 4.1.3**. On the one hand, the mass yield and elemental composition of char is calculated as average in the non-catalytic and catalytic experiments. As will be discussed in more detail in the next section, char could be valorised as a solid biofuel, but it should have a lower atomic O/C ratio in order to be categorised as a coal. Char fraction shows a high HHV compared to raw biomass (29.4 vs. 19.0 MJ/kg), which is mainly attributed to its higher carbon and lower oxygen contents.

On the other hand, coke is another by-product of CFP and is formed by oligomerisation and polymerisation reactions reducing catalytic activity by blocking the pores and depositing on the external surfaces of the catalysts. Thus, coke formation is not beneficial because it implies the need to regenerate the catalyst in continuous CFP processes [6]. Coming back to **Table 4.1.3**, it can be observed that coke mass yields augmented with C/B ratio, especially in the case of attapulgite, since it shows the highest surface area and concentration of acid active sites, which are responsible of these oligomerisation and polymerisation reactions [104]. In addition, cokes from these tests with attapulgite retain more energy from ws-ac than those of bentonite, which is translated in cokes with more carbon and less oxygen content, as C/B ratio is increased.

**Table 4.1.3.** Compositions and HHVs of char and coke obtained in the fast pyrolysis of ws-ac over BNT and ATP at different C/B ratios, including reference thermal test.

Experiment	Fraction	Coke in catalyst (wt.%)	Mass yield (wt.%)	Elemental analysis (wt.%, dry basis)				HHV (MJ/kg)
				C	H	N	O	
N-C	Char	–	17.8	78.7	2.7	0.9	10.5	29.4
BNT-0.2	Coke	10.8	2.1	36.1	5.6	–	58.3	12.7
BNT-0.6		9.3	5.4	39.8	5.4	–	54.8	14.3
ATP-0.2		18.4	3.5	46.7	3.8	–	49.5	15.6
ATP-0.6		13.3	7.5	54.9	4.5	–	40.6	20.0

The interest in using bentonite for the production of high-added value bio-based chemicals from CFP of ws-ac instead of attapulgite has been verified by its GC-MS analyses. **Figures 4.1.6.a** and **4.1.6.b** show the mass yields and proportions of detected compounds concerning the total bio-oil\*. The bio-oil\* obtained in the non-catalytic experiment presented only 19 % of detected compounds out of 57 wt.% of total mass

#### 4.1. Catalytic fast pyrolysis of wheat straw and cellulose over clay catalysts

yield, being most of them not quantified due to their complex composition. Concretely, these compounds are formed by the partial decomposition of original biomass biopolymers. On the other hand, the use of clay catalysts in CFP of ws-ac promotes the transformation of these oligomeric species into simpler compounds. It is observed that bentonite can convert more than 45 % of total bio-oil\* into quantifiable compounds at a C/B ratio of 0.2, and increases to 48 % when C/B ratio is 0.6. To a lesser extent, only 38 % of total bio-oil\* is quantified for a C/B ratio of 0.2 of attapulgite, and a negligible increase was observed with catalyst loading. The higher basicity to acidity ratio of bentonite appears to play a more important role in transforming oligomers into detectable components than that of attapulgite (7.4 vs. 3.4 mol<sub>CO2</sub>/mol<sub>NH3</sub>).

The products distribution per families in bio-oil\* is depicted in **Figure 4.1.6.c**. Main compound families found in bio-oil\* are carboxylic acids (AC); light oxygenates (LO), including aldehydes, ethers, esters and ketones; furans (FUR); oxygated aromatics (O-AR); and anhydrosugars (SUG). The non-catalytic test shows a yield of 6 wt.% of anhydrosugars, whereas other compound families (AC, LO, FUR and O-AR) do not exceed 2 wt.%. However, cracking reactions are promoted, and sugars are decomposed by the use of a catalyst with acid properties in the process, such as attapulgite [4,104]. For this clay, the sugar content of bio-oil\* in the test with C/B ratio of 0.2 is less than half of the content of thermal bio-oil\* and is depleted when C/B ratio is 0.6, confirming the effect of attapulgite on sugar content. Consequently, the concentration of the rest of the families is enhanced, highlighting the production of carboxylic acids, among others. However, the production of anhydrosugars (mainly levoglucosan) stands out when bentonite is employed, especially at lower catalyst loadings (C/B ratio = 0.2), which is in line with the literature. Levoglucosan production in presence of bentonite is maximised at 20 wt.% of catalyst [36]. The improvement of the levoglucosan yield could justify the high bio-oil\* yield compared to the other catalytic tests. Levoglucosan is the primary intermediate of cellulose thermal pyrolysis and the passage of pyrovapours through bentonite bed prevents its decomposition into lighter compounds by secondary reactions [108]. Concretely, the SUG mass yield is almost doubled compared to the non-catalytic test (11.6 vs. 6.0 wt.%), whereas the yields of the other compound families are similar to those obtained with attapulgite and for both C/B ratios. There is a reduction in SUG yield when C/B ratio was

increased to 0.6 and the SUG concentration does not improve (22 wt.% of both bio-oils\* are composed by anhydrosugars), so it is advisable to work with lower catalyst loadings due to the higher bio-oil\* yield and the saving on raw materials.

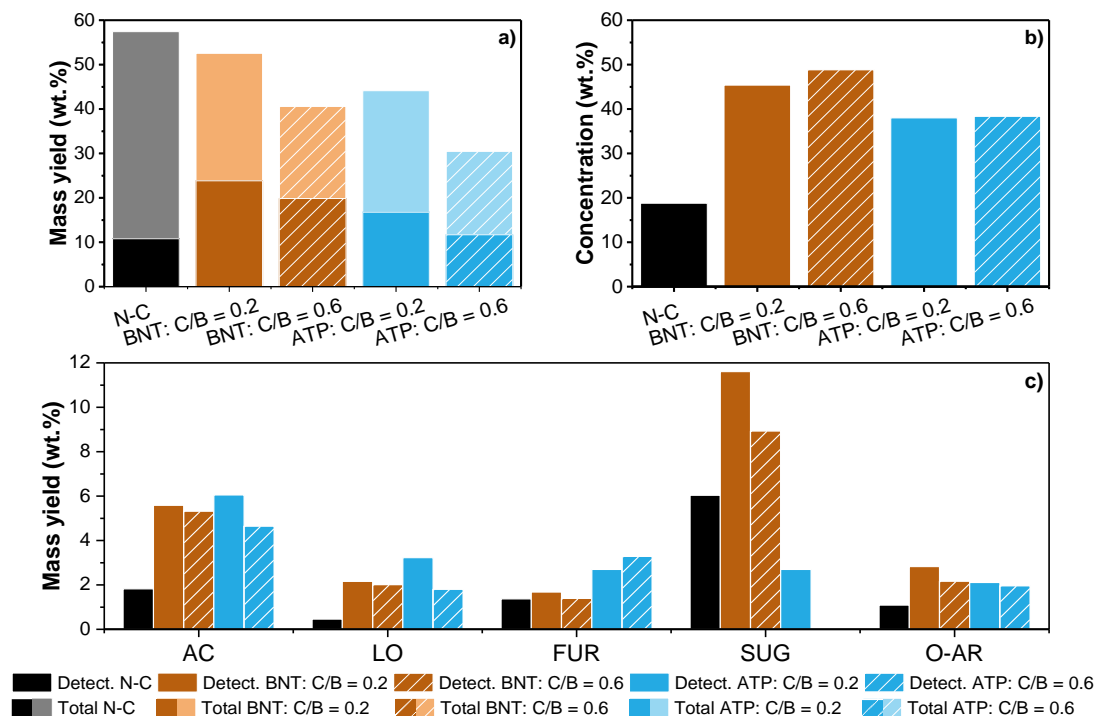


**Figure 4.1.6.** Quantitative GC-MS analyses of the bio-oil\* obtained in the fast pyrolysis of ws-ac over BNT and ATP at different C/B ratios, including reference thermal test: a) total and GC-MS detected mass yields; b) concentration of GC-MS detected components; and c) GC-MS detected mass yields of compound families (AC: carboxylic acids, LO: light oxygenates, FUR: furans, SUG: anhydrosugars and O-AR: oxygenated aromatics).

In addition to the production of anhydrosugars, carboxylic acids are present to a great extent in bio-oils\* from the experiments with both catalysts (BNT: 5.6 to 5.3 wt.%; ATP: 6.1 to 4.7 wt.%; when C/B ratio is increased from 0.2 to 0.6). Acetic acid is the most abundant compound in this family and could be separated as a bio-based chemical of commercial interest, but its presence in bio-oil can be deleterious as it affects bio-oil properties by increasing pH and corrosivity, making it very unstable. In the case of LO and O-AR for both catalysts, bio-oils\* have similar decreasing yields with increasing C/B ratios, but those of attapulgite have slightly higher and increasing FUR yields due to the degradation of anhydrosugars in more stable molecules, such as furfural [3]. Anhydrosugars are dehydrated into furans, which is favoured by acidic sites [8] and attapulgite presents more acidity than bentonite (**Table 4.1.2**).

#### 4.1. Catalytic fast pyrolysis of wheat streaw and cellulose over clay catalysts

In summary, the use of bentonite as catalyst in the process seems to be more appropriate due to its higher bio-oil\* yields and its lower formation of undesired by-products, which facilitates CFP operability; and despite having higher bio-oil\* oxygen concentrations. Anhydrosugars are the most abundant compounds in the bio-oil\* produced by CFP of ws-ac using bentonite as catalyst. This fact can be attributed to the synergistic effect of its textural properties and high weak-mild basicity, which seem to improve SUG mass yield. In order to clarify these results, in the next section, pure cellulose is used as pyrolysis feedstock and bentonite as catalyst. Thus, the catalyst features and reaction mechanisms will be studied in more detail since anhydrosugars are also the main products of cellulose pyrolysis [3].

##### 4.1.3.2 Cellulose pyrolysis over bentonite

Cellulose is one of the major components of lignocellulose, being in the case of wheat straw, approximately one-third of the overall biomass (**Table 4.1.1**) [28]. For this reason, in the CFP experiments carried out employing this feedstock, the C/B ratio is maintained considering this relationship between cellulose and wheat straw. In other words, for a C/B ratio of 0.2, the amount of cellulose introduced in the feeding system was 4 g, and the catalyst bed was 2.4 g instead of 0.8 g, as in the case of acid-washed wheat straw. The same proportion was kept for the C/B ratio of 0.6. The catalyst employed in the pyrolysis tests was bentonite, and a non-catalytic test with cellulose was also included as reference in the study. As in the previous case, char obtained from thermal pyrolysis of cellulose has an average value of 15.9 wt.% and is common to all experiments performed with the same feedstock.

Mass yields of the different fractions obtained from ws-ac and cellulose CFP are compared in **Figure 4.1.7.a**. The difference between char yields of both feedstocks does not have a great negative influence on the rest of the fraction yields since these values are very close to each other (17.8 vs. 15.9 wt.% for ws-ac and cellulose, respectively). Char from CFP of ws-ac has a higher yield due to the presence of lignin in the original biomass, which is not easy to degrade fully. As was observed in CFP of ws-ac over bentonite, bio-oil\* yield decreases with increasing C/B ratio in cellulose pyrolysis, since bio-oil\* is converted into the other fractions. However, cellulose pyrolysis produces lower yields of bio-oil\*, even when no catalyst was used. Consecutively, the rest of fraction yields is augmented with C/B ratio. On the one hand,

water yield reaches a constant value of approximately 32 wt.% at a C/B ratio of 0.2. In any case, water yields of cellulose CFP are higher at any C/B ratio than that of the non-catalytic test due to the promotion of dehydration reactions.

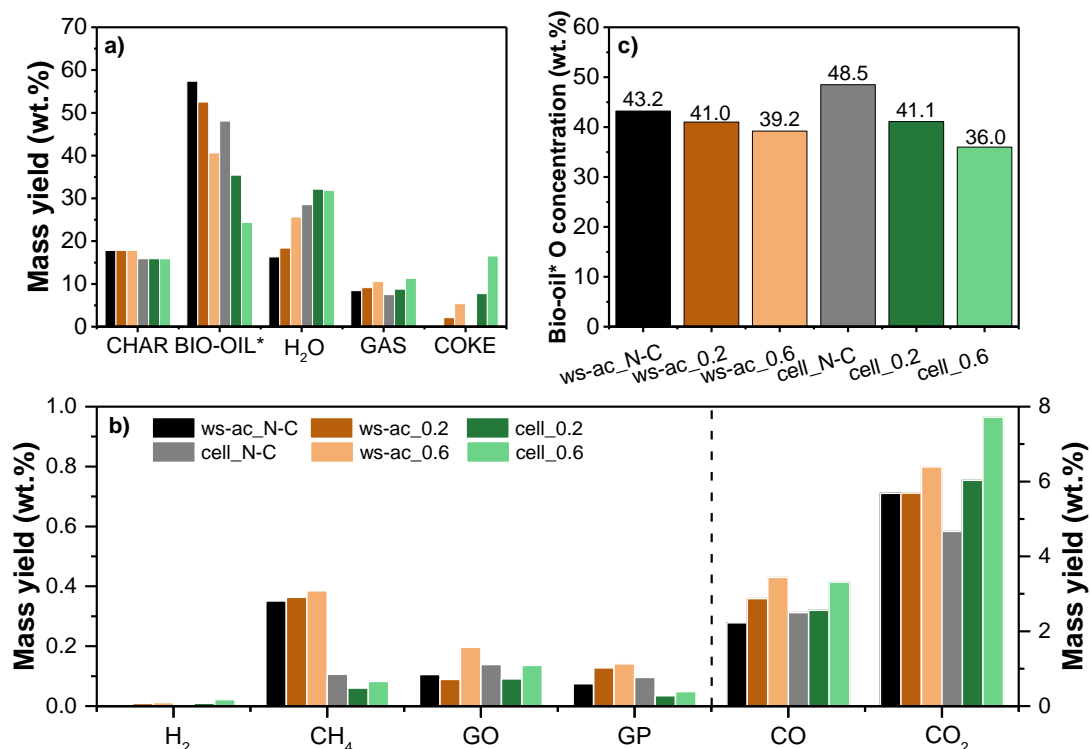


**Figure 4.1.7.** Fast pyrolysis of ws-ac and cellulose over BNT, including reference thermal tests: a) fraction yields; b) gaseous components yields (GO: gaseous olefins, GP: gaseous paraffins); c) bio-oil\* oxygen concentration.

On the other hand, gas yields also increase with the C/B ratio and have similar values between both feedstocks. The composition of gas yields for both series of experiments (denoted as *ws-ac<sub>x</sub>* and *cell<sub>x</sub>*, where *x* corresponds to C/B ratio) is further indicated in **Figure 4.1.7.b**. In the case of using cellulose as feedstock, C<sub>1</sub>-C<sub>4</sub> gaseous hydrocarbons are produced to a lesser extent, highlighting the reduction in methane formation, whose production is mainly linked to lignin degradation by dealkylation reactions [13]. Nevertheless, CO produced by non-catalytic and CFP of both feedstocks has similar yields. Otherwise, the highest production of CO<sub>2</sub> is observed for the cellulose test with the highest catalyst loading (C/B = 0.6), despite the fact that cellulose thermal test had the lowest value of CO<sub>2</sub> yield. M. Sulman et al. explain in their work about low-temperature pyrolysis of peat over bentonite that the increase of clay concentration results in the increase of H<sub>2</sub> and CO<sub>2</sub> yields, which are product of

#### 4.1. Catalytic fast pyrolysis of wheat straw and cellulose over clay catalysts

the exothermal reaction of CO and water [109] In this line, a slight increase in the mass yield of hydrogen is observed for the cellulose test with C/B = 0.6.

Turning back to **Figure 4.1.7.c**, where bio-oil\* oxygen concentrations are compared, bio-oils\* that come from cellulose fast pyrolysis show higher oxygen content when no catalyst was used, but as C/B ratio increases, bio-oil\* oxygen concentration descends to the point that it becomes lower than that of acid-washed wheat straw with the highest C/B ratio (36.0 vs. 39.2 wt.%). The elimination of oxygen from bio-oil\* via the formation of water, CO and CO<sub>2</sub> are represented in **Figure 4.1.8**, where catalytic deoxygenation selectivities are compared between feedstocks and C/B ratios. It is observed that in cellulose CFP, decarboxylation has an important contribution in the deoxygenation of bio-oil\*, even at a low catalyst loading (C/B = 0.2). When C/B ratio is increased to 0.6, decarboxylation selectivity becomes higher than that of dehydration, which is the most predominant deoxygenation pathway in CFP of ws-ac. As it was explained in the previous section, elimination of oxygen via CO<sub>2</sub> is more effective than any other deoxygenation route, resulting in a bio-oil\* with 36.0 wt.% of oxygen content in the case of using a C/B ratio of 0.6 of bentonite over cellulose. Thus, using cellulose in CFP over bentonite gives rise to a better quality bio-oil\* due to its lower oxygen content.

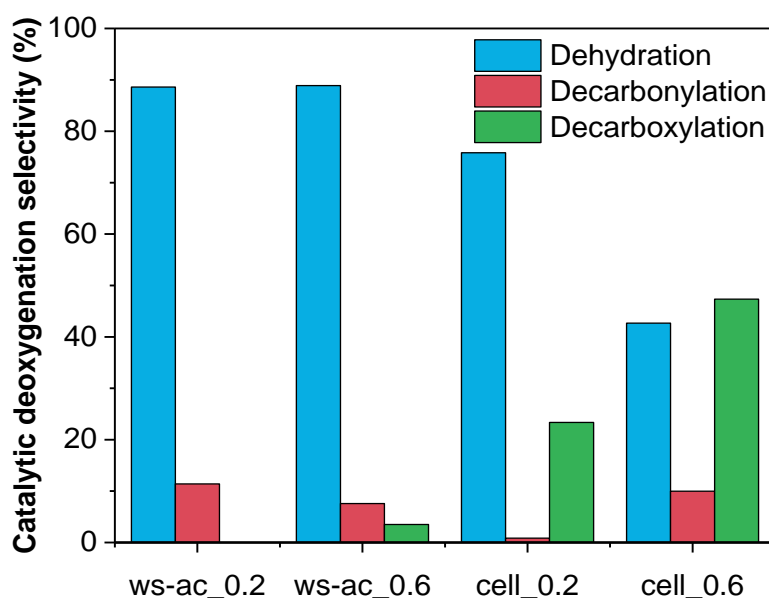


**Figure 4.1.8.** Catalytic deoxygenation selectivity obtained in the fast pyrolysis of ws-ac and cellulose over BNT at different C/B ratios.



**Table 4.1.4.** Compositions and HHVs of char and coke obtained in the fast pyrolysis of ws-ac and cellulose over BNT at different C/B ratios, including reference thermal tests.

Sample	Experiment	Fraction	Coke in catalyst (wt.%)	Mass yield (wt.%)	Elemental analysis (wt.%, dry basis)				HHV (MJ/kg)
					C	H	N	O	
ws-ac	N-C	Char	–	17.8	78.7	2.7	0.9	10.5	29.4
	BNT-0.2	Coke	10.8	2.1	36.1	5.6	–	58.3	12.7
	BNT-0.6	Coke	9.3	5.4	39.8	5.4	–	54.8	14.3
Cellulose	N-C	Char	–	15.9	81.9	3.3	–	10.0	31.4
	BNT-0.2	Coke	10.0	7.7	31.7	4.9	–	63.4	10.3
	BNT-0.6	Coke	8.8	16.5	29.0	4.8	–	66.3	8.9

Char and coke yields, elemental analyses and higher heating values of ws-ac and cellulose CFP are compared in further detail in **Table 4.1.4**. The higher heating value of char from cellulose experiments is slightly higher than that of ws-ac (31.4 vs. 29.4 MJ/kg), which is in line with their elemental analyses. Char from cellulose tests present lower mass yields with higher carbon and lower oxygen contents than those from ws-ac tests. Their possible valorisation as solid biofuels is illustrated in **Figure 4.1.9**. Both chars present compositions close to coals, but their atomic O/C ratios are slightly high, as can be observed in the Van Krevelen diagram. In addition, it is observed that coke yields augmented with C/B ratio, being more pronounced when cellulose is used as feedstock. Cellulose pyrolysis produces more coke than that of xylan (most common unit of hemicellulose) and lignin [110].

#### 4.1. Catalytic fast pyrolysis of wheat straw and cellulose over clay catalysts

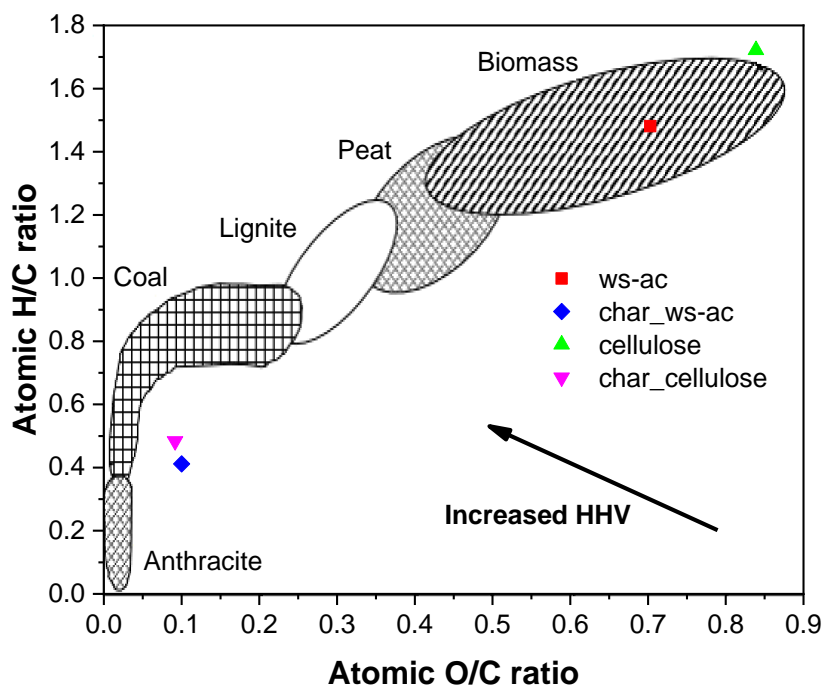


**Figure 4.1.9.** Van Krevelen diagram, comparing ws-ac and cellulose feedstocks and their respective pyrolytic chars [111].

GC-MS quantitative results of fast pyrolysis of ws-ac over bentonite from the previous section are compared with those using cellulose as feedstock. Total and GC-MS detected mass yields, as well as concentrations of quantifiable compounds, are illustrated in **Figures 4.1.10.a** and **4.1.10.b**, respectively. Based on the results of the non-catalytic tests, bio-oil\* from cellulose CFP has a considerably higher proportion of detected compounds than that of thermal pyrolysis of ws-ac (33 vs. 19 wt.%) because the complexity of the single cellulose polymer is not as great as in the lignocellulosic biomass, where hollocellulose and lignin are cross-linked. In this way, this tendency is maintained when comparing experiments with different C/B ratios. An increase in the C/B ratio implies a higher proportion of detected compounds in bio-oil\*, achieving a value of 69 wt.% in the test with cellulose over bentonite at a C/B ratio of 0.6. However, it should be noted that the total bio-oil\* yield of this particular test is reduced to half of the value of the non-catalytic test. To get a better insight into the nature of these detected species, quantified bio-oil\* yields are separated into different compound families in **Figure 4.1.10.c**.

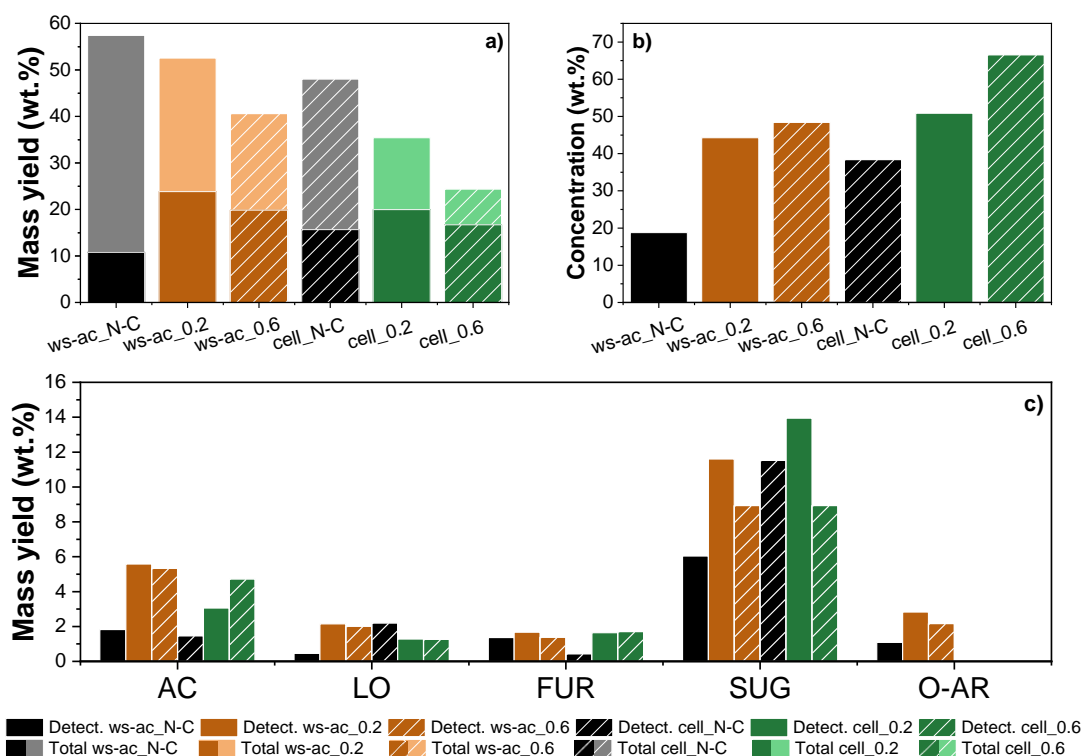


**Figure 4.1.10.** Quantitative GC-MS analyses of the bio-oil\* obtained in the fast pyrolysis of ws-ac and cellulose over bentonite, including reference thermal tests: a) total and GC-MS detected mass yields; b) concentration of GC-MS detected components; and c) GC-MS detected mass yields of compound families (AC: carboxylic acids, LO: light oxygenates, FUR: furans, SUG: anhydrosugars and O-AR: oxygenated aromatics).

As cellulose is formed by glucose units linked by glycosidic bonds, when it is pyrolysed without catalyst, these linkages are cleaved and intermediates are dehydrated, giving rise to anhydrosugars [13]. Low mass yields of AC, LO and FUR are also found in the bio-oil\* of N-C test with cellulose, as it is observed in **Figure 4.1.10.c**. Levoglucosan, the only detected and quantifiable anhydrosugar by GC-MS, presents a mass yield of 11.5 wt.%, compared to 6.0 wt.% of non-catalytic test employing ws-ac as feedstock. AC and FUR yields are lower than in the thermal pyrolysis of ws-ac, but instead LO production is moderately improved. O-AR are not detected in the bio-oil\* of N-C test with cellulose because these compounds are mainly obtained from the pyrolysis of lignin, which is only present in acid-washed wheat straw.

#### 4.1. Catalytic fast pyrolysis of wheat straw and cellulose over clay catalysts

Regarding cellulose CFP over bentonite, SUG yield is enhanced when a C/B ratio of 0.2 is employed, as it occurred with acid-washed wheat straw. The maximum value of levoglucosan is obtained for cellulose CFP over bentonite at this ratio (13.9 wt.%). Analogously to CFP of ws-ac, SUG yield decreases when the C/B ratio is 0.6. Lighter compounds, such as carboxylic acids exhibit a higher yield when catalyst loading increases (C/B ratio = 0.6). Nevertheless, FUR yields have negligible differences between catalytic tests with both C/B ratios, and LO yields are slightly lower than those of CFP of ws-ac, unlike in the case of cellulose. As in the thermal test with cellulose as feedstock, no O-AR were found in bio-oil\*. These compounds have their origin in the degradation of lignin, which is absent in this feedstock [5].

In conclusion, the use of bentonite as catalyst in lignocellulosic biomass CFP enhances levoglucosan production, unlike other highly acidic or basic catalysts that easily decompose it into other by-products. Moreover, a low catalyst to biomass ratio is preferred to increase levoglucosan yields in CFP of both cellulose and ws-ac in order to avoid the reduction in bio-oil\* yield and save on catalyst costs.

## 4.2. Catalytic fast pyrolysis of wheat straw over metal oxides

Basic alkaline earth metal oxides, like MgO, catalyse C–C bond-forming reactions, such as aldol condensation and ketonisation reactions. Certain transition metal oxides, like ZrO<sub>2</sub>, also promote this kind of reactions, as well as acid-catalysed reactions, such as cracking and deoxygenation, since this particular metal oxide exhibits amphoteric properties. Taking into account this background, a Mg-Zr mixed metal oxide was prepared by co-precipitation of Mg and zirconyl nitrates in order to obtain a multifunctional catalyst with improved acid-basic properties.

In this section, MgO, ZrO<sub>2</sub> and the Mg-Zr mixed oxide have been probed in the catalytic fast pyrolysis of acid-washed wheat straw to produce a less oxygenated bio-oil with enhanced properties and rich in bio-based chemicals. Among these products, long-chain ketones are being sought, as they are formed by ketonisation and aldol condensation of low-molecular weight oxygenated compounds usually found in bio-oil, which are promoted by basic active sites.

### 4.2.1. Characterisation of the catalysts

The Mg-Zr mixed oxide was synthesised by co-precipitation with a theoretical Mg/(Mg+Zr) atomic ratio of 0.75 and was denoted as 75MgZr. MgO and ZrO<sub>2</sub> were synthesised in the same conditions using exclusively their respective precursor inorganic salts.

X-Ray Diffraction was used to identify the crystallinity of the different phases of the Mg and Zr single and mixed oxides. The XRD patterns for all the samples are depicted in **Figure 4.2.1.a**. Both cubic MgO ( $2\theta = 36.8^\circ, 42.7^\circ, 62.1^\circ$  and  $74.5^\circ$ ) and tetragonal ZrO<sub>2</sub> ( $2\theta = 30.4^\circ, 35.1^\circ, 50.5^\circ, 60.2^\circ, 63.0^\circ, 74.5^\circ$  and  $78.5^\circ$ ) diffraction peaks can be observed in their respective single oxides. Conversely, 75MgZr presents typical diffraction peaks of both cubic MgO and cubic Mg<sub>x</sub>Zr<sub>1-x</sub>O<sub>2-x</sub> ( $2\theta = 30.7^\circ, 51.0^\circ$  and  $74.5^\circ$ ), according to Inorganic Crystal Structure Database #060443 [88]. The latter ones are displaced with respect to tetragonal ZrO<sub>2</sub> in the case of the Mg-Zr mixed oxide because of the formation of these dual species. However, a small and broad signal is found at  $74.5^\circ$ , which can be related to cubic MgO or cubic Mg<sub>x</sub>Zr<sub>1-x</sub>O<sub>2-x</sub>. It should be noted that the intensities of the diffraction peaks depend on the concentration of each oxide in the coprecipitate, being the cubic MgO peaks more intense than those

## 4.2. Catalytic fast pyrolysis of wheat straw over metal oxides

of cubic  $\text{Mg}_x\text{Zr}_{1-x}\text{O}_{2-x}$ . Apart from that, no hexagonal  $\text{Mg}(\text{OH})_2$  patterns are observed due to suitable calcination conditions employed for mixed oxide synthesis [88,112].

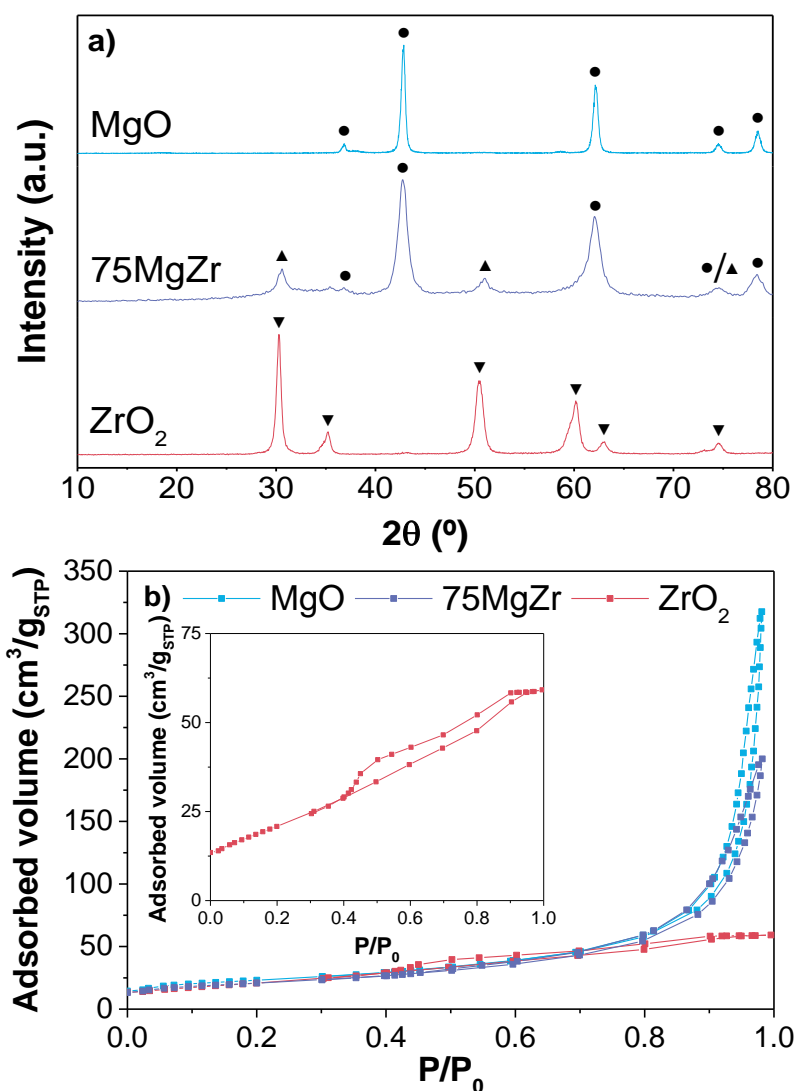


**Figure 4.2.1.** a) XRD patterns (● Cubic MgO; ▲ Cubic  $\text{Mg}_x\text{Zr}_{1-x}\text{O}_{2-x}$ ; ▼ Tetragonal  $\text{ZrO}_2$ ); b)  $\text{N}_2$  adsorption-desorption isotherms at 77 K; of the Mg and Zr single and mixed oxides.

$\text{N}_2$  physisorption isotherms at 77 K are identified as type IV according to IUPAC classification [100], which is characteristic of mesoporous materials (**Figure 4.2.1.b**). Differences among shapes and hysteresis loops depend on whether Mg and/or Zr are present in the oxides studied. Mg single and mixed oxides present type H3 hysteresis loops, which are typical of non-rigid agglomerates of plate-like particles, whereas  $\text{ZrO}_2$  exhibits type H2b loop, which is associated with pore blocking during  $\text{N}_2$  desorption. All oxides have relatively low values of BET surface area (70-80  $\text{m}^2/\text{g}$ ),

which matches with their external surface area. MgO exhibits the highest BET surface area, and as the Mg/(Mg+Zr) ratio decreases, lower values are observed. The values and trends of BET surface area are in agreement with the literature [88,105]. A more evident ascending trend is observed in their total pore volumes with Mg/(Mg+Zr) ratio (Table 4.2.1).

**Table 4.2.1.** Physicochemical properties of the Mg and Zr single and mixed oxides.

Catalyst	Mg/(Mg+Zr) atomic ratio	<sup>a</sup> S <sub>BET</sub> (m <sup>2</sup> /g)	<sup>b</sup> V <sub>T</sub> (cm <sup>3</sup> /g)	Acidity (μmolNH <sub>3</sub> /g)	Basicity (mmolCO <sub>2</sub> /g)
MgO	1.00	82	0.47	40	4.13
ZrO <sub>2</sub>	—	71	0.09	73	1.39
75MgZr	0.71	75	0.30	85	2.06

<sup>a</sup>BET surface area; <sup>b</sup>Total pore volume (P/P<sub>0</sub> ≈ 0.98)

Mg and Zr contents of the sample were determined by ICP-OES. Thus, a Mg/(Mg+Zr) atomic ratio of 0.71 was obtained (Table 4.2.1), which is slightly lower than the theoretical value since magnesium hydroxide species could have been formed during co-precipitation and removed during the centrifugation step [88]. Acid-base properties of the Mg and Zr single and mixed oxides have been studied by Temperature Programmed Desorption (TPD) of probe molecules.

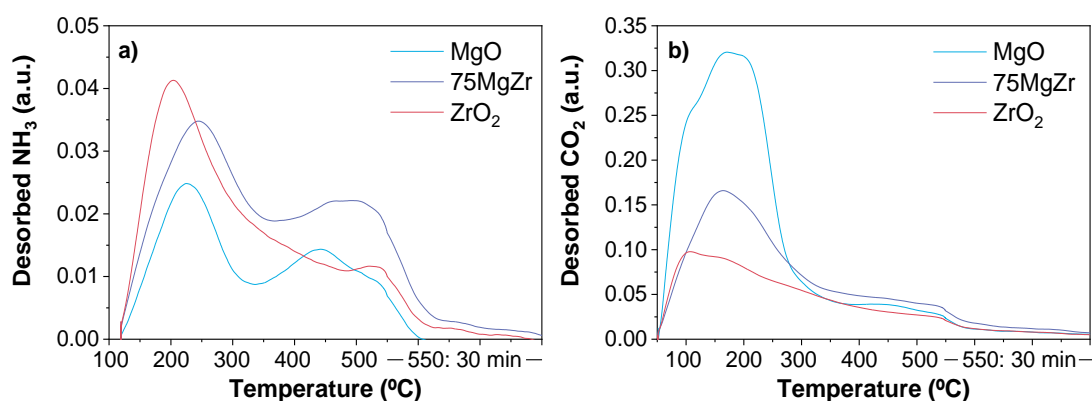


**Figure 4.2.2.** Acid-base properties of the Mg and Zr single and mixed oxides: a) NH<sub>3</sub>-TPD; b) CO<sub>2</sub>-TPD.

Acid-base properties of the samples are gathered in Table 4.2.1. On the one hand, the mixed oxide is the material with the highest overall acidity (85 μmolNH<sub>3</sub>/g). Its NH<sub>3</sub>-TPD curve shows a more intense peak at a maximum temperature of 244 °C and a smaller and broader peak centred at 494 °C (Figure 4.2.2.a). The shape of this curve

## 4.2. Catalytic fast pyrolysis of wheat straw over metal oxides

matches with that found in the work of Faba et al. [113], but the desorption peaks are displaced with respect to those obtained for the 75MgZr sample. In this work, a saturation temperature of 50 °C was used for the NH<sub>3</sub>-TPD of a Mg-Zr mixed oxide with an atomic ratio of 11.7. The peak found at lower temperature corresponds partly to NH<sub>3</sub> physisorption over weak acidic sites and its desorption is affected by the saturation temperature. Conversely, the peak at higher temperature corresponds to stronger acidity and its wider shape is attributed to the superposition of two peaks, which correspond to strong acidic sites from the two single oxides. When the two single oxides are considered separately, more intense desorption peaks of milder acidity are observed at 225 and 204 °C for the MgO and ZrO<sub>2</sub> samples, respectively. These results are consistent with the literature: MgO shows a NH<sub>3</sub> desorption peak at 230 °C [114] and ZrO<sub>2</sub> at 216 °C [115].

On the other hand, MgO is the material with the highest basicity (4.13 mmolCO<sub>2</sub>/g) and its CO<sub>2</sub>-TPD curve shows an intense and broad peak centred at 168 °C (**Figure 4.2.2.b**), which is close to that of 190 °C found in the work of Liang et al. [116]. Conversely, the mixed oxide has an intermediate value of basicity between the two single oxides and its maximum peak temperature matches with the MgO sample (168 °C), which has a higher contribution in overall basicity because of its high Mg concentration (Mg/(Mg+Zr) ratio of 0.71). A broad signal was found for the ZrO<sub>2</sub> sample with a maximum temperature of 108 °C that corresponds to weak-medium basicity, in accordance with that found at 130 °C in the work of Liang et al [116].

Both NH<sub>3</sub>- and CO<sub>2</sub>-TPD curves were deconvoluted for comparison purposes (**Figure 4.2.3**). Firstly, NH<sub>3</sub>-TPD curves were deconvoluted in three single curves based on the strength of acidic sites: weak (temperature range of 120-250 °C), medium (250-400 °C) and strong (>400 °C) [114]. Secondly, CO<sub>2</sub>-TPD curves were deconvoluted in four single curves based on the formed species during CO<sub>2</sub> desorption: bicarbonates (weak basic sites); bidentate carbonates (bridged and chelating, medium basic sites) and monodentate carbonates (strong basic sites). Bicarbonates are desorbed in the temperature range of 25 – 100 °C, bridged and chelating bidentate carbonates at 100 – 200 and 200 – 300 °C, respectively, and monodentate carbonates over 300 °C [116]. Strength types and concentrations of both acidic and basic sites in the Mg and Zr single and mixed oxides are listed in **Table 4.2.2**.



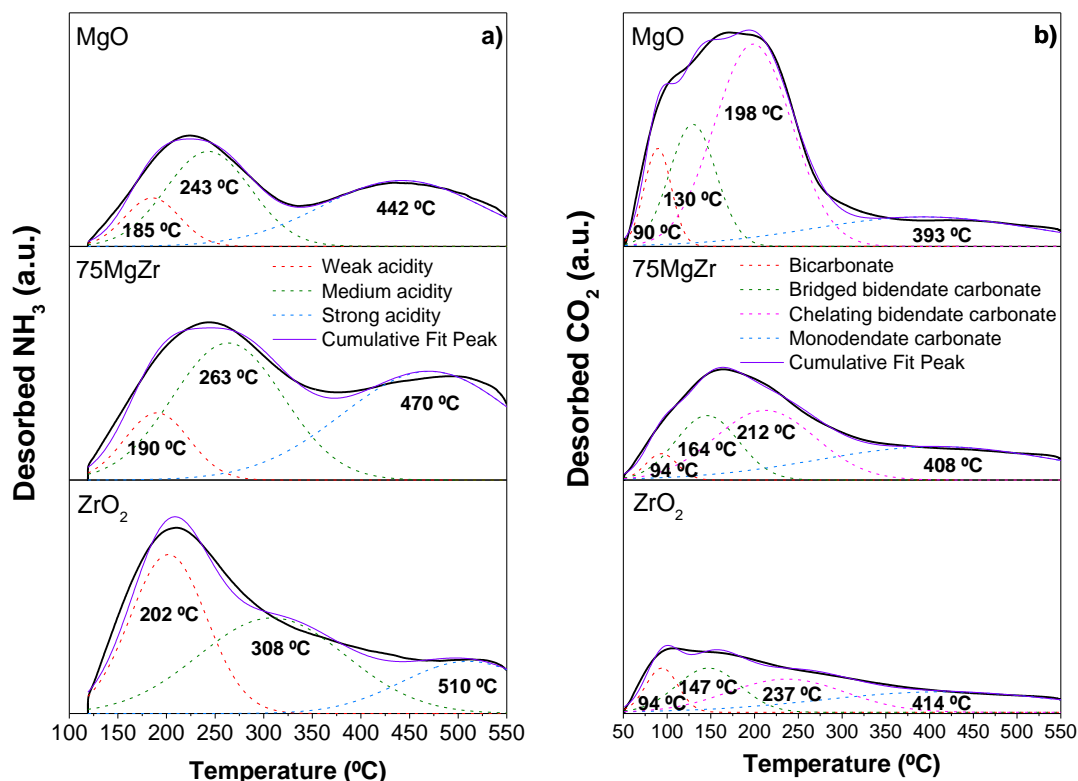


**Figure 4.2.3.** Deconvolution analyses of: a)  $\text{NH}_3$ -TPD; and b)  $\text{CO}_2$ -TPD curves; of the Mg and Zr single and mixed oxides.

In terms of acidity,  $\text{ZrO}_2$  presents the highest concentration of weak acidic sites among the three materials, whereas the Mg-Zr mixed oxide shows the highest proportion of medium and strong acidic sites, confirming the synergistic effect of the two single oxides when co-precipitated. In contrast, MgO exhibits the lowest overall acidity ( $40 \mu\text{mol}_{\text{NH}_3}/\text{g}$ ) with negligible weak acidity and low medium-strong acidities compared to 75MgZr. Regarding basicity, MgO presents the highest overall basicity with a contribution of 71 % of medium basicity. Basic centres associated to bidentates are known to catalyse aldol condensation reactions [113]. In particular, chelating bidentate carbonates are predominant over the other formed species. When comparing basicities of Zr-containing oxides,  $\text{ZrO}_2$  shows higher proportion of weak-medium basic sites than 75MgZr. In return, Mg-Zr mixed oxide exhibits higher contribution of medium-strong basic sites due to the presence of MgO in its structure.

## 4.2. Catalytic fast pyrolysis of wheat straw over metal oxides

**Table 4.2.2.** Strength types and concentration (conc.) of both acidic and basic sites in the Mg and Zr single and mixed oxides.

Catalyst	Acidic sites (NH <sub>3</sub> -TPD)		Basic sites (CO <sub>2</sub> -TPD)	
	<sup>a</sup> Strength type	Conc. (μmol/g)	<sup>b</sup> Strength type	Conc. (mmol/g)
MgO	Weak	5	Bicarbonates	0.36
	Medium	15	Bridged bidentate carbonate	0.78
			Chelating bidentate carbonate	2.15
	Strong	20	Monodentate carbonate	0.84
75MgZr	Weak	10	Bicarbonates	0.09
	Medium	34	Bridged bidentate carbonate	0.43
			Chelating bidentate carbonate	0.75
	Strong	42	Monodentate carbonate	0.79
ZrO <sub>2</sub>	Weak	27	Bicarbonates	0.20
	Medium	31	Bridged bidentate carbonate	0.32
			Chelating bidentate carbonate	0.41
	Strong	15	Monodentate carbonate	0.46

<sup>a</sup>Strength of acidic sites: weak (120 – 250 °C); medium (250 – 400 °C); strong (>400 °C)

<sup>b</sup>Strength of basic sites: weak: bicarbonates (25 – 100 °C); medium: bridged bidentate carbonate (100 – 200 °C) and chelating bidentate carbonate (200 – 300 °C); strong: monodentate carbonate (>300 °C)

### 4.2.2. Wheat straw catalytic tests

Single and mixed oxides have been tested in catalytic fast pyrolysis (CFP) of acid-washed wheat straw (ws-ac). The main variable of this study was the catalyst type, whereas the rest of the parameters were maintained constant in all trials: the catalyst to biomass ratio (C/B) ratio was 0.2 g/g, and the temperatures of the pyrolytic and catalytic zones were 550 and 450 °C, respectively. In addition, a reference non-catalytic (N-C) test was also included in the study (Tables A.1, A.9 – A.11 in the Appendix). An average value of 17.8 wt.% of char mass yield was calculated for all experiments.

Mass yields of bio-oil\* (water-free bio-oil), water, permanent gases and coke are represented in Figure 4.2.4.a. It is observed that the non-catalytic test has the highest yield of bio-oil\* (57.4 wt.%) and when a catalyst is employed, this yield exhibits a remarkable decrease. The catalyst with the lowest bio-oil\* yield is the Mg-Zr mixed oxide (75MgZr) because it has the highest acidity among the three catalysts studied. The inclusion of a catalyst in the fast pyrolysis of biomass is translated into the increase of the formation of water, permanent gases and the deposition of coke on the surface of the catalysts. Water, CO and CO<sub>2</sub> are formed by deoxygenation reactions, whereas

gaseous hydrocarbons are produced by cracking reactions. Conversely, coke is formed by oligomerisation and polymerisation reactions. These reactions are promoted differently by both acidic and basic sites, which are present to a greater or lesser extent in the three oxides studied.

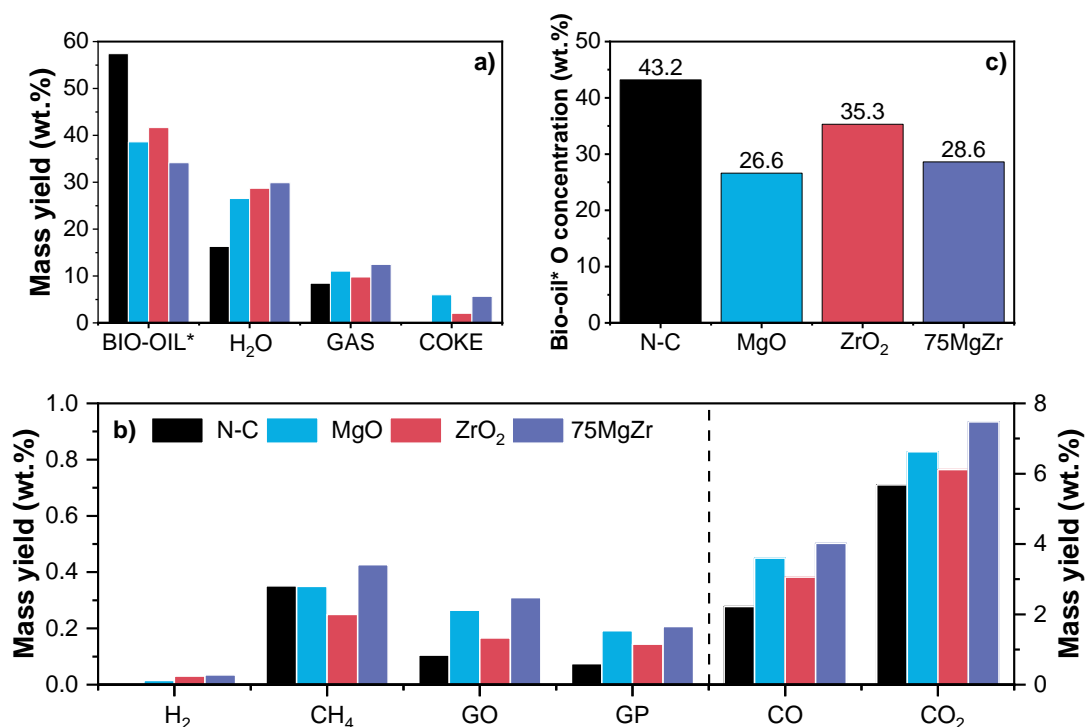


**Figure 4.2.4.** Fast pyrolysis of ws-ac over Mg and Zr single and mixed oxides: a) fraction yields; b) gaseous components yields (GO: gaseous olefins, GP: gaseous paraffins); c) bio-oil\* oxygen concentration.

Firstly, bio-oil is deoxygenated in the form of water, which is formed by dehydration and promoted by both acidic and basic sites, and aldol condensation reactions catalysed by medium basic sites [113,117]. The Mg-Zr mixed oxide has the highest water yield because of the presence of both types of active sites. Although MgO has higher basicity than 75MgZr, the lower concentration of acidic sites makes it the least active catalyst for water formation. Secondly, the permanent gases yield increases when a catalyst is employed compared to the non-catalytic test. The mixed oxide has the highest yield of permanent gases, followed by MgO and ZrO<sub>2</sub>. Permanent gases are separated into different gaseous components in **Figure 4.2.4.b**. Higher acidity favours cracking, decarbonylation and decarboxylation reactions, which produce gaseous hydrocarbons, CO and CO<sub>2</sub>, respectively. Simultaneously, C–C bond formation reactions that release CO<sub>2</sub> are promoted by basic sites [117]. Thus, 75MgZr

## 4.2. Catalytic fast pyrolysis of wheat straw over metal oxides

is the catalyst with the highest yields of  $H_2$ , gaseous hydrocarbons and  $CO_x$ . Contrarily,  $ZrO_2$  has the lowest activity in the transformation of biomass into permanent gases due to its lower basicity and pore volume despite having similar acidity to 75MgZr. Otherwise, MgO presents higher yields of gaseous  $C_2$ - $C_4$  hydrocarbons and  $CO_x$  than  $ZrO_2$  although it is the oxide with the lowest acidity, but it has the highest textural properties and overall basicity.

Finally, coke is deposited on the surface of the oxides during catalytic pyrolysis. The catalyst with the lowest coke production is  $ZrO_2$  because it has the mildest basicity among the three oxides and its acidity is less than twice that of MgO.  $ZrO_2$  is followed by 75MgZr, which exhibits intermediate basicity between the single oxides and the highest acidity although it is very similar to that of  $ZrO_2$ . Lastly, MgO has considerably higher basicity compared to the mixed oxide, which causes the highest deposition of coke among the three materials.

On the other hand, in terms of deoxygenation, the bio-oil\* from the non-catalytic experiment has a high oxygen concentration with a value of 43.2 wt.% (**Figure 4.2.4.c**), which negatively affects its properties. The decrease in the oxygen content depends on the acid-base properties of the catalysts, which affect the production of deoxygenation products, such as water and  $CO_x$ . These deoxygenation pathways are compared in the form of catalytic selectivities in **Figure 4.2.5**, which are calculated by the incremental production of water, CO and  $CO_2$  concerning the thermal test. The three catalytic systems show similar catalytic selectivities, with dehydration being the predominant route of bio-oil deoxygenation\* in all cases. It should be noted that 75MgZr exhibits the highest decarboxylation selectivity, which is advantageous in terms of deoxygenation because two atoms of oxygen are effectively removed from bio-oil\* as part of the same molecule.  $CO_2$  is eliminated by the action of both acidic and basic sites of the mixed oxide during ws-ac CFP. In spite of having the highest production of water and  $CO_x$ , 75MgZr does not show the lowest bio-oil\* oxygen concentration. It is the bio-oil\* from the MgO test which exhibits the lowest oxygen content (26.6 wt.%), whereas that of  $ZrO_2$  has a considerable higher value due to its poorer basicity and coke and gas productions. The compositions of the coke deposits formed on the surface of the catalysts need to be examined for further explanation.

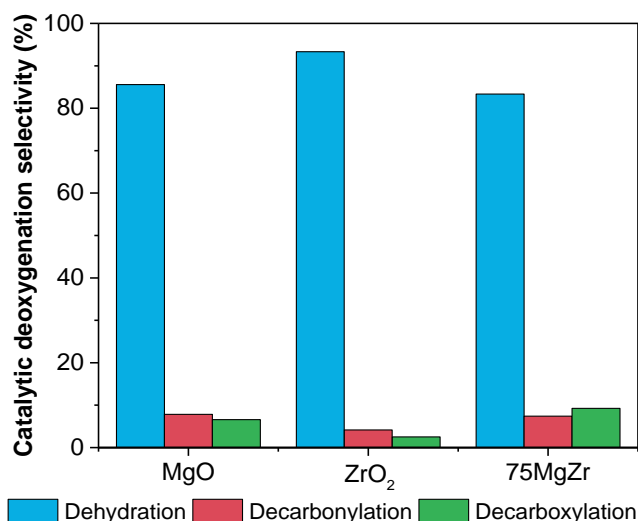


**Figure 4.2.5.** Catalytic deoxygenation selectivity obtained in the fast pyrolysis of ws-ac over Mg and Zr single and mixed oxides.

In addition to the coke compositions, mass yields and higher heating values of char and the spent catalysts are gathered in **Table 4.2.3**. On the one hand, MgO has the drawback that it produced the highest coke yield. However, almost half of its composition is oxygen, suggesting that these are carbonaceous deposits of sugars rather than coke (levoglucosan has an oxygen content of 49.3 wt.%). On the other hand, 75MgZr produced slightly lower amount of coke, but less oxygen is found than in that of MgO. Due to the higher carbon and lower oxygen contents, coke over Mg-Zr mixed oxide showed higher HHV than that over MgO, which is not beneficial in terms of energy valorisation of lignocellulosic biomass. Finally, although ZrO<sub>2</sub> was the metal oxide with the lowest coke yield due to its milder acid-base properties, its bio-oil\* oxygen content is not comparable with those of Mg-containing catalysts (35.3 vs. 26.6 – 28.3 wt.%).

**Table 4.2.3.** Compositions and HHVs of char and coke obtained in the fast pyrolysis of ws-ac over Mg and Zr single and mixed oxides.

Experiment	Fraction	Coke in catalyst (wt.%)	Mass yield (wt.%)	Elemental analysis (wt.%, dry basis)				HHV (MJ/kg)
				C	H	N	O	
N-C	Char	–	17.8	78.7	2.7	0.9	10.5	29.4
MgO	Coke	34.0	6.0	47.3	2.8	–	49.9	14.7
ZrO <sub>2</sub>		11.1	2.0	61.3	3.2	–	35.4	21.6
75MgZr		31.6	5.7	51.3	3.0	–	45.7	16.8

## 4.2. Catalytic fast pyrolysis of wheat straw over metal oxides

GC-MS quantification was used to determine the components of the bio-oil\*. Total bio-oil\* yields are compared with the yields of detected compounds in **Figure 4.2.6.a**, whereas the proportions of detected compounds found in the bio-oils\* are shown in **Figure 4.2.6.b**. Only 18.8 wt.% of thermal bio-oil\* could be quantified, corresponding to 10.8 wt.% of total mass yield. When a catalyst is used, these concentrations are enhanced ( $\text{ZrO}_2$ : 39.3 wt.%; 75MgZr: 57.9 wt.%; MgO: 61.5 wt.%). This behaviour can be related to the oligomers produced by the partial decomposition of biomass interacting with the acidic and basic sites of the metal oxides to produce more straightforward and quantifiable compounds. Despite having the highest total bio-oil\* yield,  $\text{ZrO}_2$  is the catalyst with the lowest proportion of detected compounds. It has noticeable acid properties which allow the formation of water, gaseous hydrocarbons and coke, among others, but its not so high basicity did not contribute greatly to the formation of compounds in the bio-oil\* quantifiable by GC-MS. On the contrary, MgO and 75MgZr, which have high basicity, show high proportions of detected compounds in their bio-oils\* (61 and 57 wt.%, respectively). Thus, MgO is preferred in terms of detection rate because not only does 75MgZr have a lower proportion of detected compounds, but it also has lower total bio-oil\* yield.

GC-MS detected mass yields are divided into compound families in **Figure 4.2.6.c**. The production of SUG (mainly levoglucosan) is highlighted in the thermal bio-oil\* with a 6.0 wt.%. However, the other fractions have low mass yields not exceeding 2.0 wt.%. When  $\text{ZrO}_2$  is employed, part of the unidentifiable oligomers and anhydrosugars are transformed into simpler compounds, among which AC (mainly acetic acid) stand out. AC production is even higher when MgO is employed. In addition, a noticeable increase in the formation of LO, FUR and O-AR is observed, whereas SUG yield is slightly reduced. As discussed earlier, basic sites promote C–C bond formation reactions, and numerous ketones and condensation products are found between the LO and O-AR families. MgO test exhibits slightly higher AC and SUG mass yields than those obtained using 75MgZr as catalyst, but more notable differences are observed in the LO and O-AR families. The Mg single oxide has higher yields of O-AR, whereas the Mg-Zr mixed oxide has higher yields of LO. Conversely, MgO has the highest FUR mass yield. Furans are mainly produced by dehydration of hollocelulose fragments, with anhydrosugars as intermediates. It has been observed that typical base metal oxides, such as CaO [118] and MgO [119], can also promote dehydration

reactions and ring-opening reactions of anhydrosugars to form furans when used at high temperatures in CFP of lignocellulosic biomass.

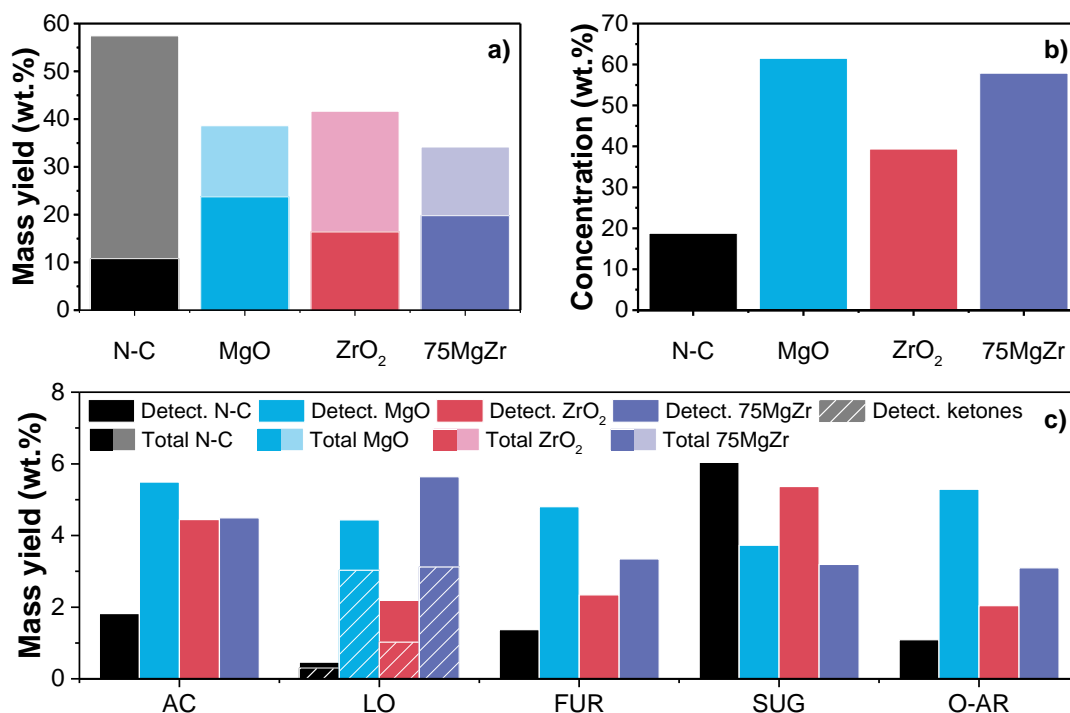


**Figure 4.2.6.** Quantitative GC-MS analyses of the bio-oil\* obtained in the fast pyrolysis of ws-ac over Mg and Zr single and mixed oxides: a) total and GC-MS detected mass yields; b) concentration of GC-MS detected components; and c) GC-MS detected mass yields of compound families (AC: carboxylic acids, LO: light oxygenates, FUR: furans, SUG: anhydrosugars and O-AR: oxygenated aromatics).

Concentrations of the different subfamilies found in the LO fraction without catalyst and using the three oxides are compared in **Table 4.2.4**. It is observed that the thermal bio-oil\* presents a low overall concentration of light oxygenates (0.8 wt.%), followed by ZrO<sub>2</sub> (5.3 wt.%) and MgO (11.5 wt.%). It is 75MgZr that which showed the bio-oil\* with the highest overall LO concentration (16.5 wt.%).

This bio-oil\* exhibits the highest concentration of acetals of all bio-oils\*. These compounds are produced by acetalisation of aldehydes with alcohols [120]. These reactions are promoted by acidic sites and it was proved that 75MgZr presents the highest acidity among the three oxides. Overlapping peaks of low-molecular-weight alcohols were found in the chromatograms at low retention times but could not be adequately quantified since the solvent used for the dilutions was ethanol, so it can be envisaged that these alcohols formed during CFP of ws-ac can act as intermediates of acetalisation reactions.

## 4.2. Catalytic fast pyrolysis of wheat straw over metal oxides

**Table 4.2.4.** Concentration (wt.%) of the LO subfamilies present in the bio-oil\* produced by ws-ac CFP over Mg and Zr single and mixed oxides.

Catalyst	N-C	MgO	ZrO <sub>2</sub>	75MgZr
<b>Acetals</b>	<b>0.061</b>	<b>1.068</b>	<b>1.159</b>	<b>4.232</b>
Diethoxyethane	–	0.935	1.017	4.109
<b>Aldehydes</b>	<b>0.083</b>	<b>0.371</b>	<b>0.162</b>	<b>0.385</b>
<b>Esters</b>	<b>0.040</b>	<b>2.200</b>	<b>0.369</b>	<b>2.765</b>
<b>Ketones</b>	<b>0.525</b>	<b>7.844</b>	<b>2.450</b>	<b>9.131</b>
<i>Cyclic ketones</i>	<i>0.117</i>	<i>4.744</i>	<i>2.110</i>	<i>4.809</i>
Cyclohexanone	0.007	2.217	1.091	1.535
Dimethylcyclopentenone	–	1.227	–	1.019
Cyclopentenone	–	0.532	0.361	0.960
Cyclopentanone	–	0.402	0.193	0.707
Methylcyclopentenone	0.009	–	–	0.587
<i>Linear ketones</i>	<i>0.408</i>	<i>3.100</i>	<i>0.340</i>	<i>4.322</i>
Hydroxyacetone	0.027	1.569	–	1.689
Hydroxybutanone	0.012	0.750	0.183	0.406
Pentenone	–	0.491	–	0.640
<b>Oxacycles</b>	<b>0.033</b>	–	–	–
<b>Pyranones</b>	<b>0.052</b>	–	<b>1.112</b>	–
<b>Total LO</b>	<b>0.795</b>	<b>11.484</b>	<b>5.251</b>	<b>16.513</b>

On the other hand, MgO and 75MgZr present similar concentrations of esters (2.2 and 2.7 wt.%, respectively). These compounds are formed by Tishchenko reaction, which is catalysed by basic and bifunctional catalysts. Aldehydes with no  $\alpha$ -H are directly converted to esters by basic alkaline earth metal oxides, such as MgO, whereas in the esterification of aldehydes with  $\alpha$ -H, Tishchenko reaction competes with aldol condensation and acidic sites are required in order to produce esters [45]. This fact could explain the higher concentration of esters in the CFP test over bifunctional 75MgZr since both types of aldehydes are transformed.

Regarding the percentages of ketones in LO subfamilies, these are consistent with the basicity values of their respective catalysts ( $\text{ZrO}_2 < 75\text{MgZr} < \text{MgO}$ , see **Figure 4.2.6.c**), since aldol condensation and ketonisation reactions are promoted by basic sites. Except in the case thermal bio-oil\*, cyclic ketones are more abundant than linear ketones in catalytic bio-oils\*. A recent work of Gupta et. al [61] could give an explanation to the high production of cyclic ketones in the case of MgO. In this work, a basic CaO catalyst is used to transform furfural into cyclopentanone and



cyclopentenone by successive hydrogenation, dehydroxylation, rearrangement and dehydration reactions.

Finally, thermal bio-oil\* shows negligible concentrations of oxacycles and pyranones. The latter are obtained from the degradation of sugars [121], and their production is improved when  $\text{ZrO}_2$  with milder acid-base properties is used. However, these compounds are not observed in the case of catalysts with higher basicity.

Similarly, concentrations of the different subfamilies found in the O-AR fraction are listed in **Table 4.2.5**. Methoxybenzenes constitute 79 wt.% of O-AR subfamily in the thermal bio-oil\*, where 63 % are guaiacols. However, the total concentration of O-AR subfamily in thermal bio-oil\* does not exceed 2 wt.%. This concentration augmented to almost double its value when  $\text{ZrO}_2$  was used as catalyst, being 60 % of this subfamily composed by methoxybenzenes. Moreover, syringols and trimethoxybenzenes are almost tripled compared to those of the non-catalytic test. Taking into account that methoxybenzenes are formed by the cleavage of lignin C–C bonds in thermal pyrolysis, the addition of a slightly acid catalyst seems to favour the cracking reactions, giving rise to more methoxybenzenes [5]. Conversely, MgO shows the highest concentration of methoxybenzenes (8.4 wt.%, where 78 % are guaiacols). In the literature, it was found that guaiacols exhibit their maximum concentrations at mild temperature conditions (400 – 450 °C) and low catalyst to biomass ratios (C/B = 0.2) over solid base catalysts [122]. Since 75MgZr has a lower basicity than MgO, it shows an intermediate concentration of methoxybenzenes between both single oxides.

On the other hand, acetophenones are formed by the cross-ketonisation of acetates found in the ester subfamily and benzyl acetates, which should act as reaction intermediates due to their absence in the O-AR family. This reaction is mainly catalysed by basic sites [47] and therefore the highest concentration of acetophenones (3.0 wt.%) is observed in the MgO bio-oil\*.

Finally, MgO and 75MgZr present similar values of hydroxybenzenes (1.9 and 2.2 wt.%, respectively), but with different distributions of phenols and benzenediols. Demethylation and demethoxylation of syringols and guaiacols give rise to catechols and other phenolic compounds, both reactions being promoted by base metal oxides [3,5].

## 4.2. Catalytic fast pyrolysis of wheat straw over metal oxides

**Table 4.2.5.** Concentration of the O-AR subfamilies present in the bio-oil\* produced by ws-ac CFP over Mg and Zr single and mixed oxides.

Catalyst	N-C	MgO	ZrO <sub>2</sub>	75MgZr
<b>Acetophenones</b>	<b>0.104</b>	<b>3.049</b>	<b>1.356</b>	<b>2.182</b>
Hydroxymethylacetophenone	—	2.438	1.166	1.666
<b>Benzalacetones</b>	<b>0.016</b>	<b>0.149</b>	—	<b>0.103</b>
<b>Benzaldehydes</b>	<b>0.141</b>	<b>0.236</b>	<b>0.178</b>	<b>0.164</b>
<b>Hydroxybenzenes</b>	<b>0.138</b>	<b>1.908</b>	<b>0.425</b>	<b>2.164</b>
<i>Phenols</i>	<i>0.130</i>	<i>1.099</i>	<i>0.425</i>	<i>1.511</i>
<i>Benzenediols</i>	<i>0.008</i>	<i>0.809</i>	—	<i>0.653</i>
<b>Methoxybenzenes</b>	<b>1.496</b>	<b>8.369</b>	<b>2.945</b>	<b>4.737</b>
<i>Guaiacols</i>	<i>1.191</i>	<i>6.517</i>	<i>2.091</i>	<i>3.215</i>
Guaiacol	0.140	2.996	0.508	0.768
Creosol	0.216	1.284	0.562	1.058
Isoeugenol	0.142	1.048	0.556	0.690
Ethylguaiacol	0.162	0.765	0.341	0.392
Dihydroeugenol	0.049	0.425	0.123	0.307
<i>Syringols</i>	<i>0.219</i>	<i>1.208</i>	<i>0.631</i>	<i>0.979</i>
<i>Trimethoxybenzenes</i>	<i>0.086</i>	<i>0.643</i>	<i>0.223</i>	<i>0.543</i>
<b>Total O-AR (wt.%)</b>	<b>1.895</b>	<b>13.711</b>	<b>4.903</b>	<b>9.351</b>

In summary, MgO and the 75MgZr mixed oxide showed the most promising results in CFP of ws-ac in terms of deoxygenation of bio-oil\* and production of high-added value bio-based chemicals. However, unlike ZrO<sub>2</sub>, their bio-oil\* yields are considerably reduced. On the one hand, basic MgO gave rise to a highly deoxygenated bio-oil\* (oxygen content of 26.6 wt.%) with a great share of LO (11.5 wt.%) and O-AR (13.7 wt.%). Cyclic ketones, such as cyclopentenones, stand out among other LO, due to its versatility in organic reactions as chemical intermediates for natural products and drug molecules [123]. In addition, production of acetophenones and guaiacols is highlighted among other O-AR because of their application in cosmetics and pharmaceutical industries [124,125]. On the other hand, bifunctional 75MgZr produced a not-so-highly deoxygenated bio-oil\* (oxygen content of 28.6 wt.%) rich in LO (16.5 wt.%), including acetals and both linear and cyclic ketones, although its production of O-AR is somewhat diminished compared to MgO (9.4 wt.%). Diethoxyethane stands out due to its use as a precursor in the synthesis of pharmaceuticals, perfumes, polyacetal resins and alkyl vinyl ethers [126], whereas hydroxyacetone is employed as an intermediate to produce low-molecular-weight chemicals and a food flavouring [127].

### 4.3. Catalytic fast pyrolysis of wheat straw over K-incorporated zeolites

The addition of alkali metals to protonated zeolites is an interesting way to increase their basicity and, at the same time, to reduce their cracking activity due to their high acidity leading to a considerable decrease in bio-oil yield and further deactivation due to the formation of coke deposits.

In this section, two different protonic zeolites and potassium incorporation methods have been studied. On the one hand, a nanocrystalline zeolite H-ZSM-5 was ion-exchanged with an aqueous KCl solution. On the other hand, an Ultrastable Y (USY) zeolite was potassium grafted with KOH in alcoholic medium.

Basic properties of KH-ZSM-5 and K-USY zeolites have been evaluated in the catalytic fast pyrolysis of acid-washed wheat straw. Catalyst to biomass ratios were varied for the catalytic tests with both zeolites, whereas catalytic step temperature was only varied for the catalytic tests with K-grafted USY. Parent H-ZSM-5 and USY zeolites have also been included in their respective studies. The use of protonated zeolites in CFP of lignocellulose is usually oriented to the production of biofuels. However, when K-incorporated zeolites are employed instead of their protonated forms, the focus is more on obtaining high-added value bio-based chemicals from bio-oil.

The results of catalytic tests with different K-incorporated zeolites cannot be easily compared since the procedures followed for bio-oil recovery and permanent gases collection were different. It was decided to follow Procedure 2 for the fast pyrolysis tests of ws-ac over K-USY zeolite instead of Procedure 1, since bio-oil recovery with acetone may affect the concentration of light oxygenates (LO) and anhydrosugars (SUG) in bio-oils. In addition, due to the different collection procedures of the individual product fractions, their mass yields were calculated differently.

#### 4.3.1 K-exchanged and parent H-ZSM-5 zeolites

##### 4.3.1.1. Characterisation of the catalysts

The KH-ZSM-5 sample has been prepared by repeated ion-exchange (three-times) of the parent H-ZSM-5 material, which has afforded the partial replacement of H<sup>+</sup> protons

### 4.3. Catalytic fast pyrolysis of wheat straw over K-incorporated zeolites

by  $K^+$  cations. Thus, as shown in **Table 4.3.1**, the KH-ZSM-5 sample presents a K/Al ratio of 0.5, clearly below the maximum theoretical value ( $K/Al = 1$ ) that could be attained if all the negative charges associated with Al atoms in the zeolite framework are counterbalanced by  $K^+$  species. This partial ion-exchange does not affect negatively the zeolite crystallinity since both H-ZSM-5 and KH-ZSM-5 materials show very similar XRD patterns (**Figure 4.3.1.a**).

**Table 4.3.1.** Physicochemical properties of the H-ZSM-5-based samples.

Sample	K/Al <sup>a</sup>	Si/Al <sup>a</sup>	S <sub>BET</sub> <sup>b</sup> (m <sup>2</sup> /g)	S <sub>MES+EXT</sub> <sup>c</sup> (m <sup>2</sup> /g)	S <sub>MIC</sub> <sup>d</sup> (m <sup>2</sup> /g)	V <sub>T</sub> <sup>e</sup> (cm <sup>3</sup> /g)	V <sub>MIC</sub> <sup>f</sup> (cm <sup>3</sup> /g)	Acidity (mmol NH <sub>3</sub> /g)	Basicity (mmol CO <sub>2</sub> /g)
H-ZSM-5	—	39.5	384	53	331	0.36	0.197	0.314	0.018
KH-ZSM-5	0.5	36.8	397	83	314	0.39	0.187	0.160	0.460

<sup>a</sup> Atomic ratio; <sup>b</sup> BET surface area; <sup>c</sup> Mesopore + external surface area;

<sup>d</sup> Micropore surface area; <sup>e</sup> Total pore volume ( $P/P_0 \approx 0.98$ ); <sup>f</sup> Micropore volume

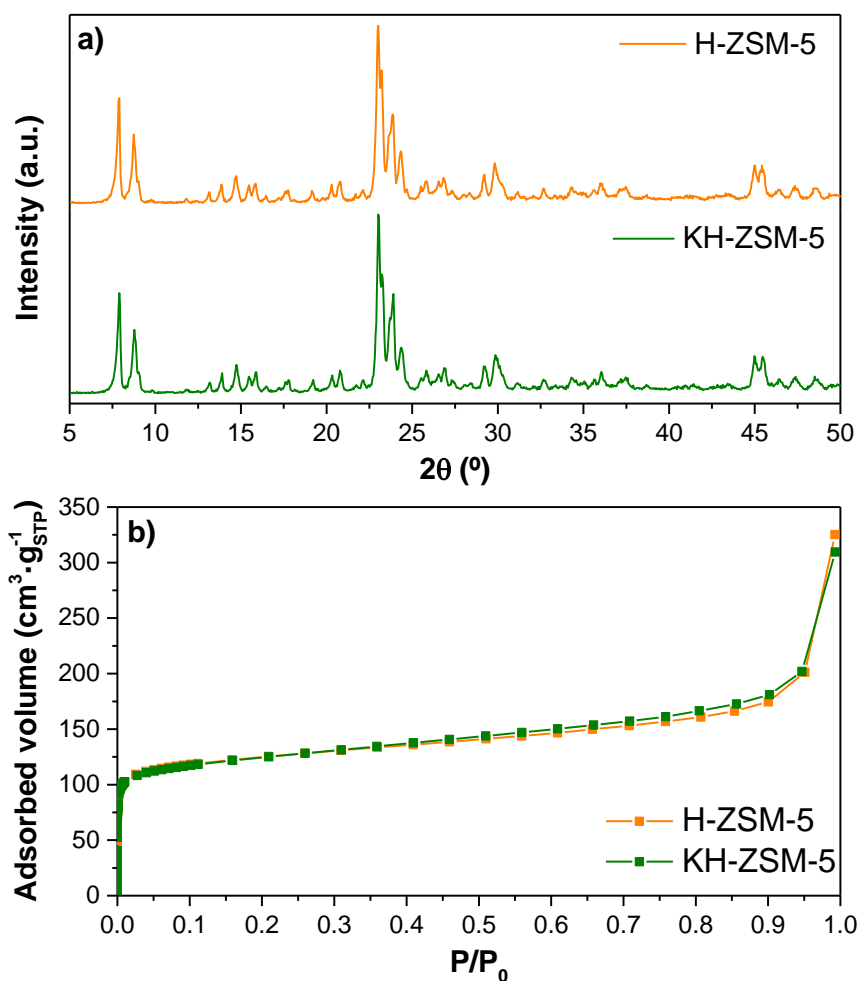


**Figure 4.3.1.** XRD patterns (a) and Ar adsorption isotherms at -87 K (b) of the catalyst samples.

In the same way, just small variations are observed in the textural properties of the H-ZSM-5 sample after the introduction of  $K^+$  cations. Thus, as illustrated in **Figure 4.3.1.b**, both materials present very similar Ar adsorption isotherms. The presence of a relatively pronounced slope in the adsorption curve at intermediate pressures is consistent with the nanocrystalline features of these samples that provide them with a significant external surface. This fact has been confirmed by TEM images (**Figure 4.3.2**), showing that both samples are formed by aggregates of nanocrystals with sizes in the range 25-50 nm [56]. This is a convenient property for favouring the catalyst accessibility, in particular in the conversion of bulky compounds, as many of those derived from the lignocellulose pyrolysis.

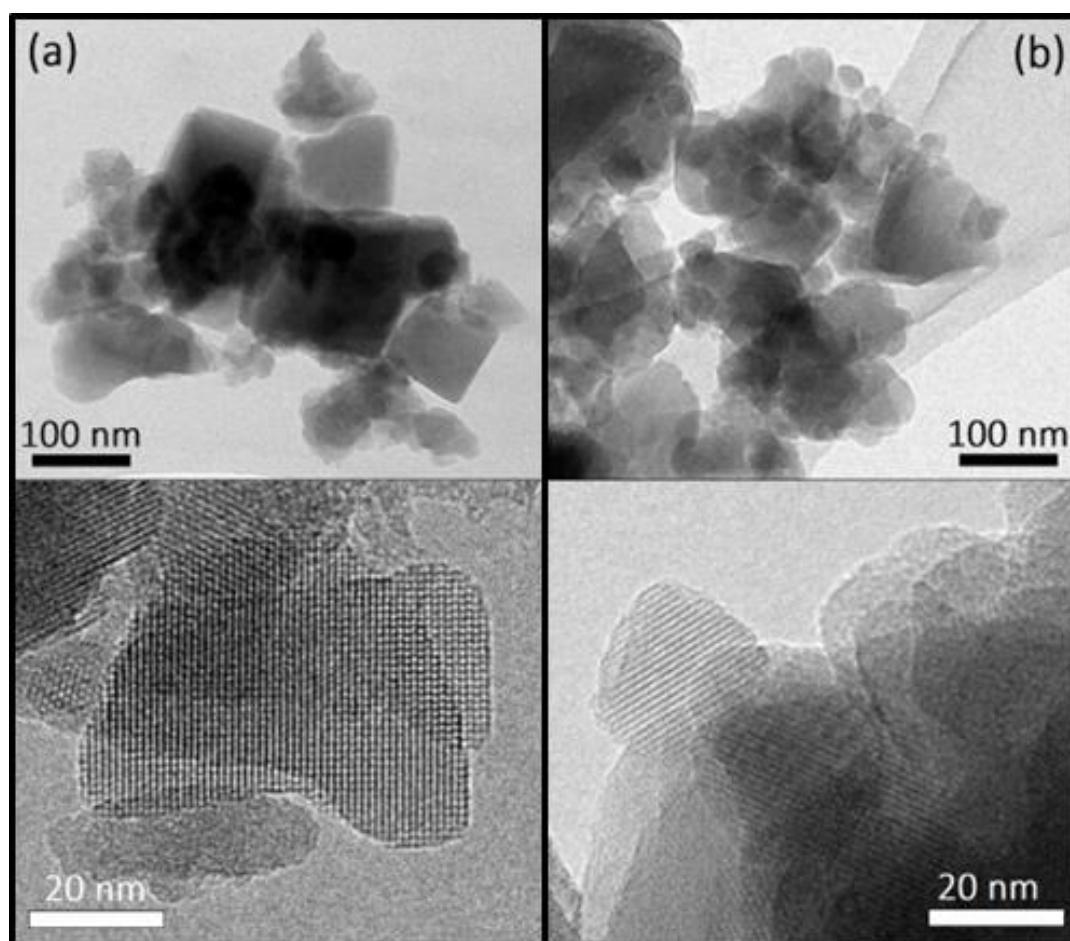


**Figure 4.3.2.** TEM images of: (a) parent H-ZSM-5 zeolite and (b) K-exchanged H-ZSM-5 zeolite.

The KH-ZSM-5 sample possesses BET and external surface areas slightly higher, and lower micropore surface, in comparison with the parent H-ZSM-5 material. Although these differences are close to the experimental error of the Ar adsorption

### 4.3. Catalytic fast pyrolysis of wheat straw over K-incorporated zeolites

measurements, it could also indicate that some mesoporosity has been created during the ion-exchange treatment, probably by desilication of the zeolite framework, as suggested by the slight decrease observed in the Si/Al ratio (**Table 4.3.1**).

In contrast with the small changes in the crystallinity and textural properties of the zeolite as a consequence of the partial  $K^+$  ion-exchange, this treatment has a strong effect on its acid-base properties. The acidity of the zeolite samples has been probed by ammonia TPD. As shown in **Figure 4.3.3.a**, two peaks are clearly seen in the ammonia TPD curve of the parent H-ZSM-5 catalyst that correspond with weak and strong acidic sites, having maxima at 187 and 358 °C, respectively. The first one represents about 35 % of the overall acidity in this sample, showing that most of its acidic sites are of high strength. Ion-exchange with  $K^+$  provokes a significant reduction of the acidity, in spite of the fact that alkali cations, ion-exchanged in zeolites, have been reported to behave as weak Lewis acidic sites [52,99,128]. In this way, the intensity of the signals corresponding to both weak and strong acidic sites is reduced in the KH-ZSM-5 sample, but with a more pronounced effect on the latter. Thus, whereas the peak corresponding to the weak acidic sites is still clearly visible for this material, the signal associated to the strong acidic sites is transformed into a broad signal in the range 250 – 400 °C. In overall, after the  $K^+$  ion-exchange, the total acidity of the zeolite probed by  $NH_3$ -TPD is almost reduced to half regarding the parent sample (**Table.4.3.1**).

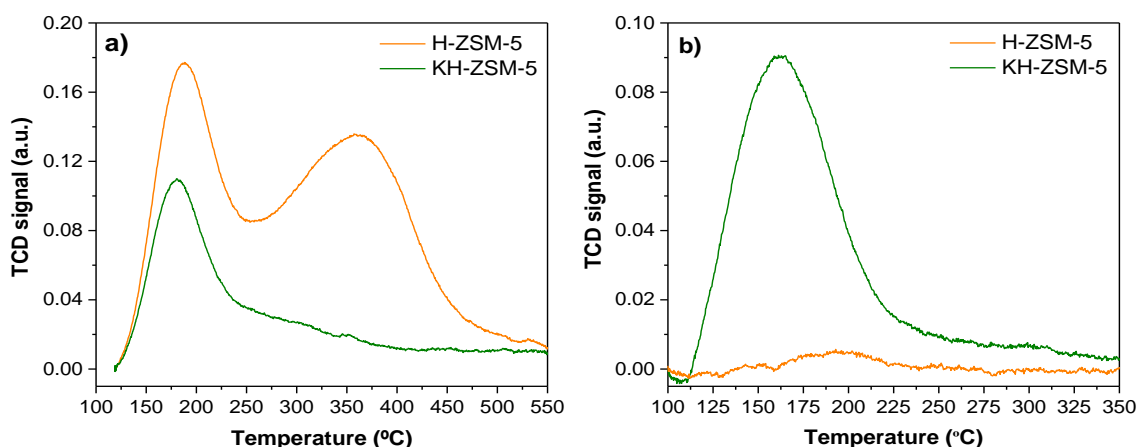


**Figure 4.3.3.** Acid-base properties of the catalyst samples: a)  $NH_3$ -TPD; b)  $CO_2$ -TPD.

On the other hand, the presence of basic properties in both zeolite samples has been investigated by  $CO_2$ -TPD. As depicted in **Figure 4.3.3.b**, just a very small and broad

signal is observed in the case of the H-ZSM-5 sample, denoting the lack of basicity in this material. However, an intense signal, centred at 160 °C, is present in the CO<sub>2</sub> TPD of the KH-ZSM-5 sample. This finding shows that basic sites have been generated in the zeolite sample as a consequence of the ion-exchange with K<sup>+</sup>. The overall basicity so estimated for this material is 0.46 mmol<sub>CO<sub>2</sub></sub>·g<sup>-1</sup>, value that is about twice the potassium content (0.21 mmol·g<sup>-1</sup>). Since in alkali-exchanged zeolites the basic properties arise from the framework oxygen sites [52,129], it can be envisaged that two CO<sub>2</sub> molecules are adsorbed in two oxygen atoms located in the vicinity of the ion-exchanged K<sup>+</sup> cations.

In conclusion, characterisation of the catalysts indicates that the zeolite crystallinity and its textural properties are mostly retained after partial ion-exchange with K<sup>+</sup> cations. However, this treatment strongly modifies and decreases the acidity of the parent sample, whereas it provokes the generation of basic sites. Accordingly, the KH-ZSM-5 material exhibits a combination of acid and basic properties with a good balance of both types of active sites.

### 4.3.1.2. Wheat straw catalytic tests

The performance of the KH-ZSM-5 catalyst in biomass pyrolysis (ws-ac as feedstock) has been investigated varying the catalyst to biomass ratio (C/B) in the range 0.2 – 0.8. All the experiments have been carried out using the same combination of temperatures for the thermal and catalytic zones: 550 and 450 °C, respectively. Under these conditions the amount of char, formed and accumulated in the thermal zone of the reactor, was very similar (about 17.1 wt.%). Fast pyrolysis tests carried out following the procedure 1 of bio-oil recovery are found in **Tables A.12 – A.18** in the Appendix.

**Figure 4.3.4.a** illustrates the evolution of the product distribution per fractions with the variation of the C/B ratio, including also the results obtained in a reference thermal test, carried out in the same conditions but with no catalyst in the second reaction zone. As it was expected, increasing the catalyst loading provokes important changes in the yield of the different fractions: progressive reduction of the bio-oil\* yield with and enhancement in the production of gases, water and coke, confirming that the organic liquid fraction is an intermediate product, being formed by pyrolysis of the biomass in the thermal zone and subsequently converted in the catalytic section of the reactor. This strong reduction in the bio-oil\* yield leads to a value of 28.8 % for the test with



### 4.3. Catalytic fast pyrolysis of wheat straw over K-incorporated zeolites

C/B = 0.8 that is almost half of that corresponding to the thermal experiment (57.9 %). Nevertheless, as shown in **Figure 4.3.4.b**, conversion of the bio-oil\* fraction is accompanied by a decrease of the bio-oil\* oxygen content from about 39.5 % in the thermal test down to 25.6 % for the catalytic test with C/B = 0.8.

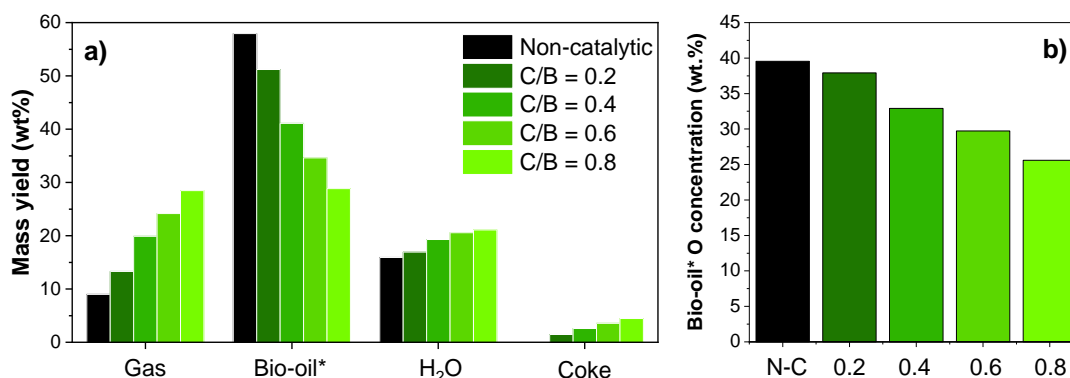


**Figure 4.3.4.** Catalytic fast pyrolysis of ws-ac over KH-ZSM-5 as a function of the C/B ratio: (a) mass yield of the fractions; (b) bio-oil\* oxygen content.

The variation of the C/B ratio caused also a strong increase in the yield of most of the non-condensable gases, as it can be appreciated in **Figure 4.3.5**. This effect is quite remarkable regarding the production of CO and, in a lesser extension of CO<sub>2</sub>, which are the final products formed in decarbonylation and decarboxylation reactions, respectively. Likewise, the yield of gaseous hydrocarbons is progressively enhanced with the C/B ratio, in particular of gaseous olefins (mainly propylene), formed by a combination of cracking and deoxygenation reactions. Finally, although in low concentration, the KH-ZSM-5 catalyst increases the production of H<sub>2</sub> in comparison with the thermal test.

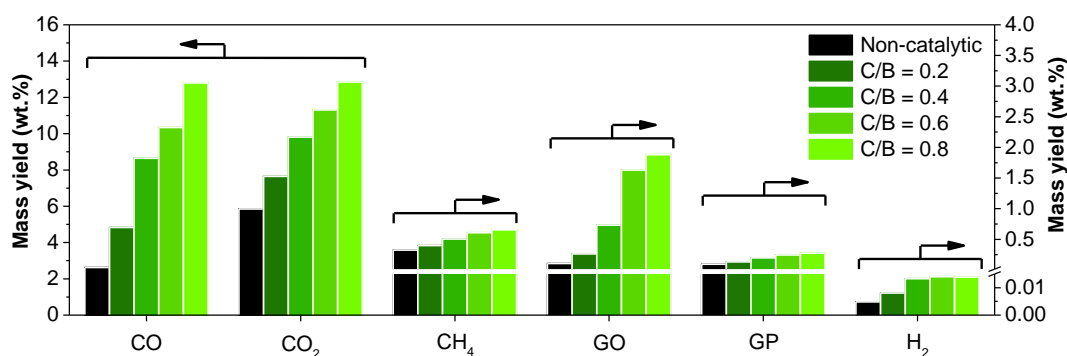


**Figure 4.3.5.** Catalytic fast pyrolysis of ws-ac over KH-ZSM-5 as a function of the C/B ratio: yield of the main components in the gas fraction. GO: gaseous olefins (C<sub>2</sub>–C<sub>4</sub>); GP: gaseous paraffins (C<sub>2</sub>–C<sub>4</sub>).



As reported in previous works of our research group [53,54,130], the overall efficiency of the bio-oil deoxygenation process can be assessed by the relationship between the yield and oxygen content of the organic liquid phase. Thereby, this relationship has been depicted in **Figure 4.3.6**. This figure illustrates the behaviour of the KH-ZSM-5 catalyst in regard to the parent H-ZSM-5 sample when varying the C/B ratio.

If both materials are compared at the same catalyst loading (i.e. for C/B = 0.2 and 0.6), it is evident that KH-ZSM-5 is less active than the parent zeolite, leading to a lower extension of deoxygenation and cracking reactions, as indicated by the higher yield and oxygen content of the bio-oil\* so produced. This is an expected result taking into account the lower overall acidity of the zeolite after the partial K<sup>+</sup> ion-exchange. However, this catalyst shows a more efficient deoxygenation pathway since, for the same or even lower oxygen contents, the bio-oil\* fraction is produced in clearly larger mass yields. The improved bio-oil\* deoxygenation efficiency of the KH-ZSM-5 could be assigned either to the attenuation of the acidity of H-ZSM-5 zeolite, to the generation of basic sites or to a combination of both effects.

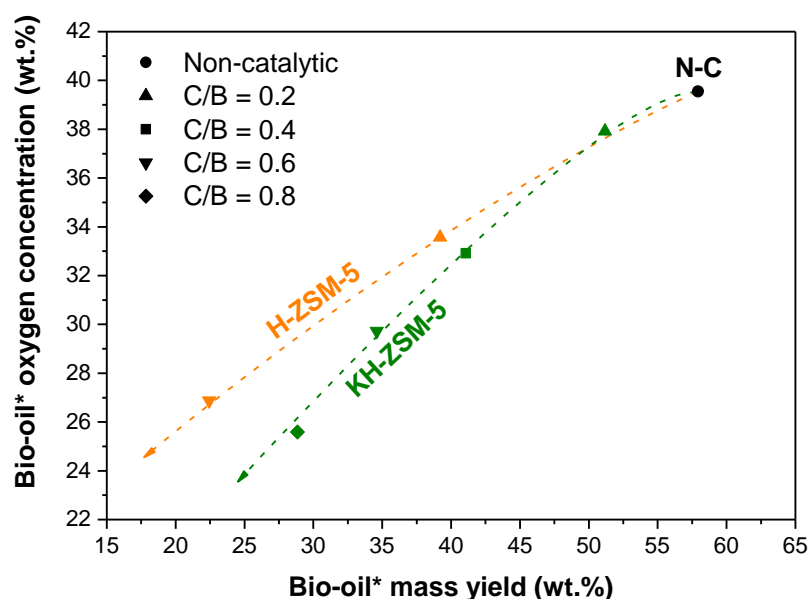


**Figure 4.3.6.** Relationship between mass yield and oxygen content of the bio-oil\* fraction in the catalytic fast pyrolysis of WS-ac over H-ZSM-5 and KH-ZSM-5 when varying the C/B ratio.

As previously mentioned, bio-oil deoxygenation involves three main deoxygenation pathways: dehydration, decarbonylation and decarboxylation. Using the thermal test as reference, the deoxygenation selectivities corresponding to the catalytic step can be

### 4.3. Catalytic fast pyrolysis of wheat straw over K-incorporated zeolites

estimated from the incremental productions of water, CO and CO<sub>2</sub> that occur when the pyrolysis products are passed through the catalyst bed. **Figure 4.3.7** illustrates the catalytic deoxygenation selectivities corresponding to the experiments carried out with C/B = 0.2 and 0.6 over the two catalysts. For the H-ZSM-5 catalyst the major pathway is decarbonylation, which reaches a selectivity of 52.7 % for C/B = 0.6, whereas dehydration has a very small contribution. When using the KH-ZSM-5 sample, the selectivity pattern is quite well balanced among the three deoxygenation routes. Thus, for C/B = 0.6 the three routes present a similar selectivity. The lower contribution of decarbonylation when using KH-ZSM-5 in comparison with the parent zeolite is a positive fact since it also contributes to improve the efficiency of the bio-oil\* deoxygenation process. This effect can be related to the removal of a great part of the strong acidic sites present in the zeolite by ion-exchange with K<sup>+</sup>, which catalyse decarbonylation reactions. In addition, the generation of basicity in the KH-ZSM-5 samples may have also a role in the changes observed in the deoxygenation selectivity since basic catalysts have been reported to promote ketonisation and aldol condensation reactions between the components of the bio-oil, leading to the formation of C–C bonds and the release of oxygen in the form of water and/or CO<sub>2</sub> [105,106,131,132].

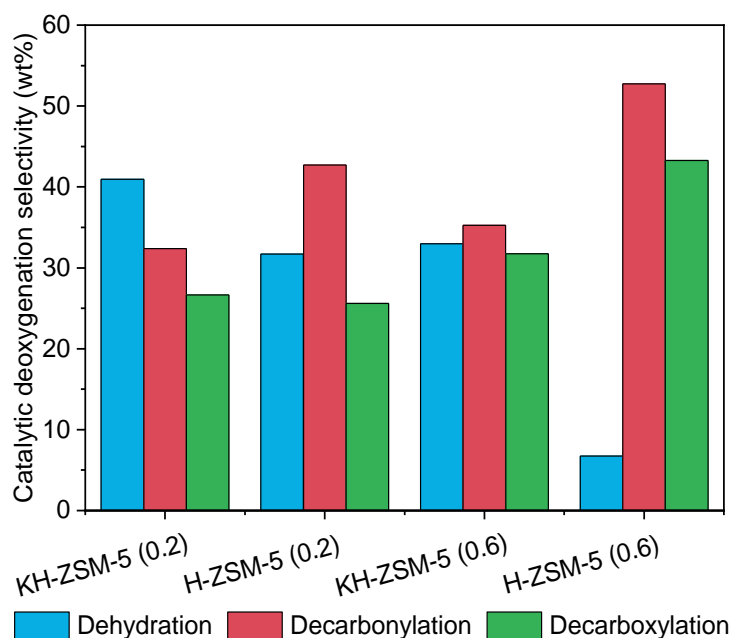


**Figure 4.3.7.** Catalytic fast pyrolysis of ws-ac over KH-ZSM-5 and H-ZSM-5 catalysts (C/B = 0.2 and 0.6): deoxygenation selectivity.

The components present in the bio-oil\* fraction have been determined by GC-MS, being grouped into families according to their chemical nature. By calibration of the most abundant components, the yield of each family has been determined. Moreover, by difference in respect to the total bio-oil\* yield, it has been possible to quantify the yield of the components in bio-oil\*, which are not detected or identified by the GC-MS analyses. The results so obtained with the KH-ZSM-5 and H-ZSM-5 catalysts for C/B = 0.2 are shown in **Figure 4.3.8.a** in terms of mass yields of both GC-MS detected and non-detected components. As a reference, this figure includes also the yields corresponding to the bio-oil\* produced in a pure thermal test. In this last case, the mass yield of the GC-MS detected species is 17 %, which represents just about 29 % of the overall bio-oil\* production, showing that oligomers are predominant in the organic liquid obtained in the thermal test. When using the H-ZSM-5 catalyst, the proportion of GC-MS detected species is increased up to 44 %. However, the mass yields of both GC-MS detected and non-detected components are reduced in respect to the thermal test. These results denote that the H-ZSM-5 catalyst is little effective for transforming the oligomers into compounds with molecular size / boiling points within the bio-oil\* fraction. In contrast, the KH-ZSM-5 material leads to quite larger yields of the GC-MS detected components in comparison with both the parent zeolite and the thermal test, which evidences that it is able of converting the oligomers into bio-oil\* components in a more effective way than the sole acid zeolite.

The positive effect on the conversion of oligomers, evidenced with the KH-ZSM-5 catalyst, can be assigned to the modifications produced in the acid-base properties of the zeolite by partial ion-exchange with  $K^+$ . In particular, it can be envisaged that the so created basic sites play an important role catalysing the transformation of oligomeric fragments into smaller species, but with a molecular size large enough to remain in the bio-oil\* fraction. In contrast, for the parent H-ZSM-5 material the predominant pathway seems to be the conversion of oligomers into gaseous components due to its high decarbonylation and cracking activity, in addition to its higher tendency for coke formation, all these results arising from the presence of strong acidic sites [53,133].

### 4.3. Catalytic fast pyrolysis of wheat straw over K-incorporated zeolites

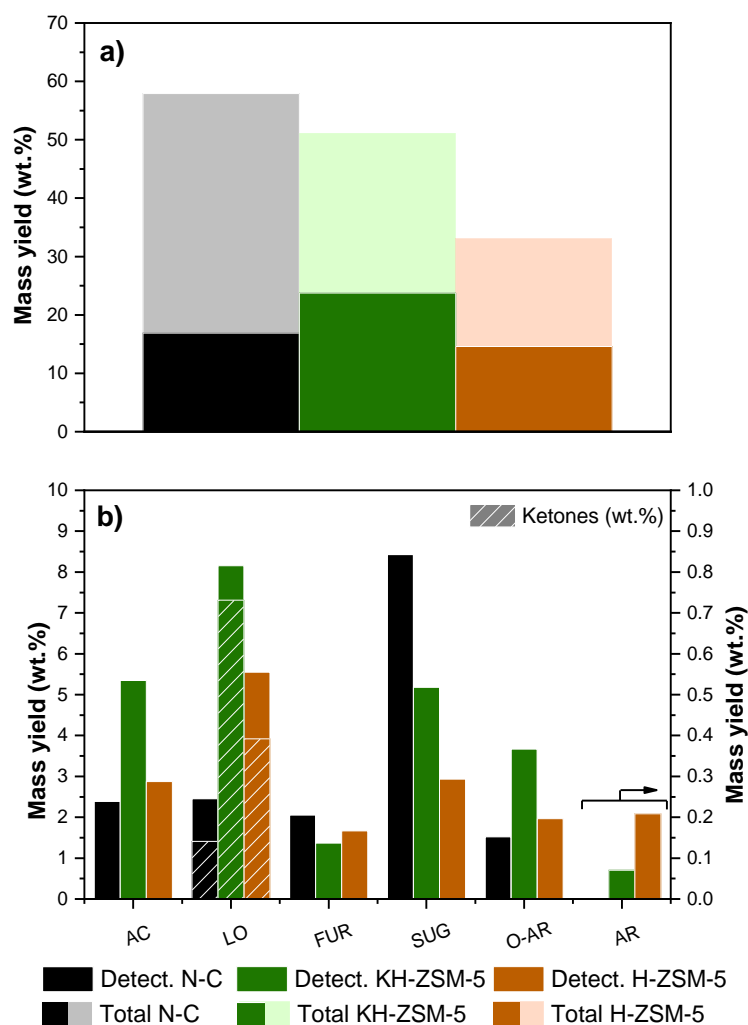


**Figure 4.3.8.** GC-MS analysis of the bio-oil\* obtained in the ws-ac pyrolysis over KH-ZSM-5 and H-ZSM-5 catalysts (C/B = 0.2): (a) mass yields of total/quantified components; (b) mass yield of the quantified components according to families of compounds.

Regarding the distribution of compounds in the bio-oil\* per families (**Figure 4.3.8.b**), in the case of the thermal test the main components are sugars (mainly levoglucosan) with a mass yield of 8.4 %, while the rest of the families (AC, LO, FUR and O-AR) are present with yields in the range 1.5 – 2.4 %). As expected, no hydrocarbons are detected in the thermal bio-oil\*. A drastic change in the distribution of these families occurs when using the H-ZSM-5 catalyst. Thus, a strong decrease of the SUG yield (down to 2.9 %) is observed whereas that of LO is augmented (up to 5.5 %) in respect to the thermal test, and just small variations are observed for the AC, FUR and O-AR families. In addition, although present in low concentrations, aromatic hydrocarbons are detected in the bio-oil obtained with the H-ZSM-5 material. These results are qualitatively in line with those reported in previous literature [28]. Significant

differences are observed when assessing the product distribution in the bio-oil\* produced over the KH-ZSM-5 catalyst. Thus, an enhanced production of AC, LO and O-AR takes place with this material in comparison with both the thermal test and the parent H-ZSM-5 catalyst. These results agree partially with those earlier reported by Mullen et al. [122], who observed that K-exchanged ZSM-5 catalysts favored significantly the formation of alkyl phenols. However, these authors also detected a strong increase in the production of furans, which is not the case of the current work. This fact is probably originated by the important differences existing between the reaction conditions employed, as in the earlier work the biomass catalytic pyrolysis tests were performed in a micropyrolyser operating with C/B ratios about 10 times higher than the ones here applied. In the current work, the largest variation in the bio-oil\* components over the KH-ZSM-5 catalyst is observed for the LO family, with a great share of ketones, which could be assigned to the ketonisation activity reported for basic catalysts. Although the reaction networks involving all these families, formed by hundreds of components, within the bio-oil\* fraction are really complex, these findings indicate that the lack of strong acidic sites and the presence of basicity in the KH-ZSM-5 catalyst provokes a significant change in the products distribution, increasing the yield of specific components that could be employed as raw chemicals.

### 4.3.2. K-grafted and parent USY zeolites

#### 4.3.2.1. Characterisation of the catalysts

K-USY sample was prepared by grafting of  $K^+$  cations over the surface of the parent USY zeolite, replacing  $H^+$  protons from silanol groups [33]. ICP-OES analysis showed that 1.59 wt.% of potassium was incorporated into the resulting material. This treatment involved exposure to a strong base solution, which caused a decrease in the Si/Al ratio (see **Table 4.3.2**), denoting the occurrence of some desilication of the zeolite framework. This fact is also reflected in the rougher surface and less defined morphology of the K-USY crystals in comparison with the parent zeolite, as observed in TEM and SEM images (**Figures 4.3.9 and 4.3.10**).

#### 4.3. Catalytic fast pyrolysis of wheat straw over K-incorporated zeolites

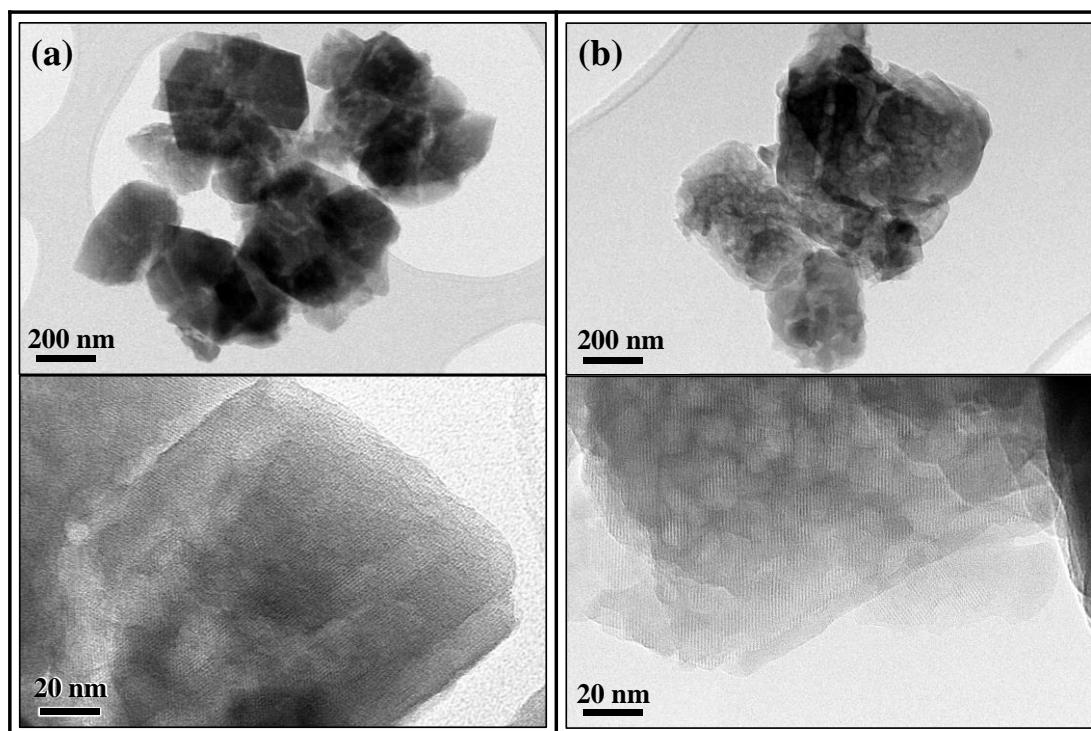


**Figure 4.3.9.** TEM images of: a) parent USY zeolite and b) K-grafted USY zeolite.

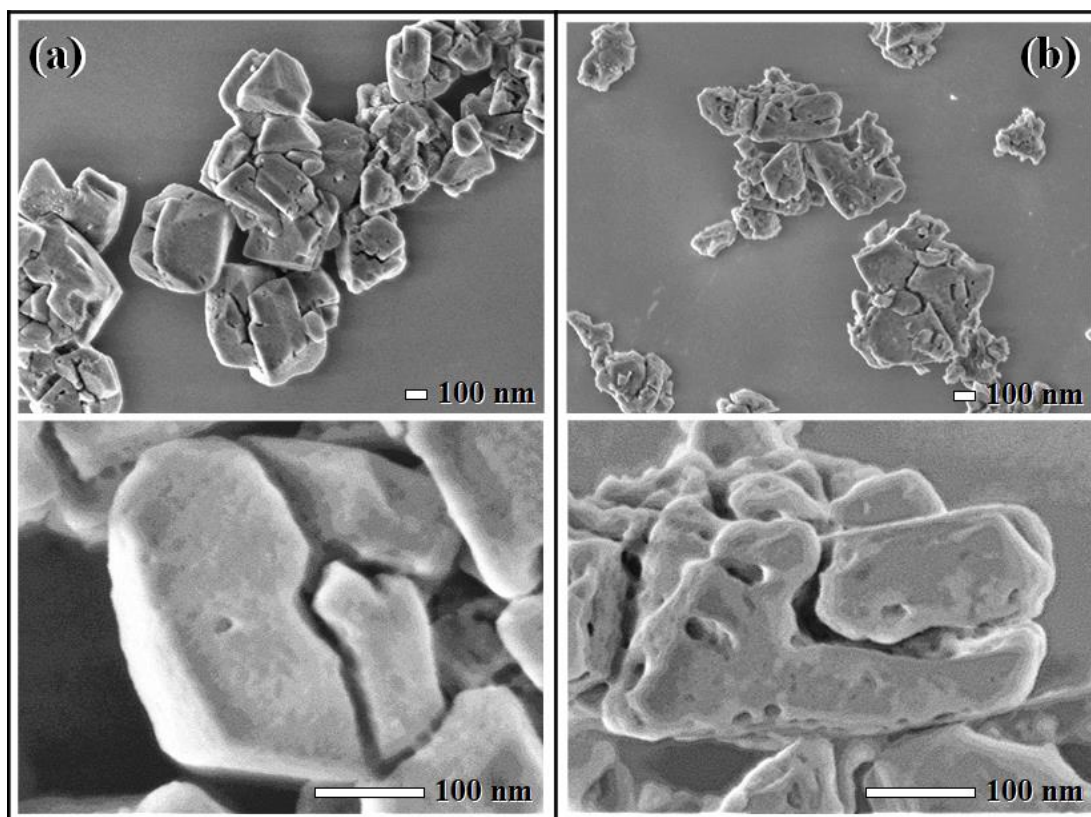


**Figure 4.3.10.** SEM images of: a) parent USY zeolite and b) K-grafted USY zeolite.



XRD patterns show the high crystallinity of the K-grafted USY sample (**Figure 4.3.11.a**), although with some decrease in the peaks intensity in comparison with the parent zeolite, which can be also related to the framework desilication as it may cause the formation of minor amounts of amorphous silica. On the other hand, the textural properties of the original USY zeolite were affected by potassium grafting. Both samples present basically type I  $N_2$  physisorption isotherms (**Figure 4.3.11.b**), which are typical of microporous materials. However, the application of the t-plot method shows the presence of significant external/mesopore surface area (**Table 4.3.2**). This fact can be related to the presence of some mesoporosity in both samples as denoted by the BJH pore size distribution depicted in **Figure 4.3.11.c**. In this way, mesopores are clearly seen in both TEM and SEM images (**Figures 4.3.9** and **4.3.10**), which are generated during the dealumination treatment applied for the USY preparation. After the potassium grafting treatment, a reduction in the values of the textural properties is observed. Thus, the micropore volume and surface area are decreased by about 18-19%, which can be assigned to some degradation of the zeolite structure, although the bulkier size of the incorporated  $K^+$  cations in respect to  $H^+$  may have also an effect on the micropore volume reduction. Conversely, as seen in the EDX analyses depicted in **Figure 4.3.12**, the potassium is evenly distributed over the entire surface of the K-USY sample.

**Table 4.3.2.** Physicochemical properties of the USY-based catalysts.

Sample	$m_K$ (wt.%)	Si/Al <sup>a</sup>	$S_{BET}^b$ (m <sup>2</sup> /g)	$S_{MES+EXT}^c$ (m <sup>2</sup> /g)	$S_{MIC}^d$ (m <sup>2</sup> /g)	$V_{TOT}^e$ (cm <sup>3</sup> /g)	$V_{MIC}^f$ (cm <sup>3</sup> /g)	Acidity <sup>g</sup> (mmol/g)		Basicity (mmol CO <sub>2</sub> /g)
								C <sub>B</sub>	C <sub>L</sub>	
USY	–	419	687	95	592	0.51	0.296	–	–	0.097
K-USY	1.59	346	574	88	486	0.46	0.239	–	0.018	0.587

<sup>a</sup>Atomic ratio; <sup>b</sup>BET surface area; <sup>c</sup>Mesopore+external surface area; <sup>d</sup>Micropore surface area; <sup>e</sup>Total pore volume ( $P/P_0 \approx 0.98$ ); <sup>f</sup>Micropore volume; <sup>g</sup>Determined by FT-IR/pyridine with C<sub>B</sub> and C<sub>L</sub> as concentration of Brønsted and Lewis acidic sites at 150 °C, respectively.

### 4.3. Catalytic fast pyrolysis of wheat straw over K-incorporated zeolites

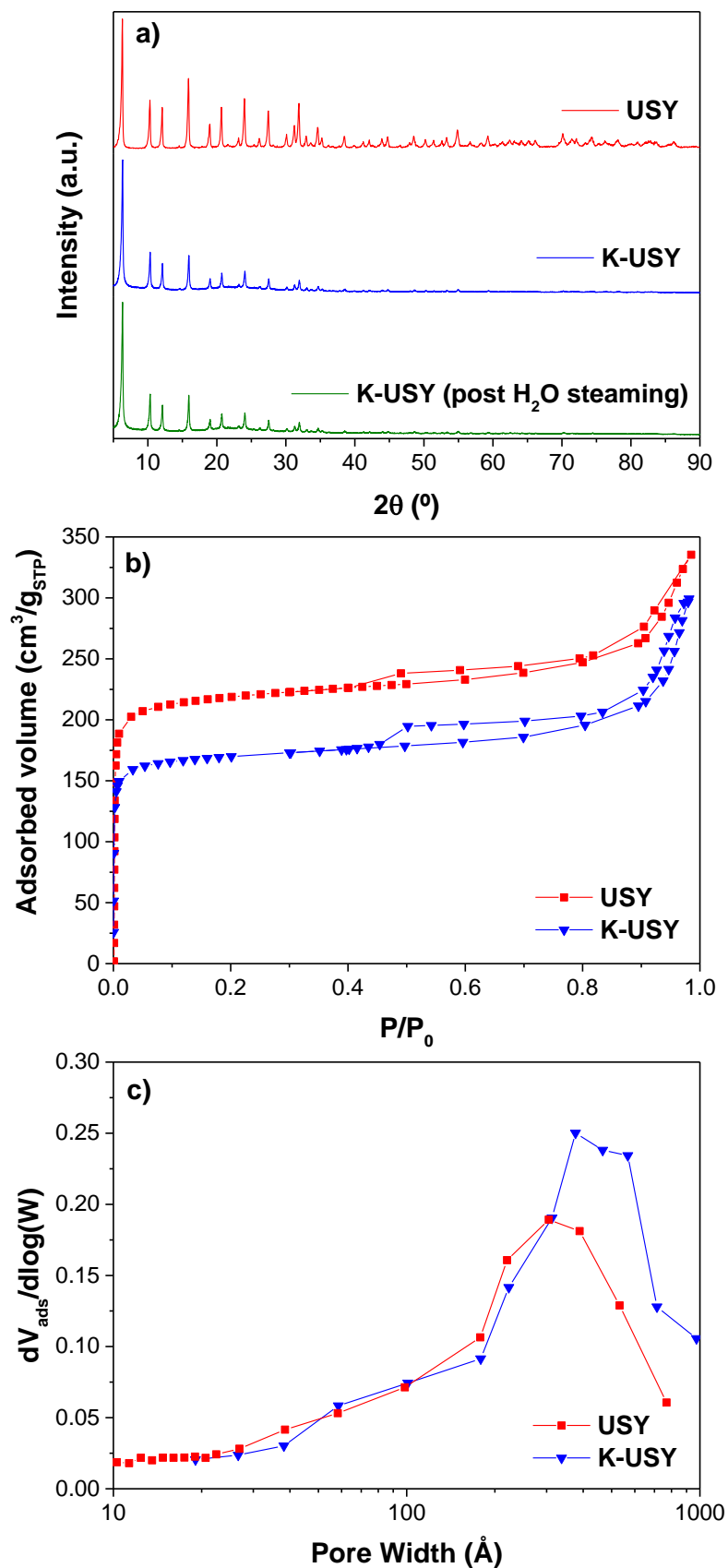


**Figure 4.3.11.** a) XRD patterns; b) N<sub>2</sub> adsorption-desorption isotherms at 77 K; c) BJH pore size distribution of the USY – based catalysts.



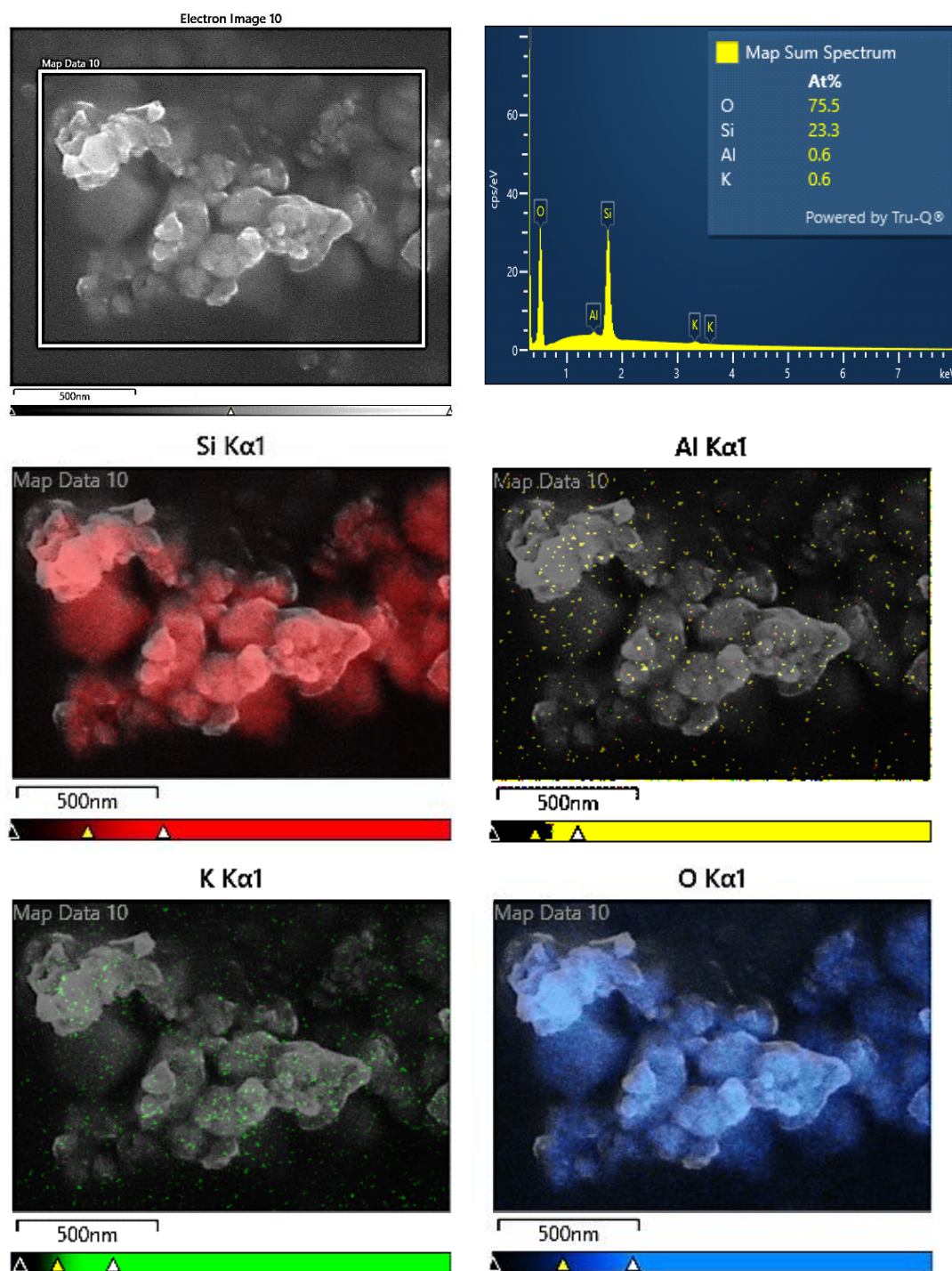


**Figure 4.3.12.** EDX analysis performed on K-grafted USY zeolite.

Acid-base properties of the parent USY zeolite were also significantly altered after K-grafting. The acidity of the samples was probed by ammonia TPD (**Figure 4.3.13.a**). Both samples present very low acidity, which is consistent with their high Si/Al ratios (346 and 419 for K-USY and USY, respectively). Nevertheless, K-USY catalyst showed a more marked ammonia TPD peak, centred at 177 °C. In the same way, FT-

### 4.3. Catalytic fast pyrolysis of wheat straw over K-incorporated zeolites

IR/pyridine measurements showed that for USY zeolite the concentration of acidic sites was below the detection limit (**Table 4.3.2** and **Figure 4.3.14**). In the case of the K-USY catalyst, only a low population of weak Lewis acidic sites (0.018 mmol/g at 150 °C), that did not remain at higher evacuation temperatures, was present. This residual Lewis acidity could be originated by a small proportion of  $K^+$  species being incorporated by ion-exchange with Al-associated protons (signals located at 1607 and 1588  $\text{cm}^{-1}$  in **Figure 4.3.14**). Weak Lewis acid sites were also detected at 1446  $\text{cm}^{-1}$  (H-bonded Py) [134]. Conversely, the interest of potassium grafting relies on the generation of basic sites, which was assessed by  $\text{CO}_2$  TPD (**Figure 4.3.13.b**). USY zeolite exhibited a small and broad signal with a peak maximum at 220 °C. In contrast, an intense signal was observed in the  $\text{CO}_2$  TPD of the K-USY sample, confirming that the grafting was successful in generating basic sites. The peak maximum in this case is placed at 83 °C, although the signal is quite asymmetrical and extends up to significantly higher temperature, showing the presence of basic sites with different strength. The overall basicity of the K-USY sample (0.587  $\text{mmol}_{\text{CO}_2}/\text{g}_{\text{sample}}$ ) is six times higher than that of the parent zeolite, confirming that potassium grafting fulfils its purpose of generating basic sites with weak-medium strength.

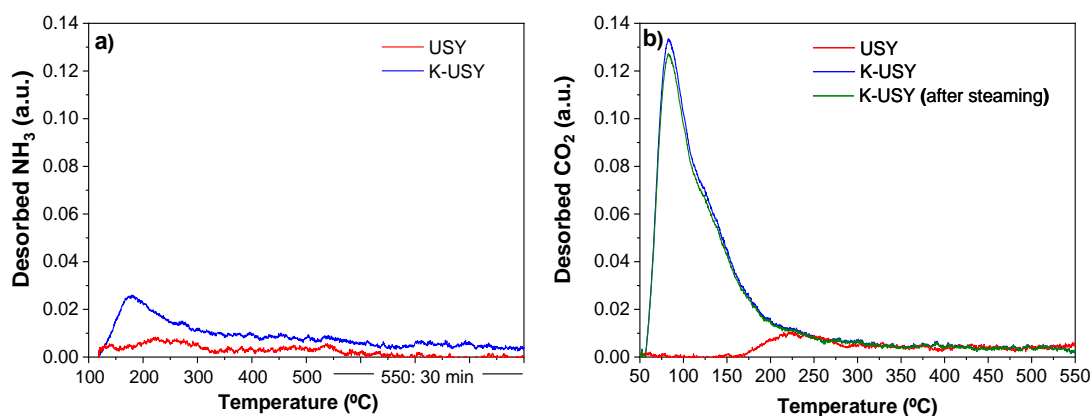


**Figure 4.3.13.** Acid-base properties of the USY-based catalysts: a)  $\text{NH}_3$ -TPD; b)  $\text{CO}_2$ -TPD.

In addition, stability tests for the K-USY zeolite were performed by steaming 2 g/h  $\text{H}_2\text{O}$  over K-USY zeolite at 450 °C for 30 min, using a catalyst/water ratio (1.6:1 g/g) similar to that occurring during the pyrolysis tests performed. XRD patterns show that the zeolite barely loses crystallinity and preserves its integrity (**Figure 4.3.11.a**). On the other hand, the total surface area was decreased by 10 % respecting the fresh K-

USY zeolite, which is within the error of this analysis. Finally, to assess the possible hydrolysis of the K-OSi linkages, which are the origin of the basic properties of this material, CO<sub>2</sub>-TPD was also performed for the sample after the steaming treatment (**Figure 4.3.13.b**). The profile of the curve and the overall basicity of the steamed material were practically identical to those of the fresh K-USY zeolite, showing that the concentration and strength of the basic sites are not modified by the applied steaming treatment.

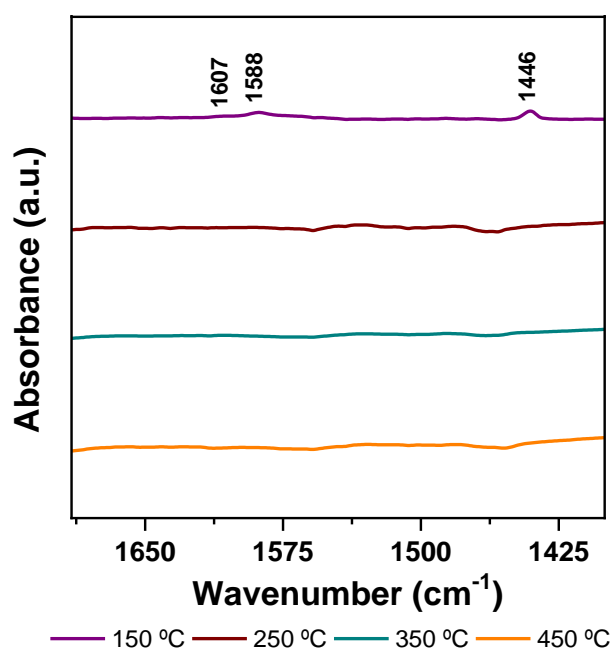


**Figure 4.3.14.** Pyridine adsorption FT-IR spectra after treating the K-grafted USY zeolite at different desorption temperatures (150, 250, 350, and 450 °C).

#### 4.3.2.2. Effect of catalyst to biomass ratio on K-grafted and parent USY zeolites

USY and K-USY samples were tested in catalytic fast pyrolysis (CFP) of acid-washed wheat straw (ws-ac). Experiments were carried out varying the catalyst to biomass ratio (C/B) from 0.2 to 0.6. A reference non-catalytic (N-C) experiment was also performed for comparison purposes (**Tables A.1, A.19 – A.22** in the Appendix) . The conditions employed initially for the thermal and catalytic zones were 550 and 450 °C, respectively. Nevertheless, the effect of the catalytic bed temperature was further investigated in the range 400 – 500 °C. Since the thermal pyrolysis step is common to all trials, the amount of char formed in the upper part of the reactor was very similar with an average value of 17.8 wt.% rate. Mass yields of the different fractions obtained

### 4.3. Catalytic fast pyrolysis of wheat straw over K-incorporated zeolites

in the catalytic pyrolysis of the acid-washed wheat straw over both USY and K-USY zeolites at two different C/B ratios is shown in **Figure 4.3.15.a**, including also the results of the reference thermal test.

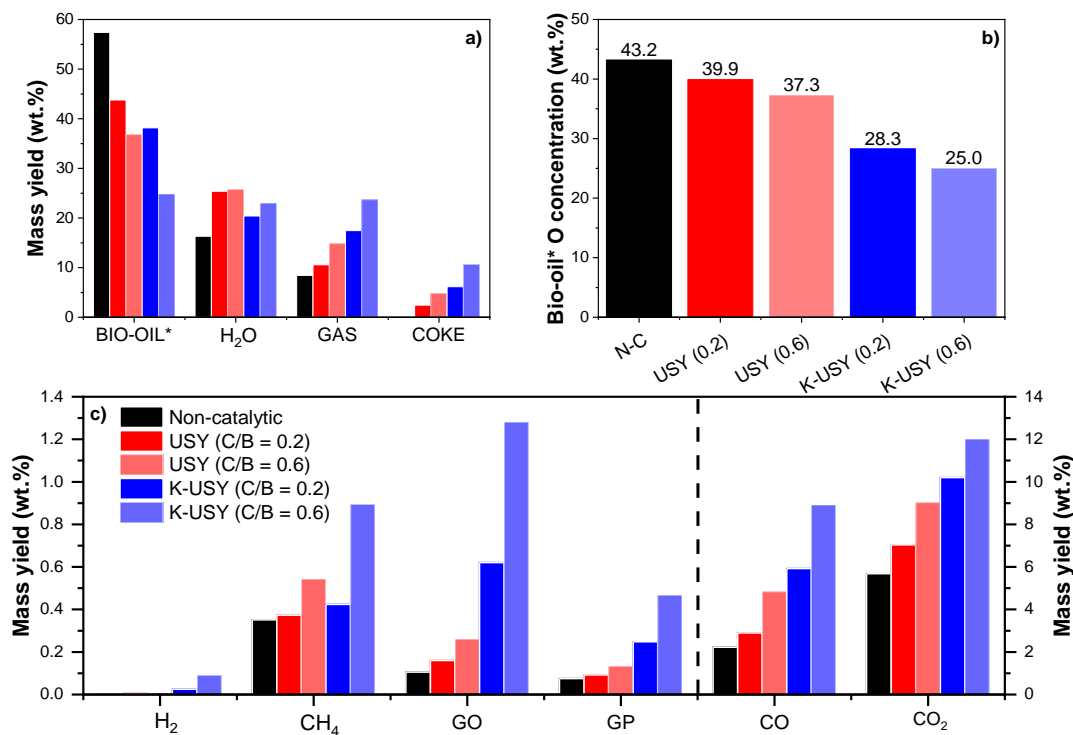


**Figure 4.3.15.** Catalytic pyrolysis of ws-ac over USY-based samples: a) fractions yield; b) bio-oil\* oxygen concentration (dry basis); c) gaseous components yield (GO: gaseous olefins, GP: gaseous paraffins).

It is observed that the presence of the catalyst, and the increase of the C/B ratio, resulted in a significant reduction of the bio-oil\* yield and a subsequent enhancement of the production of coke, water, and non-condensable gases. This finding is a consequence of the variety of transformations undergone by the bio-oil\* vapours when passing through the catalyst bed, such as deoxygenation and cracking. The changes in the product distribution are quite more pronounced for the K-USY catalyst, denoting the high activity of their basic sites, which are practically absent in the parent zeolite. This effect is also clearly seen in the bio-oil\* oxygen content (**Figure 4.3.15.b**), which is strongly reduced over the K-USY catalysts, passing from 43.2 wt.% in the thermal test to 25 wt.% for C/B = 0.6. In contrast, this parameter is quite less modified when using the USY sample due to its low concentration of both acidic and basic sites.

The deoxygenation of the bio-oil\* can occur via three main pathways: decarbonylation, decarboxylation and dehydration, leading to the formation of CO, CO<sub>2</sub> and H<sub>2</sub>O, respectively [107,135]. As seen in **Figure 4.3.14.c**, the main components of the non-condensable gases were CO and CO<sub>2</sub>, whose yield increased sharply with the C/B ratio, this fact being more pronounced for the K-USY catalyst in good agreement with its higher activity in comparison with the USY sample. However, the opposite is observed regarding the water yield which is higher over the USY sample than when using the basic zeolite. The deoxygenation selectivity of the two catalysts have been calculated from the incremental production of H<sub>2</sub>O, CO and CO<sub>2</sub> with respect to the thermal test, being represented in **Figure 4.3.16**. Dehydration is the predominant pathway over USY zeolite, although it seems to be little effective to reduce the oxygen content of the bio-oil\*. Conversely, the basic K-USY catalyst exhibits a more balanced deoxygenation pattern with a rather higher contribution of both decarbonylation and decarboxylation than the parent zeolite. Moreover, the deoxygenation selectivity of the K-USY sample is just slightly modified by the increase of the C/B ratio.

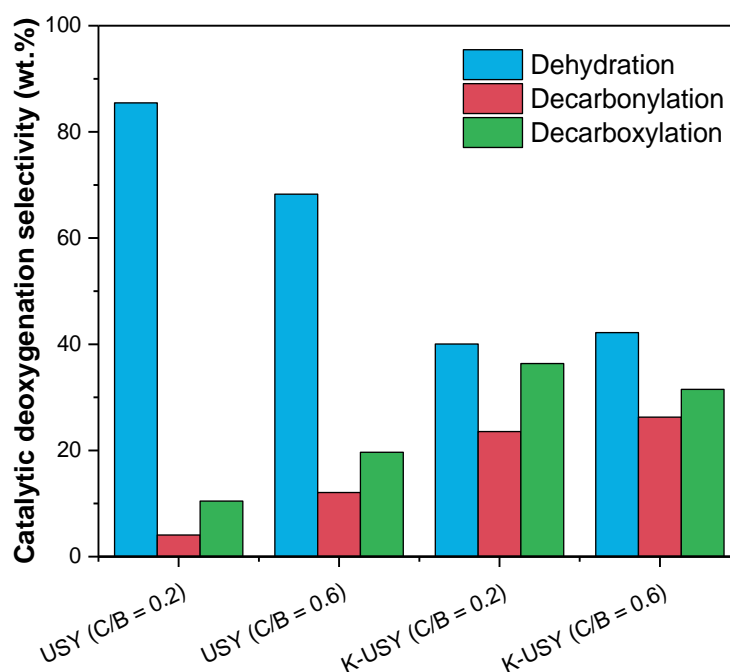


**Figure 4.3.16.** Catalytic deoxygenation selectivity, estimated from the incremental production of H<sub>2</sub>O, CO and CO<sub>2</sub> regarding the thermal pyrolysis test, obtained in the ws-ac pyrolysis over USY - based catalysts.

### 4.3. Catalytic fast pyrolysis of wheat straw over K-incorporated zeolites

In addition to deoxygenation, other types of reactions taking place in the presence of the catalysts are cracking and coke formation, which in general are non-desired transformations as they contribute to reduce the bio-oil yield and/or provoke the catalyst deactivation. Severe cracking reactions, combined with deoxygenation, lead to the formation of different types of gaseous hydrocarbons (methane and both light olefins and paraffins), as shown in **Figure 4.3.15.c**. For the highest C/B ratio, the K-USY sample exhibits a rather enhanced production of methane, as well as of C<sub>2</sub> – C<sub>4</sub> olefins, regarding the parent zeolite. Thus, under these conditions, up to about 0.9 wt.% and 1.3 wt.% yields of methane and gaseous olefins, respectively, are obtained over K-USY. The superior activity of the basic zeolite sample in comparison with the parent USY is also reflected in the increased production of H<sub>2</sub> at C/B = 0.6 due to the extension of dehydrogenation reactions.

Coke formation is also more pronounced over the K-USY catalysts, as illustrated in **Figure 4.3.15.a**. This carbonaceous solid is produced through successive oligomerisation and polymerisation reactions and deposited on the surface of the catalysts, blocking the access to the zeolite channels and active sites. In general terms, the coke amounts here measured during the ws-ac catalytic pyrolysis over the USY zeolite is significantly higher than those obtained over medium pore slites, such as ZSM-5 [136], with this type of feedstock. The presence of large pores and cavities in zeolites with faujasite structure are the major reasons that explain the high coke contents of the catalysts, being in the range 7.4 – 23.2 wt.% (**Table 4.3.3**). The formation of this undesirable by-product was enhanced linearly with the C/B ratio and was especially noticeable over the K-USY sample as a consequence of their superior activity. This means that, from a practical point of view, reaction systems affording a fast catalyst regeneration would be necessary, such as circulating fluidised-bed reactors. On the other hand, significant variations can be noticed in **Table 4.3.3** between the coke elemental composition for both zeolite catalysts. Thus, the coke produced over the USY catalyst at C/B = 0.6 possesses more hydrogen but lower oxygen content. The removal of this oxygen is expected to have proceeded mainly in the form of water, according to the above commented high dehydration selectivity over USY. Therefore, a part of the increased water production over the parent zeolite is not really linked to bio-oil\* deoxygenation but it is due to coke dehydration reactions. However, this is not the case of the K-grafted zeolite as the coke fraction contains a



high share of oxygen (up to 29.9 wt.% for C/B = 0.6, **Table 4.3.3**). This fact indicates a change in the nature of the species retained in this catalyst with the increase of the C/B ratio, shifting towards the accumulation of highly oxygenated species, originated probably from levoglucosan and furfural, which are the main components of the sugar and furan families, respectively, as commented below when discussing the bio-oil\* GC-MS analyses. In summary, the introduction of basic sites in the K-USY sample induces important changes in the amount and nature of the carbonaceous matter deposited over the catalyst surface.

**Table 4.3.3.** Char and coke composition obtained in the catalytic pyrolysis of ws-ac over USY-based samples.

Experiment	Fraction	Coke in catalyst (wt.%)	Mass yield (wt.%)	Elemental analysis (wt.%, dry basis)			
				C	H	N	O
N-C	Char	–	17.8	78.7	2.7	0.9	10.5
USY-0.2	Coke	10.9	2.4	77.9	5.8	–	16.3
USY-0.6		7.4	4.8	87.6	5.9	–	6.5
K-USY-0.2		23.2	6.1	78.7	3.4	–	17.9
K-USY-0.6		14.1	10.6	67.2	3.0	–	29.9

Detailed information about the molecular composition of bio-oils\* has been obtained by means of GC-MS analyses, using calibration methods of the major components present in each family to get quantitative data in terms of mass yield and concentration. Moreover, from these results it has been possible to calculate the overall yield and concentration of both GC-MS detected and non-detected components, the latter being estimated by difference. As illustrated in **Figures 4.3.17.a** and **4.3.17.b**, for the bio-oil\* obtained in the thermal pyrolysis test, the yield of the GC-MS detected components is about 10 wt.%, whereas their overall concentration in the organic liquid fraction is just 19 wt.%. Therefore, the major part of this bio-oil\* is formed by heavy species (oligomers) that may have different origins. They can be compounds coming from the partial decomposition of the lignocellulose biopolymers (cellulose, hemicellulose and lignin). Alternatively, they could be bulky species generated in secondary condensation reactions involving the most reactive components present in bio-oil\*.

### 4.3. Catalytic fast pyrolysis of wheat straw over K-incorporated zeolites

As observed in **Figure 4.3.17**, the USY catalyst exhibited negligible beneficial effects for transforming biopolymers into simpler compounds, not even increasing their concentration. Accordingly, the yield nor the proportion of GC-MS detected components do not improve when increasing the C/B ratio over the USY sample. Conversely, the K-USY catalyst leads to a noticeable increase in the yield of GC-MS detected species when working at C/B = 0.2, suggesting that the basic sites of this material are able to catalyse the conversion of oligomeric compounds into lighter ones (**Figure 4.3.17.a**). Thus, the bio-oils\* produced over the K-USY catalyst possess concentrations of GC-MS detected components in the range 37 – 40 wt.%, i.e. double than that corresponding to the thermal pyrolysis test (**Figure 4.3.17.b**).

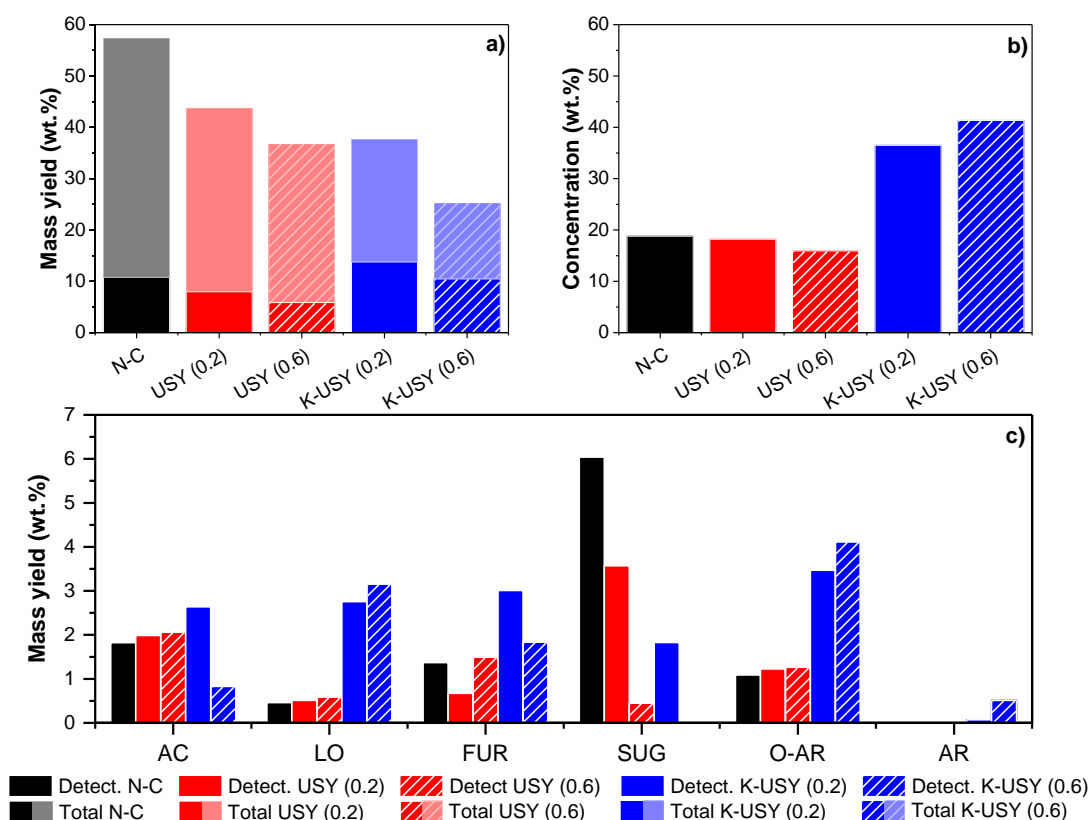


**Figure 4.3.17.** GC-MS analyses of the bio-oil\* obtained in the ws-ac catalytic pyrolysis over USY-based samples: a) overall mass yields; b) overall concentration of GC-MS detected components; and c) mass yields of compound families (AC: carboxylic acids, LO: light oxygenates, FUR: furans, SUG: anhydrosugars, O-AR: oxygenated aromatics and AR: aromatic hydrocarbons).

**Figure 4.3.17.c** illustrates the product distribution per family in the bio-oil\* fraction. Concretely, bio-oil\* from the non-catalytic test contained mainly sugars (assimilable to levoglucosan) with a mass yield of 6 wt.%. Other families found in this bio-oil\*



(AC, LO, FUR and O-AR) do not exceed 2 wt.% yields, whereas aromatic hydrocarbons were absent. When using USY zeolite, the mass yields of most of these families did not vary significantly with the increase of the C/B ratio. However, the levoglucosan yield declined sharply with the USY catalyst loading, being transformed into non-condensable gases and coke. This finding confirms the lack of effectiveness of the USY zeolite for bio-oil\* upgrading.

In contrast, a very different picture arises when assessing the composition of the bio-oils\* produced over the K-USY catalyst. In this case, whereas the SUG yield declined with the C/B ratio until their total depletion, an increase was observed in the production of the rest of the families for C/B = 0.2 regarding the thermal experiment. On the other hand, for the highest C/B ratio (0.6), i.e. for longer contact times, the production of AC and FUR decreased whereas those of LO, O-AR and AR further augmented. The important reduction in the AC yield can be connected with the occurrence of acetic acid cracking reactions, thus contributing to the sharp increase observed in the yield of methane, CO and CO<sub>2</sub> with the C/B ratio (see **Figure 4.3.15.c**). It can be envisaged that the presence of basic sites in the catalyst favours the interaction with acetic acid and its subsequent conversion. In the case of FUR, consisting of furfural as the major component, the oxygen content of the coke fraction reported in **Table 4.3.3** (29.9 wt.%) is quite close to that of this component (33.3 wt.%), suggesting that it may act as one of the main precursors for the formation and accumulation of carbonaceous matter over the catalyst at C/B = 0.6. The increase in the O-AR and AR yields denotes the capability of the K-USY catalyst to achieve the conversion of lignin oligomers into lighter and more valuable aromatic compounds. Substituted monoaromatics become the major family of AR compounds, most of them formed by toluene and xylene, representing around 65 wt.% of this family, whereas the rest correspond to indenenes and polyaromatics. Therefore, the incorporation of basicity via K-grafting of the USY zeolite presents clear advantages in biomass CFP, provoking a deeper bio-oil\* deoxygenation and doubling the concentration of valuable components. Further insights about the composition of these upgraded bio-oils\*, as well as on the different reactions taking place, is provided in the next section.

### 4.3. Catalytic fast pyrolysis of wheat straw over K-incorporated zeolites

#### 4.3.2.3. Effect of both catalytic zone temperature and catalyst to biomass ratio on K-grafted USY zeolite

In order to complete the study of the K-USY performance in ws-ac CFP, as well as to maximise the production of valuable compounds in the bio-oil\*, the temperature of the catalytic zone was varied from 400 to 500 °C. For each temperature, two C/B ratios (0.2 and 0.6) were employed. In addition, the results of the thermal pyrolysis test were included as a reference, similarly to the previous section (**Tables A.1, A.21 – A.26** in the Appendix).

The results obtained in these experiments in terms of fraction yields and bio-oil\* oxygen content are depicted in **Figures 4.3.18.a** and **4.3.18.b**, respectively. In general, it can be appreciated that the effect of the temperature is less marked than that of the C/B ratio. Moreover, the increase of the temperature presents in some cases opposite trends depending on the value of the C/B ratio. This is particularly observed in the case of the bio-oil\* yield that is slightly enhanced with the temperature for C/B = 0.2, (from about 34 up to 39 wt.%), whereas a decreasing effect is observed at C/B = 0.6 (from about 25 to 20 %). This finding can be interpreted as a result of the intermediate character of many bio-oil components, which are formed from primary cracking reactions but are subsequently converted into other fractions (gases, water and coke) through secondary transformations, which become predominant when working at high C/B ratios.

On the other hand, the variation of the temperature in the catalytic zone does not almost change the bio-oil\* oxygen content, showing values of 29 and 25 wt.% for C/B = 0.2 and 0.6, respectively. When using acid catalysts in biomass catalytic pyrolysis, the major pathway contributing to bio-oil deoxygenation is the formation of aromatic hydrocarbons. However, the extension of aromatisation reactions is very low over the K-USY catalyst. Accordingly, a limit of bio-oil\* oxygen content of about 25 wt.% is reached when increasing the temperature and the C/B ratio.

While no clear trend is noticed for the temperature effect on the water yield, the production of non-condensable gases augmented with this variable, especially when working with C/B = 0.6. **Figure 4.3.18.c** shows the evolution of the different gaseous components with the temperature at the two investigated C/B ratios. The production of GO, GP, CO and H<sub>2</sub> increases continuously with both the temperature and the C/B

ratio, showing that these variables favour the occurrence of cracking, decarbonylation and dehydrogenation reactions. In the case of methane production, the variation is not linear but a sharp increase in its yield is appreciated when augmenting the temperature from 450 to 500 °C.

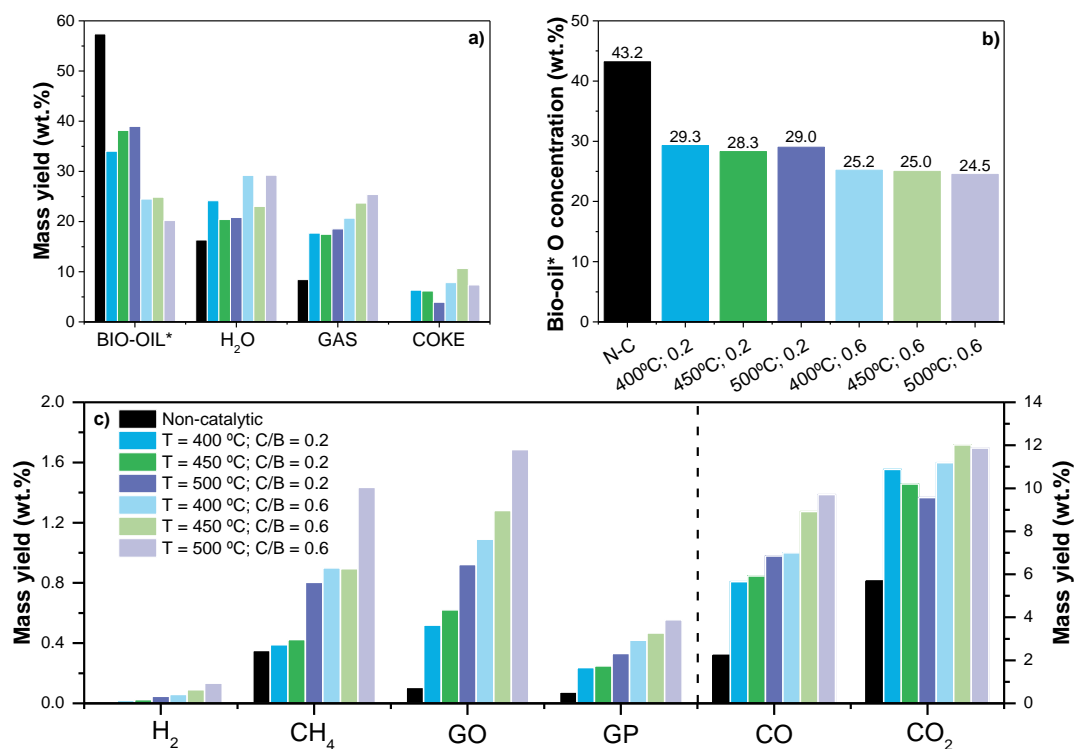


**Figure 4.3.18.** Catalytic pyrolysis of ws-ac over K-USY sample at different temperatures and C/B ratios: a) fractions yield; b) bio-oil\* oxygen concentration (dry basis); c) gaseous components yield (wt.%) (GO: gaseous olefins, GP: gaseous paraffins).

On the other hand, the evolution of the CO<sub>2</sub> yield with the temperature presents a relatively complex behaviour, as it shows a decreasing trend at C/B = 0.2 but tends to be enhanced at C/B = 0.6. To explain this finding, it should be considered that CO<sub>2</sub> can be formed by decarboxylation of a variety of oxygenated groups. Moreover, decarboxylation and decarbonylation are in part competitive deoxygenation processes, being affected in a different manner by the increase of the temperature. As shown in **Figure 4.3.19**, the CO/CO<sub>2</sub> ratio is augmented with both the C/B ratio and the temperature. This last fact indicates that, overall, the activation energy of the decarbonylation reactions is higher than that of decarboxylation processes over the basic K-USY catalyst.

### 4.3. Catalytic fast pyrolysis of wheat straw over K-incorporated zeolites

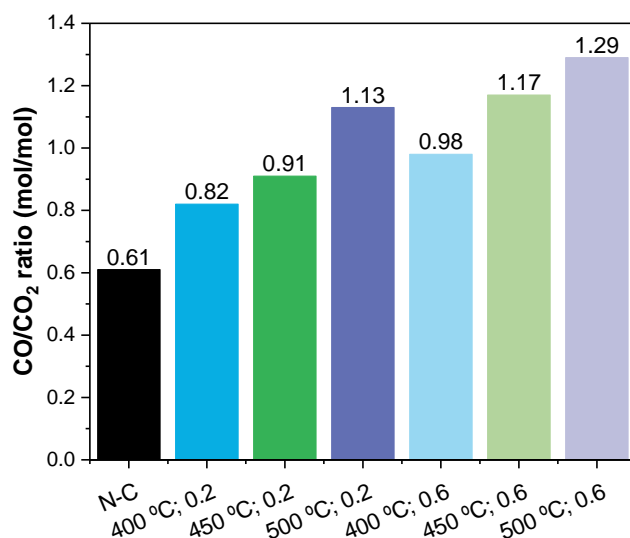


**Figure 4.3.19.** CO/CO<sub>2</sub> ratio obtained in the pyrolysis of ws-ac over K-USY zeolites at different temperatures and C/B ratios.

Analogously to the previous section, GC-MS was employed to determine and identify the components present in the bio-oil\* fraction. As depicted in **Figure 4.3.20.a**, the overall yield of GC-MS detected components remains practically constant with the temperature but showing lower values for the tests performed at C/B = 0.6. Moreover, for this catalyst loading, the overall yield of non-detected GC-MS species is progressively reduced with the temperature. Accordingly, as shown in **Figure 4.3.20.b**, the concentration in the bio-oil\* of GC-MS detected components is significantly enhanced with the temperature reaching a value of c.a. 47 wt.% at 500 °C. In other words, extensive conversion of bio-oil\* into other fractions occurred when the C/B ratio was increased to 0.6, but this organic liquid phase become richer in valuable compounds, especially when working at 500 °C and C/B = 0.6.

The distribution of GC-MS components per family obtained in these experiments using the K-USY catalyst is shown in **Figure 4.3.20.c**. The results obtained varying the two operational parameters (temperature and C/B ratio) confirm most of the conclusions stated in the previous section. In this way, SUG (i.e. levoglucosan), which is formed from the decomposition of holocellulose fragments, are converted into FUR first and then to smaller oxygenated molecules (LO and AC) in series, in addition to the likely transformation of sugars into the other fractions (mainly gases and coke). Due to the weak-mild strength of the basic sites present in the studied K-grafted zeolite, it seems these transformations are more pronounced with the increase of the C/B ratio rather than by rising the temperature.

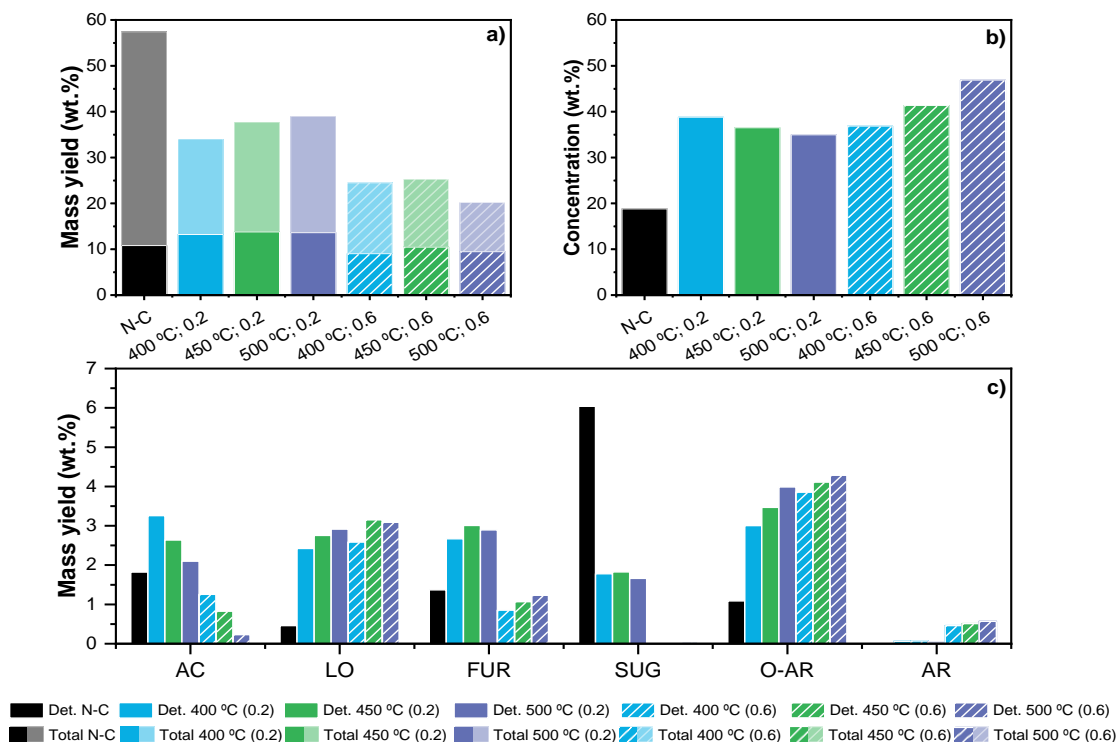


**Figure 4.3.20.** GC-MS analyses of the bio-oil\* obtained in the ws-ac catalytic pyrolysis over K-USY sample: a) overall mass yields; b) overall concentration of GC-MS detected components; and c) mass yields of compound families (AC: carboxylic acids, LO: light oxygenates, FUR: furans, SUG: anhydrosugars, O-AR: oxygenated aromatics and AR: aromatic hydrocarbons).

Another noticeable fact is the progressive reduction of the AC yield when increasing the temperature, which can be assigned to cracking into gaseous compounds as the yield of CH<sub>4</sub> and CO is also enhanced. Finally, the conversion of lignin fragments over the potassium grafted USY zeolite is also favoured at higher temperatures, as denoted by the increasing yields of O-AR and AR, which reach values of 4.3 and 0.6 wt.%, respectively. In short, it is observed how the production of compounds of interest included in LO and O-AR families are enhanced when both C/B ratio and temperature of the catalytic zone are increased, reaching a maximum at C/B = 0.6 and 500 °C, while the yield of SUG, FUR and AC families is sharply reduced. Accordingly, K-USY not only favours the production of added-value compounds, but it also reduces the presence of the most reactive molecules (sugar derivatives), which hinder their latter purification via distillation, and of carboxylic acids (mainly acetic acid), responsible of the low bio-oil\* pH, preventing corrosion problems that could appear in the subsequent processing of this fraction.

### 4.3. Catalytic fast pyrolysis of wheat straw over K-incorporated zeolites

**Table 4.3.4** discloses the concentration in the bio-oil\* fraction of the main components included in the O-AR family. Mono-O-AR are important raw materials in the chemical industry, which at present are obtained mainly from fossil sources [137]. Among the O-AR produced over the K-USY catalyst, guaiacols and phenols subfamilies are predominant, being reaction intermediates and final products, respectively, as concluded from their variation with the increment of both temperature and catalyst loading. Most of the guaiacols are produced with maximum concentrations at C/B=0.2 and temperatures between 400-450 °C. Creosol, guaiacol, isoeugenol and ethylguaiacol are the most important compounds of this group. They present a variety of uses in industry, such as starting materials for the preparation of cosmetics and pesticides and as platform molecules in pharmacy [125].

**Table 4.3.4.** Concentration (wt.%) of the main O-AR components present in the bio-oil\* produced by ws-ac catalytic pyrolysis over K-USY sample at different temperatures and C/B ratios.

C/B ratio (g/g)	N-C	0.2			0.6		
T <sub>catalysis</sub> (°C)	450	400	450	500	400	450	500
<b>Acetophenones</b>	<b>0.10</b>	<b>0.32</b>	<b>0.28</b>	<b>0.35</b>	<b>0.19</b>	<b>0.25</b>	<b>0.23</b>
<b>Anisols</b>	-	-	-	-	<b>0.16</b>	-	<b>0.65</b>
<b>Benzalacetones</b>	<b>0.02</b>	-	-	-	<b>0.06</b>	-	<b>0.14</b>
<b>Benzaldehydes</b>	<b>0.14</b>	<b>0.19</b>	<b>0.11</b>	<b>0.43</b>	<b>1.03</b>	<b>0.35</b>	<b>0.94</b>
<b>Benzyl alcohols</b>	-	<b>0.03</b>	-	-	<b>0.12</b>	-	-
<b>Guaiacols</b>	<b>1.19</b>	<b>3.87</b>	<b>3.35</b>	<b>3.21</b>	<b>1.28</b>	<b>1.35</b>	<b>0.48</b>
Creosol	0.22	0.73	0.81	0.61	0.41	0.44	0.16
Guaiacol	0.14	0.64	0.53	0.51	0.43	-	-
Isoeugenol	0.14	0.60	0.66	0.42	-	0.07	-
Ethylguaiacol	0.16	0.57	0.09	0.48	0.27	0.40	0.15
<b>O-polyaromatics</b>	-	<b>0.17</b>	<b>0.44</b>	<b>0.31</b>	<b>1.13</b>	<b>1.15</b>	<b>1.18</b>
<b>Phenols</b>	<b>0.14</b>	<b>3.13</b>	<b>3.49</b>	<b>5.08</b>	<b>11.51</b>	<b>12.05</b>	<b>17.02</b>
Dimethylphenol	0.02	0.39	0.49	0.64	1.92	2.00	2.09
Ethylmethylphenol	-	-	-	-	0.50	1.01	1.16
Ethylphenol	0.02	0.41	0.67	0.72	0.43	2.49	2.47
Methylphenol	0.05	0.60	0.48	1.07	2.88	2.05	3.96
Phenol	0.03	1.02	1.01	1.62	4.44	4.02	6.06
<b>Phenyl esters</b>	-	-	-	-	-	-	<b>0.60</b>
<b>Syringols</b>	<b>0.22</b>	<b>0.74</b>	<b>1.15</b>	<b>0.55</b>	<b>0.12</b>	-	-
Methoxyeugenol	0.09	0.32	0.35	0.18	-	-	-
Syringol	0.12	0.42	0.80	0.38	0.12	-	-
<b>Trimethoxybenzenes</b>	0.09	0.37	0.38	0.31	0.16	0.17	-
<b>Total O-AR</b>	<b>1.89</b>	<b>8.84</b>	<b>9.20</b>	<b>10.24</b>	<b>15.76</b>	<b>15.32</b>	<b>21.24</b>

More severe conditions of C/B and/or temperature contribute to the rupture of the labile  $-OCH_3$  group, provoking that great part of guaiacols is converted into phenols [122,138]. Within this subfamily, phenol is the most abundant compound, showing a concentration of up to 6 wt.%. Phenol is widely used for the formulation of pesticides, explosives, paints, pharmaceuticals, dyes and textiles, among others. Moreover, phenol is an intermediate in the production of bisphenol A (BPA), which is used in the manufacture of polycarbonates and epoxy resins [137,139]. In addition, alkylphenols, such as methyl-phenol, ethyl-phenol, dimethylphenol and ethyl-methyl-phenol are also produced to a great extent in these conditions, being valuable compounds for the synthesis of surfactants, fuel additives and a variety of fine chemicals [139,140].

On the other hand, the LO family represents an important source of valuable products with industrial applications, whose composition is provided in **Table 4.3.5** in the form of concentration referred to the whole bio-oil\* fraction. In the thermal pyrolysis test, the LO family possessed a concentration of just 0.79 % in the whole bio-oil\*, showing a broad composition in terms of individual components (acetals, aldehydes, esters and ketones). However, the use of the K-USY catalyst provokes a sharp enhancement in the yield and concentration of light oxygenates, reaching values for the latter within the range 7.04 – 15.32 wt.%. Increasing both the temperature and the C/B ratios led to higher LO concentrations. These variations affected mostly to the ketones sub-family, which reached a share of about 94 % of the whole LO group for the test performed in the most severe conditions (C/B = 0.6 and T = 500 °C), while the ketone yield was almost ten times higher than that of the reference thermal pyrolysis test. A number of both linear and cyclic ketones can be found as major components in this sub-family, as detailed in **Table 4.3.5**. The transformation of **SUG** and **FUR** through ring-rearrangement reactions is probably the major route for the production of the cyclic ketones, as it has been observed in **ws-ac CFP** tests over **KH-ZSM-5** in **Section 4.3.2.1**. In this way, Gupta et al. have reported the transformation of furfural into both cyclopentenone and cyclopentanone in vapour phase over basic CaO catalyst [61], proposing a pathway that starts with a hydrogenation step into furfuryl alcohol, followed by dehydroxylation, rearrangement and further dehydration to form 2-cyclopentenone. The authors propose that the required hydrogen is in-situ generated from coke formation and water gas shift reactions. Likewise, it has been reported that the presence of water may enhance the conversion of furfural towards cyclic ketones

### 4.3. Catalytic fast pyrolysis of wheat straw over K-incorporated zeolites

over TiO<sub>2</sub> supported Ru and Pd catalysts [79]. These components are of great interest to be used as building blocks for the synthesis of a variety of natural products, drug molecules and chemical intermediates, as well as fuel precursors and additives [123,141].

**Table 4.3.5.** Concentration (wt.%) of the main LO components in the bio-oil\* produced by ws-ac catalytic pyrolysis over K-USY sample at different temperatures and C/B ratios.

C/B ratio (g/g)	N-C	0.2			0.6		
T <sub>catalysis</sub> (°C)	450	400	450	500	400	450	500
Acetals	0.06	0.00	0.15	0.02	0.00	0.00	0.11
Aldehydes	0.08	0.68	0.32	0.49	0.67	0.54	0.69
Esters	0.04	0.77	0.38	0.56	0.07	0.00	0.07
Ketones	0.52	5.68	6.18	6.41	9.84	11.33	14.44
<i>Cyclic ketones</i>	0.12	3.62	3.56	3.8	5.98	6.75	8.68
Cyclopentanone	0.00	0.14	0.13	0.19	0.46	0.35	0.41
Cyclopentenone	0.00	1.74	1.77	1.64	0.00	2.57	2.56
Methyl cyclopentenone	0.01	0.63	0.74	0.92	4.17	3.15	3.53
Methyl cyclopentanedione	0.03	0.65	0.40	0.34	0.17	0.00	0.00
Dimethyl cyclopentenone	0.00	0.00	0.31	0.50	0.29	0.68	1.72
<i>Linear ketones</i>	0.41	2.05	2.62	2.61	3.86	4.59	5.76
Butanone	0.00	0.00	0.93	0.33	1.63	2.20	2.06
Methyl vinyl ketone	0.00	0.35	0.74	0.89	0.95	0.76	1.11
Hydroxyacetone	0.03	0.83	0.31	0.55	0.00	0.00	0.28
Pentenone	0.02	0.56	0.24	0.60	1.12	1.27	1.43
<b>Total LO</b>	<b>0.79</b>	<b>7.13</b>	<b>7.04</b>	<b>7.48</b>	<b>10.58</b>	<b>11.87</b>	<b>15.32</b>

In summary, the use of the K-USY catalyst, having a high concentration of weak basic sites, drastically affects the bio-oil\* composition, leading to more uniform product distribution and favouring the formation of high-added value compounds, mainly phenols and ketones. Considered together, these type of products reaches a concentration in the bio-oil\* fraction of 31.5 wt.% for the catalytic test performed in the most severe conditions, which is a value quite higher in comparison with the one (0.66 wt.%) corresponding to the thermal pyrolysis experiment. After a proper separation, these compounds could be valorised as raw chemicals, mainly for fine chemistry applications.



#### 4.4. Fast pyrolysis of wheat straw by dual-catalyst tandem system

Acid catalysts, such as H-ZSM-5 zeolite, have been used in catalytic fast pyrolysis of lignocellulosic biomass due to its ability to produce bio-oils with high concentrations of aromatic hydrocarbons, whereas basic metal oxides have been proven to be a good alternative to efficiently remove oxygen in the form of CO<sub>2</sub>. In this way, several authors [142–145] suggest that a dual-catalyst staged catalytic pyrolysis is an innovative way to produce aromatic hydrocarbons while deoxygenating bio-oil by sequentially using catalysts with different pore sizes and acid-base properties.

In this section, a nanocrystalline zeolite H-ZSM-5 with mainly microporous structure and high overall acidity was chosen as the only acid catalyst, whereas bentonite and magnesium oxide were chosen as basic catalysts, having different mesoporous structures and overall basicities. Acid H-ZSM-5 zeolite and basic BNT/MgO have been evaluated in the catalytic fast pyrolysis of acid-washed wheat straw. Two different catalytic studies have been conducted by varying the basic catalyst tested in the three-stage thermocatalytic cascade reaction system. In addition, two different coupling configurations have been employed depending on whether the acid or the basic catalyst bed was placed first.

##### 4.4.1. Characterisation of the catalysts

The three catalysts used in this chapter are different in nature and their physicochemical properties do not have many similarities to each other. Although these catalysts were described in previous chapters, their physicochemical and crystalline properties are briefly explained here.

XRD patterns of the catalysts are shown in **Figure 4.4.1.a**. As discussed in **Section 4.1.2**, Na-montmorillonite (Na-Al-Si-OH) and quartz (SiO<sub>2</sub>) patterns can be identified in the BNT diffractogram. Na-Al-Si-OH patterns are found at  $2\theta = 8.4^\circ$ ,  $19.3^\circ$ ,  $34.7^\circ$  and  $60.5^\circ$ ; whereas SiO<sub>2</sub> diffraction peaks are observed at  $2\theta = 24.5^\circ$  and  $27.4^\circ$  [97–99]. MgO diffractogram was described in **Section 4.2.1**. Its characteristic cubic MgO patterns are found at  $2\theta = 36.9^\circ$ ,  $42.7^\circ$  and  $62.1^\circ$  [88]. Conversely, XRD patterns of H-ZSM-5 match with IZA standards of MFI framework [146].

#### 4.4. Fast pyrolysis of wheat straw by dual-catalyst tandem system

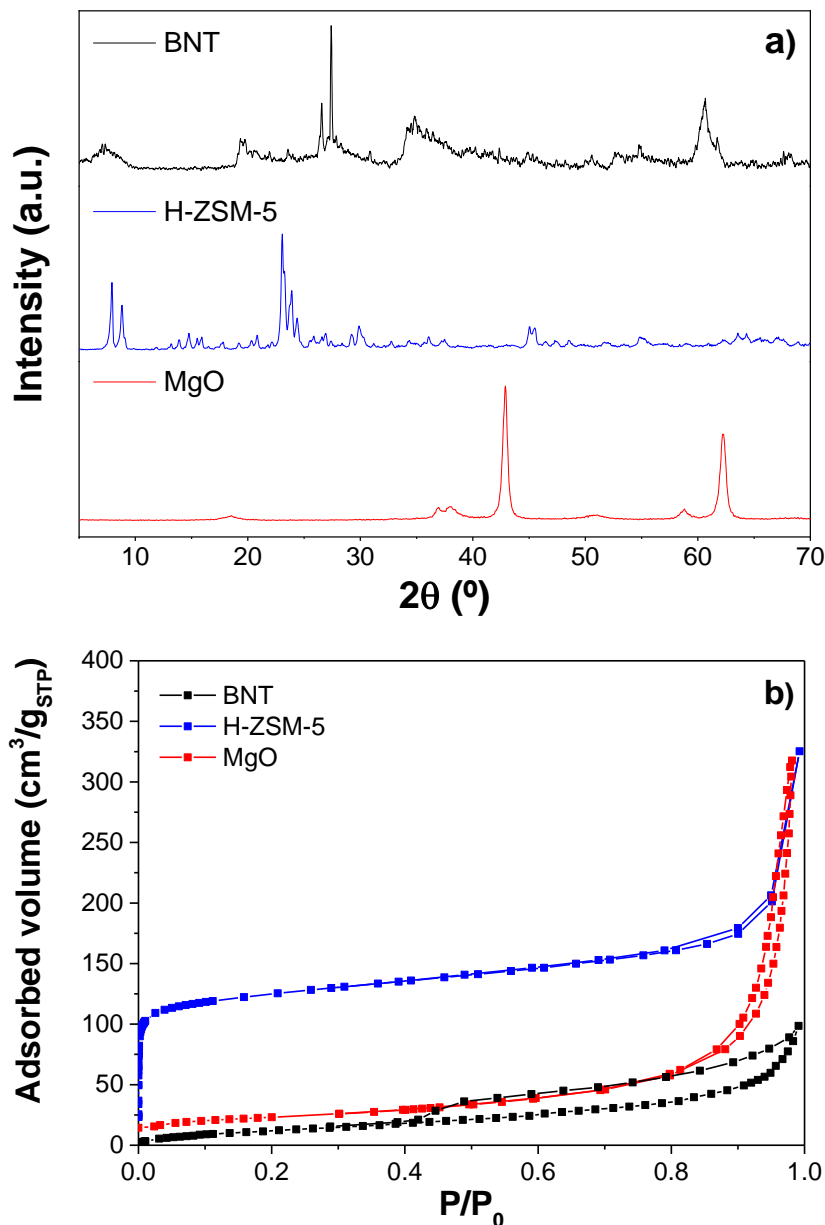


**Figure 4.4.1.** a) XRD patterns; b) N<sub>2</sub> and Ar adsorption-desorption isotherms; of the catalysts.

Ar and N<sub>2</sub> physisorption isotherms and the corresponding textural properties are shown in **Figure 4.4.1.b** and **Table 4.4.1**, respectively. Bentonite and magnesium oxide exhibit type IV N<sub>2</sub> physisorption isotherms and H3 hysteresis loops according to IUPAC classification, which are typical of plate-like particles. On the other hand, nanocrystalline H-ZSM-5 shows type IV Ar physisorption isotherm, with both micro- and mesoporosity. For this reason, Ar physisorption isotherms at 87 K were employed for H-ZSM-5, since using argon as adsorbate is more adequate for the micropore filling step during physisorption [100]. H-ZSM-5 has the highest BET surface (384 m<sup>2</sup>/g), where 86 % corresponds to micropore surface area. On the contrary, BNT and MgO

have low BET surface areas ( $40 - 80 \text{ m}^2/\text{g}$ ), which match with their mesopore and external surface areas due to their lack of micropores. Conversely, MgO has the highest total pore volume ( $0.470 \text{ cm}^3/\text{g}$ ), followed by H-ZSM-5 and BNT. Despite H-ZSM-5 has high density of micropores, larger pores like those of MgO are translated into a higher total pore volume.

**Table 4.4.1.** Physicochemical properties of the coupling catalysts.

Catalyst	$S_{\text{BET}}^a$ ( $\text{m}^2/\text{g}$ )	$S_{\text{MZ-EXT}}^b$ ( $\text{m}^2/\text{g}$ )	$S_{\text{MICRO}}^c$ ( $\text{m}^2/\text{g}$ )	$V_{\text{T}}^d$ ( $\text{cm}^3/\text{g}$ )	$V_{\text{MZ-EXT}}^e$ ( $\text{cm}^3/\text{g}$ )	$V_{\text{MIC}}^f$ ( $\text{cm}^3/\text{g}$ )	Acidity ( $\text{mmol}_{\text{NH}_3}/\text{g}$ )	Basicity ( $\text{mmol}_{\text{CO}_2}/\text{g}$ )
BNT	43	43	–	0.126	0.126	–	0.080	0.596
H-ZSM-5	384	53	331	0.360	0.163	0.197	0.314	0.018
MgO	82	82	–	0.470	0.470	–	0.040	4.127

<sup>a</sup>BET surface area; <sup>b</sup>Mesopore+external surface area; <sup>c</sup>Micropore surface area; <sup>d</sup>Total pore volume ( $P/P_0 \approx 0.98$ ); <sup>e</sup>Mesopore+external volume; <sup>f</sup>Micropore volume

The focus of this chapter is on the use of two different catalysts in a thermo-catalytic cascade reaction system consisting of an acid and a basic catalyst in different configurations. For this reason, their acid-base properties have been quantified by  $\text{NH}_3$ - and  $\text{CO}_2$ -TPD. Acidity of the samples was measured using ammonia as adsorbate (**Figure 4.4.2.a** and **Table 4.4.1**). H-ZSM-5 shows the highest acidity ( $0.314 \text{ mmol}_{\text{NH}_3}/\text{g}$ ) among the three catalysts, which is in good agreement with its Al content (Si/Al ratio = 39.5). Its  $\text{NH}_3$ -TPD curve presents two clear peaks: a more intense peak of weak acidity centred at  $187^\circ\text{C}$ , which corresponds to  $\text{NH}_3$  molecules adsorbed onto silanol groups, and a broader peak of medium acidity centred at  $358^\circ\text{C}$ , which is attributed to the interaction of  $\text{NH}_3$  molecules with framework Al species [53]. Both BNT and MgO have low acidities ( $0.040$  and  $0.080 \text{ mmol}_{\text{NH}_3}/\text{g}$ , respectively) compared to H-ZSM-5. On the other hand,  $\text{CO}_2$  is the adsorbate employed for the quantification of basicity (**Figure 4.4.2.b** and **Table 4.4.1**). In this case, MgO is the catalyst with the highest basicity, which is considerably more basic than BNT ( $4.127$  vs.  $0.589 \text{ mmol}_{\text{CO}_2}/\text{g}$ ). Magnesium oxide exhibits an intense and broad peak centred at  $168^\circ\text{C}$ , which is deconvoluted in three different curves of weak-medium basicity (see **Section 4.2.1**), whereas bentonite has a less intense peak of weak basicity centred at  $96^\circ\text{C}$ . H-ZSM-5 shows a small and broad peak of medium basicity at  $192^\circ\text{C}$ , which is negligible compared to those of the other two catalysts.

#### 4.4. Fast pyrolysis of wheat straw by dual-catalyst tandem system

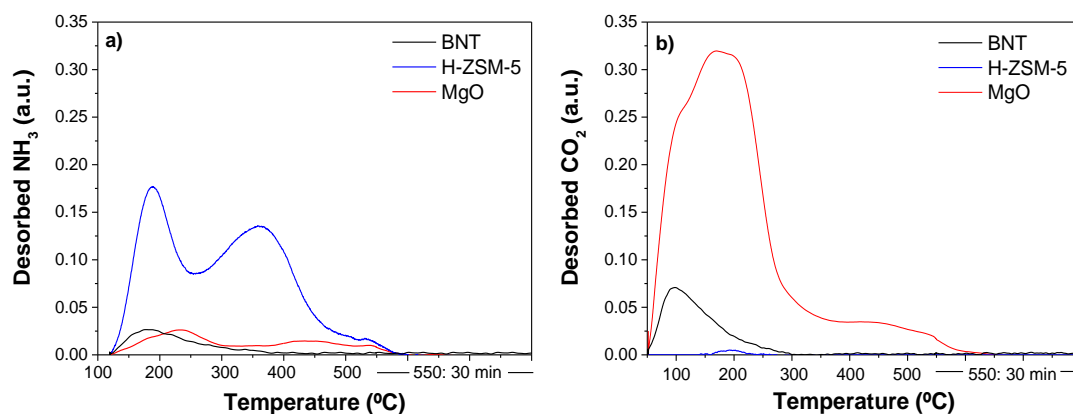


**Figure 4.4.2.** Acid and base properties of the catalysts: a) NH<sub>3</sub>-TPD; b) CO<sub>2</sub>-TPD.

#### 4.4.2. Wheat straw catalytic tests

Catalytic fast pyrolysis (CFP) of acid-washed wheat straw (ws-ac) was carried out employing two catalysts with different acid and basic properties coupled in the catalytic zone. The objective of this study is to obtain aromatic hydrocarbons through the synergetic effect of acid and basic catalysts. The pyrolysis tests were performed at atmospheric pressure and temperatures of 550 °C and 450 °C for the pyrolysis and catalytic zones, respectively. The catalyst to biomass (C/B) ratio was set at 0.2 g/g in single-catalyst tests and 0.4 g/g in the sequential coupling tests (0.2 in each catalyst bed). The acid and basic catalysts are denoted as A and B, respectively. Two different coupling configurations were studied depending on whether the pyrolytic vapours (pyrovapours) first passed through the acid (A+B) or the basic (B+A) catalyst bed. Reference non-catalytic (N-C) and single-catalyst (A and B) tests are also included in the study (Tables A.1, A.2, A.9 and A.27 – 31 in the Appendix). The amount of char formed in the thermal zone presented an average value of 17.8 wt.% for all trials.

##### 4.4.2.1. CFP by coupling H-ZSM-5 and basic-bentonite as catalysts

The distribution in mass yields of bio-oil\* and the rest of by-products are depicted in **Figure 4.4.3.a**. The use of two catalysts in the catalytic zone gave rise to the lower bio-oil\* and higher gas yields than the single-catalyst tests due to the larger number of transformations (including cracking, deoxygenation, and C–C bond formation reactions, among others [105–107]) that pyrovapours undergo when they pass through both catalyst beds, regardless of the coupling configuration. When comparing both configurations, A+B presents a slightly higher bio-oil\* yield than the opposite

configuration. The lower bio-oil\* yields obtained employing a tandem of catalysts lead to an increase of by-products compared to the single-catalyst tests. The water yield is close to that of H-ZSM-5 with a difference of less than  $< 1$  wt.%, whether the acid or basic catalyst is placed on top. However, differences between coke yields are greater, since that of H-ZSM-5 is almost doubled when using B+A configuration. These results are in agreement with the oxygen contents of the bio-oils\*, compared in **Figure 4.4.3.b**. The combination of both catalysts favours the deoxygenation of bio-oil\*, reducing it the oxygen content to 25.6 wt.% in the best scenario (B+A configuration). This finding confirms the effectiveness of coupling two different catalysts rather than using a single catalyst bed.

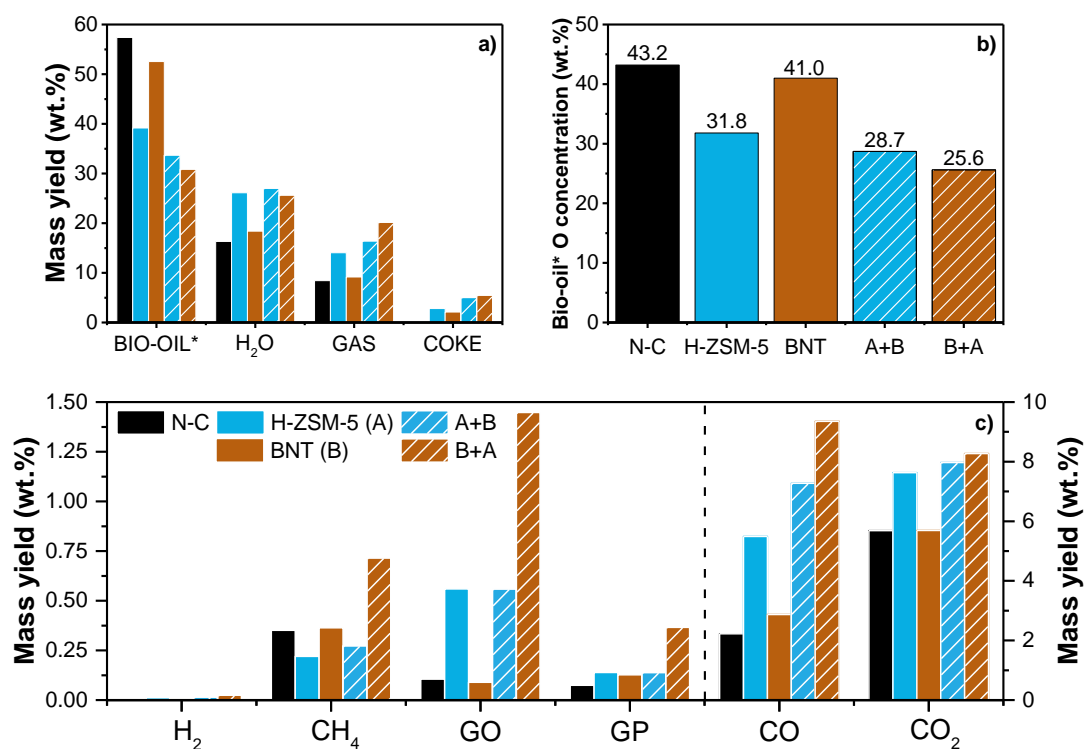


**Figure 4.4.3.** Catalytic pyrolysis of ws-ac over H-ZSM-5 and BNT in single-catalyst and coupling configurations: a) fraction yields; b) bio-oil\* oxygen concentration; c) gaseous components yields (GO: gaseous olefins, GP: gaseous paraffins).

The composition of non-condensable gases determined by micro-GC are depicted in **Figure 4.4.3.c**. When comparing both coupling configurations, the production of C<sub>1</sub>-C<sub>4</sub> hydrocarbons stands out in the case of B+A configuration because of the sharp increase in its gas yield. Methoxyl groups from lignin structure are degraded by demethylation reactions, whereas gaseous olefins are product of decarbonylation reactions of light oxygenates intermediates in pyrovapours, confirming the high yields

#### 4.4. Fast pyrolysis of wheat straw by dual-catalyst tandem system

of CH<sub>4</sub>, GO and CO [56]. Likewise, the highest CO<sub>2</sub> yield between the single catalyst and the staged catalytic tests is observed for the B+A configuration. However, A+B configuration has similar levels of gaseous hydrocarbons and CO<sub>2</sub> to those of the sole H-ZSM-5.

Catalytic deoxygenation selectivities to H<sub>2</sub>O, CO, and CO<sub>2</sub> regarding the thermal test are illustrated in **Figure 4.4.4**. In the single-catalyst tests, it is observed that dehydration is the main deoxygenation pathway, especially in the case of bentonite because decarboxylation selectivity is almost negligible. However, the three reaction pathways are more balanced when the sequential coupling is used since CO<sub>x</sub> production is enhanced. B+A configuration stands out due to its higher decarbonylation and decarboxylation selectivities, being the latter the most remarkable because deoxygenation is more efficient by removing two atoms of oxygen in the same molecule. These results are consistent with the lowest bio-oil\* oxygen content (25.6 wt.%) of B+A configuration.

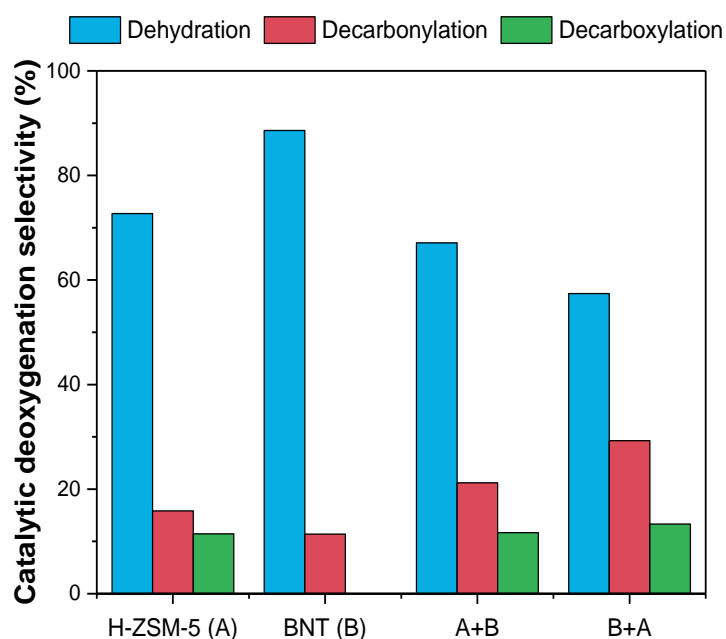


**Figure 4.4.4.** Catalytic deoxygenation selectivity obtained in the fast pyrolysis of ws-ac over H-ZSM-5 and BNT in single-catalyst and coupling configurations.

The variation of the elemental composition of the bio-oils\* in the CFP tests performed using different catalyst configurations is shown in **Figures 4.4.5.a** and **4.4.5.b** in the form of van Krevelen diagrams, representing overall and effective H/C ratios versus O/C one [147]. According to **Figure 4.4.5.a**, the reduction in the O/C ratios is more

pronounced for the coupling configurations than the single-catalyst tests, which is in line with the oxygen contents of the bio-oils\*. Conversely, the H/C ratio of the B+A configuration is similar to that of the sole H-ZSM-5. When analysed together, BNT presents a relationship between H/C and O/C ratios very close to that of the thermal test and shows a decreasing trend with the single-H-ZSM-5 and A+B configurations. However, when correlating the values obtained from B+A configuration and the thermal test, a different trend is observed. This curve has a slope closer to the gasoline-diesel region of the Van Krevelen diagram, which is even clearer when comparing  $H/C_{eff}$  and O/C ratios (**Figure 4.4.5.b**). As previously discussed, catalytic deoxygenation selectivities were more balanced in the case of B+A configuration (**Figure 4.4.4**), confirming the increasing trend towards potential low-oxygen biofuels.

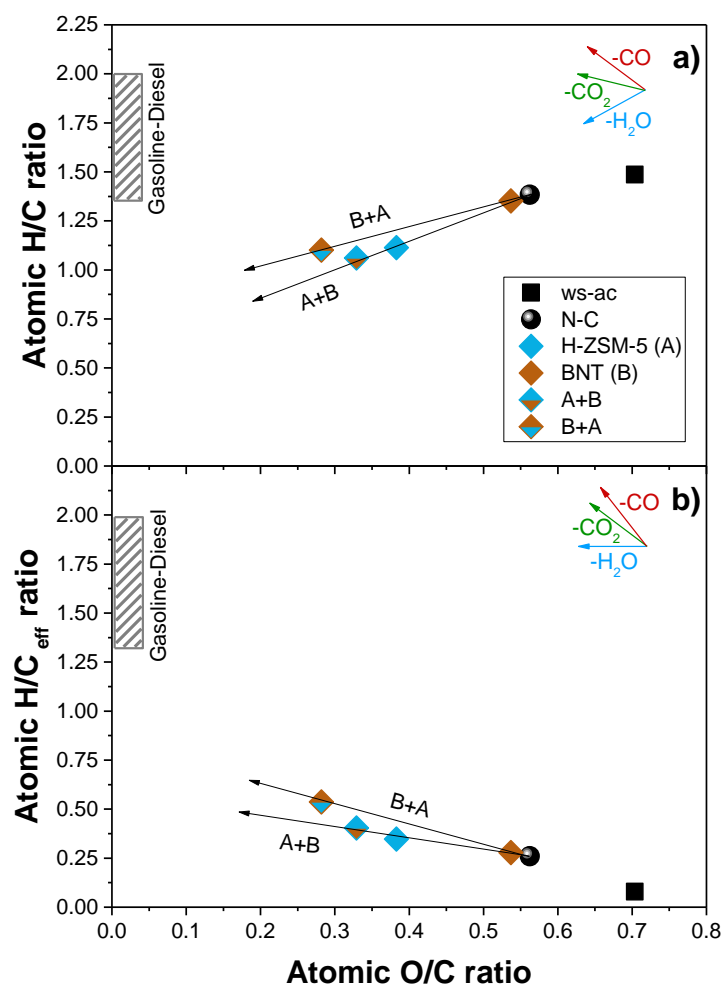


**Figure 4.4.5.** Van Krevelen diagram [147], comparing elemental compositions of bio-oils\* in the fast pyrolysis of ws-ac over H-ZSM-5 and BNT in single-catalyst and coupling configurations.

#### 4.4. Fast pyrolysis of wheat straw by dual-catalyst tandem system

Distribution of the energy contained in the different product fractions regarding initial biomass for the different configurations is illustrated in **Figure 4.4.6**. Bio-oil\* energy yield are considerably reduced when H-ZSM-5 and BNT are employed as part of a coupling configuration, since their respective mass yields are considerably reduced due to the severe cracking reactions carried out in their corresponding staged-CFP tests. As higher mass yields of gas and coke are produced in single-step and staged-catalytic tests, especially in those which include H-ZSM-5, their respective energy yields are also enhanced. Particularly, gas fractions with higher concentrations of CO and GO give rise to higher energy yields due to their higher HHVs. B+A configuration stands out among the rest of configurations with a gas yield of 11.2 %, which is 1.6 and 3.7 times higher than its opposite configuration and the thermal test, respectively.

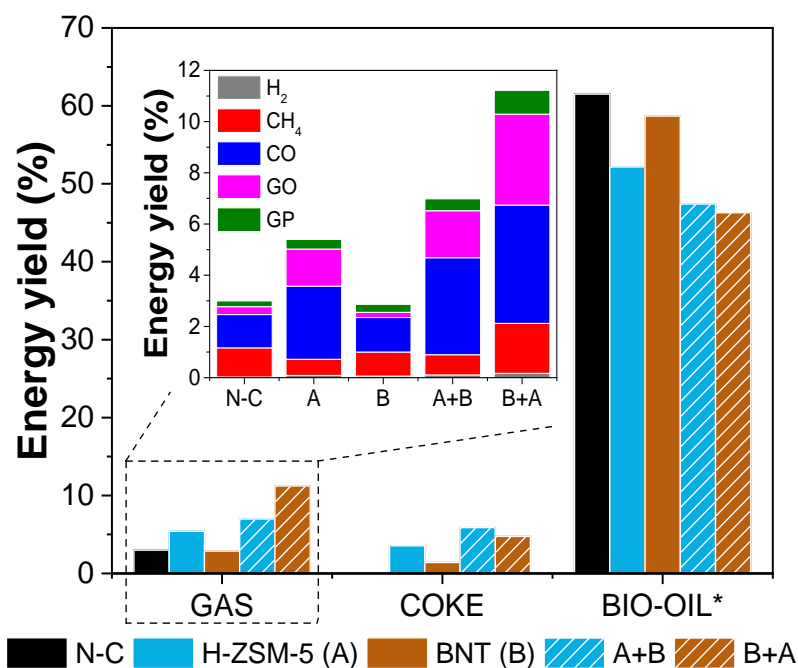


**Figure 4.4.6.** Energy yield distribution obtained in fast pyrolysis of ws-ac over H-ZSM-5 and BNT in single-catalyst and coupling configurations.

Additionally, ultimate analyses and higher heating values of char and coke, as well as their fraction yields and coke content in catalysts, are included in **Table 4.4.2**. Char presents an average elemental composition and oxygen removed common to all trials, but coke elemental composition depends on the catalyst(s) and configurations employed. It is observed that BNT coke contains more oxygen than H-ZSM-5 due to the oxygenated nature of the compounds found in pyrovapours that oligomerise when



they pass through this catalyst and are retained. As will be discussed later, H-ZSM-5 produces oxygen-free aromatic hydrocarbons that tend to polymerise and are deposited as coke within its pores, blocking its acidic active sites [6]. These cokes present greater HHVs (23.2 – 24.2 MJ/kg) due to their higher carbon contents. However, the coke retained on the surface and within the pores of BNT is richer in oxygen than in the case of H-ZSM-5, especially when used as the sole or top catalyst (B+A configuration), reducing their higher heating values and, therefore, their energy yields (**Figure 4.4.6**).

**Table 4.4.2.** Compositions and HHVs of char and coke obtained in the fast pyrolysis of ws-ac over H-ZSM-5 and BNT in single-catalyst and coupling configurations.

Experiment	Fraction	Coke in catalyst (wt.%)	Mass yield (wt.%)	Elemental analysis (wt.%, dry basis)				HHV (MJ/kg)
				C	H	N	O	
N-C	Char	–	17.8	78.7	2.7	0.9	10.5	29.4
H-ZSM-5 (A)	Coke	13.9	2.8	63.5	4.4	–	32.1	24.0
BNT (B)	Coke	10.8	2.1	36.1	5.6	–	58.3	12.7
A+B	Coke A	13.4	2.6	61.8	4.4	–	33.9	23.2
	Coke B	12.6	2.4	56.5	4.8	–	38.8	21.3
B+A	Coke B	14.7	2.8	29.7	4.6	–	65.8	8.9
	Coke A	14.3	2.7	63.6	4.5	–	31.9	24.2

The composition of the bio-oils\* from the CFP tests are quantified by GC-MS. **Figure 4.4.7.a** shows the mass yields of the detected compounds in the bio-oil\* fraction. Proportions of detected compounds can be calculated by the relationship between detected and total mass yields. Despite having the highest bio-oil\* yield, the thermal test has a lower proportion of detected compounds than the catalytic tests (19 vs. 40 – 45 wt.%). The undetected species are formed mainly by the partial decomposition of original biomass biopolymers. It is observed that bio-oils\* from coupling configurations present lower total mass yields and, particularly, in the case of B+A configuration, the proportion of detected compounds is even lower than that of BNT as the top catalyst (40.3 vs. 44.5 wt.%), which is not favourable for the valorisation of ws-ac as bio-oil\*. Decreasing trends of total mass yields with C/B ratio are also observed in total energy yields (**Figure 4.4.7.b**).

#### 4.4. Fast pyrolysis of wheat straw by dual-catalyst tandem system

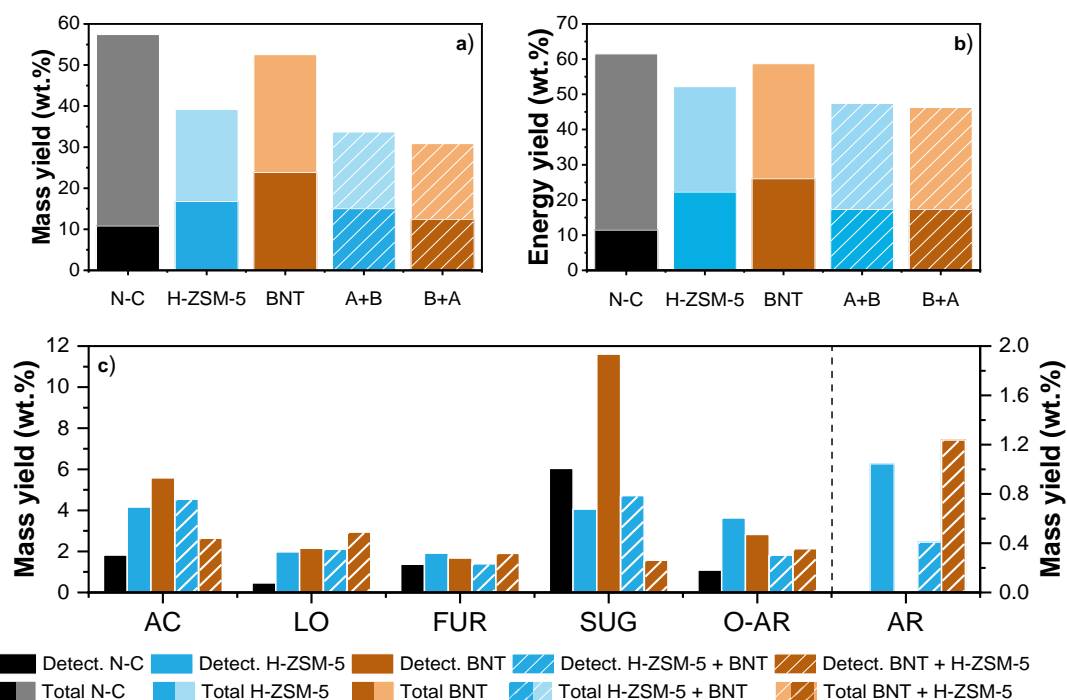


**Figure 4.4.7.** Quantitative GC-MS analyses of the bio-oil\* obtained in the ws-ac catalytic pyrolysis over H-ZSM-5 and BNT in single-catalyst and coupling configurations: a) total and GC-MS detected mass yields; b) total and GC-MS detected energy yields; and c) GC-MS detected mass yields of compound families (AC: carboxylic acids, LO: light oxygenates, FUR: furans, SUG: anhydrosugars and O-AR: oxygenated aromatics).

When the quantified mass yield is separated into the different families found in bio-oil\* (**Figure 4.4.7.c**), it is observed that B+A configuration has a slightly higher production of LO and AR concerning the other configurations. In addition, the SUG family (mainly composed of levoglucosan, which is formed by approx. 50 wt.% of oxygen) is considerably reduced in this configuration (1.6 wt.%), which could explain the low oxygen content of this bio-oil (25.6 wt.%). Levoglucosan is dehydrated by H-ZSM-5 acidic sites into furans, which interact with gaseous olefins from cracking reactions giving rise to aromatic hydrocarbons through Diels-Alder condensation reactions [66,148]. In addition, acid properties of H-ZSM-5 zeolite promote an increase in the amount of gaseous olefins and their successive oligomerisation-cyclisation-aromatisation chain reactions [149]. However, the increase in AR yields compared to the catalytic test with the sole H-ZSM-5 is of little significance (1.0 vs. 1.2 wt.%). On the other hand, basic sites of BNT promote ketonisation and aldol condensation reactions, giving rise to longer-chain oxygenated compounds, as is slightly observed in the LO yield. Water and CO<sub>2</sub> yields are consistent with the

deoxygenation reactions involved in the CFP of ws-ac over both acid and basic catalysts.

#### 4.4.2.2. CFP by coupling H-ZSM-5 and basic-MgO as catalysts

Similarly to the previous section, **Figure 4.4.8.a.** summarised the fraction yields of bio-oil\*, water, permanent gases and coke obtained in the catalytic and thermal tests. Compared to the thermal test, the yields of catalytic bio-oil\* decrease with a consequent increase in the yield of the other fractions. H-ZSM-5 and MgO exhibit similar bio-oil\* yields, but they are reduced when both catalysts are used sequentially, as a consequence of the variety of reactions that take place in staged-CFP [142]. The lowest bio-oil\* yield was obtained with B+A coupling configuration, as occurred in the staged-catalytic pyrolysis test with bentonite. In this way, A+B configuration presents once more higher water yield than the opposite configuration. Conversely, MgO yields fewer permanent gases than H-ZSM-5, but it has the highest gas production when used as the top catalyst in a coupling configuration. In contrast, coke formation is enhanced when MgO is employed as sole or top catalyst.

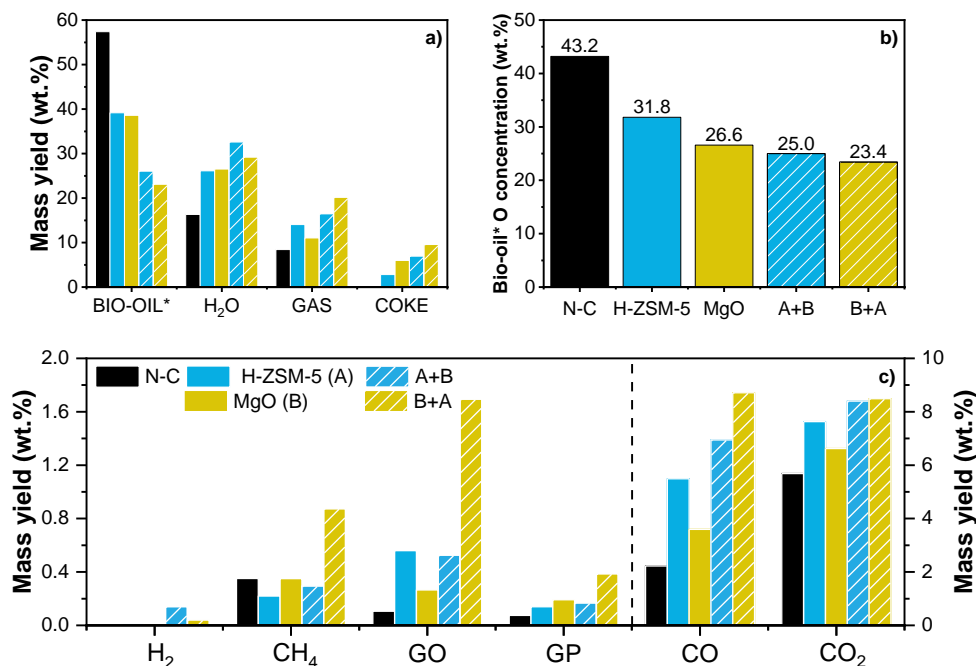


**Figure 4.4.8.** Catalytic pyrolysis of ws-ac over H-ZSM-5 and MgO in single-catalyst and coupling configurations: a) fraction yields; b) bio-oil\* oxygen concentration (dry basis); c) gaseous components yields (GO: gaseous olefins, GP: gaseous paraffins).

Bio-oil\* oxygen concentrations are depicted in **Figure 4.4.8.b.** Compared to the reference thermal test, H-ZSM-5 has a degree of deoxygenation of 26.3 %, whereas

#### 4.4. Fast pyrolysis of wheat straw by dual-catalyst tandem system

MgO has one of 38.4 % despite having lower CO<sub>x</sub> yields, since oxygen can also be removed in the form of other by-products, such as coke. Thus, the more basic character of MgO appears to be beneficial for the deoxygenation of bio-oil\*. Oxygen contents of bio-oils\* from staged-catalytic pyrolysis tests are even lower than those with BNT. These values are consistent with their production of water and CO<sub>x</sub>, with B+A configuration having the highest degree of deoxygenation (45.8 %).

Distribution of different non-condensable gases are compared in **Figure 4.4.8.c**. Since the overall MgO gas yield is lower than the other catalytic tests, it is reasonable that specific gas yields are lower than those of H-ZSM-5 and both coupling configurations. In the case of A+B configuration, gaseous C<sub>1</sub>-C<sub>4</sub> hydrocarbons have similar yields to those of H-ZSM-5. However, the production of these gases is highly enhanced when the opposite configuration is employed, especially in the case of gaseous olefins (GO). Regarding CO<sub>x</sub>, H-ZSM-5 presents higher yields of CO and CO<sub>2</sub> than MgO. A greater difference can be observed between CO than CO<sub>2</sub> yields, since decarbonylation reactions mainly take place over acidic centres, whereas decarboxylation reactions are promoted by both acidic and basic active sites. Thus, CO<sub>2</sub>/CO ratio is significantly higher with basic MgO than with acid H-ZSM-5 (1.8 vs. 1.4), which is in agreement with that found in literature [57]. In addition, CO<sub>x</sub> yields are also affected by the placement order of the catalyst beds. CO<sub>2</sub> yields are very similar in both coupling configurations, but CO production increases when H-ZSM-5 is used as the bottom catalyst. These events also occurred when BNT was employed instead of MgO.

The catalytic deoxygenation selectivities from **Figure 4.4.9** are calculated analogously to those in the previous section. No remarkable differences are noticed between single-H-ZSM-5 and A+B configurations. In the case of MgO, this catalyst presents the highest dehydration selectivity, which is reasonable because H<sub>2</sub>O is a by-product of ketonisation and aldol condensation reactions that are promoted by basic sites [105,106]. Moreover, decarboxylation selectivity is also increased in the pyrolysis reactions over the basic sites of MgO. Therefore, the deoxygenation effectivity is improved, being observed to a greater extent in the B+A configuration, where the three deoxygenation pathways are more balanced. In this case, decarbonylation selectivity is also enhanced, but CO production is attributed to the acid properties of the second catalyst [56]. A similar trend was observed for the coupling configurations with BNT as basic catalyst.

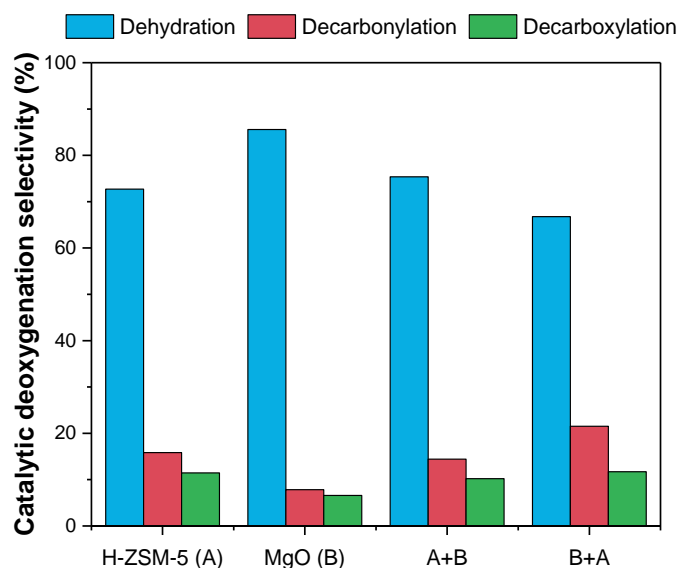


**Figure 4.4.9.** Catalytic deoxygenation selectivity obtained in the fast pyrolysis of ws-ac over H-ZSM-5 and MgO in single-catalyst and coupling configurations.

Van Krevelen diagrams comparing elemental composition of bio-oils\* are depicted in **Figures 4.4.10.a** and **4.4.10.b**. As occurred with MgO, the reduction in the O/C ratios is more pronounced for the coupling configuration than the single-catalyst tests. However, O/C ratio of the bio-oil\* obtained in the CFP over MgO has a similar value to those of the coupling configurations leaving aside those of the thermal and single-H-ZSM-5 tests. Therefore, these values of O/C ratio are reasonable since the oxygen contents of the bio-oils\* of the CFP that include MgO are very close to each other.

When comparing H/C ratios in **Figure 4.4.10.a**, single-catalyst and A+B configurations show comparable values and their relationship with their respective O/C values result in trends with a similar slope regarding the non-catalytic test. In contrast, B+A coupling configuration presents a more ascending slope closer to the gasoline-diesel region of the Van Krevelen diagram when related with the non-catalytic test. Like in the case of the same configuration with BNT, this slope is more pronounced when  $H/C_{eff}$  and O/C ratios are compared (**Figure 4.4.10.b**). The fact that the catalytic deoxygenation selectivities were more balanced in this particular case (**Figure 4.4.9**) is reflected in the Van Krevelen diagram. The  $H/C_{eff}$  vs. O/C curve of B+A configuration regarding the thermal test shows a slope more similar to that of decarboxylation reactions, whereas the other configurations have a behaviour closer to that of dehydration reactions. These slopes, along with that of decarbonylation

#### 4.4. Fast pyrolysis of wheat straw by dual-catalyst tandem system

reactions, were calculated by subtracting oxygen from the thermal bio-oil in the form of  $H_2O$ ,  $CO$  and  $CO_2$  until the complete elimination of oxygen.

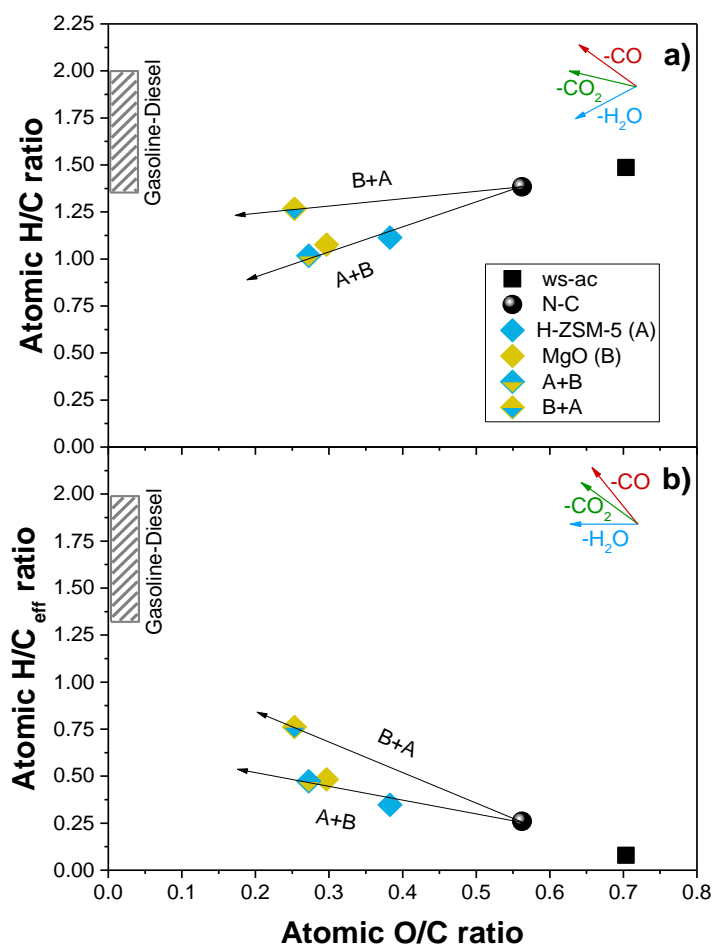


**Figure 4.4.10.** Van Krevelen diagram [147], comparing elemental compositions of bio-oils\* in the ws-ac fast pyrolysis over H-ZSM-5 and MgO in single-catalyst and coupling configurations.

Energy yields of the different product fractions for the single-catalyst and coupling configurations are compared in **Figure 4.4.11**. Similarly to the CFP tests with BNT, bio-oil\* energy yield is considerably reduced when staged-CFP are carried out. In addition, gas and coke energy yields are enhanced with the increase of their respective mass yields. CFP tests that include H-ZSM-5 show higher gas energy yields than the other configurations, especially both coupling configurations. Their higher production of  $CO$  and  $GO$  give rise to higher energy yields, as discussed in the previous section. In the case of A+B, the energy contained in the  $H_2$  fraction stands out. Despite having a low mass yield, slight increase results in a significant contribution to the overall gas yield due to the high HHV of  $H_2$ . Nevertheless, B+A configuration is the coupling

configuration with the highest gas energy yield (12.1 %), even higher than the analogous test with BNT.

Char and coke yields, and their ultimate analyses and contained energies, are summarised in **Table 4.4.3**. Coke from CFP of ws-ac over MgO presents a mass yield that doubles that of H-ZSM-5 and the oxygen content in this coke is half of its overall mass yield, which explains the decay in the oxygen concentration of the bio-oil\* obtained in this CFP test. H-ZSM-5 has an oxygen content in coke in the range of furans (33.3 wt.% in the case of furfural), whereas MgO has one in the range of anhydrosugars (49.3 wt.% in the case of levoglucosan). However, these values are slightly altered when these catalysts are placed in the secondary beds of the coupling configurations. Finally, the higher C and H contents of coke result in greater HHVs, so more energy should be retained in cokes of spent H-ZSM-5 samples than in the spent MgO ones. However, the lower coke concentrations of H-ZSM-5 samples are translated into lower energy yields (see **Figure 4.4.11**).

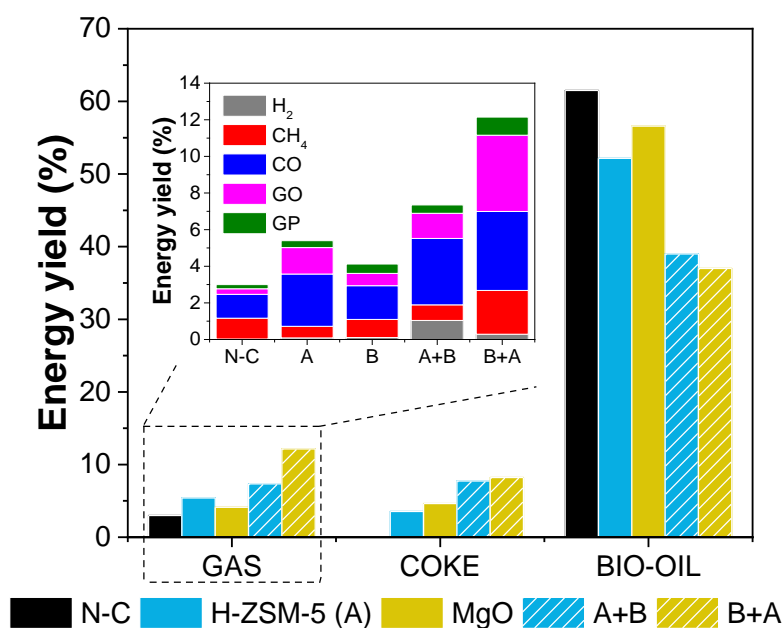


**Figure 4.4.11.** Energy yield distribution obtained in fast pyrolysis of ws-ac over H-ZSM-5 and MgO in single-catalyst and coupling configurations.

#### 4.4. Fast pyrolysis of wheat straw by dual-catalyst tandem system

**Table 4.4.3.** Compositions and HHVs of char and coke obtained in the fast pyrolysis of ws-ac over H-ZSM-5 and MgO in single-catalyst and coupling configurations.

Experiment	Fraction	Coke in catalyst (wt.%)	Mass yield (wt.%)	Elemental analysis (wt.%, dry basis)				HHV (MJ/kg)
				C	H	N	O	
N-C	Char	–	17.8	78.7	2.7	0.9	10.5	29.4
H-ZSM-5 (A)	Coke	13.9	2.8	63.5	4.4	–	32.1	24.0
MgO (B)	Coke	34.0	6.0	47.3	2.8	–	49.9	14.7
A+B	Coke A	14.4	2.7	63.3	4.1	–	32.6	23.5
	Coke B	22.2	4.3	56.9	3.1	–	40.0	19.4
B+A	Coke B	30.8	6.3	50.1	2.4	–	47.5	15.4
	Coke A	16.2	3.3	52.4	3.6	–	44.0	18.0

GC-MS detected and total mass yields are depicted in **Figure 4.4.12.a**. It is observed that total mass yields of the single-catalyst tests are very close to each other, but MgO shows a higher proportion of detected compounds than H-ZSM-5 (61.5 vs. 42.8 wt.%). In the case of employing MgO as the bottom catalyst, the proportion of detected compounds maintains its value around 60 wt.%, but its total mass yield decreased considerably because of the action of the two catalysts. However, in the B+A configuration, a decay in both total mass yield and proportion of detected compounds is observed. As occurred with BNT tests, a remarkable decrease in energy yields is observed when two catalysts are employed in staged-CFP, being B+A configuration the one with the lowest total energy yield (**Figure 4.4.12.b**).



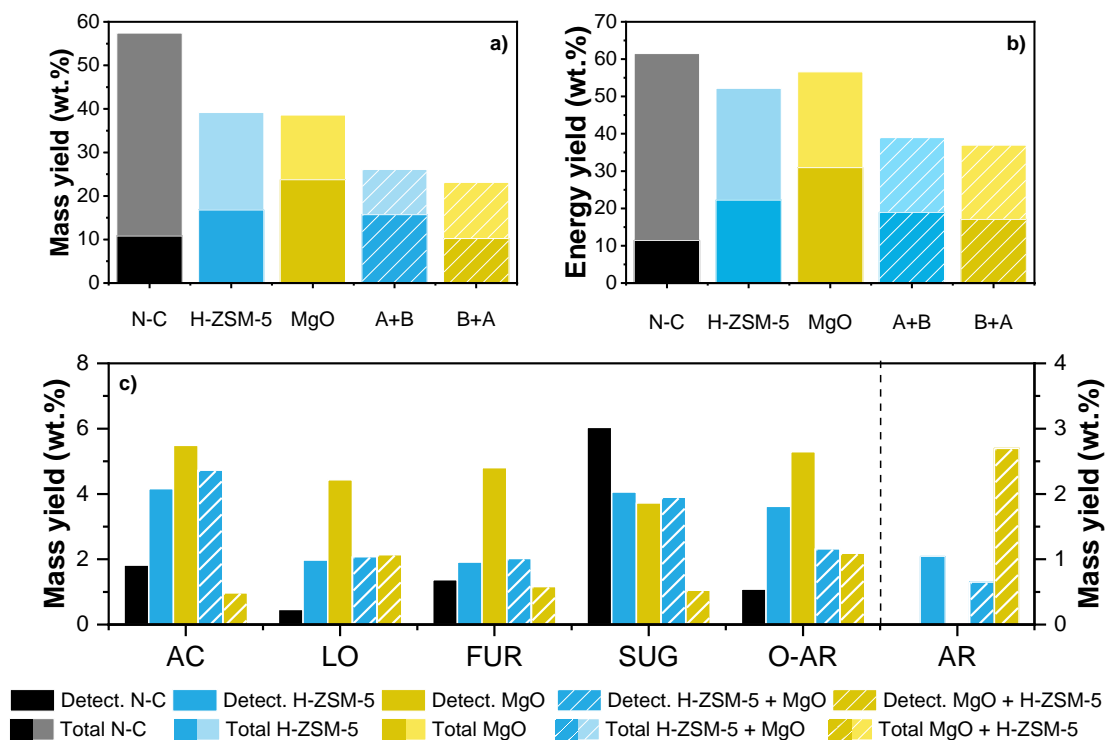


**Figure 4.4.12.** Quantitative GC-MS analyses of the bio-oil\* obtained in the ws-ac catalytic pyrolysis over H-ZSM-5 and MgO in single-catalyst and coupling configurations: a) total and GC-MS detected mass yields; b) total and GC-MS detected energy yields; and c) GC-MS detected mass yields of compound families (AC: carboxylic acids, LO: light oxygenates, FUR: furans, SUG: anhydrosugars and O-AR: oxygenated aromatics).

In order to explain these behaviours, it is necessary to examine the compositions of the quantifiable fractions of the bio-oils\* (**Figure 4.4.12.c**). MgO presents the highest proportion of detected compounds, with the highest yields of AC, LO, FUR and O-AR families. In contrast, SUG yield is lower than that of the non-catalyst test, but similar to H-ZSM-5. Anhydrosugars are first dehydrated into furans and then decomposed into low-molecular-weight oxygenates, such as carboxylic acids. In addition, the production of light oxygenates is enhanced because MgO basic sites promote ketonisation and aldol condensation reactions. Moreover, basic MgO properties favour lignin decomposition into oxygenated aromatic compounds. However, unlike the CFP tests that include H-ZSM-5 as a single or combined catalyst, MgO does not produce aromatic hydrocarbons. Although MgO was part of both coupling configurations, the production of LO, FUR and O-AR decreased compared to the single-catalyst test. In contrast, AC and SUG yields with MgO are very similar to that of A+B configuration. Anhydrosugars are similarly transformed into aromatic hydrocarbons as explained in

#### 4.4. Fast pyrolysis of wheat straw by dual-catalyst tandem system

the previous section. However, AR yield of A+B configuration is slightly lower than that of H-ZSM-5 due to the presence of the MgO catalyst bed beneath, where aromatic hydrocarbons may undergo some transformations as they pass through it. In the case of staged B+A catalytic pyrolysis configuration, AR production stands out. AC and LO from MgO bed act as GO precursors [57,73], which are then transformed into AR through Diels-Alder condensation reactions with FUR and oligomerisation-cyclisation-aromatisation reactions in the H-ZSM-5 bed, proving that B+A coupling configuration is the most efficient in this regard.

##### 4.4.2.3. Comparison of high-added value bio-based chemicals obtained by CFP employing single-catalyst and coupling configurations

As aromatic hydrocarbons are the most relevant compounds found in bio-oils\* of acid-basic coupling configurations, the AR concentrations are disclosed into their different subfamilies in **Table 4.4.4**.

As shown in **Figures 4.4.7.c** and **4.4.12.c**, no aromatic hydrocarbons were found in the non-catalytic and single BNT and MgO tests. It can be observed that bio-oils\* from B+A configurations present higher total AR concentrations than that of single H-ZSM-5 configuration (2.7 vs. 1.2 and 2.5 wt.% for BNT and MgO, respectively). However, substituted benzenes become more abundant when a secondary basic catalyst is used (from 46 to 52 and 61 % for BNT and MgO, respectively). Polycyclic aromatic hydrocarbons (PAHs) are simplified into single aromatic ring components when they pass through the basic catalyst beds. When B+A configurations are employed, the total AR concentrations improve from 1.5 to 4.4 times with respect to that of the single-H-ZSM-5 test, for BNT and MgO, respectively. In the case of MgO, substituted benzenes represent more than 65 % of AR subfamily, with xylenes being the most abundant compounds. Mixed xylenes (composed of m-xylene, p-xylene, o-xylene and ethyl benzene in varying proportions), in conjunction with toluene and mesitylene, are components of high-octane number in gasolines, whereas, together with styrene, xylenes are fundamental building blocks in the plastics industry. Furthermore, xylenes are extensively used as thinners and solvents in adhesives, inks, paints and varnishes [150–152].

**Table 4.4.4.** Concentration (wt.%) of the main AR components present in the bio-oil\* produced by fast pyrolysis of ws-ac over H-ZSM-5 in single-catalyst and coupling configurations with BNT/MgO (catalyst A: H-ZSM-5; catalyst B: MgO). Polycyclic aromatic hydrocarbons (PAHs) in *italics*.

Catalyst(s)	H-ZSM-5	H-ZSM-5 & BNT		H-ZSM-5 & MgO	
Configuration	A	A+B	B+A	A+B	B+A
<i>Anthracenes</i>	<b>&lt;0.01</b>	<b>&lt;0.01</b>	<b>0.04</b>	<b>0.03</b>	<b>0.10</b>
<i>Biphenyls</i>	<b>&lt;0.01</b>	–	<b>0.09</b>	–	<b>0.13</b>
<i>Fluorenes</i>	<b>0.04</b>	<b>0.01</b>	<b>0.10</b>	<b>0.03</b>	<b>0.18</b>
<i>Indenes</i>	<b>0.66</b>	<b>0.28</b>	<b>0.66</b>	<b>0.35</b>	<b>1.63</b>
Methylindene	0.19	0.06	–	0.10	0.49
Indane	0.13	0.05	0.14	0.11	0.41
Dimethylindene	0.17	0.01	0.14	0.08	0.29
<i>Naphthalenes</i>	<b>0.71</b>	<b>0.28</b>	<b>1.25</b>	<b>0.56</b>	<b>1.97</b>
Methylnaphthalene	0.25	0.14	0.32	0.20	0.56
Naphthalene	0.20	–	0.27	0.10	0.49
Dimethylnaphthalene	0.19	0.09	0.27	0.15	0.43
<i>Phenanthrenes</i>	<b>0.02</b>	<b>0.00</b>	<b>0.03</b>	–	–
<b>Substituted benzenes</b>	<b>1.22</b>	<b>0.64</b>	<b>1.79</b>	<b>1.53</b>	<b>7.60</b>
Xylene	0.56	0.36	0.68	0.72	2.96
Toluene	0.25	0.18	0.40	0.30	1.70
Ethylbenzene	0.07	–	0.20	0.16	0.50
Mesitylene	0.08	0.03	0.09	0.09	0.37
Styrene	0.05	0.03	0.09	0.06	0.28
<b>Total AR</b>	<b>2.66</b>	<b>1.21</b>	<b>3.97</b>	<b>2.49</b>	<b>11.62</b>

Moreover, PAHs are also abundant in bio-oils\* of B+A configurations, especially in the case of MgO, which almost doubles its concentration compared to that of BNT. In general, PAHs are formed by oligomerisation of substituted benzenes, and these reactions are carried out by the acidic active sites of H-ZSM-5 in the second catalytic bed [6]. Indenes and naphthalenes stand out among other PAHs found in these bio-oils\*. Indenes have numerous applications in manufacturing pharmaceutically active compounds, functional molecules, and ligands for metal complexes [87], whereas naphthalenes are used directly as pesticides and as precursors in the production of dyes, plasticisers, and resins [86].

In summary, the combination of acid and basic catalysts in sequential pyrolysis of lignocellulosic biomass gives rise to a more deoxygenated bio-oil\* at the expense of a decrease in its total mass yield. It was demonstrated that the bio-oils\* from the B+A

#### **4.4. Fast pyrolysis of wheat straw by dual-catalyst tandem system**

configurations have lower proportions of detected compounds. However, in return they have higher aromatic hydrocarbons concentration, especially when using a catalyst with high concentration of basic sites in the upper bed, such as MgO. This bio-oil\* shows a total concentration of 11.6 wt.% of aromatic hydrocarbons, where substituted benzenes stand out over PAHs.

### 4.5. Comparison of studied catalysts and coupling configurations

This section compiles the most relevant results of the previous sections with the goal of establishing a comparison between the different catalytic systems in terms of products that may have a commercial value.

Firstly, and aimed to the possible use of the whole bio-oil as a biofuel, the relationship between oxygen contents and bio-oil\* mass and energy yields of selected catalytic tests, performed at the same operating conditions ( $C/B$  ratio = 0.2 and  $T_{\text{catalysis}} = 450$  °C), are compared in **Figures 4.5.1.a** and **4.5.1.b**, respectively. In addition, non-catalytic tests performed following the two different bio-oil recovery procedures are also included in the study for reference (denoted as  $N-C_x$ , where  $x$  corresponds to the number of the procedure). Apart from the reference thermal test, the only catalytic test carried out following Procedure 1 that involved the use of acetone in the recovery of bio-oil, is the one performed with KH-ZSM-5 zeolite.

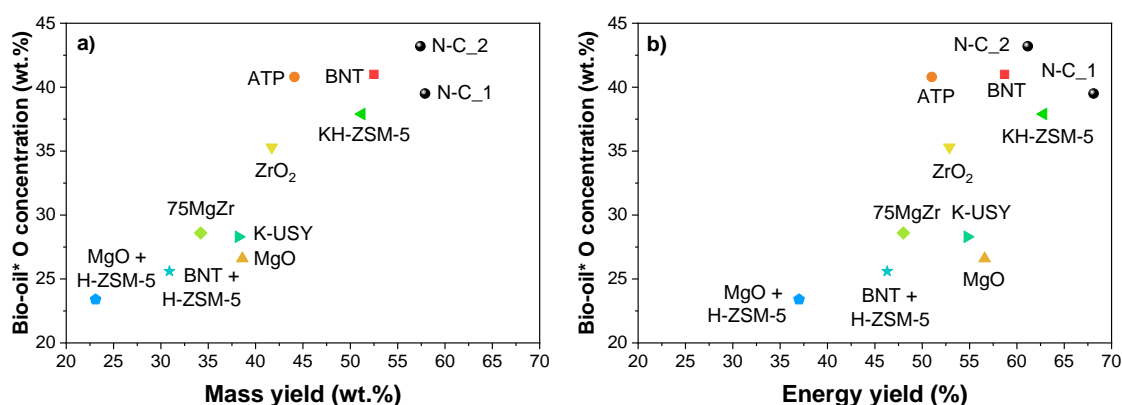


**Figure 4.5.1.** Relationship between the oxygen content and yields of the bio-oil\* fraction in the fast pyrolysis of wheat straw over the different catalysts and coupling configurations studied when  $C/B$  ratio = 0.2 and  $T_{\text{catalysis}} = 450$  °C: a) mass yield; b) energy yield.

Coupling catalyst tests exhibit the lowest oxygen concentrations of bio-oils\*, showing also the greatest difference between mass and energy yields regarding those of their respective thermal test. Having these low oxygen contents should imply higher energy yields of both bio-oils\*. However, due to the low mass yields obtained for both dual-catalyst catalytic tests, these values are at the lower left-hand side of the graphs. In addition, bio-oils\* obtained over MgO and K-USY catalysts can be also interesting as biofuels since they present a significantly lower oxygen content than the thermal ones

#### 4.5. Comparison of studied catalysts and coupling configurations

whereas their energy yields are over 50 %, which are very close to that of the non-catalytic test. Thus, the use of MgO and K-grafted USY zeolite in catalytic fast pyrolysis of wheat straw is not only interesting in their valorisation as a source of high-added value bio-based chemicals, but also as potential biofuels.

On the other hand, the interest of this catalyst screening is to analyse the influence of the nature of the catalysts studied on the compound families obtained in each bio-oil\*. In this way, **Figure 4.5.2** represents the yield of GC-MS detected species. As has been commented throughout the discussion, the non-catalytic tests exhibit low mass yields of GC-MS detected compounds (10.8 – 16.9 wt.%), only accounting for 18.8 – 29.2 wt.% of the total bio-oil\*. The inclusion of catalysts in the fast pyrolysis of acid-washed wheat straw results in bio-oils\* with more detected compounds due to the relatively simpler chemical structures of the molecules so obtained. The highest increase in this parameter corresponds with the use of BNT and MgO catalysts, reaching yields that are more than twice higher than that of their respective thermal bio-oil\*.

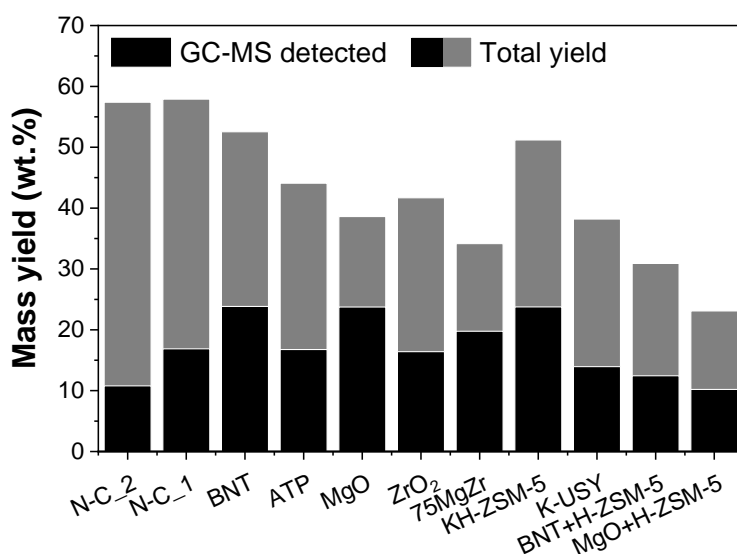


**Figure 4.5.2.** GC-MS analyses of the bio-oil\* obtained in the bio-oil\* produced by fast pyrolysis of wheat straw over different catalysts and coupling configurations: overall mass yields of GC-MS detected components.

When detected compounds are considered individually by families (**Figure 4.5.3**), the nature of the catalysts, as well as their textural and acid-base properties, have a great impact on the composition of bio-oils\*.

Firstly, carboxylic acids are present to a great extent in bio-oils\* of most single-step catalytic tests under mild conditions of C/B ratio and catalytic temperature, especially in the case of attapulgite. Conversely, production of furans stands out in bio-oils\* from tests involving basic Mg-containing metal oxides, as dehydration of anhydrosugars into furans is promoted.

Secondly, the most notorious compound family in thermal tests is that of anhydrosugars (6.0 – 8.4 wt.%). Unlike other catalytic systems, bentonite clay showed the highest yield of anhydrosugars (11.6 wt.%), concretely levoglucosan, which appears to be the most abundant product of cellulose fast pyrolysis.

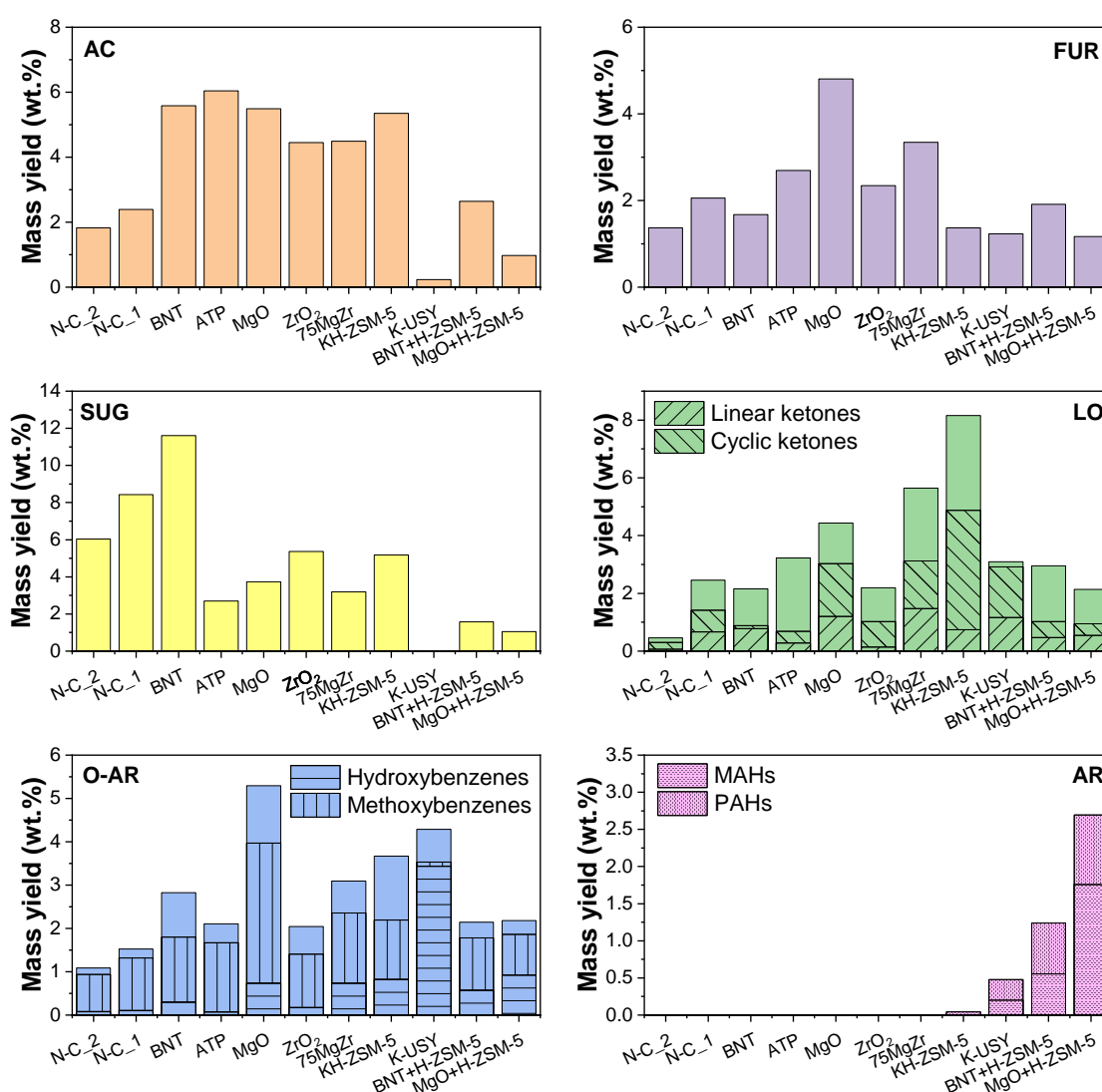


**Figure 4.5.3.** GC-MS detected mass yields of compound families present in the bio-oil\* produced by fast pyrolysis of ws-ac over different catalysts and coupling configurations (AC: carboxylic acids, LO: light oxygenates, FUR: furans, SUG: anhydrosugars, O-AR: oxygenated aromatics, and AR: aromatic hydrocarbons).

#### 4.5. Comparison of studied catalysts and coupling configurations

Thirdly, Mg-containing metal oxides and K-incorporated zeolites showed moderate-high yields of both light oxygenates (3.1 – 8.2 wt.%) and oxygenated aromatics (3.1 – 5.3 wt.%). The former are derived from cellulose and hemicellulose pyrolysis, whereas the latter are product of the transformation of lignin oligomers. Ketones, specifically cyclic ketones, are the most abundant compounds in the light oxygenates family, whereas methoxybenzenes and hydroxybenzenes are those of the oxygenated aromatics family. As discussed previously, hydroxybenzenes are more abundant at more severe conditions of C/B ratio and temperature, as observed in the K-USY bio-oil\* obtained at C/B = 0.6 and 500 °C, since methoxybenzenes act as their precursors. Moreover, in this particular case, ketones account for 94 % of the total light oxygenates. Conversely, among Mg-containing metal oxides and K-incorporated zeolites, catalysts with more balanced acid-base properties, such as the Mg-Zr mixed metal oxide and the KH-ZSM-5 zeolite, exhibit higher yields of light oxygenates than oxygenated aromatics. In contrast, those with higher basicity to acidity ratio, like MgO and K-grafted USY zeolite, produce more oxygenated aromatics than light oxygenates, since C–C bond formation reactions predominate over cracking reactions, resulting in compounds of higher molecular weight.

Finally, catalytic tests involving zeolites exhibit low-moderate yields of aromatic hydrocarbons. Dual-catalyst catalytic tests stand out over single-catalyst tests, specifically, that of MgO + H-ZSM-5 shows a remarkable yield of aromatic hydrocarbons (2.7 wt.%). The synergistic effect of a highly basic catalyst and a highly acid catalyst result in the transformation of carboxylic acids, light oxygenates and furans into aromatic hydrocarbons through sequential reaction mechanisms described in the previous section. Furthermore, the proportion between mono- and polycyclic aromatic hydrocarbons of such configuration (1.9 : 1) is higher than in any other catalytic systems.



## **5. General conclusions**



The main conclusions of this Doctoral Thesis are summarised below, aiming to respond in general terms to the objectives set out at the beginning of the research:

- Bentonite clay showed high bio-oil\* yields with low formation of undesirable by-products. Anhydrosugars are the most abundant compounds in both bio-oils\* produced by catalytic pyrolysis of acid-washed wheat straw and cellulose. This fact can be attributed to the synergistic effect of its textural properties and high weak-mild basicity. Their production is maximised at a catalyst to biomass ratio of 0.2 (11.6 and 13.9 wt.%, respectively).
- Compared to bentonite clay, attapulgite clay exhibited considerably reduced bio-oil\* yields due to its higher textural and acid-base properties leading to excessive cracking and deoxygenation reactions. However, this fact benefits the formation of gaseous hydrocarbons and the reduction in the oxygen concentration of bio-oil\*. Regarding the composition of bio-oil\*, the highest yield of carboxylic acids (6.0 wt.%) is observed for a catalyst to biomass ratio of 0.2.
- Magnesium oxide presents the highest overall basicity (4.13 mmolCO<sub>2</sub>/g) among all catalysts studied with a high contribution of medium basicity (71 %). Bio-oil\* yield is significantly reduced due to the more efficient deoxygenation and extensive C–C bond formation reactions, including aldol condensation and ketonisation reactions, promoted by its high concentrations of basic sites. Thus, basic MgO gives rise to a highly deoxygenated bio-oil\* (oxygen content of 26.6 wt.%), but its energy yield remains very similar to the reference thermal test despite the reduction in its mass yield. The bio-oil\* so obtained shows the highest concentration of detected compounds by GC-MS and remarkable yields of light oxygenates (4.4 wt.%) and oxygenated aromatics (5.3 wt.%). Cyclic ketones, such as cyclopentenones, stand out among other light oxygenates, whereas production of acetophenones and guaiacols is highlighted among other oxygenated aromatics. In addition, the highest yield of furans (4.8 wt.%) is observed for this catalytic test.
- Zirconium oxide showed amphoteric acid-base properties, but its overall basicity is not comparable with the other Mg-containing oxides. Thus, ZrO<sub>2</sub> exhibited low activity in the fast pyrolysis of wheat straw, which is reflected in the highest bio-oil yield\* and oxygen concentration among catalytic tests with the other materials studied. Regarding the composition of bio-oil\*, the most predominant compounds are carboxylic acids and anhydrosugars.

## 5. General conclusions

- A Mg-Zr mixed oxide with a Mg/(Mg+Zr) ratio of 0.71, synthesised by co-precipitation of magnesium and zirconyl nitrates, results in an enhanced overall acidity due to synergistic effect of both single oxides and an intermediate overall basicity between the two single oxides. As in the case of MgO, bio-oil\* yield was considerably reduced due to its remarkable acid-base properties. 75MgZr produced a not-so-highly deoxygenated bio-oil\* (oxygen content of 28.6 wt.%) rich in light oxygenates (5.6 wt.%), including acetals and ketones, although its production of oxygenated aromatics is somewhat diminished compared to MgO (3.1 wt.%).
- The K-exchanged H-ZSM-5 zeolite showed similar crystallinity and textural properties to its parent material. However, ion-exchange strongly modified its acid-base properties, decreasing the concentration of strong acid sites, while generating basic sites of weak-mild strength. When tested in the catalytic pyrolysis of wheat straw, the increase of the KH-ZSM-5 catalyst to biomass ratio provokes a progressive reduction of the bio-oil\* yield with and enhancement in the production of gases, water and coke. It showed a more efficient behaviour than parent H-ZSM-5 zeolite since, for the same or even lower oxygen contents, the bio-oil\* is produced in clearly larger mass yields. In terms of bio-oil\* composition, KH-ZSM-5 zeolite showed quite larger yields of GC-MS detected components with an enhanced production of carboxylic acids, oxygenated aromatics and light oxygenates, with a great share of ketones, which could be assigned to ketonisation activity arising from its generated basic sites.
- The K-grafted USY zeolite showed a high concentration of basic sites of weak-mild strength, but with reduced textural properties caused by partial desilication/amorphisation of the parent zeolite. The stability of the K-USY zeolite was tested by steaming at 450 °C, showing that its crystallinity and basicity were not affected. The K-USY zeolite showed enhanced activity for the catalytic pyrolysis of acid-washed wheat straw in comparison with the USY sample. This fact was clearly reflected in the reduction of both the yield and oxygen content of the bio-oil\* fraction when increasing the catalyst to biomass ratio. Remarkable changes were also observed in the bio-oil\* composition when using the K-USY catalyst. Thus, an increase in the yield of GC-MS detected components was denoted, showing that this basic catalyst promotes the transformation of oligomers and heavy species into lighter and more valuable compounds, such as light oxygenates and oxygenated aromatics. Moreover, varying the temperature of the

catalyst bed and the C/B ratio allowed the bio-oil\* composition to be further optimised. Accordingly, when working at 500 °C in the catalytic zone of the reaction system and with a catalyst to biomass ratio of 0.6, the formation of both ketones (with a great share of cyclic ketones) and phenolics was favoured.

- The combination of bentonite and H-ZSM-5 zeolite in sequential pyrolysis of wheat straw gives rise to a more deoxygenated bio-oil\* at the expense of a decrease in its total mass yield. A little positive effect on aromatic hydrocarbons concentration is observed with respect to the catalytic test with the sole H-ZSM-5 zeolite (1.2 vs. 1.0 wt.%, respectively). As in this case, polycyclic aromatic hydrocarbons predominate over substituted benzenes.
- In contrast, the combination of MgO and H-ZSM-5 zeolite in sequential pyrolysis of wheat straw significantly enhances the production of aromatic hydrocarbons. Oligomeric fragments are transformed into smaller species that are precursors of furans and light olefins in a primary step over basic MgO and are further converted into aromatic hydrocarbons in a secondary step over a mainly microporous and acid catalyst like H-ZSM-5 zeolite. The highest yield of aromatic hydrocarbons (2.7 wt.%) with the highest proportion of monoaromatic/polycyclic aromatic hydrocarbons (1.9 : 1) was achieved for this dual-catalyst catalytic test.



## **6. Recommendations for future work**





## 6. Recommendations for future work

As a consequence of the results and conclusions obtained in the present Doctoral Thesis on the ex-situ catalytic fast pyrolysis of acid-washed wheat straw over diverse acid-base catalysts and coupling configurations, the following recommendations for future research are suggested:

- To prepare multifunctional catalysts by loading metals with different functionalities on either Mg-containing metal oxides or K-incorporated zeolites.
- To deepen the use of the basic+acid coupling catalyst configuration by testing innovative combinations of acid-base catalysts.
- To study the nature of the carbonaceous deposits on the surface of the catalysts, their deactivation and their regenerability.
- To bring bio-oil upgrading over basic or both basic and acid catalysts to larger scales.
- To consider both material and energy valorisation of other by-products of catalytic fast pyrolysis, such as char and gaseous hydrocarbons.
- To evaluate the environmental impact and the techno-economic viability of the process under optimised conditions.
- To develop an effective system of separation/fractionation of the components present in the bio-oil finally obtained.



## **7. References**



- [1] U.S. Energy Information Administration, Biomass explained. (2021). <https://www.eia.gov/energyexplained/biomass/> (accessed April 19, 2022).
- [2] R. Gurjar, A. Raychaudhuri, S. Bagchi, M. Behera, Biomass to Fuel and Chemicals: Enabling Technologies, in: Biomass, Biofuels, Biochemicals, Elsevier, 2021: 57–90. <https://doi.org/10.1016/B978-0-12-821878-5.00021-0>.
- [3] K.N. Yogalakshmi, T. Poornima Devi, P. Sivashanmugam, S. Kavitha, R. Yukesh Kannah, S. Varjani, S. AdishKumar, G. Kumar, J. Rajesh Banu, Lignocellulosic biomass-based pyrolysis: A comprehensive review. *Chemosphere*, 286 (2022) 1–16. <https://doi.org/10.1016/j.chemosphere.2021.131824>.
- [4] I.G. Hakeem, P. Halder, M.H. Marzbali, S. Patel, S. Kundu, J. Paz-Ferreiro, A. Surapaneni, K. Shah, Research progress on levoglucosan production via pyrolysis of lignocellulosic biomass and its effective recovery from bio-oil. *Journal of Environmental Chemical Engineering*, 9 (2021). <https://doi.org/10.1016/j.jece.2021.105614>.
- [5] L. Dai, Y. Wang, Y. Liu, C. He, R. Ruan, Z. Yu, L. Jiang, Z. Zeng, Q. Wu, A review on selective production of value-added chemicals via catalytic pyrolysis of lignocellulosic biomass. *Science of the Total Environment*, 749 (2020). <https://doi.org/10.1016/j.scitotenv.2020.142386>.
- [6] J. Liang, G. Shan, Y. Sun, Catalytic fast pyrolysis of lignocellulosic biomass: Critical role of zeolite catalysts. *Renewable and Sustainable Energy Reviews*, 139 (2021). <https://doi.org/10.1016/j.rser.2021.110707>.
- [7] L. Dai, N. Zhou, H. Li, W. Deng, Y. Cheng, Y. Wang, Y. Liu, K. Cobb, H. Lei, P. Chen, R. Ruan, Recent advances in improving lignocellulosic biomass-based bio-oil production. *Journal of Analytical and Applied Pyrolysis*, 149 (2020). <https://doi.org/10.1016/j.jaap.2020.104845>.
- [8] P. Khemthong, C. Yimsukanan, T. Narkkun, A. Srifa, T. Witoon, S. Pongchaiphol, S. Kiatphuengporn, K. Faungnawakij, Advances in catalytic production of value-added biochemicals and biofuels via furfural platform derived lignocellulosic biomass. *Biomass and Bioenergy*, 148 (2021). <https://doi.org/10.1016/j.biombioe.2021.106033>.
- [9] V. de Buck, M. Polanska, J. van Impe, Modeling Biowaste Biorefineries: A Review. *Frontiers in Sustainable Food Systems*, 4 (2020). <https://doi.org/10.3389/fsufs.2020.00011>.
- [10] International Energy Agency, Bioenergy. (2022). <https://www.iea.org/fuels-and-technologies/bioenergy> (accessed September 4, 2022).
- [11] S. Wang, G. Dai, H. Yang, Z. Luo, Lignocellulosic biomass pyrolysis mechanism: A state-of-the-art review. *Progress in Energy and Combustion Science*, 62 (2017) 33–86. <https://doi.org/10.1016/j.pecs.2017.05.004>.

## 7. References

- [12] International Energy Agency, Technology Roadmap - Biofuels for Transport, 2011.
- [13] X. Chen, Q. Che, S. Li, Z. Liu, H. Yang, Y. Chen, X. Wang, J. Shao, H. Chen, Recent developments in lignocellulosic biomass catalytic fast pyrolysis: Strategies for the optimization of bio-oil quality and yield. *Fuel Processing Technology*, 196 (2019). <https://doi.org/10.1016/j.fuproc.2019.106180>.
- [14] Y. Wang, A. Akbarzadeh, L. Chong, J. Du, N. Tahir, M.K. Awasthi, Catalytic pyrolysis of lignocellulosic biomass for bio-oil production: A review. *Chemosphere*, 297 (2022). <https://doi.org/10.1016/j.chemosphere.2022.134181>.
- [15] S.G. Karp, E. Bittencourt Sydney, A. Lorenci Woiciechowski, L.A.J. Letti, J.C. de Carvalho, L.A. Zevallos Torres, G. Sprotte Kumlehn, E. de Souza Candéo, C.R. Soccol, Lignocellulosic Biorefinery for Value-Added Products: The Emerging Bioeconomy, in: *Biomass, Biofuels, Biochemicals*, Elsevier, 2021: 291–321. <https://doi.org/10.1016/B978-0-12-821878-5.00002-7>.
- [16] J.A. Ruiz, M.C. Juárez, M.P. Morales, P. Muñoz, M.A. MENDÍVIL, Biomass gasification for electricity generation: Review of current technology barriers. *Renewable and Sustainable Energy Reviews*, 18 (2013) 174–183. <https://doi.org/10.1016/j.rser.2012.10.021>.
- [17] Y.H. Xu, M.F. Li, Hydrothermal liquefaction of lignocellulose for value-added products: Mechanism, parameter and production application. *Bioresource Technology*, 342 (2021). <https://doi.org/10.1016/j.biortech.2021.126035>.
- [18] T. Kan, V. Strezov, T.J. Evans, Lignocellulosic biomass pyrolysis: A review of product properties and effects of pyrolysis parameters. *Renewable and Sustainable Energy Reviews*, 57 (2016) 1126–1140. <https://doi.org/10.1016/j.rser.2015.12.185>.
- [19] M. Tawalbeh, A. Al-Othman, T. Salamah, M. Alkasrawi, R. Martis, Z.A. El-Rub, A critical review on metal-based catalysts used in the pyrolysis of lignocellulosic biomass materials. *Journal of Environmental Management*, 299 (2021). <https://doi.org/10.1016/j.jenvman.2021.113597>.
- [20] T. Kan, V. Strezov, T. Evans, J. He, R. Kumar, Q. Lu, Catalytic pyrolysis of lignocellulosic biomass: A review of variations in process factors and system structure. *Renewable and Sustainable Energy Reviews*, 134 (2020). <https://doi.org/10.1016/j.rser.2020.110305>.
- [21] C. Liu, H. Wang, A.M. Karim, J. Sun, Y. Wang, Catalytic fast pyrolysis of lignocellulosic biomass. *Chemical Society Reviews*, 43 (2014) 7594–7623. <https://doi.org/10.1039/c3cs60414d>.
- [22] L.J. Jönsson, C. Martín, Pretreatment of lignocellulose: Formation of inhibitory by-products and strategies for minimizing their effects. *Bioresource*

- Technology, 199 (2016) 103–112.  
<https://doi.org/10.1016/j.biortech.2015.10.009>.
- [23] E. Butler, G. Devlin, D. Meier, K. McDonnell, A review of recent laboratory research and commercial developments in fast pyrolysis and upgrading. *Renewable and Sustainable Energy Reviews*, 15 (2011) 4171–4186.  
<https://doi.org/10.1016/j.rser.2011.07.035>.
- [24] A. v. Bridgwater, Review of fast pyrolysis of biomass and product upgrading. *Biomass and Bioenergy*, 38 (2012) 68–94.  
<https://doi.org/10.1016/j.biombioe.2011.01.048>.
- [25] C. Hu, R. Xiao, H. Zhang, Ex-situ catalytic fast pyrolysis of biomass over HZSM-5 in a two-stage fluidized-bed/fixed-bed combination reactor. *Bioresource Technology*, 243 (2017) 1133–1140.  
<https://doi.org/10.1016/j.biortech.2017.07.011>.
- [26] Y. Picó, D. Barceló, Pyrolysis gas chromatography-mass spectrometry in environmental analysis: Focus on organic matter and microplastics. *TrAC - Trends in Analytical Chemistry*, 130 (2020).  
<https://doi.org/10.1016/j.trac.2020.115964>.
- [27] S. Douvartzides, N.D. Charisiou, W. Wang, V.G. Papadakis, K. Polychronopoulou, M.A. Goula, Catalytic fast pyrolysis of agricultural residues and dedicated energy crops for the production of high energy density transportation biofuels. Part II: Catalytic research. *Renewable Energy*, 189 (2022) 315–338. <https://doi.org/10.1016/j.renene.2022.02.106>.
- [28] H. Hernando, S. Jiménez-Sánchez, J. Feroso, P. Pizarro, J.M. Coronado, D.P. Serrano, Assessing biomass catalytic pyrolysis in terms of deoxygenation pathways and energy yields for the efficient production of advanced biofuels. *Catalysis Science and Technology*, 6 (2016) 2829–2843.  
<https://doi.org/10.1039/c6cy00522e>.
- [29] T.R. Carlson, Y.T. Cheng, J. Jae, G.W. Huber, Production of green aromatics and olefins by catalytic fast pyrolysis of wood sawdust. *Energy and Environmental Science*, 4 (2011) 145–161.  
<https://doi.org/10.1039/c0ee00341g>.
- [30] H. Hattori, Y. Ono, Catalysts and catalysis for acid-base reactions, in: *Metal Oxides in Heterogeneous Catalysis*, Elsevier, 2018: 133–209.  
<https://doi.org/10.1016/B978-0-12-811631-9.00004-1>.
- [31] J.C. Védrine, Recent developments and perspectives of acid-base and redox catalytic processes by metal oxides. *Applied Catalysis A: General*, 575 (2019) 170–179. <https://doi.org/10.1016/j.apcata.2019.02.012>.
- [32] Y. Ono, H. Hattori, *Solid Base Catalysis*, Springer Berlin Heidelberg, Berlin, Heidelberg, 2011. <https://doi.org/10.1007/978-3-642-18339-3>.

## 7. References

- [33] T.C. Keller, K. Desai, S. Mitchell, J. Pérez-Ramírez, Design of Base Zeolite Catalysts by Alkali-Metal Grafting in Alcoholic Media. *ACS Catalysis*, 5 (2015) 5388–5396. <https://doi.org/10.1021/acscatal.5b00761>.
- [34] J.A. Cecilia, C.P. Jiménez-Gómez, Catalytic applications of clay minerals and hydrotalcites. *Catalysts*, 11 (2021) 1–4. <https://doi.org/10.3390/catal11010068>.
- [35] N. Kumari, C. Mohan, Basics of Clay Minerals and Their Characteristic Properties, in: *Clay and Clay Minerals*, IntechOpen, 2021. <https://doi.org/10.5772/intechopen.97672>.
- [36] A. Doroshenko, I. Pylypenko, K. Heaton, S. Cowling, J. Clark, V. Budarin, Selective Microwave-Assisted Pyrolysis of Cellulose towards Levoglucosenone with Clay Catalysts. *ChemSusChem*, 12 (2019) 5224–5227. <https://doi.org/10.1002/cssc.201903026>.
- [37] P. Rutkowski, Pyrolytic behavior of cellulose in presence of montmorillonite K10 as catalyst. *Journal of Analytical and Applied Pyrolysis*, 98 (2012) 115–122. <https://doi.org/10.1016/j.jaap.2012.07.012>.
- [38] M.F. Brigatti, E. Galan, B.K.G. Theng, Chapter 2 Structures and Mineralogy of Clay Minerals. *Developments in Clay Science*, 1 (2006) 19–86. [https://doi.org/10.1016/S1572-4352\(05\)01002-0](https://doi.org/10.1016/S1572-4352(05)01002-0).
- [39] A. Veses, M. Aznar, J.M. López, M.S. Callén, R. Murillo, T. García, Production of upgraded bio-oils by biomass catalytic pyrolysis in an auger reactor using low cost materials. *Fuel*, 141 (2015) 17–22. <https://doi.org/10.1016/j.fuel.2014.10.044>.
- [40] O.Y. Golubeva, E.N. Korytkova, V. v Gusarov, Hydrothermal Synthesis of Magnesium Silicate Montmorillonite for Polymer/Clay Nanocomposites, 2005.
- [41] W.F. Bradley, The structural scheme of attapulgite. *American Mineralogist*, 25 (1940) 405–410. <https://pubs.geoscienceworld.org/msa/ammin/article-abstract/25/6/405/538015/The-structural-scheme-of-attapulgite> (accessed June 1, 2022).
- [42] Y. Zhou, Z. Chen, H. Gong, L. Chen, H. Yu, W. Wu, Characteristics of dehydration during rice husk pyrolysis and catalytic mechanism of dehydration reaction with NiO/ $\gamma$ -Al<sub>2</sub>O<sub>3</sub> as catalyst. *Fuel*, 245 (2019) 131–138. <https://doi.org/10.1016/j.fuel.2019.02.059>.
- [43] S.D. Stefanidis, K.G. Kalogiannis, E.F. Iliopoulou, A.A. Lappas, P.A. Pilavachi, In-situ upgrading of biomass pyrolysis vapors: Catalyst screening on a fixed bed reactor. *Bioresource Technology*, 102 (2011) 8261–8267. <https://doi.org/10.1016/j.biortech.2011.06.032>.
- [44] T. Mochizuki, D. Atong, S.Y. Chen, M. Toba, Y. Yoshimura, Effect of SiO<sub>2</sub> pore size on catalytic fast pyrolysis of Jatropha residues by using pyrolyzer-



- GC/MS. *Catalysis Communications*, 36 (2013) 1–4. <https://doi.org/10.1016/j.catcom.2013.02.018>.
- [45] H. Hattori, Solid base catalysts: Fundamentals and their applications in organic reactions. *Applied Catalysis A: General*, 504 (2015) 103–109. <https://doi.org/10.1016/j.apcata.2014.10.060>.
- [46] S.D. Stefanidis, S.A. Karakoulia, K.G. Kalogiannis, E.F. Iliopoulou, A. Delimitis, H. Yiannoulakis, T. Zampetakis, A.A. Lappas, K.S. Triantafyllidis, Natural magnesium oxide (MgO) catalysts: A cost-effective sustainable alternative to acid zeolites for the in situ upgrading of biomass fast pyrolysis oil. *Applied Catalysis B: Environmental*, 196 (2016) 155–173. <https://doi.org/10.1016/j.apcatb.2016.05.031>.
- [47] R. Kumar, N. Enjamuri, S. Shah, A.S. Al-Fatesh, J.J. Bravo-Suárez, B. Chowdhury, Ketoneization of oxygenated hydrocarbons on metal oxide based catalysts. *Catalysis Today*, 302 (2018) 16–49. <https://doi.org/10.1016/j.cattod.2017.09.044>.
- [48] Q. Lu, Y. Zhang, Z. Tang, W.Z. Li, X.F. Zhu, Catalytic upgrading of biomass fast pyrolysis vapors with titania and zirconia/titania based catalysts. *Fuel*, 89 (2010) 2096–2103. <https://doi.org/10.1016/j.fuel.2010.02.030>.
- [49] Sheldon R A, van Bekkum H, Solid-base Catalysis, in: *Fine Chemicals through Heterogeneous Catalysis*, Wiley-VCH Verlag GmbH, Weinheim, Germany, 2007: 309–349. <https://doi.org/10.1002/9783527612963.ch07>.
- [50] M. Zabeti, T.S. Nguyen, L. Lefferts, H.J. Heeres, K. Seshan, In situ catalytic pyrolysis of lignocellulose using alkali-modified amorphous silica alumina. *Bioresource Technology*, 118 (2012) 374–381. <https://doi.org/10.1016/j.biortech.2012.05.034>.
- [51] R.M. Navarro, R. Guil-Lopez, J.L.G. Fierro, N. Mota, S. Jiménez, P. Pizarro, J.M. Coronado, D.P. Serrano, Catalytic fast pyrolysis of biomass over Mg-Al mixed oxides derived from hydrotalcite-like precursors: Influence of Mg/Al ratio. *Journal of Analytical and Applied Pyrolysis*, 134 (2018) 362–370. <https://doi.org/10.1016/j.jaap.2018.07.001>.
- [52] G. Busca, Acidity and basicity of zeolites: A fundamental approach. *Microporous and Mesoporous Materials*, 254 (2017) 3–16. <https://doi.org/10.1016/j.micromeso.2017.04.007>.
- [53] H. Hernando, I. Moreno, J. Feroso, C. Ochoa-Hernández, P. Pizarro, J.M. Coronado, J. Čejka, D.P. Serrano, Biomass catalytic fast pyrolysis over hierarchical ZSM-5 and Beta zeolites modified with Mg and Zn oxides. *Biomass Conversion and Biorefinery*, 7 (2017) 289–304. <https://doi.org/10.1007/s13399-017-0266-6>.

## 7. References

- [54] J. Feroso, H. Hernando, P. Jana, I. Moreno, J. Přech, C. Ochoa-Hernández, P. Pizarro, J.M. Coronado, J. Čejka, D.P. Serrano, Lamellar and pillared ZSM-5 zeolites modified with MgO and ZnO for catalytic fast-pyrolysis of eucalyptus woodchips. *Catalysis Today*, 277 (2016) 171–181. <https://doi.org/10.1016/j.cattod.2015.12.009>.
- [55] P. Li, X. Chen, X. Wang, J. Shao, G. Lin, H. Yang, Q. Yang, H. Chen, Catalytic Upgrading of Fast Pyrolysis Products with Fe-, Zr-, and Co-Modified Zeolites Based on Pyrolyzer-GC/MS Analysis. *Energy and Fuels*, 31 (2017) 3979–3986. <https://doi.org/10.1021/acs.energyfuels.6b03105>.
- [56] H. Hernando, A.M. Hernández-Giménez, C. Ochoa-Hernández, P.C.A. Bruijninx, K. Houben, M. Baldus, P. Pizarro, J.M. Coronado, J. Feroso, J. Čejka, B.M. Weckhuysen, D.P. Serrano, Engineering the acidity and accessibility of the zeolite ZSM-5 for efficient bio-oil upgrading in catalytic pyrolysis of lignocellulose. *Green Chemistry*, 20 (2018) 3499–3511. <https://doi.org/10.1039/c8gc01722k>.
- [57] A.C. Psarras, C.M. Michailof, E.F. Iliopoulou, K.G. Kalogiannis, A.A. Lappas, E. Heracleous, K.S. Triantafyllidis, Acetic acid conversion reactions on basic and acidic catalysts under biomass fast pyrolysis conditions. *Molecular Catalysis*, 465 (2019) 33–42. <https://doi.org/10.1016/j.mcat.2018.12.012>.
- [58] Y. Zhang, H. Lei, Z. Yang, D. Duan, E. Villota, R. Ruan, From glucose-based carbohydrates to phenol-rich bio-oils integrated with syngas production via catalytic pyrolysis over an activated carbon catalyst. *Green Chemistry*, 20 (2018) 3346–3358. <https://doi.org/10.1039/c8gc00593a>.
- [59] M.M. Ramirez-Corredores, Pathways and Mechanisms of Fast Pyrolysis: Impact on Catalyst Research, in: *The Role of Catalysis for the Sustainable Production of Bio-Fuels and Bio-Chemicals*, Elsevier Inc., 2013: 161–216. <https://doi.org/10.1016/B978-0-444-56330-9.00006-1>.
- [60] L. Faba, E. Díaz, S. Ordóñez, Base-catalyzed reactions in biomass conversion: Reaction mechanisms and catalyst deactivation, in: *Reaction Pathways and Mechanisms in Thermocatalytic Biomass Conversion I: Cellulose Structure, Depolymerization and Conversion by Heterogeneous Catalysts*, Springer Singapore, 2015: 87–122. [https://doi.org/10.1007/978-981-287-688-1\\_5](https://doi.org/10.1007/978-981-287-688-1_5).
- [61] J. Gupta, K. Papadakis, E.Y. Konyshova, Y. Lin, I. v. Kozhevnikov, J. Li, CaO catalyst for multi-route conversion of oakwood biomass to value-added chemicals and fuel precursors in fast pyrolysis. *Applied Catalysis B: Environmental*, 285 (2021). <https://doi.org/10.1016/j.apcatb.2020.119858>.
- [62] P.M. Mortensen, J.D. Grunwaldt, P.A. Jensen, K.G. Knudsen, A.D. Jensen, A review of catalytic upgrading of bio-oil to engine fuels. *Applied Catalysis A: General*, 407 (2011) 1–19. <https://doi.org/10.1016/j.apcata.2011.08.046>.

- [63] C.D. Chang, A.J. Silvestri, The conversion of methanol and other O-compounds to hydrocarbons over zeolite catalysts. *Journal of Catalysis*, 47 (1977) 249–259. [https://doi.org/10.1016/0021-9517\(77\)90172-5](https://doi.org/10.1016/0021-9517(77)90172-5).
- [64] J. Huang, X. Li, D. Wu, H. Tong, W. Li, Theoretical studies on pyrolysis mechanism of guaiacol as lignin model compound. *Journal of Renewable and Sustainable Energy*, 5 (2013). <https://doi.org/10.1063/1.4816497>.
- [65] C.C. Chang, H. Je Cho, J. Yu, R.J. Gorte, J. Gulbinski, P. Dauenhauer, W. Fan, Lewis acid zeolites for tandem Diels-Alder cycloaddition and dehydration of biomass-derived dimethylfuran and ethylene to renewable p-xylene. *Green Chemistry*, 18 (2016) 1368–1376. <https://doi.org/10.1039/c5gc02164b>.
- [66] Y.T. Cheng, G.W. Huber, Production of targeted aromatics by using Diels-Alder classes of reactions with furans and olefins over ZSM-5. *Green Chemistry*, 14 (2012) 3114–3125. <https://doi.org/10.1039/c2gc35767d>.
- [67] M. Vandichel, D. Lesthaeghe, J. van der Mynsbrugge, M. Waroquier, V. van Speybroeck, Assembly of cyclic hydrocarbons from ethene and propene in acid zeolite catalysis to produce active catalytic sites for MTO conversion. *Journal of Catalysis*, 271 (2010) 67–78. <https://doi.org/10.1016/j.jcat.2010.02.001>.
- [68] Y. Cai, Y. Fan, X. Li, L. Chen, J. Wang, Preparation of refined bio-oil by catalytic transformation of vapors derived from vacuum pyrolysis of rape straw over modified HZSM-5. *Energy*, 102 (2016) 95–105. <https://doi.org/10.1016/j.energy.2016.02.051>.
- [69] Y.T. Cheng, Z. Wang, C.J. Gilbert, W. Fan, G.W. Huber, Production of p-Xylene from Biomass by Catalytic Fast Pyrolysis Using ZSM-5 Catalysts with Reduced Pore Openings. *Angewandte Chemie International Edition*, 51 (2012) 11097–11100. <https://doi.org/10.1002/anie.201205230>.
- [70] D.J. Mihalcik, C.A. Mullen, A.A. Boateng, Screening acidic zeolites for catalytic fast pyrolysis of biomass and its components. *Journal of Analytical and Applied Pyrolysis*, 92 (2011) 224–232. <https://doi.org/10.1016/j.jaap.2011.06.001>.
- [71] D.B. Lukyanov, N.S. Gnep, M.R. Guisnet, Kinetic modeling of ethene and propene aromatization over HZSM-5 and GaHZSM-5. *Industrial & Engineering Chemistry Research*, 33 (1994) 223–234. <https://doi.org/10.1021/ie00026a008>.
- [72] L. Faba, E. Díaz, S. Ordóñez, Improvement on the catalytic performance of Mg-Zr mixed oxides for furfural-acetone aldol condensation by supporting on mesoporous carbons. *ChemSusChem*, 6 (2013) 463–473. <https://doi.org/10.1002/cssc.201200710>.
- [73] M. Montaña, M.B. Navas, H.P. Bideberripe, M.L. Barbelli, I.D. Lick, M.L. Casella, A heterogeneous catalytic process to mitigate the acidity of bio-oils

## 7. References

- caused by the presence of volatile organic acids. *Fuel*, 299 (2021). <https://doi.org/10.1016/j.fuel.2021.120919>.
- [74] M.R. Rover, A. Aui, M.M. Wright, R.G. Smith, R.C. Brown, Production and purification of crystallized levoglucosan from pyrolysis of lignocellulosic biomass. *Green Chemistry*, 21 (2019) 5980–5989. <https://doi.org/10.1039/c9gc02461a>.
- [75] X. Huang, J. Ren, J.Y. Ran, C.L. Qin, Z.Q. Yang, J.P. Cao, Recent advances in pyrolysis of cellulose to value-added chemicals. *Fuel Processing Technology*, 229 (2022). <https://doi.org/10.1016/j.fuproc.2022.107175>.
- [76] S.J. Oh, G.G. Choi, J.S. Kim, Production of acetic acid-rich bio-oils from the fast pyrolysis of biomass and synthesis of calcium magnesium acetate deicer. *Journal of Analytical and Applied Pyrolysis*, 124 (2017) 122–129. <https://doi.org/10.1016/j.jaap.2017.01.032>.
- [77] T. Sarchami, N. Batta, F. Berruti, Production and separation of acetic acid from pyrolysis oil of lignocellulosic biomass: a review. *Biofuels, Bioproducts and Biorefining*, 15 (2021) 1912–1937. <https://doi.org/10.1002/bbb.2273>.
- [78] J. Guo, G. Xu, Z. Han, Y. Zhang, Y. Fu, Q. Guo, Selective conversion of furfural to cyclopentanone with CuZnAl catalysts. *ACS Sustainable Chemistry and Engineering*, 2 (2014) 2259–2266. <https://doi.org/10.1021/sc5003566>.
- [79] T. Omotoso, L. v. Herrera, T. Vann, N.M. Briggs, L.A. Gomez, L. Barrett, D. Jones, T. Pham, B. Wang, S.P. Crossley, Stabilization of furanics to cyclic ketone building blocks in the vapor phase. *Applied Catalysis B: Environmental*, 254 (2019) 491–499. <https://doi.org/10.1016/j.apcatb.2019.04.079>.
- [80] Q. Bu, H. Lei, L. Wang, Y. Wei, L. Zhu, X. Zhang, Y. Liu, G. Yadavalli, J. Tang, Bio-based phenols and fuel production from catalytic microwave pyrolysis of lignin by activated carbons. *Bioresource Technology*, 162 (2014) 142–147. <https://doi.org/10.1016/j.biortech.2014.03.103>.
- [81] N. Montazeri, A.C.M. Oliveira, B.H. Himelbloom, M.B. Leigh, C.A. Crapo, Chemical characterization of commercial liquid smoke products. *Food Science & Nutrition*, 1 (2013) 102–115. <https://doi.org/10.1002/fsn3.9>.
- [82] S.R. Chandrasekaran, D. Murali, K.A. Marley, R.A. Larson, K.M. Doll, B.R. Moser, J. Scott, B.K. Sharma, Antioxidants from Slow Pyrolysis Bio-Oil of Birch Wood: Application for Biodiesel and Biobased Lubricants. *ACS Sustainable Chemistry and Engineering*, 4 (2016) 1414–1421. <https://doi.org/10.1021/acssuschemeng.5b01302>.
- [83] K.H. Kim, H.S. Jeong, J.Y. Kim, G.S. Han, I.G. Choi, J.W. Choi, Evaluation of the antifungal effects of bio-oil prepared with lignocellulosic biomass using fast pyrolysis technology. *Chemosphere*, 89 (2012) 688–693. <https://doi.org/10.1016/j.chemosphere.2012.06.010>.

- [84] M. Chaouch, P.N. Diouf, A. Laghdir, S. Yin, Bio-oil from whole-tree feedstock in resol-type phenolic resins. *Journal of Applied Polymer Science*, 131 (2014). <https://doi.org/10.1002/app.40014>.
- [85] C.M. Lok, J. van Doorn, G. Aranda Almansa, Promoted ZSM-5 catalysts for the production of bio-aromatics, a review. *Renewable and Sustainable Energy Reviews*, 113 (2019). <https://doi.org/10.1016/j.rser.2019.109248>.
- [86] C. Jia, S. Batterman, A critical review of naphthalene sources and exposures relevant to indoor and outdoor air. *International Journal of Environmental Research and Public Health*, 7 (2010) 2903–2939. <https://doi.org/10.3390/ijerph7072903>.
- [87] A. Rinaldi, D. Scarpi, E.G. Occhiato, Recent Advances in the Synthesis of Indenes. *European Journal of Organic Chemistry*, 2019 (2019) 7401–7419. <https://doi.org/10.1002/ejoc.201901425>.
- [88] I. Sádaba, M. Ojeda, R. Mariscal, J.L.G. Fierro, M.L. Granados, Catalytic and structural properties of co-precipitated Mg-Zr mixed oxides for furfural valorization via aqueous aldol condensation with acetone. *Applied Catalysis B: Environmental*, 101 (2011) 638–648. <https://doi.org/10.1016/j.apcatb.2010.11.005>.
- [89] C.P. Nicolaidis, M. Wapiennik, K.I.G. Weiss, I.-I. van den Akker, B. van Zalk, P. Wielaard, Alkali metal cation exchange of HZSM-5 and the catalytic properties of the alkalized zeolites. *Applied Catalysis*, 68 (1991) 31–39. [https://doi.org/10.1016/S0166-9834\(00\)84091-9](https://doi.org/10.1016/S0166-9834(00)84091-9).
- [90] C.A. Emeis, Determination of Integrated Molar Extinction Coefficients for Infrared Absorption Bands of Pyridine Adsorbed on Solid Acid Catalysts. *Journal of Catalysis*, 141 (1993) 347–354. <https://doi.org/10.1006/jcat.1993.1145>.
- [91] J. Fermoso, H. Hernando, S. Jiménez-Sánchez, A.A. Lappas, E. Heracleous, P. Pizarro, J.M. Coronado, D.P. Serrano, Bio-oil production by lignocellulose fast-pyrolysis: Isolating and comparing the effects of indigenous versus external catalysts. *Fuel Processing Technology*, 167 (2017) 563–574. <https://doi.org/10.1016/j.fuproc.2017.08.009>.
- [92] S.A. Channiwala, P.P. Parikh, A unified correlation for estimating HHV of solid, liquid and gaseous fuels. *Fuel*, 81 (2002) 1051–1063. [https://doi.org/10.1016/S0016-2361\(01\)00131-4](https://doi.org/10.1016/S0016-2361(01)00131-4).
- [93] N.Y. Chen, T.F. Degnan, L.R. Koenig, Liquid fuels from carbohydrates. *Chemical Technology*, 16 (1986) 506–511.
- [94] M.S. Hassan, N.A. Abdel-Khalek, Beneficiation and applications of an Egyptian bentonite, 1998.

## 7. References

- [95] B. Caglar, B. Afsin, A. Tabak, E. Eren, Characterization of the cation-exchanged bentonites by XRPD, ATR, DTA/TG analyses and BET measurement. *Chemical Engineering Journal*, 149 (2009) 242–248. <https://doi.org/10.1016/j.cej.2008.10.028>.
- [96] R. Giustetto, R. Compagnoni, An unusual occurrence of palygorskite from Montestrutto, Sesia-Lanzo zone, internal Western Alps (Italy). *Clay Minerals*, 46 (2011) 371–385. <https://doi.org/10.1180/claymin.2011.046.3.371>.
- [97] L. Zhirong, M. Azhar Uddin, S. Zhanxue, FT-IR and XRD analysis of natural Na-bentonite and Cu(II)-loaded Na-bentonite. *Spectrochimica Acta - Part A: Molecular and Biomolecular Spectroscopy*, 79 (2011) 1013–1016. <https://doi.org/10.1016/j.saa.2011.04.013>.
- [98] H. Liu, T. Chen, D. Chang, D. Chen, R.L. Frost, Catalytic cracking of tars derived from rice hull gasification over goethite and palygorskite. *Applied Clay Science*, 70 (2012) 51–57. <https://doi.org/10.1016/j.clay.2012.09.006>.
- [99] H. Hernando, C. Ochoa-Hernández, M. Shamzhy, I. Moreno, J. Feroso, P. Pizarro, J.M. Coronado, J. Čejka, D.P. Serrano, The crucial role of clay binders in the performance of ZSM-5 based materials for biomass catalytic pyrolysis. *Catalysis Science and Technology*, 9 (2019) 789–802. <https://doi.org/10.1039/c8cy02116c>.
- [100] M. Thommes, K. Kaneko, A. v. Neimark, J.P. Olivier, F. Rodriguez-Reinoso, J. Rouquerol, K.S.W. Sing, Physisorption of gases, with special reference to the evaluation of surface area and pore size distribution (IUPAC Technical Report). *Pure and Applied Chemistry*, 87 (2015) 1051–1069. <https://doi.org/10.1515/pac-2014-1117>.
- [101] Z. Duan, Q. Zhao, S. Wang, Z. Yuan, Y. Zhang, X. Li, Y. Wu, Y. Jiang, H. Tai, Novel application of attapulgite on high performance and low-cost humidity sensors. *Sensors and Actuators, B: Chemical*, 305 (2020). <https://doi.org/10.1016/j.snb.2019.127534>.
- [102] Z. Vajglová, I.L. Simakova, K. Eränen, P. Mäki-Arvela, N. Kumar, M. Peurla, S. Tolvanen, A. Efimov, L. Hupa, J. Peltonen, D.Y. Murzin, The physicochemical and catalytic properties of clay extrudates in cyclization of citronellal. *Applied Catalysis A: General*, 629 (2022). <https://doi.org/10.1016/j.apcata.2021.118426>.
- [103] L. Novikova, F. Roessner, L. Belchinskaya, M. AlSawalha, V. Krupskaya, Study of surface acid-base properties of natural clays and zeolites by the conversion of 2-methylbut-3-yn-2-ol. *Applied Clay Science*, 101 (2014) 229–236. <https://doi.org/10.1016/j.clay.2014.08.005>.
- [104] T. Han, S. Ding, W. Yang, P. Jönsson, Catalytic pyrolysis of lignin using low-cost materials with different acidities and textural properties as catalysts.



- Chemical Engineering Journal, 373 (2019) 846–856. <https://doi.org/10.1016/j.cej.2019.05.125>.
- [105] L. Faba, E. Díaz, S. Ordóñez, Gas phase acetone self-condensation over unsupported and supported Mg-Zr mixed-oxides catalysts. *Applied Catalysis B: Environmental*, 142–143 (2013) 387–395. <https://doi.org/10.1016/j.apcatb.2013.05.043>.
- [106] I. Sádaba, M. Ojeda, R. Mariscal, R. Richards, M. López Granados, Preparation and characterization of Mg-Zr mixed oxide aerogels and their application as aldol condensation catalysts. *ChemPhysChem*, 13 (2012) 3282–3292. <https://doi.org/10.1002/cphc.201200440>.
- [107] J. Feroso, P. Pizarro, J.M. Coronado, D.P. Serrano, Advanced biofuels production by upgrading of pyrolysis bio-oil. *Wiley Interdisciplinary Reviews: Energy and Environment*, 6 (2017). <https://doi.org/10.1002/wene.245>.
- [108] A. Doroshenko, I. Pylypenko, S. Gromovaite, J. Clark, V. Budarin, Effect of Exchangeable Cation in Clays on the Yield and Quality of the Bio-Oil during Microwave Pyrolysis of Cellulose. *Sustainable Chemistry*, 1 (2020) 315–324. <https://doi.org/10.3390/suschem1030021>.
- [109] M. Sulman, Y. Kosivtsov, E. Sulman, V. Alfyorov, Y. Lugovoy, V. Molchanov, I. Tyamina, O. Misnikov, A. Afanasjev, N. Kumar, D. Murzin, Influence of aluminosilicate materials on the peat low-temperature pyrolysis and gas formation. *Chemical Engineering Journal*, 154 (2009) 355–360. <https://doi.org/10.1016/j.cej.2009.04.001>.
- [110] B. Li, X. Xie, L. Zhang, D. Lin, S. Wang, S. Wang, H. Xu, J. Wang, Y. Huang, S. Zhang, D. Liu, Coke formation during rapid quenching of volatile vapors from fast pyrolysis of cellulose. *Fuel*, 306 (2021). <https://doi.org/10.1016/j.fuel.2021.121658>.
- [111] M.J. Prins, Thermodynamic analysis of biomass gasification and torrefaction, Technische Universiteit Eindhoven, 2005. <https://doi.org/10.6100/IR583729>.
- [112] I. Sádaba, M. Ojeda, R. Mariscal, R. Richards, M.L. Granados, Mg-Zr mixed oxides for aqueous aldol condensation of furfural with acetone: Effect of preparation method and activation temperature, in: *Catalysis Today*, 2011: 77–83. <https://doi.org/10.1016/j.cattod.2010.11.059>.
- [113] L. Faba, E. Díaz, S. Ordóñez, Aqueous-phase furfural-acetone aldol condensation over basic mixed oxides. *Applied Catalysis B: Environmental*, 113–114 (2012) 201–211. <https://doi.org/10.1016/j.apcatb.2011.11.039>.
- [114] S. Jeong, G.L. Sudibya, J.K. Jeon, Y.M. Kim, C.M.A. Swamidoss, S. Kim, The use of a  $\gamma$ -Al<sub>2</sub>O<sub>3</sub> and MgO mixture in the catalytic conversion of 1,1,1,2-tetrafluoroethane (Hfc-134a). *Catalysts*, 9 (2019). <https://doi.org/10.3390/catal9110901>.

## 7. References

- [115] G. Zhou, Y. Pei, Z. Jiang, K. Fan, M. Qiao, B. Sun, B. Zong, Doping effects of B in ZrO<sub>2</sub> on structural and catalytic properties of Ru/B-ZrO<sub>2</sub> catalysts for benzene partial hydrogenation. *Journal of Catalysis*, 311 (2014) 393–403. <https://doi.org/10.1016/j.jcat.2013.12.022>.
- [116] D. Liang, G. Li, Y. Liu, J. Wu, X. Zhang, Controllable self-aldol condensation of cyclopentanone over MgO-ZrO<sub>2</sub> mixed oxides: Origin of activity & selectivity. *Catalysis Communications*, 81 (2016) 33–36. <https://doi.org/10.1016/j.catcom.2016.04.008>.
- [117] B. Puértolas, T.C. Keller, S. Mitchell, J. Pérez-Ramírez, Deoxygenation of bio-oil over solid base catalysts: From model to realistic feeds. *Applied Catalysis B: Environmental*, 184 (2016) 77–86. <https://doi.org/10.1016/j.apcatb.2015.11.017>.
- [118] X. Chen, S. Li, Z. Liu, Y. Chen, H. Yang, X. Wang, Q. Che, W. Chen, H. Chen, Pyrolysis characteristics of lignocellulosic biomass components in the presence of CaO. *Bioresource Technology*, 287 (2019). <https://doi.org/10.1016/j.biortech.2019.121493>.
- [119] R. Yuan, Y. Shen, Catalytic pyrolysis of biomass-plastic wastes in the presence of MgO and MgCO<sub>3</sub> for hydrocarbon-rich oils production. *Bioresource Technology*, 293 (2019). <https://doi.org/10.1016/j.biortech.2019.122076>.
- [120] X. Hu, R. Gunawan, D. Maurant, C. Lievens, X. Li, S. Zhang, W. Chaiwat, C.Z. Li, Acid-catalysed reactions between methanol and the bio-oil from the fast pyrolysis of mallee bark. *Fuel*, 97 (2012) 512–522. <https://doi.org/10.1016/j.fuel.2012.02.032>.
- [121] P.E. Shaw, J.H. Tatum, R.E. Berry, 2,3-Dihydro-3,5-dihydroxy-6-methyl-4H-pyran-4-one, a degradation product of hexose. *Carbohydrate Research*, 16 (1971) 207–211. [https://doi.org/10.1016/S0008-6215\(00\)86115-7](https://doi.org/10.1016/S0008-6215(00)86115-7).
- [122] C.A. Mullen, P.C. Tarves, A.A. Boateng, Role of Potassium Exchange in Catalytic Pyrolysis of Biomass over ZSM-5: Formation of Alkyl Phenols and Furans. *ACS Sustainable Chemistry and Engineering*, 5 (2017) 2154–2162. <https://doi.org/10.1021/acssuschemeng.6b02262>.
- [123] X. Li, Q. Deng, L. Yu, R. Gao, Z. Tong, C. Lu, J. Wang, Z. Zeng, J.J. Zou, S. Deng, Double-metal cyanide as an acid and hydrogenation catalyst for the highly selective ring-rearrangement of biomass-derived furfuryl alcohol to cyclopentenone compounds. *Green Chemistry*, 22 (2020) 2549–2557. <https://doi.org/10.1039/c9gc04432a>.
- [124] S. Gutiérrez-Rubio, M. Shamzhy, J. Čejka, D.P. Serrano, I. Moreno, J.M. Coronado, Vapor phase acylation of guaiacol with acetic acid over micro, nano and hierarchical MFI and BEA zeolites. *Applied Catalysis B: Environmental*, 285 (2021). <https://doi.org/10.1016/j.apcatb.2020.119826>.



- [125] D.R. Naron, F.X. Collard, L. Tyhoda, J.F. Görgens, Production of phenols from pyrolysis of sugarcane bagasse lignin: Catalyst screening using thermogravimetric analysis – Thermal desorption – Gas chromatography – Mass spectroscopy. *Journal of Analytical and Applied Pyrolysis*, 138 (2019) 120–131. <https://doi.org/10.1016/j.jaap.2018.12.015>.
- [126] X. He, H. Liu, Efficient synthesis of 1,1-diethoxyethane via sequential ethanol reactions on silica-supported copper and H-Y zeolite catalysts. *Catalysis Today*, 233 (2014) 133–139. <https://doi.org/10.1016/j.cattod.2014.01.023>.
- [127] C.R. Vitasari, G.W. Meindersma, A.B. de Haan, Conceptual process design of an integrated bio-based acetic acid, glycolaldehyde, and acetol production in a pyrolysis oil-based biorefinery. *Chemical Engineering Research and Design*, 95 (2015) 133–143. <https://doi.org/10.1016/j.cherd.2015.01.010>.
- [128] O. Kikhtyanin, R. Bulánek, K. Frolich, J. Čejka, D. Kubička, Aldol condensation of furfural with acetone over ion-exchanged and impregnated potassium BEA zeolites. *Journal of Molecular Catalysis A: Chemical*, 424 (2016) 358–368. <https://doi.org/10.1016/j.molcata.2016.09.014>.
- [129] J.C. Lavalley, *Infrared spectrometric studies of the surface basicity of metal oxides and zeolites using adsorbed probe molecules*, 1996.
- [130] H. Hernando, J. Feroso, C. Ochoa-Hernández, M. Opanasenko, P. Pizarro, J.M. Coronado, J. Čejka, D.P. Serrano, Performance of MCM-22 zeolite for the catalytic fast-pyrolysis of acid-washed wheat straw. *Catalysis Today*, 304 (2018) 30–38. <https://doi.org/10.1016/j.cattod.2017.09.043>.
- [131] G. Pacchioni, Ketonization of carboxylic acids in biomass conversion over TiO<sub>2</sub> and ZrO<sub>2</sub> surfaces: A DFT perspective. *ACS Catalysis*, 4 (2014) 2874–2888. <https://doi.org/10.1021/cs500791w>.
- [132] J.A. Bennett, C.M.A. Parlett, M.A. Isaacs, L.J. Durndell, L. Olivi, A.F. Lee, K. Wilson, Acetic Acid Ketonization over Fe<sub>3</sub>O<sub>4</sub>/SiO<sub>2</sub> for Pyrolysis Bio-Oil Upgrading. *ChemCatChem*, 9 (2017) 1648–1654. <https://doi.org/10.1002/cctc.201601269>.
- [133] A.M. Hernández-Giménez, H. Hernando, R.M. Danisi, E.T.C. Vogt, K. Houben, M. Baldus, D.P. Serrano, P.C.A. Bruijninx, B.M. Weckhuysen, Deactivation and regeneration of solid acid and base catalyst bodies used in cascade for bio-oil synthesis and upgrading. *Journal of Catalysis*, 405 (2022) 641–651. <https://doi.org/10.1016/j.jcat.2021.09.029>.
- [134] J.M. Jimenez-Martin, A. Orozco-Saumell, H. Hernando, M. Linares, R. Mariscal, M. López Granados, A. García, J. Iglesias, Efficient Conversion of Glucose to Methyl Lactate with Sn-USY: Retro-aldol Activity Promotion by Controlled Ion Exchange. *ACS Sustainable Chemistry & Engineering*, 10 (2022) 8885–8896. <https://doi.org/10.1021/acssuschemeng.2c01987>.

## 7. References

- [135] M. Asadieraghi, W.M. Ashri Wan Daud, H.F. Abbas, Heterogeneous catalysts for advanced bio-fuel production through catalytic biomass pyrolysis vapor upgrading: A review. *RSC Advances*, 5 (2015) 22234–22255. <https://doi.org/10.1039/c5ra00762c>.
- [136] J. Jae, G.A. Tompsett, A.J. Foster, K.D. Hammond, S.M. Auerbach, R.F. Lobo, G.W. Huber, Investigation into the shape selectivity of zeolite catalysts for biomass conversion. *Journal of Catalysis*, 279 (2011) 257–268. <https://doi.org/10.1016/j.jcat.2011.01.019>.
- [137] A. Kabir, A. Mocan, M. Santoleri, M. de Simone, F. Cacciagrano, A. Tartaglia, H.I. Ulusoy, M. Locatelli, Analysis of monophenols, in: *Recent Advances in Natural Products Analysis*, Elsevier, 2020: 19–37. <https://doi.org/10.1016/B978-0-12-816455-6.00002-0>.
- [138] H. Hernando, G. Gómez-Pozuelo, J.A. Botas, D.P. Serrano, Evaluating fractional pyrolysis for bio-oil speciation into holocellulose and lignin derived compounds. *Journal of Analytical and Applied Pyrolysis*, 154 (2021). <https://doi.org/10.1016/j.jaap.2021.105019>.
- [139] Z. Fang, R.L.J. Smith, L. Xu, *Production of Biofuels and Chemicals with Pyrolysis*, Springer Singapore, Singapore, 2020. <https://doi.org/10.1007/978-981-15-2732-6>.
- [140] C.P. Groshart, P.C. Okkerman, W.B.A. Wassenberg, A.M.C.M. Pijnenburg, Chemical study on alkylphenols, 2001. <https://edepot.wur.nl/174304> (accessed April 22, 2022).
- [141] J. Ma, S. Shi, X. Jia, F. Xia, H. Ma, J. Gao, J. Xu, Advances in catalytic conversion of lignocellulose to chemicals and liquid fuels. *Journal of Energy Chemistry*, 36 (2019) 74–86. <https://doi.org/10.1016/j.jechem.2019.04.026>.
- [142] H. Hernando, B. Puértolas, P. Pizarro, J. Feroso, J. Pérez-Ramírez, D.P. Serrano, Cascade Deoxygenation Process Integrating Acid and Base Catalysts for the Efficient Production of Second-Generation Biofuels. *ACS Sustainable Chemistry and Engineering*, 7 (2019) 18027–18037. <https://doi.org/10.1021/acssuschemeng.9b04921>.
- [143] J. Wang, Z. Zhong, K. Ding, A. Deng, N. Hao, X. Meng, H. Ben, R. Ruan, A.J. Ragauskas, Catalytic fast pyrolysis of bamboo sawdust via a two-step bench scale bubbling fluidized bed/fixed bed reactor: Study on synergistic effect of alkali metal oxides and HZSM-5. *Energy Conversion and Management*, 176 (2018) 287–298. <https://doi.org/10.1016/j.enconman.2018.09.029>.
- [144] K. Ding, Z. Zhong, J. Wang, B. Zhang, L. Fan, S. Liu, Y. Wang, Y. Liu, D. Zhong, P. Chen, R. Ruan, Improving hydrocarbon yield from catalytic fast co-pyrolysis of hemicellulose and plastic in the dual-catalyst bed of CaO and

- HZSM-5. *Bioresource Technology*, 261 (2018) 86–92. <https://doi.org/10.1016/j.biortech.2018.03.138>.
- [145] Q. Che, M. Yang, X. Wang, X. Chen, W. Chen, Q. Yang, H. Yang, H. Chen, Aromatics production with metal oxides and ZSM-5 as catalysts in catalytic pyrolysis of wood sawdust. *Fuel Processing Technology*, 188 (2019) 146–152. <https://doi.org/10.1016/j.fuproc.2019.02.016>.
- [146] M.M.J. Treacy, J.B. Higgins, ZSM-5, Calcined, in: *Collection of Simulated XRD Powder Patterns for Zeolites*, Elsevier, 2007: 278–279. <https://doi.org/10.1016/B978-044453067-7/50604-3>.
- [147] H. Hernando, A.M. Hernández-Giménez, S. Gutiérrez-Rubio, T. Fakin, A. Horvat, R.M. Danisi, P. Pizarro, J. Fermoso, E. Heracleous, P.C.A. Bruijninx, A.A. Lappas, B.M. Weckhuysen, D.P. Serrano, Scaling-Up of Bio-Oil Upgrading during Biomass Pyrolysis over ZrO<sub>2</sub>/ZSM-5-Attapulgate. *ChemSusChem*, 12 (2019) 2428–2438. <https://doi.org/10.1002/cssc.201900534>.
- [148] C. Dorado, C.A. Mullen, A.A. Boateng, Origin of carbon in aromatic and olefin products derived from HZSM-5 catalyzed co-pyrolysis of cellulose and plastics via isotopic labeling. *Applied Catalysis B: Environmental*, 162 (2015) 338–345. <https://doi.org/10.1016/j.apcatb.2014.07.006>.
- [149] R. Ramos, A. García, J.A. Botas, D.P. Serrano, Enhanced Production of Aromatic Hydrocarbons by Rapeseed Oil Conversion over Ga and Zn Modified ZSM-5 Catalysts. *Industrial and Engineering Chemistry Research*, 55 (2016) 12723–12732. <https://doi.org/10.1021/acs.iecr.6b03050>.
- [150] G. Busca, Production of gasolines and monocyclic aromatic hydrocarbons: From fossil raw materials to green processes. *Energies*, 14 (2021). <https://doi.org/10.3390/en14134061>.
- [151] R. Arora, Manila, Styrene: Risk assessment, environmental, and health hazard, in: *Hazardous Gases*, Elsevier, 2021: 363–374. <https://doi.org/10.1016/B978-0-323-89857-7.00015-3>.
- [152] E. Aransiola, M.O. Daramola, T.V. Ojumu, Xylenes: Production technologies and uses, 2013. <https://www.researchgate.net/publication/288477593>.



## List of tables

<b>Table 1.1.</b> Maximum bio-oil yields according to pyrolysis types [7,13,18,19,21] ...	27
<b>Table 3.1.</b> X-ray diffraction parameters as a function of the type of catalyst studied.....	58
<b>Table 4.1.1.</b> Proximate, ultimate and biopolymers analyses of the raw (ws), acid-washed (ws-ac) wheat straw and cellulose samples [28].....	74
<b>Table 4.1.2.</b> Physicochemical properties of the clay catalysts. ....	77
<b>Table 4.1.3.</b> Compositions and HHVs of char and coke obtained in the fast pyrolysis of ws-ac over BNT and ATP at different C/B ratios, including reference thermal test. ....	81
<b>Table 4.1.4.</b> Compositions and HHVs of char and coke obtained in the fast pyrolysis of ws-ac and cellulose over BNT at different C/B ratios, including reference thermal tests. ....	87
<b>Table 4.2.1.</b> Physicochemical properties of the Mg and Zr single and mixed oxides. ....	93
<b>Table 4.2.2.</b> Strength types and concentration (conc.) of both acidic and basic sites in the Mg and Zr single and mixed oxides.....	96
<b>Table 4.2.3.</b> Compositions and HHVs of char and coke obtained in the fast pyrolysis of ws-ac over Mg and Zr single and mixed oxides.....	99
<b>Table 4.2.4.</b> Concentration (wt.%) of the LO subfamilies present in the bio-oil* produced by ws-ac CFP over Mg and Zr single and mixed oxides. ....	102
<b>Table 4.2.5.</b> Concentration of the O-AR subfamilies present in the bio-oil* produced by ws-ac CFP over Mg and Zr single and mixed oxides.....	104
<b>Table 4.3.1.</b> Physicochemical properties of the H-ZSM-5-based samples.....	106
<b>Table 4.3.2.</b> Physicochemical properties of the USY-based catalysts. ....	117
<b>Table 4.3.3.</b> Char and coke composition obtained in the catalytic pyrolysis of ws-ac over USY-based samples. ....	125
<b>Table 4.3.4.</b> Concentration (wt.%) of the main O-AR components present in the bio-oil* produced by ws-ac catalytic pyrolysis over K-USY sample at different temperatures and C/B ratios.....	132

## List of tables

<b>Table 4.3.5.</b> Concentration (wt.%) of the main LO components in the bio-oil* produced by ws-ac catalytic pyrolysis over K-USY sample at different temperatures and C/B ratios.....	134
<b>Table 4.4.1.</b> Physicochemical properties of the coupling catalysts .....	137
<b>Table 4.4.2.</b> Compositions and HHVs of char and coke obtained in the fast pyrolysis of ws-ac over H-ZSM-5 and BNT in single-catalyst and coupling configurations...	143
<b>Table 4.4.3.</b> Compositions and HHVs of char and coke obtained in the fast pyrolysis of ws-ac over H-ZSM-5 and MgO in single-catalyst and coupling configurations...	150
<b>Table 4.4.4.</b> Concentration (wt.%) of the main AR components present in the bio-oil* produced by fast pyrolysis of ws-ac over H-ZSM-5 in single-catalyst and coupling configurations with BNT/MgO (catalyst A: H-ZSM-5; catalyst B: MgO). Polycyclic aromatic hydrocarbons (PAHs) in <i>italics</i> . ....	153

# List of figures

<b>Figure 1.1.</b> Chemical structure of lignocellulosic biomass [9].	24
<b>Figure 1.2.</b> Conversion technologies, products and utilisation of lignocellulosic biomass [14]. S: solid; L: liquid; G: gaseous.	25
<b>Figure 1.3.</b> Types of biomass pyrolysis reactors from the smallest to the largest scale: a) Py-GC/MS (micro-scale) [26]; b) fixed-bed reactor (bench-scale) [27]; c) fluidised bed reactor (pilot- or commercial-scale) [3].	30
<b>Figure 1.4.</b> Configuration of in-situ, ex-situ and staged ex-situ CFP [13].	31
<b>Figure 1.5.</b> Classification of mineral clays, metal oxides and zeolites according to their acid-base properties [13,27,30–33].	33
<b>Figure 1.6.</b> Crystalline structure and particle morphology of montmorillonite [40] and attapulgite [41].	34
<b>Figure 1.7.</b> Catalytic effects of metal oxides on fast pyrolysis of lignocellulosic biomass [13].	37
<b>Figure 1.8.</b> Obtainable high-added value bio-based chemicals from bio-oil classified by compound family. LG: levoglucosan; LGO: levoglucosenone; HMF: 5-hydroxy-methyl-furfural; MAHs: monocyclic aromatic hydrocarbons; PAHs: polycyclic aromatic hydrocarbons.	46
<b>Figure 3.1.</b> Schematic diagram of the experimental set-up used for the fast pyrolysis tests	62
<b>Figure 4.1.1.</b> TG/DTG curves in nitrogen of parent bentonite and attapulgite.	75
<b>Figure 4.1.2.</b> a) XRD patterns; b) N <sub>2</sub> adsorption-desorption isotherms at 77 K; of the clay catalysts.	76
<b>Figure 4.1.3.</b> Acid-base properties of the clay catalysts: a) NH <sub>3</sub> -TPD; b) CO <sub>2</sub> -TPD.	78
<b>Figure 4.1.4.</b> Fast pyrolysis of ws-ac over BNT and ATP at different C/B ratios, including reference thermal test: a) fraction yields; b) bio-oil* oxygen concentration; c) gaseous components yields (GO: gaseous olefins, GP: gaseous paraffins).	79
<b>Figure 4.1.5.</b> Catalytic deoxygenation selectivity obtained in the fast pyrolysis of ws-ac over BNT and ATP at different C/B ratios.	80
<b>Figure 4.1.6.</b> Quantitative GC-MS analyses of the bio-oil* obtained in the fast pyrolysis of ws-ac over BNT and ATP at different C/B ratios, including reference	

## List of figures

thermal test: a) total and GC-MS detected mass yields; b) concentration of GC-MS detected components; and c) GC-MS detected mass yields of compound families (AC: carboxylic acids, LO: light oxygenates, FUR: furans, SUG: anhydrosugars and O-AR: oxygenated aromatics).....	83
<b>Figure 4.1.7.</b> Fast pyrolysis of ws-ac and cellulose over BNT, including reference thermal tests: a) fraction yields; b) gaseous components yields (GO: gaseous olefins, GP: gaseous paraffins); c) bio-oil* oxygen concentration. ....	85
<b>Figure 4.1.8.</b> Catalytic deoxygenation selectivity obtained in the fast pyrolysis of ws-ac and cellulose over BNT at different C/B ratios.....	86
<b>Figure 4.1.9.</b> Van Krevelen diagram, comparing ws-ac and cellulose feedstocks and their respective pyrolytic chars [113]. ....	88
<b>Figure 4.1.10.</b> Quantitative GC-MS analyses of the bio-oil* obtained in the fast pyrolysis of ws-ac and cellulose over bentonite, including reference thermal tests: a) total and GC-MS detected mass yields; b) concentration of GC-MS detected components; and c) GC-MS detected mass yields of compound families (AC: carboxylic acids, LO: light oxygenates, FUR: furans, SUG: anhydrosugars and O-AR: oxygenated aromatics).....	89
<b>Figure 4.2.1.</b> a) XRD patterns (● Cubic MgO; ▲ Cubic $\text{Mg}_x\text{Zr}_{1-x}\text{O}_{2-x}$ ; ▼ Tetragonal $\text{ZrO}_2$ ); b) $\text{N}_2$ adsorption-desorption isotherms at 77 K; of the Mg and Zr single and mixed oxides. ....	92
<b>Figure 4.2.2.</b> Acid-base properties of the Mg and Zr single and mixed oxides: a) $\text{NH}_3$ -TPD; b) $\text{CO}_2$ -TPD. ....	93
<b>Figure 4.2.3.</b> Deconvolution analyses of: a) $\text{NH}_3$ -TPD; and b) $\text{CO}_2$ -TPD curves; of the Mg and Zr single and mixed oxides. ....	95
<b>Figure 4.2.4.</b> Fast pyrolysis of ws-ac over Mg and Zr single and mixed oxides: a) fraction yields; b) gaseous components yields (GO: gaseous olefins, GP: gaseous paraffins); c) bio-oil* oxygen concentration. ....	97
<b>Figure 4.2.5.</b> Catalytic deoxygenation selectivity obtained in the fast pyrolysis of ws-ac over Mg and Zr single and mixed oxides.....	99
<b>Figure 4.2.6.</b> Quantitative GC-MS analyses of the bio-oil* obtained in the fast pyrolysis of ws-ac over Mg and Zr single and mixed oxides: a) total and GC-MS detected mass yields; b) concentration of GC-MS detected components; and c) GC-MS detected mass yields of compound families (AC: carboxylic acids, LO: light	



oxygenates, FUR: furans, SUG: anhydrosugars and O-AR: oxygenated aromatics).....	101
<b>Figure 4.3.1.</b> XRD patterns (a) and Ar adsorption isotherms at -87 K (b) of the catalyst samples.....	106
<b>Figure 4.3.2.</b> TEM images of: (a) parent H-ZSM-5 zeolite and (b) K-exchanged H-ZSM-5 zeolite. ....	107
<b>Figure 4.3.3.</b> Acid-base properties of the catalyst samples: a) NH <sub>3</sub> -TPD; b) CO <sub>2</sub> -TPD.....	108
<b>Figure 4.3.4.</b> Catalytic fast pyrolysis of ws-ac over KH-ZSM-5 as a function of the C/B ratio: (a) mass yield of the fractions; (b) bio-oil* oxygen content.....	110
<b>Figure 4.3.5.</b> Catalytic fast pyrolysis of ws-ac over KH-ZSM-5 as a function of the C/B ratio: yield of the main components in the gas fraction. GO: gaseous olefins (C <sub>2</sub> –C <sub>4</sub> ); GP: gaseous paraffins (C <sub>2</sub> –C <sub>4</sub> ). ....	110
<b>Figure 4.3.6.</b> Relationship between mass yield and oxygen content of the bio-oil* fraction in the catalytic fast pyrolysis of WS-ac over H-ZSM-5 and KH-ZSM-5 when varying the C/B ratio.....	111
<b>Figure 4.3.7.</b> Catalytic fast pyrolysis of ws-ac over KH-ZSM-5 and H-ZSM-5 catalysts (C/B = 0.2 and 0.6): deoxygenation selectivity. ....	112
<b>Figure 4.3.8.</b> GC-MS analysis of the bio-oil* obtained in the ws-ac pyrolysis over KH-ZSM-5 and H-ZSM-5 catalysts (C/B = 0.2): (a) mass yields of total/quantified components; (b) mass yield of the quantified components according to families of compounds.....	114
<b>Figure 4.3.9.</b> TEM images of: a) parent USY zeolite and b) K-grafted USY zeolite.....	116
<b>Figure 4.3.10.</b> SEM images of: a) parent USY zeolite and b) K-grafted USY zeolite.....	116
<b>Figure 4.3.11.</b> a) XRD patterns; b) N <sub>2</sub> adsorption-desorption isotherms at 77 K; c) BJH pore size distribution of the USY – based catalysts. ....	118
<b>Figure 4.3.12.</b> EDX analysis performed on K-grafted USY zeolite. ....	119
<b>Figure 4.3.13.</b> Acid-base properties of the USY-based catalysts: a) NH <sub>3</sub> -TPD; b) CO <sub>2</sub> -TPD.....	120
<b>Figure 4.3.14.</b> Pyridine adsorption FT-IR spectra after treating the K-grafted USY zeolite at different desorption temperatures (150, 250, 350, and 450 °C). ....	121

## List of figures

<b>Figure 4.3.15.</b> Catalytic pyrolysis of ws-ac over USY-based samples: a) fractions yield; b) bio-oil* oxygen concentration (dry basis); c) gaseous components yield (GO: gaseous olefins, GP: gaseous paraffins). .....	122
<b>Figure 4.3.16.</b> Catalytic deoxygenation selectivity, estimated from the incremental production of H <sub>2</sub> O, CO and CO <sub>2</sub> regarding the thermal pyrolysis test, obtained in the ws-ac pyrolysis over USY - based catalysts. ....	123
<b>Figure 4.3.17.</b> GC-MS analyses of the bio-oil* obtained in the ws-ac catalytic pyrolysis over USY-based samples: a) overall mass yields; b) overall concentration of GC-MS detected components; and c) mass yields of compound families (AC: carboxylic acids, LO: light oxygenates, FUR: furans, SUG: anhydrosugars, O-AR: oxygenated aromatics and AR: aromatic hydrocarbons). ....	126
<b>Figure 4.3.18.</b> Catalytic pyrolysis of ws-ac over K-USY sample at different temperatures and C/B ratios: a) fractions yield; b) bio-oil* oxygen concentration (dry basis); c) gaseous components yield (wt.%) (GO: gaseous olefins, GP: gaseous paraffins). ....	129
<b>Figure 4.3.19.</b> CO/CO <sub>2</sub> ratio obtained in the pyrolysis of ws-ac over K-USY zeolites at different temperatures and C/B ratios. ....	130
<b>Figure 4.3.20.</b> GC-MS analyses of the bio-oil* obtained in the ws-ac catalytic pyrolysis over K-USY sample: a) overall mass yields; b) overall concentration of GC-MS detected components; and c) mass yields of compound families (AC: carboxylic acids, LO: light oxygenates, FUR: furans, SUG: anhydrosugars, O-AR: oxygenated aromatics and AR: aromatic hydrocarbons). ....	131
<b>Figure 4.4.1.</b> a) XRD patterns; b) N <sub>2</sub> and Ar adsorption-desorption isotherms; of the catalysts. ....	136
<b>Figure 4.4.2.</b> Acid and base properties of the catalysts: a) NH <sub>3</sub> -TPD; b) CO <sub>2</sub> -TPD. ....	138
<b>Figure 4.4.3.</b> Catalytic pyrolysis of ws-ac over H-ZSM-5 and BNT in single-catalyst and coupling configurations: a) fraction yields; b) bio-oil* oxygen concentration; c) gaseous components yields (GO: gaseous olefins, GP: gaseous paraffins). ....	139
<b>Figure 4.4.4.</b> Catalytic deoxygenation selectivity obtained in the fast pyrolysis of ws-ac over H-ZSM-5 and BNT in single-catalyst and coupling configurations. ....	140
<b>Figure 4.4.5.</b> Van Krevelen diagram [149], comparing elemental compositions of bio-oils* in the fast pyrolysis of ws-ac over H-ZSM-5 and BNT in single-catalyst and coupling configurations. ....	141

<b>Figure 4.4.6.</b> Energy yield distribution obtained in fast pyrolysis of ws-ac over H-ZSM-5 and BNT in single-catalyst and coupling configurations. ....	142
<b>Figure 4.4.7.</b> Quantitative GC-MS analyses of the bio-oil* obtained in the ws-ac catalytic pyrolysis over H-ZSM-5 and BNT in single-catalyst and coupling configurations: a) total and GC-MS detected mass yields; b) total and GC-MS detected energy yields; and c) GC-MS detected mass yields of compound families (AC: carboxylic acids, LO: light oxygenates, FUR: furans, SUG: anhydrosugars and O-AR: oxygenated aromatics). ....	144
<b>Figure 4.4.8.</b> Catalytic pyrolysis of ws-ac over H-ZSM-5 and MgO in single-catalyst and coupling configurations: a) fraction yields; b) bio-oil* oxygen concentration (dry basis); c) gaseous components yields (GO: gaseous olefins, GP: gaseous paraffins). ....	145
<b>Figure 4.4.9.</b> Catalytic deoxygenation selectivity obtained in the fast pyrolysis of ws-ac over H-ZSM-5 and MgO in single-catalyst and coupling configurations. ....	147
<b>Figure 4.4.10.</b> Van Krevelen diagram [149], comparing elemental compositions of bio-oils* in the ws-ac fast pyrolysis over H-ZSM-5 and MgO in single-catalyst and coupling configurations. ....	148
<b>Figure 4.4.11.</b> Energy yield distribution obtained in fast pyrolysis of ws-ac over H-ZSM-5 and MgO in single-catalyst and coupling configurations. ....	149
<b>Figure 4.4.12.</b> Quantitative GC-MS analyses of the bio-oil* obtained in the ws-ac catalytic pyrolysis over H-ZSM-5 and MgO in single-catalyst and coupling configurations: a) total and GC-MS detected mass yields; b) total and GC-MS detected energy yields; and c) GC-MS detected mass yields of compound families (AC: carboxylic acids, LO: light oxygenates, FUR: furans, SUG: anhydrosugars and O-AR: oxygenated aromatics). ....	151
<b>Figure 4.5.1.</b> Relationship between the oxygen content and yields of the bio-oil* fraction in the fast pyrolysis of wheat straw over the different catalysts and coupling configurations studied when C/B ratio = 0.2 and $T_{\text{catalysis}} = 450\text{ }^{\circ}\text{C}$ : a) mass yield; b) energy yield. ....	155
<b>Figure 4.5.2.</b> GC-MS analyses of the bio-oil* obtained in the bio-oil* produced by fast pyrolysis of wheat straw over different catalysts and coupling configurations: overall mass yields of GC-MS detected components. ....	156
<b>Figure 4.5.3.</b> GC-MS detected mass yields of compound families present in the bio-oil* produced by fast pyrolysis of ws-ac over different catalysts and coupling	

## List of figures

configurations (AC: carboxylic acids, LO: light oxygenates, FUR: furans, SUG: anhydrosugars, O-AR: oxygenated aromatics, and AR: aromatic hydrocarbons). ..157

## **Appendix**



**Table A.1. Fast pyrolysis of ws-ac (N-C test; procedure 2)**

Reaction conditions		Catalyst properties	
Raw biomass	ws-ac	$S_{\text{BET}}$ (m <sup>2</sup> /g)	–
Catalyst sample	N-C	$S_{\text{MES+EXT}}$ (m <sup>2</sup> /g)	–
$T_{\text{pyrolysis}}/T_{\text{catalysis}}$ (°C)	550/450	$V_{\text{T}}$ (cm <sup>3</sup> /g)	–
C/B ratio (g/g)	0.0	Acidity (mmol <sub>NH3</sub> /g)	–
Procedure for bio-oil recovery	2	Basicity (mmol <sub>CO2</sub> /g)	–

Products distribution		
Solid phase	Mass yield (wt.%)	Energy yield (%)
<b>Char</b>	<b>17.8</b>	<b>27.6</b>
<b>Coke</b>	–	–
Liquid phase	Mass yield (wt.%)	Energy yield (%)
<b>Bio-oil*</b>	<b>57.4</b>	<b>61.5</b>
Carboxylic acids	1.8	1.8
Light oxygenates	0.5	0.9
Furans	1.4	1.9
Sugars	6.0	6.4
Oxygenated aromatics	1.1	2.0
Aromatic hydrocarbons	–	–
Non-detected compounds	46.6	48.6
<b>Water</b>	<b>16.3</b>	–
Gaseous phase	Mass yield (wt.%)	Energy yield (%)
<b>Hydrogen</b>	<b>0.003</b>	<b>0.028</b>
<b>Methane</b>	<b>0.351</b>	<b>1.136</b>
<b>Gaseous olefins</b>	<b>0.105</b>	<b>0.306</b>
Ethylene	0.047	0.140
Propylene	0.041	0.119
Butylene	0.017	0.048
<b>Gaseous paraffins</b>	<b>0.075</b>	<b>0.227</b>
Ethane	0.054	0.166
Propane	0.017	0.053
Butane	0.003	0.008
<b>Carbon oxide</b>	<b>2.223</b>	1.302
<b>Carbon dioxide</b>	<b>5.684</b>	–

Fraction	Proximate and ultimate analysis (wt.%)					HHV (MJ/kg)
	C	H	N	O	Ash	
Biomass	47.8	5.9	0.2	44.8	1.3	19.0
Char	78.7	2.7	0.9	10.5	7.2	29.4
Coke	–	–	–	–	–	–
Bio-oil*	53.3	3.3	0.2	<b>43.2</b>	–	20.4

**Table A.2. Fast pyrolysis of ws-ac over BNT (C/B = 0.2)**

Reaction conditions		Catalyst properties	
Raw biomass	ws-ac	$S_{\text{BET}}$ (m <sup>2</sup> /g)	43
Catalyst sample	BNT	$S_{\text{MES+EXT}}$ (m <sup>2</sup> /g)	43
$T_{\text{pyrolysis}}/T_{\text{catalysis}}$ (°C)	550/450	$V_{\text{T}}$ (cm <sup>3</sup> /g)	0.126
C/B ratio (g/g)	0.2	Acidity (mmol <sub>NH3</sub> /g)	0.080
Procedure for bio-oil recovery	2	Basicity (mmol <sub>CO2</sub> /g)	0.596

Products distribution		
Solid phase	Mass yield (wt.%)	Energy yield (%)
<b>Char</b>	<b>17.8</b>	<b>27.6</b>
<b>Coke</b>	<b>2.1</b>	<b>1.4</b>
Liquid phase	Mass yield (wt.%)	Energy yield (%)
<b>Bio-oil*</b>	<b>52.5</b>	<b>58.7</b>
Carboxylic acids	5.6	4.9
Light oxygenates	2.2	3.6
Furans	1.7	2.1
Sugars	11.6	10.9
Oxygenated aromatics	2.8	4.5
Aromatic hydrocarbons	—	—
Non-detected compounds	28.7	32.7
<b>Water</b>	<b>18.4</b>	—
Gaseous phase	Mass yield (wt.%)	Energy yield (%)
<b>Hydrogen</b>	<b>0.009</b>	<b>0.061</b>
<b>Methane</b>	<b>0.363</b>	<b>0.941</b>
<b>Gaseous olefins</b>	<b>0.089</b>	<b>0.206</b>
Ethylene	0.007	0.017
Propylene	0.054	0.126
Butylene	0.028	0.062
<b>Gaseous paraffins</b>	<b>0.127</b>	<b>0.310</b>
Ethane	0.086	0.210
Propane	0.027	0.065
Butane	0.015	0.035
<b>Carbon oxide</b>	<b>2.870</b>	<b>1.346</b>
<b>Carbon dioxide</b>	<b>5.690</b>	<b>0.061</b>

Fraction	Proximate and ultimate analysis (wt.%)					HHV (MJ/kg)
	C	H	N	O	Ash	
Biomass	47.8	5.9	0.2	44.8	1.3	19.0
Char	78.7	2.7	0.9	10.5	7.2	29.4
Coke	36.1	5.6	—	58.3	—	12.7
Bio-oil*	53.3	5.6	—	<b>41.0</b>	—	21.0



**Table A.3. Fast pyrolysis of ws-ac over BNT (C/B = 0.6)**

Reaction conditions		Catalyst properties	
Raw biomass	ws-ac	$S_{\text{BET}}$ (m <sup>2</sup> /g)	43
Catalyst sample	BNT	$S_{\text{MES+EXT}}$ (m <sup>2</sup> /g)	43
$T_{\text{pyrolysis}}/T_{\text{catalysis}}$ (°C)	550/450	$V_{\text{T}}$ (cm <sup>3</sup> /g)	0.126
C/B ratio (g/g)	0.6	Acidity (mmol <sub>NH3</sub> /g)	0.080
Procedure for bio-oil recovery	2	Basicity (mmol <sub>CO2</sub> /g)	0.596

Products distribution	
Solid phase	Mass yield (wt.%)
<b>Char</b>	<b>17.8</b>
<b>Coke</b>	<b>5.4</b>
Liquid phase	Mass yield (wt.%)
<b>Bio-oil*</b>	<b>40.6</b>
Carboxylic acids	5.3
Light oxygenates	2.0
Furans	1.4
Sugars	8.9
Oxygenated aromatics	2.2
Aromatic hydrocarbons	–
Non-detected compounds	20.8
<b>Water</b>	<b>25.6</b>
Gaseous phase	Mass yield (wt.%)
<b>Hydrogen</b>	<b>0.012</b>
<b>Methane</b>	<b>0.385</b>
<b>Gaseous olefins</b>	<b>0.197</b>
Ethylene	0.090
Propylene	0.071
Butylene	0.035
<b>Gaseous paraffins</b>	<b>0.141</b>
Ethane	0.096
Propane	0.030
Butane	0.015
<b>Carbon oxide</b>	<b>3.439</b>
<b>Carbon dioxide</b>	<b>6.391</b>

Fraction	Proximate and ultimate analysis (wt.%)					HHV (MJ/kg)
	C	H	N	O	Ash	
Biomass	47.8	5.9	0.2	44.8	1.3	19.0
Char	78.7	2.7	0.9	10.5	7.2	29.4
Coke	39.8	5.4	–	54.8	–	14.3
Bio-oil*	54.9	5.9	0.1	<b>39.2</b>	–	22.1

**Table A.4. Fast pyrolysis of ws-ac over ATP (C/B = 0.2)**

Reaction conditions		Catalyst properties	
Raw biomass	ws-ac	$S_{\text{BET}}$ (m <sup>2</sup> /g)	117
Catalyst sample	ATP	$S_{\text{MES+EXT}}$ (m <sup>2</sup> /g)	117
$T_{\text{pyrolysis}}/T_{\text{catalysis}}$ (°C)	550/450	$V_{\text{T}}$ (cm <sup>3</sup> /g)	0.526
C/B ratio (g/g)	0.2	Acidity (mmol <sub>NH3</sub> /g)	0.200
Procedure for bio-oil recovery	2	Basicity (mmol <sub>CO2</sub> /g)	0.689

Products distribution	
Solid phase	Mass yield (wt.%)
<b>Char</b>	<b>17.8</b>
<b>Coke</b>	<b>3.5</b>
Liquid phase	Mass yield (wt.%)
<b>Bio-oil*</b>	<b>44.1</b>
Carboxylic acids	6.0
Light oxygenates	3.2
Furans	2.7
Sugars	2.7
Oxygenated aromatics	2.1
Aromatic hydrocarbons	—
Non-detected compounds	27.4
<b>Water</b>	<b>21.8</b>
Gaseous phase	Mass yield (wt.%)
<b>Hydrogen</b>	<b>0.013</b>
<b>Methane</b>	<b>0.388</b>
<b>Gaseous olefins</b>	<b>0.166</b>
Ethylene	0.091
Propylene	0.067
Butylene	0.008
<b>Gaseous paraffins</b>	<b>0.120</b>
Ethane	0.091
Propane	0.024
Butane	0.005
<b>Carbon oxide</b>	<b>4.208</b>
<b>Carbon dioxide</b>	<b>7.935</b>

Fraction	Proximate and ultimate analysis (wt.%)					HHV (MJ/kg)
	C	H	N	O	Ash	
Biomass	47.8	5.9	0.2	44.8	1.3	19.0
Char	78.7	2.7	0.9	10.5	7.2	29.4
Coke	46.7	3.8	—	49.5	—	15.6
Bio-oil*	52.9	6.2	0.1	<b>40.8</b>	—	21.5

**Table A.5. Fast pyrolysis of ws-ac over ATP (C/B = 0.6)**

Reaction conditions		Catalyst properties	
Raw biomass	ws-ac	$S_{\text{BET}}$ (m <sup>2</sup> /g)	117
Catalyst sample	ATP	$S_{\text{MES+EXT}}$ (m <sup>2</sup> /g)	117
$T_{\text{pyrolysis}}/T_{\text{catalysis}}$ (°C)	550/450	$V_{\text{T}}$ (cm <sup>3</sup> /g)	0.526
C/B ratio (g/g)	0.6	Acidity (mmol <sub>NH3</sub> /g)	0.200
Procedure for bio-oil recovery	2	Basicity (mmol <sub>CO2</sub> /g)	0.689

Products distribution	
Solid phase	Mass yield (wt.%)
<b>Char</b>	<b>17.8</b>
<b>Coke</b>	<b>7.5</b>
Liquid phase	Mass yield (wt.%)
<b>Bio-oil*</b>	<b>30.5</b>
Carboxylic acids	4.7
Light oxygenates	1.8
Furans	3.3
Sugars	–
Oxygenated aromatics	2.0
Aromatic hydrocarbons	–
Non-detected compounds	18.8
<b>Water</b>	<b>27.9</b>
Gaseous phase	Mass yield (wt.%)
<b>Hydrogen</b>	<b>0.019</b>
<b>Methane</b>	<b>0.408</b>
<b>Gaseous olefins</b>	<b>0.359</b>
Ethylene	0.171
Propylene	0.162
Butylene	0.026
<b>Gaseous paraffins</b>	<b>0.176</b>
Ethane	0.132
Propane	0.032
Butane	0.012
<b>Carbon oxide</b>	<b>6.533</b>
<b>Carbon dioxide</b>	<b>8.800</b>

Fraction	Proximate and ultimate analysis (wt.%)					HHV (MJ/kg)
	C	H	N	O	Ash	
Biomass	47.8	5.9	0.2	44.8	1.3	19.0
Char	78.7	2.7	0.9	10.5	7.2	29.4
Coke	54.9	4.5	–	40.6	–	20.0
Bio-oil*	57.8	6.1	0.1	<b>36.0</b>	–	23.7

**Table A.6. Fast pyrolysis of cellulose (N-C test)**

Reaction conditions		Catalyst properties	
Raw biomass	cellulose	$S_{\text{BET}}$ ( $\text{m}^2/\text{g}$ )	–
Catalyst sample	N-C	$S_{\text{MES+EXT}}$ ( $\text{m}^2/\text{g}$ )	–
$T_{\text{pyrolysis}}/T_{\text{catalysis}}$ ( $^{\circ}\text{C}$ )	550/450	$V_{\text{T}}$ ( $\text{cm}^3/\text{g}$ )	–
C/B ratio (g/g)	0.0	Acidity ( $\text{mmol}_{\text{NH}_3}/\text{g}$ )	–
Procedure for bio-oil recovery	2	Basicity ( $\text{mmol}_{\text{CO}_2}/\text{g}$ )	–

Products distribution	
Solid phase	Mass yield (wt.%)
<b>Char</b>	<b>15.9</b>
<b>Coke</b>	–
Liquid phase	Mass yield (wt.%)
<b>Bio-oil*</b>	<b>48.1</b>
Carboxylic acids	1.5
Light oxygenates	2.2
Furans	0.4
Sugars	11.5
Oxygenated aromatics	–
Aromatic hydrocarbons	–
Non-detected compounds	32.4
<b>Water</b>	<b>28.5</b>
Gaseous phase	Mass yield (wt.%)
<b>Hydrogen</b>	<b>0.006</b>
<b>Methane</b>	<b>0.107</b>
<b>Gaseous olefins</b>	<b>0.139</b>
Ethylene	0.064
Propylene	0.058
Butylene	0.016
<b>Gaseous paraffins</b>	<b>0.096</b>
Ethane	0.070
Propane	0.020
Butane	0.006
<b>Carbon oxide</b>	<b>2.496</b>
<b>Carbon dioxide</b>	<b>4.667</b>

Fraction	Proximate and ultimate analysis (wt.%)					HHV (MJ/kg)
	C	H	N	O	Ash	
Biomass	43.9	6.3	–	49.1	0.8	17.6
Char	81.9	3.3	–	10.0	4.8	31.4
Coke	–	–	–	–	–	–
Bio-oil*	46.4	5.1	–	<b>48.5</b>	46.4	17.3

**Table A.7. Fast pyrolysis of cellulose over BNT (C/B = 0.2)**

Reaction conditions		Catalyst properties	
Raw biomass	cellulose	$S_{\text{BET}}$ ( $\text{m}^2/\text{g}$ )	43
Catalyst sample	BNT	$S_{\text{MES+EXT}}$ ( $\text{m}^2/\text{g}$ )	43
$T_{\text{pyrolysis}}/T_{\text{catalysis}}$ ( $^{\circ}\text{C}$ )	550/450	$V_{\text{T}}$ ( $\text{cm}^3/\text{g}$ )	0.126
C/B ratio (g/g)	0.2	Acidity ( $\text{mmol}_{\text{NH}_3}/\text{g}$ )	0.080
Procedure for bio-oil recovery	2	Basicity ( $\text{mmol}_{\text{CO}_2}/\text{g}$ )	0.596

Products distribution	
Solid phase	Mass yield (wt.%)
<b>Char</b>	<b>15.9</b>
<b>Coke</b>	<b>7.7</b>
Liquid phase	Mass yield (wt.%)
<b>Bio-oil*</b>	<b>35.4</b>
Carboxylic acids	3.1
Light oxygenates	1.3
Furans	1.6
Sugars	13.9
Oxygenated aromatics	—
Aromatic hydrocarbons	—
Non-detected compounds	15.4
<b>Water</b>	<b>32.2</b>
Gaseous phase	Mass yield (wt.%)
<b>Hydrogen</b>	<b>0.009</b>
<b>Methane</b>	<b>0.060</b>
<b>Gaseous olefins</b>	<b>0.091</b>
Ethylene	0.039
Propylene	0.040
Butylene	0.011
<b>Gaseous paraffins</b>	<b>0.034</b>
Ethane	0.025
Propane	0.009
Butane	0.001
<b>Carbon oxide</b>	<b>2.558</b>
<b>Carbon dioxide</b>	<b>6.034</b>

Fraction	Proximate and ultimate analysis (wt.%)					HHV (MJ/kg)
	C	H	N	O	Ash	
Biomass	43.9	6.3	—	49.1	0.8	17.6
Char	81.9	3.3	—	10.0	4.8	31.4
Coke	31.7	4.9	—	63.4	—	10.3
Bio-oil*	52.4	6.5	—	<b>41.2</b>	—	21.7

**Table A.8. Fast pyrolysis of cellulose over BNT (C/B = 0.6)**

Reaction conditions		Catalyst properties	
Raw biomass	cellulose	$S_{\text{BET}}$ (m <sup>2</sup> /g)	43
Catalyst sample	BNT	$S_{\text{MES+EXT}}$ (m <sup>2</sup> /g)	43
$T_{\text{pyrolysis}}/T_{\text{catalysis}}$ (°C)	550/450	$V_{\text{T}}$ (cm <sup>3</sup> /g)	0.126
C/B ratio (g/g)	0.6	Acidity (mmol <sub>NH3</sub> /g)	0.080
Procedure for bio-oil recovery	2	Basicity (mmol <sub>CO2</sub> /g)	0.596

Products distribution	
Solid phase	Mass yield (wt.%)
<b>Char</b>	<b>15.9</b>
<b>Coke</b>	<b>16.5</b>
Liquid phase	Mass yield (wt.%)
<b>Bio-oil*</b>	<b>24.4</b>
Carboxylic acids	4.7
Light oxygenates	1.3
Furans	1.7
Sugars	8.9
Oxygenated aromatics	0.1
Aromatic hydrocarbons	—
Non-detected compounds	7.7
<b>Water</b>	<b>31.9</b>
Gaseous phase	Mass yield (wt.%)
<b>Hydrogen</b>	<b>0.022</b>
<b>Methane</b>	<b>0.082</b>
<b>Gaseous olefins</b>	<b>0.136</b>
Ethylene	0.053
Propylene	0.059
Butylene	0.024
<b>Gaseous paraffins</b>	<b>0.049</b>
Ethane	0.034
Propane	0.013
Butane	0.002
<b>Carbon oxide</b>	<b>3.315</b>
<b>Carbon dioxide</b>	<b>7.717</b>

Fraction	Proximate and ultimate analysis (wt.%)					HHV (MJ/kg)
	C	H	N	O	Ash	
Biomass	43.9	6.3	—	49.1	43.9	17.6
Char	81.9	3.3	—	10.0	81.9	31.4
Coke	29.0	4.8	—	66.3	29.0	8.9
Bio-oil*	58.9	5.1	—	<b>36.0</b>	58.9	22.8

**Table A.9. Fast pyrolysis of ws-ac over MgO (C/B = 0.2)**

Reaction conditions		Catalyst properties	
Raw biomass	ws-ac	Mg/(Mg+Zr) atomic ratio	1.00
Catalyst sample	MgO	$S_{\text{BET}}/S_{\text{MES+EXT}}$ (m <sup>2</sup> /g)	82/82
T <sub>pyrolysis</sub> /T <sub>catalysis</sub> (°C)	550/450	V <sub>T</sub> (cm <sup>3</sup> /g)	0.47
C/B ratio (g/g)	0.2	Acidity (μmol <sub>NH3</sub> /g)	40
Procedure for bio-oil recovery	2	Basicity (mmolCO <sub>2</sub> /g)	4.13

Products distribution		
Solid phase	Mass yield (wt.%)	Energy yield (%)
<b>Char</b>	<b>17.8</b>	<b>27.6</b>
<b>Coke</b>	<b>6.0</b>	<b>4.6</b>
Liquid phase	Mass yield (wt.%)	Energy yield (%)
<b>Bio-oil*</b>	<b>38.6</b>	<b>56.6</b>
Carboxylic acids	5.5	4.8
Light oxygenates	4.4	7.4
Furans	4.8	5.9
Sugars	3.7	4.5
Oxygenated aromatics	5.3	8.4
Aromatic hydrocarbons	–	–
Non-detected compounds	14.9	25.7
<b>Water</b>	<b>26.5</b>	<b>–</b>
Gaseous phase	Mass yield (wt.%)	Energy yield (%)
<b>Hydrogen</b>	<b>0.015</b>	<b>0.109</b>
<b>Methane</b>	<b>0.350</b>	<b>0.988</b>
<b>Gaseous olefins</b>	<b>0.265</b>	<b>0.672</b>
Ethylene	0.123	0.316
Propylene	0.095	0.240
Butylene	0.048	0.117
<b>Gaseous paraffins</b>	<b>0.192</b>	<b>0.509</b>
Ethane	0.127	0.340
Propane	0.050	0.131
Butane	0.015	0.038
<b>Carbon oxide</b>	<b>3.598</b>	<b>1.842</b>
<b>Carbon dioxide</b>	<b>6.622</b>	<b>0.109</b>

Fraction	Proximate and ultimate analysis (wt.%)					HHV (MJ/kg)
	C	H	N	O	Ash	
Biomass	47.8	5.9	0.2	44.8	1.3	19.0
Char	78.7	2.7	0.9	10.5	7.2	29.4
Coke	47.3	2.8	–	49.9	–	14.7
Bio-oil*	67.3	6.0	0.1	<b>26.6</b>	–	27.8

**Table A.10. Fast pyrolysis of ws-ac over ZrO<sub>2</sub> (C/B = 0.2)**

Reaction conditions		Catalyst properties	
Raw biomass	ws-ac	Mg/(Mg+Zr) atomic ratio	–
Catalyst sample	ZrO <sub>2</sub>	S <sub>BET</sub> /S <sub>MES+EXT</sub> (m <sup>2</sup> /g)	71/71
T <sub>pyrolysis</sub> /T <sub>catalysis</sub> (°C)	550/450	V <sub>T</sub> (cm <sup>3</sup> /g)	0.09
C/B ratio (g/g)	0.2	Acidity (μmol <sub>NH3</sub> /g)	73
Procedure for bio-oil recovery	2	Basicity (mmol <sub>CO2</sub> /g)	1.39

Products distribution	
Solid phase	Mass yield (wt.%)
<b>Char</b>	<b>17.8</b>
<b>Coke</b>	<b>2.0</b>
Liquid phase	Mass yield (wt.%)
<b>Bio-oil*</b>	<b>41.7</b>
Carboxylic acids	4.4
Light oxygenates	2.2
Furans	2.3
Sugars	5.4
Oxygenated aromatics	2.0
Aromatic hydrocarbons	–
Non-detected compounds	25.3
<b>Water</b>	<b>28.7</b>
Gaseous phase	Mass yield (wt.%)
<b>Hydrogen</b>	<b>0.030</b>
<b>Methane</b>	<b>0.250</b>
<b>Gaseous olefins</b>	<b>0.166</b>
Ethylene	0.093
Propylene	0.073
Butylene	0.000
<b>Gaseous paraffins</b>	<b>0.144</b>
Ethane	0.106
Propane	0.028
Butane	0.010
<b>Carbon oxide</b>	<b>3.059</b>
<b>Carbon dioxide</b>	<b>6.119</b>

Fraction	Proximate and ultimate analysis (wt.%)					HHV (MJ/kg)
	C	H	N	O	Ash	
Biomass	47.8	5.9	0.2	44.8	1.3	19.0
Char	78.7	2.7	0.9	10.5	7.2	29.4
Coke	61.3	3.2	–	35.4	–	21.6
Bio-oil*	58.3	6.3	0.1	<b>35.3</b>	–	24.1



**Table A.11. Fast pyrolysis of ws-ac over 75MgZr (C/B = 0.2)**

Reaction conditions		Catalyst properties	
Raw biomass	ws-ac	Mg/(Mg+Zr) atomic ratio	0.71
Catalyst sample	75MgZr	$S_{\text{BET}}/S_{\text{MES+EXT}}$ (m <sup>2</sup> /g)	75/75
T <sub>pyrolysis</sub> /T <sub>catalysis</sub> (°C)	550/450	V <sub>T</sub> (cm <sup>3</sup> /g)	0.30
C/B ratio (g/g)	0.2	Acidity (μmol <sub>NH3</sub> /g)	85
Procedure for bio-oil recovery	2	Basicity (mmol <sub>CO2</sub> /g)	2.06

Products distribution	
Solid phase	Mass yield (wt.%)
<b>Char</b>	<b>17.8</b>
<b>Coke</b>	<b>5.7</b>
Liquid phase	Mass yield (wt.%)
<b>Bio-oil*</b>	<b>34.2</b>
Carboxylic acids	4.5
Light oxygenates	5.6
Furans	3.3
Sugars	3.2
Oxygenated aromatics	3.1
Aromatic hydrocarbons	—
Non-detected compounds	14.4
<b>Water</b>	<b>29.9</b>
Gaseous phase	Mass yield (wt.%)
<b>Hydrogen</b>	<b>0.034</b>
<b>Methane</b>	<b>0.427</b>
<b>Gaseous olefins</b>	<b>0.309</b>
Ethylene	0.141
Propylene	0.127
Butylene	0.042
<b>Gaseous paraffins</b>	<b>0.206</b>
Ethane	0.153
Propane	0.042
Butane	0.012
<b>Carbon oxide</b>	<b>4.020</b>
<b>Carbon dioxide</b>	<b>7.472</b>

Fraction	Proximate and ultimate analysis (wt.%)					HHV (MJ/kg)
	C	H	N	O	Ash	
Biomass	47.8	5.9	0.2	44.8	1.3	19.0
Char	78.7	2.7	0.9	10.5	7.2	29.4
Coke	51.3	3.0	—	45.7	—	16.8
Bio-oil*	65.6	5.7	0.1	<b>28.6</b>	—	26.7

Table A.12. Fast pyrolysis of ws-ac (N-C test; procedure 1)

Reaction conditions		Catalyst properties	
Raw biomass	ws-ac	K/Al	—
Catalyst sample	N-C	Si/Al	—
T <sub>pyrolysis</sub> /T <sub>catalysis</sub> (°C)	550/450	S <sub>BET</sub> /S <sub>MES+EXT</sub> (m <sup>2</sup> /g)	—
C/B ratio (g/g)	0.0	Acidity (mmol <sub>NH3</sub> /g)	—
Procedure for bio-oil recovery	2	Basicity (mmol <sub>CO2</sub> /g)	—

Products distribution	
Solid phase	Mass yield (wt.%)
<b>Char</b>	<b>17.1</b>
<b>Coke</b>	—
Liquid phase	Mass yield (wt.%)
<b>Bio-oil*</b>	<b>57.9</b>
Carboxylic acids	2.4
Light oxygenates	2.5
Furans	2.1
Sugars	8.4
Oxygenated aromatics	1.5
Aromatic hydrocarbons	—
Non-detected compounds	41.1
<b>Water</b>	<b>15.9</b>
Gaseous phase	Mass yield (wt.%)
<b>Hydrogen</b>	<b>0.005</b>
<b>Methane</b>	<b>0.323</b>
<b>Gaseous olefins</b>	<b>0.106</b>
Ethylene	0.057
Propylene	0.046
Butylene	0.002
<b>Gaseous paraffins</b>	<b>0.094</b>
Ethane	0.066
Propane	0.023
Butane	0.005
<b>Carbon oxide</b>	<b>2.622</b>
<b>Carbon dioxide</b>	<b>5.853</b>

Fraction	Proximate and ultimate analysis (wt.%)					HHV (MJ/kg)
	C	H	N	O	Ash	
Biomass	46.9	5.9	0.9	44.5	1.8	18.7
Char	75.0	3.0	1.9	9.7	10.3	28.5
Coke	—	—	—	—	—	—
Bio-oil*	54.3	6.0	0.1	<b>39.5</b>	—	22.0

**Table A.13. Fast pyrolysis of ws-ac over KH-ZSM-5 (C/B = 0.2)**

Reaction conditions		Catalyst properties	
Raw biomass	ws-ac	K/Al	0.5
Catalyst sample	KH-ZSM-5	Si/Al	36.8
T <sub>pyrolysis</sub> /T <sub>catalysis</sub> (°C)	550/450	S <sub>BET</sub> /S <sub>MES+EXT</sub> (m <sup>2</sup> /g)	397/83
C/B ratio (g/g)	0.2	Acidity (mmol <sub>NH3</sub> /g)	0.160
Procedure for bio-oil recovery	1	Basicity (mmol <sub>CO2</sub> /g)	0.460

Products distribution	
Solid phase	Mass yield (wt.%)
<b>Char</b>	<b>17.1</b>
<b>Coke</b>	<b>1.5</b>
Liquid phase	Mass yield (wt.%)
<b>Bio-oil*</b>	<b>51.2</b>
Carboxylic acids	5.3
Light oxygenates	8.2
Furans	1.4
Sugars	5.2
Oxygenated aromatics	3.7
Aromatic hydrocarbons	–
Non-detected compounds	27.4
<b>Water</b>	<b>16.9</b>
Gaseous phase	Mass yield (wt.%)
<b>Hydrogen</b>	<b>0.008</b>
<b>Methane</b>	<b>0.399</b>
<b>Gaseous olefins</b>	<b>0.264</b>
Ethylene	0.100
Propylene	0.140
Butylene	0.024
<b>Gaseous paraffins</b>	<b>0.134</b>
Ethane	0.088
Propane	0.031
Butane	0.014
<b>Carbon oxide</b>	<b>4.833</b>
<b>Carbon dioxide</b>	<b>7.650</b>

Fraction	Proximate and ultimate analysis (wt.%)					HHV (MJ/kg)
	C	H	N	O	Ash	
Biomass	46.9	5.9	0.9	44.5	1.8	18.7
Char	75.0	3.0	1.9	9.7	10.3	28.5
Coke	87.3	7.2	2.7	2.8	–	38.7
Bio-oil*	55.7	6.3	0.1	<b>37.9</b>	–	22.9

**Table A.14. Fast pyrolysis of ws-ac over KH-ZSM-5 (C/B = 0.4)**

Reaction conditions		Catalyst properties	
Raw biomass	ws-ac	K/Al	0.5
Catalyst sample	KH-ZSM-5	Si/Al	36.8
T <sub>pyrolysis</sub> /T <sub>catalysis</sub> (°C)	550/450	S <sub>BET</sub> /S <sub>MES+EXT</sub> (m <sup>2</sup> /g)	397/83
C/B ratio (g/g)	0.4	Acidity (mmol <sub>NH3</sub> /g)	0.160
Procedure for bio-oil recovery	1	Basicity (mmol <sub>CO2</sub> /g)	0.460

Products distribution	
Solid phase	Mass yield (wt.%)
<b>Char</b>	<b>17.1</b>
<b>Coke</b>	<b>2.6</b>
Liquid phase	Mass yield (wt.%)
<b>Bio-oil*</b>	<b>41.1</b>
Carboxylic acids	4.3
Light oxygenates	4.6
Furans	1.2
Sugars	4.4
Oxygenated aromatics	3.3
Aromatic hydrocarbons	0.2
Non-detected compounds	20.4
<b>Water</b>	<b>19.3</b>
Gaseous phase	Mass yield (wt.%)
<b>Hydrogen</b>	<b>0.013</b>
<b>Methane</b>	<b>0.505</b>
<b>Gaseous olefins</b>	<b>0.732</b>
Ethylene	0.255
Propylene	0.432
Butylene	0.045
<b>Gaseous paraffins</b>	<b>0.197</b>
Ethane	0.118
Propane	0.038
Butane	0.040
<b>Carbon oxide</b>	<b>8.639</b>
<b>Carbon dioxide</b>	<b>9.816</b>

Fraction	Proximate and ultimate analysis (wt.%)					HHV (MJ/kg)
	C	H	N	O	Ash	
Biomass	46.9	5.9	0.9	44.5	1.8	18.7
Char	75.0	3.0	1.9	9.7	10.3	28.5
Coke	86.0	7.5	4.0	2.4	—	38.6
Bio-oil*	60.2	6.7	0.1	<b>32.9</b>	—	25.5

**Table A.15. Fast pyrolysis of ws-ac over KH-ZSM-5 (C/B = 0.6)**

Reaction conditions		Catalyst properties	
Raw biomass	ws-ac	K/Al	0.5
Catalyst sample	KH-ZSM-5	Si/Al	36.8
T <sub>pyrolysis</sub> /T <sub>catalysis</sub> (°C)	550/450	S <sub>BET</sub> /S <sub>MES+EXT</sub> (m <sup>2</sup> /g)	397/83
C/B ratio (g/g)	0.6	Acidity (mmol <sub>NH3</sub> /g)	0.160
Procedure for bio-oil recovery	1	Basicity (mmol <sub>CO2</sub> /g)	0.460

Products distribution	
Solid phase	Mass yield (wt.%)
<b>Char</b>	<b>17.1</b>
<b>Coke</b>	<b>3.5</b>
Liquid phase	Mass yield (wt.%)
<b>Bio-oil*</b>	<b>34.6</b>
Carboxylic acids	2.9
Light oxygenates	2.5
Furans	0.5
Sugars	3.3
Oxygenated aromatics	3.3
Aromatic hydrocarbons	0.4
Non-detected compounds	21.7
<b>Water</b>	<b>20.6</b>
Gaseous phase	Mass yield (wt.%)
<b>Hydrogen</b>	<b>0.014</b>
<b>Methane</b>	<b>0.608</b>
<b>Gaseous olefins</b>	<b>1.631</b>
Ethylene	0.540
Propylene	0.993
Butylene	0.098
<b>Gaseous paraffins</b>	<b>0.245</b>
Ethane	0.136
Propane	0.050
Butane	0.060
<b>Carbon oxide</b>	<b>10.342</b>
<b>Carbon dioxide</b>	<b>11.312</b>

Fraction	Proximate and ultimate analysis (wt.%)					HHV (MJ/kg)
	C	H	N	O	Ash	
Biomass	46.9	5.9	0.9	44.5	1.8	18.7
Char	75.0	3.0	1.9	9.7	10.3	28.5
Coke	85.8	8.5	2.4	3.3	–	39.6
Bio-oil*	63.3	6.8	0.2	<b>29.7</b>	–	27.0

**Table A.16. Fast pyrolysis of ws-ac over KH-ZSM-5 (C/B = 0.8)**

Reaction conditions		Catalyst properties	
Raw biomass	ws-ac	K/Al	0.5
Catalyst sample	KH-ZSM-5	Si/Al	36.8
T <sub>pyrolysis</sub> /T <sub>catalysis</sub> (°C)	550/450	S <sub>BET</sub> /S <sub>MES+EXT</sub> (m <sup>2</sup> /g)	397/83
C/B ratio (g/g)	0.8	Acidity (mmol <sub>NH3</sub> /g)	0.160
Procedure for bio-oil recovery	1	Basicity (mmol <sub>CO2</sub> /g)	0.460

Products distribution	
Solid phase	Mass yield (wt.%)
<b>Char</b>	<b>17.1</b>
<b>Coke</b>	<b>4.5</b>
Liquid phase	Mass yield (wt.%)
<b>Bio-oil*</b>	<b>28.8</b>
Carboxylic acids	3.0
Light oxygenates	2.2
Furans	0.6
Sugars	1.0
Oxygenated aromatics	3.2
Aromatic hydrocarbons	0.7
Non-detected compounds	14.4
<b>Water</b>	<b>21.1</b>
Gaseous phase	Mass yield (wt.%)
<b>Hydrogen</b>	<b>0.014</b>
<b>Methane</b>	<b>0.654</b>
<b>Gaseous olefins</b>	<b>1.882</b>
Ethylene	0.619
Propylene	1.152
Butylene	0.112
<b>Gaseous paraffins</b>	<b>0.275</b>
Ethane	0.140
Propane	0.048
Butane	0.088
<b>Carbon oxide</b>	<b>12.798</b>
<b>Carbon dioxide</b>	<b>12.849</b>

Fraction	Proximate and ultimate analysis (wt.%)					HHV (MJ/kg)
	C	H	N	O	Ash	
Biomass	46.9	5.9	0.9	44.5	1.8	18.7
Char	75.0	3.0	1.9	9.7	10.3	28.5
Coke	85.5	8.8	4.8	0.9	—	40.0
Bio-oil*	66.8	7.4	0.2	<b>25.6</b>	—	29.4

**Table A.17. Fast pyrolysis of ws-ac over H-ZSM-5 (C/B = 0.2; procedure 1)**

Reaction conditions		Catalyst properties	
Raw biomass	ws-ac	K/Al	–
Catalyst sample	H-ZSM-5	Si/Al	39.5
T <sub>pyrolysis</sub> /T <sub>catalysis</sub> (°C)	550/450	S <sub>BET</sub> /S <sub>MES+EXT</sub> (m <sup>2</sup> /g)	384/53
C/B ratio (g/g)	0.2	Acidity (mmol <sub>NH3</sub> /g)	0.314
Procedure for bio-oil recovery	1	Basicity (mmol <sub>CO2</sub> /g)	0.018

Products distribution	
Solid phase	Mass yield (wt.%)
<b>Char</b>	<b>17.1</b>
<b>Coke</b>	<b>3.3</b>
Liquid phase	Mass yield (wt.%)
<b>Bio-oil*</b>	<b>33.1</b>
Carboxylic acids	2.9
Light oxygenates	5.5
Furans	1.7
Sugars	2.9
Oxygenated aromatics	2.0
Aromatic hydrocarbons	0.2
Non-detected compounds	24.0
<b>Water</b>	<b>19.4</b>
Gaseous phase	Mass yield (wt.%)
<b>Hydrogen</b>	<b>0.009</b>
<b>Methane</b>	<b>0.578</b>
<b>Gaseous olefins</b>	<b>1.079</b>
Ethylene	0.396
Propylene	0.511
Butylene	0.172
<b>Gaseous paraffins</b>	<b>0.214</b>
Ethane	0.112
Propane	0.041
Butane	0.061
<b>Carbon oxide</b>	<b>9.875</b>
<b>Carbon dioxide</b>	<b>9.273</b>

Fraction	Proximate and ultimate analysis (wt.%)					HHV (MJ/kg)
	C	H	N	O	Ash	
Biomass	46.9	5.9	0.9	44.5	1.8	18.7
Char	75.0	3.0	1.9	9.7	10.3	28.5
Coke	91.2	7.3	0.1	1.4	–	40.3
Bio-oil*	59.6	6.7	0.1	<b>33.6</b>	–	25.2

**Table A.18. Fast pyrolysis of ws-ac over H-ZSM-5 (C/B = 0.6)**

Reaction conditions		Catalyst properties	
Raw biomass	ws-ac	K/Al	–
Catalyst sample	H-ZSM-5	Si/Al	39.5
T <sub>pyrolysis</sub> /T <sub>catalysis</sub> (°C)	550/450	S <sub>BET</sub> /S <sub>MES+EXT</sub> (m <sup>2</sup> /g)	384/53
C/B ratio (g/g)	0.6	Acidity (mmol <sub>NH3</sub> /g)	0.314
Procedure for bio-oil recovery	1	Basicity (mmol <sub>CO2</sub> /g)	0.018

Products distribution	
Solid phase	Mass yield (wt.%)
<b>Char</b>	<b>17.1</b>
<b>Coke</b>	<b>4.6</b>
Liquid phase	Mass yield (wt.%)
<b>Bio-oil*</b>	<b>24.1</b>
Carboxylic acids	0.6
Light oxygenates	1.3
Furans	0.2
Sugars	1.9
Oxygenated aromatics	1.7
Aromatic hydrocarbons	0.5
Non-detected compounds	17.8
<b>Water</b>	<b>17.2</b>
Gaseous phase	Mass yield (wt.%)
<b>Hydrogen</b>	<b>0.022</b>
<b>Methane</b>	<b>0.887</b>
<b>Gaseous olefins</b>	<b>2.890</b>
Ethylene	1.244
Propylene	1.335
Butylene	0.311
<b>Gaseous paraffins</b>	<b>0.576</b>
Ethane	0.236
Propane	0.300
Butane	0.040
<b>Carbon oxide</b>	<b>17.316</b>
<b>Carbon dioxide</b>	<b>15.328</b>

Fraction	Proximate and ultimate analysis (wt.%)					HHV (MJ/kg)
	C	H	N	O	Ash	
Biomass	46.9	5.9	0.9	44.5	1.8	18.7
Char	75.0	3.0	1.9	9.7	10.3	28.5
Coke	85.4	13.5	–	1.1	–	45.6
Bio-oil*	64.3	8.7	0.2	<b>26.9</b>	–	29.9



**Table A.19. Fast pyrolysis of ws-ac over USY (C/B = 0.2)**

Reaction conditions		Catalyst properties	
Raw biomass	ws-ac	K content (wt.%)	–
Catalyst sample	USY	Si/Al	419
T <sub>pyrolysis</sub> /T <sub>catalysis</sub> (°C)	550/450	S <sub>BET</sub> /S <sub>MES+EXT</sub> (m <sup>2</sup> /g)	687/95
C/B ratio (g/g)	0.2	Lewis acidity (mmol <sub>NH3</sub> /g)	–
Procedure for bio-oil recovery	2	Overall basicity (mmol <sub>CO2</sub> /g)	0.097

Products distribution	
Solid phase	Mass yield (wt.%)
<b>Char</b>	<b>17.8</b>
<b>Coke</b>	<b>2.4</b>
Liquid phase	Mass yield (wt.%)
<b>Bio-oil*</b>	<b>43.8</b>
Carboxylic acids	2.0
Light oxygenates	0.5
Furans	0.7
Sugars	3.6
Oxygenated aromatics	1.2
Aromatic hydrocarbons	–
Non-detected compounds	35.8
<b>Water</b>	<b>25.4</b>
Gaseous phase	Mass yield (wt.%)
<b>Hydrogen</b>	<b>0.005</b>
<b>Methane</b>	<b>0.373</b>
<b>Gaseous olefins</b>	<b>0.160</b>
Ethylene	0.064
Propylene	0.058
Butylene	0.038
<b>Gaseous paraffins</b>	<b>0.092</b>
Ethane	0.068
Propane	0.020
Butane	0.004
<b>Carbon oxide</b>	<b>2.895</b>
<b>Carbon dioxide</b>	<b>7.040</b>

Fraction	Proximate and ultimate analysis (wt.%)					HHV (MJ/kg)
	C	H	N	O	Ash	
Biomass	47.8	5.9	0.2	44.8	1.3	19.0
Char	78.7	2.7	0.9	10.5	7.2	29.4
Coke	77.9	5.8	–	16.3	–	27.7
Bio-oil*	52.3	6.0	1.8	<b>39.9</b>	–	21.2

**Table A.20. Fast pyrolysis of ws-ac over USY (C/B = 0.6)**

Reaction conditions		Catalyst properties	
Raw biomass	ws-ac	K content (wt.%)	–
Catalyst sample	USY	Si/Al	419
T <sub>pyrolysis</sub> /T <sub>catalysis</sub> (°C)	550/450	S <sub>BET</sub> /S <sub>MES+EXT</sub> (m <sup>2</sup> /g)	687/95
C/B ratio (g/g)	0.6	Lewis acidity (mmol <sub>NH3</sub> /g)	–
Procedure for bio-oil recovery	2	Overall basicity (mmol <sub>CO2</sub> /g)	0.097

Products distribution	
Solid phase	Mass yield (wt.%)
<b>Char</b>	<b>17.8</b>
<b>Coke</b>	<b>4.8</b>
Liquid phase	Mass yield (wt.%)
<b>Bio-oil*</b>	<b>36.8</b>
Carboxylic acids	2.1
Light oxygenates	0.6
Furans	1.5
Sugars	0.4
Oxygenated aromatics	1.3
Aromatic hydrocarbons	–
Non-detected compounds	30.9
<b>Water</b>	<b>25.8</b>
Gaseous phase	Mass yield (wt.%)
<b>Hydrogen</b>	<b>0.008</b>
<b>Methane</b>	<b>0.543</b>
<b>Gaseous olefins</b>	<b>0.261</b>
Ethylene	0.119
Propylene	0.102
Butylene	0.040
<b>Gaseous paraffins</b>	<b>0.134</b>
Ethane	0.101
Propane	0.032
Butane	0.001
<b>Carbon oxide</b>	<b>4.837</b>
<b>Carbon dioxide</b>	<b>9.027</b>

Fraction	Proximate and ultimate analysis (wt.%)					HHV (MJ/kg)
	C	H	N	O	Ash	
Biomass	47.8	5.9	0.2	44.8	1.3	19.0
Char	78.7	2.7	0.9	10.5	7.2	29.4
Coke	87.6	5.9	–	6.5	–	33.3
Bio-oil*	54.6	6.0	2.1	<b>37.3</b>	–	22.3

**Table A.21. Fast pyrolysis of ws-ac over K-USY (C/B = 0.2; T<sub>catalysis</sub> = 450 °C)**

Reaction conditions		Catalyst properties	
Raw biomass	ws-ac	K content (wt.%)	1.59
Catalyst sample	K-USY	Si/Al	346
T <sub>pyrolysis</sub> /T <sub>catalysis</sub> (°C)	550/450	S <sub>BET</sub> /S <sub>MES+EXT</sub> (m <sup>2</sup> /g)	574/88
C/B ratio (g/g)	0.2	Lewis acidity (mmol <sub>NH3</sub> /g)	0.018
Procedure for bio-oil recovery	2	Overall basicity (mmol <sub>CO2</sub> /g)	0.597

Products distribution	
Solid phase	Mass yield (wt.%)
<b>Char</b>	<b>17.8</b>
<b>Coke</b>	<b>6.1</b>
Liquid phase	Mass yield (wt.%)
<b>Bio-oil*</b>	<b>38.2</b>
Carboxylic acids	2.6
Light oxygenates	2.8
Furans	3.0
Sugars	1.8
Oxygenated aromatics	3.5
Aromatic hydrocarbons	0.1
Non-detected compounds	24.0
<b>Water</b>	<b>20.4</b>
Gaseous phase	Mass yield (wt.%)
<b>Hydrogen</b>	<b>0.025</b>
<b>Methane</b>	<b>0.424</b>
<b>Gaseous olefins</b>	<b>0.621</b>
Ethylene	0.180
Propylene	0.254
Butylene	0.187
<b>Gaseous paraffins</b>	<b>0.248</b>
Ethane	0.163
Propane	0.027
Butane	0.059
<b>Carbon oxide</b>	<b>5.926</b>
<b>Carbon dioxide</b>	<b>10.198</b>

Fraction	Proximate and ultimate analysis (wt.%)					HHV (MJ/kg)
	C	H	N	O	Ash	
Biomass	47.8	5.9	0.2	44.8	1.3	19.0
Char	78.7	2.7	0.9	10.5	7.2	29.4
Coke	78.7	3.4	—	17.9	—	20.3
Bio-oil*	65.4	6.2	0.1	<b>28.3</b>	—	27.2

**Table A.22. Fast pyrolysis of ws-ac over K-USY (C/B = 0.6; T<sub>catalysis</sub> = 450 °C)**

Reaction conditions		Catalyst properties	
Raw biomass	ws-ac	K content (wt.%)	1.59
Catalyst sample	K-USY	Si/Al	346
T <sub>pyrolysis</sub> /T <sub>catalysis</sub> (°C)	550/450	S <sub>BET</sub> /S <sub>MES+EXT</sub> (m <sup>2</sup> /g)	574/88
C/B ratio (g/g)	0.6	Lewis acidity (mmol <sub>NH3</sub> /g)	0.018
Procedure for bio-oil recovery	2	Overall basicity (mmol <sub>CO2</sub> /g)	0.597

Products distribution	
Solid phase	Mass yield (wt.%)
<b>Char</b>	<b>17.8</b>
<b>Coke</b>	<b>10.6</b>
Liquid phase	Mass yield (wt.%)
<b>Bio-oil*</b>	<b>24.9</b>
Carboxylic acids	0.8
Light oxygenates	3.2
Furans	1.8
Sugars	–
Oxygenated aromatics	4.1
Aromatic hydrocarbons	0.5
Non-detected compounds	14.9
<b>Water</b>	<b>23.0</b>
Gaseous phase	Mass yield (wt.%)
<b>Hydrogen</b>	<b>0.091</b>
<b>Methane</b>	<b>0.894</b>
<b>Gaseous olefins</b>	<b>1.281</b>
Ethylene	0.365
Propylene	0.487
Butylene	0.429
<b>Gaseous paraffins</b>	<b>0.467</b>
Ethane	0.262
Propane	0.079
Butane	0.127
<b>Carbon oxide</b>	<b>8.916</b>
<b>Carbon dioxide</b>	<b>12.016</b>

Fraction	Proximate and ultimate analysis (wt.%)					HHV (MJ/kg)
	C	H	N	O	Ash	
Biomass	47.8	5.9	0.2	44.8	1.3	19.0
Char	78.7	2.7	0.9	10.5	7.2	29.4
Coke	67.2	3.0	–	29.9	–	19.0
Bio-oil*	67.7	7.2	0.1	<b>25.0</b>	–	29.5

**Table A.23. Fast pyrolysis of ws-ac over K-USY (C/B = 0.2; T<sub>catalysis</sub> = 400 °C)**

Reaction conditions		Catalyst properties	
Raw biomass	ws-ac	K content (wt.%)	1.59
Catalyst sample	K-USY	Si/Al	346
T <sub>pyrolysis</sub> /T <sub>catalysis</sub> (°C)	550/400	S <sub>BET</sub> /S <sub>MES+EXT</sub> (m <sup>2</sup> /g)	574/88
C/B ratio (g/g)	0.2	Lewis acidity (mmol <sub>NH3</sub> /g)	0.018
Procedure for bio-oil recovery	2	Overall basicity (mmol <sub>CO2</sub> /g)	0.597

Products distribution	
Solid phase	Mass yield (wt.%)
<b>Char</b>	<b>17.8</b>
<b>Coke</b>	<b>6.3</b>
Liquid phase	Mass yield (wt.%)
<b>Bio-oil*</b>	<b>34.0</b>
Carboxylic acids	3.3
Light oxygenates	2.4
Furans	2.7
Sugars	1.8
Oxygenated aromatics	3.0
Aromatic hydrocarbons	0.1
Non-detected compounds	20.8
<b>Water</b>	<b>24.1</b>
Gaseous phase	Mass yield (wt.%)
<b>Hydrogen</b>	<b>0.017</b>
<b>Methane</b>	<b>0.389</b>
<b>Gaseous olefins</b>	<b>0.520</b>
Ethylene	0.164
Propylene	0.228
Butylene	0.128
<b>Gaseous paraffins</b>	<b>0.238</b>
Ethane	0.151
Propane	0.043
Butane	0.043
<b>Carbon oxide</b>	<b>5.659</b>
<b>Carbon dioxide</b>	<b>10.878</b>

Fraction	Proximate and ultimate analysis (wt.%)					HHV (MJ/kg)
	C	H	N	O	Ash	
Biomass	47.8	5.9	0.2	44.8	1.3	19.0
Char	78.7	2.7	0.9	10.5	7.2	29.4
Coke	75.2	3.8	–	21.0	–	28.6
Bio-oil*	63.9	6.7	0.1	<b>29.3</b>	–	27.1

**Table A.24. Fast pyrolysis of ws-ac over K-USY (C/B = 0.6; T<sub>catalysis</sub> = 400 °C)**

Reaction conditions		Catalyst properties	
Raw biomass	ws-ac	K content (wt.%)	1.59
Catalyst sample	K-USY	Si/Al	346
T <sub>pyrolysis</sub> /T <sub>catalysis</sub> (°C)	550/400	S <sub>BET</sub> /S <sub>MES+EXT</sub> (m <sup>2</sup> /g)	574/88
C/B ratio (g/g)	0.6	Lewis acidity (mmol <sub>NH3</sub> /g)	0.018
Procedure for bio-oil recovery	2	Overall basicity (mmol <sub>CO2</sub> /g)	0.597

Products distribution	
Solid phase	Mass yield (wt.%)
<b>Char</b>	<b>17.8</b>
<b>Coke</b>	<b>7.8</b>
Liquid phase	Mass yield (wt.%)
<b>Bio-oil*</b>	<b>24.5</b>
Carboxylic acids	1.3
Light oxygenates	2.6
Furans	0.9
Sugars	–
Oxygenated aromatics	3.9
Aromatic hydrocarbons	0.4
Non-detected compounds	15.5
<b>Water</b>	<b>29.2</b>
Gaseous phase	Mass yield (wt.%)
<b>Hydrogen</b>	<b>0.059</b>
<b>Methane</b>	<b>0.900</b>
<b>Gaseous olefins</b>	<b>1.090</b>
Ethylene	0.292
Propylene	0.423
Butylene	0.375
<b>Gaseous paraffins</b>	<b>0.419</b>
Ethane	0.254
Propane	0.061
Butane	0.104
<b>Carbon oxide</b>	<b>7.002</b>
<b>Carbon dioxide</b>	<b>11.195</b>

Fraction	Proximate and ultimate analysis (wt.%)					HHV (MJ/kg)
	C	H	N	O	Ash	
Biomass	47.8	5.9	0.2	44.8	1.3	19.0
Char	78.7	2.7	0.9	10.5	7.2	29.4
Coke	87.6	4.1	–	8.3	–	34.6
Bio-oil*	67.0	7.8	0.1	<b>25.2</b>	–	29.9

**Table A.25. Fast pyrolysis of ws-ac over K-USY (C/B = 0.2; T<sub>catalysis</sub> = 500 °C)**

Reaction conditions		Catalyst properties	
Raw biomass	ws-ac	K content (wt.%)	1.59
Catalyst sample	K-USY	Si/Al	346
T <sub>pyrolysis</sub> /T <sub>catalysis</sub> (°C)	550/500	S <sub>BET</sub> /S <sub>MES+EXT</sub> (m <sup>2</sup> /g)	574/88
C/B ratio (g/g)	0.2	Lewis acidity (mmol <sub>NH3</sub> /g)	0.018
Procedure for bio-oil recovery	2	Overall basicity (mmol <sub>CO2</sub> /g)	0.597

Products distribution	
Solid phase	Mass yield (wt.%)
<b>Char</b>	<b>17.8</b>
<b>Coke</b>	<b>3.9</b>
Liquid phase	Mass yield (wt.%)
<b>Bio-oil*</b>	<b>39.0</b>
Carboxylic acids	2.1
Light oxygenates	2.9
Furans	2.9
Sugars	1.7
Oxygenated aromatics	4.0
Aromatic hydrocarbons	–
Non-detected compounds	25.3
<b>Water</b>	<b>20.8</b>
Gaseous phase	Mass yield (wt.%)
<b>Hydrogen</b>	<b>0.046</b>
<b>Methane</b>	<b>0.804</b>
<b>Gaseous olefins</b>	<b>0.922</b>
Ethylene	0.284
Propylene	0.360
Butylene	0.277
<b>Gaseous paraffins</b>	<b>0.332</b>
Ethane	0.215
Propane	0.054
Butane	0.062
<b>Carbon oxide</b>	<b>6.852</b>
<b>Carbon dioxide</b>	<b>9.566</b>

Fraction	Proximate and ultimate analysis (wt.%)					HHV (MJ/kg)
	C	H	N	O	Ash	
Biomass	47.8	5.9	0.2	44.8	1.3	19.0
Char	78.7	2.7	0.9	10.5	7.2	29.4
Coke	90.4	3.6	–	5.9	–	35.2
Bio-oil*	64.1	6.8	0.1	<b>29.0</b>	–	27.4

**Table A.26. Fast pyrolysis of ws-ac over K-USY (C/B = 0.6; T<sub>catalysis</sub> = 500 °C)**

Reaction conditions		Catalyst properties	
Raw biomass	ws-ac	K content (wt.%)	1.59
Catalyst sample	K-USY	Si/Al	346
T <sub>pyrolysis</sub> /T <sub>catalysis</sub> (°C)	550/500	S <sub>BET</sub> /S <sub>MES+EXT</sub> (m <sup>2</sup> /g)	574/88
C/B ratio (g/g)	0.6	Lewis acidity (mmol <sub>NH3</sub> /g)	0.018
Procedure for bio-oil recovery	2	Overall basicity (mmol <sub>CO2</sub> /g)	0.597

Products distribution	
Solid phase	Mass yield (wt.%)
<b>Char</b>	<b>17.8</b>
<b>Coke</b>	<b>7.4</b>
Liquid phase	Mass yield (wt.%)
<b>Bio-oil*</b>	<b>20.2</b>
Carboxylic acids	0.2
Light oxygenates	3.1
Furans	1.2
Sugars	–
Oxygenated aromatics	4.3
Aromatic hydrocarbons	0.5
Non-detected compounds	10.8
<b>Water</b>	<b>29.2</b>
Gaseous phase	Mass yield (wt.%)
<b>Hydrogen</b>	<b>0.134</b>
<b>Methane</b>	<b>1.434</b>
<b>Gaseous olefins</b>	<b>1.685</b>
Ethylene	0.513
Propylene	0.657
Butylene	0.515
<b>Gaseous paraffins</b>	<b>0.555</b>
Ethane	0.355
Propane	0.077
Butane	0.123
<b>Carbon oxide</b>	<b>9.705</b>
<b>Carbon dioxide</b>	<b>11.866</b>

Fraction	Proximate and ultimate analysis (wt.%)					HHV (MJ/kg)
	C	H	N	O	Ash	
Biomass	47.8	5.9	0.2	44.8	1.3	19.0
Char	78.7	2.7	0.9	10.5	7.2	29.4
Coke	90.1	3.4	–	6.5	–	34.8
Bio-oil*	68.6	6.8	0.2	<b>24.5</b>	–	29.4



**Table A.27. Fast pyrolysis of ws-ac over H-ZSM-5 (C/B = 0.2; procedure 2)**

Reaction conditions		Catalyst properties	
Raw biomass	ws-ac	Si/Al	39.5
Catalyst sample	H-ZSM-5	$S_{\text{BET}}/S_{\text{MES+EXT}}$ (m <sup>2</sup> /g)	384/53
$T_{\text{pyrolysis}}/T_{\text{catalysis}}$ (°C)	550/450	$V_{\text{T}}$ (cm <sup>3</sup> /g)	0.360
C/B ratio (g/g)	0.2	Acidity (mmol <sub>NH3</sub> /g)	0.314
Procedure for bio-oil recovery	2	Basicity (mmol <sub>CO2</sub> /g)	0.018

Products distribution		
Solid phase	Mass yield (wt.%)	Energy yield (%)
<b>Char</b>	<b>17.8</b>	<b>27.6</b>
<b>Coke</b>	<b>2.8</b>	<b>3.5</b>
Liquid phase	Mass yield (wt.%)	Energy yield (%)
<b>Bio-oil*</b>	<b>39.2</b>	<b>52.2</b>
Carboxylic acids	4.2	3.6
Light oxygenates	2.0	3.4
Furans	1.9	2.3
Sugars	4.1	4.9
Oxygenated aromatics	3.6	5.8
Aromatic hydrocarbons	1.0	2.3
Non-detected compounds	22.4	22.3
<b>Water</b>	<b>26.1</b>	–
Gaseous phase	Mass yield (wt.%)	Energy yield (%)
<b>Hydrogen</b>	<b>0.012</b>	<b>0.089</b>
<b>Methane</b>	<b>0.220</b>	<b>0.631</b>
<b>Gaseous olefins</b>	<b>0.559</b>	<b>1.448</b>
Ethylene	0.284	0.743
Propylene	0.249	0.640
Butylene	0.026	0.065
<b>Gaseous paraffins</b>	<b>0.139</b>	<b>0.374</b>
Ethane	0.091	0.246
Propane	0.025	0.068
Butane	0.023	0.061
<b>Carbon oxide</b>	<b>5.493</b>	<b>2.854</b>
<b>Carbon dioxide</b>	<b>7.633</b>	<b>0.089</b>

Fraction	Proximate and ultimate analysis (wt.%)					HHV (MJ/kg)
	C	H	N	O	Ash	
Biomass	47.8	5.9	0.2	44.8	1.3	19.0
Char	78.7	2.7	0.9	10.5	7.2	29.4
Coke	63.5	4.4	–	32.1	–	24.0
Bio-oil*	62.3	5.8	0.1	<b>31.8</b>	–	25.3

**Table A.28. Fast pyrolysis of ws-ac over H-ZSM-5 and BNT (C/B = 0.2)**

Reaction conditions		Catalyst properties		
Raw biomass	ws-ac	Catalyst bed	Top	Bottom
Top catalyst sample	H-ZSM-5	Si/Al	39.5	–
Bottom catalyst sample	BNT	$S_{\text{BET}}/S_{\text{MES+EXT}}$ (m <sup>2</sup> /g)	384/53	43/43
$T_{\text{pyrolysis}}/T_{\text{catalysis}}$ (°C)	550/450	$V_{\text{T}}$ (cm <sup>3</sup> /g)	0.360	0.126
C/B ratio (g/g)	0.2	Acidity (mmol <sub>NH3</sub> /g)	0.314	0.080
Procedure for bio-oil recovery	2	Basicity (mmol <sub>CO2</sub> /g)	0.018	0.596

Products distribution		
Solid phase	Mass yield (wt.%)	Energy yield (%)
<b>Char</b>	<b>17.8</b>	<b>27.6</b>
<b>Coke</b>	<b>5.0</b>	<b>5.9</b>
Coke in top catalyst bed	2.6	3.2
Coke in bottom catalyst bed	2.4	2.7
Liquid phase	Mass yield (wt.%)	Energy yield (%)
<b>Bio-oil*</b>	<b>33.7</b>	<b>47.4</b>
Carboxylic acids	4.5	3.9
Light oxygenates	2.1	3.6
Furans	1.4	1.7
Sugars	4.7	4.3
Oxygenated aromatics	1.8	2.9
Aromatic hydrocarbons	0.4	0.9
Non-detected compounds	18.7	30.1
<b>Water</b>	<b>27.0</b>	–
Gaseous phase	Mass yield (wt.%)	Energy yield (%)
<b>Hydrogen</b>	<b>0.015</b>	<b>0.108</b>
<b>Methane</b>	<b>0.273</b>	<b>0.787</b>
<b>Gaseous olefins</b>	<b>0.707</b>	<b>1.836</b>
Ethylene	0.366	0.958
Propylene	0.315	0.811
Butylene	0.027	0.067
<b>Gaseous paraffins</b>	<b>0.172</b>	<b>0.465</b>
Ethane	0.105	0.284
Propane	0.038	0.100
Butane	0.030	0.081
<b>Carbon oxide</b>	<b>7.275</b>	<b>3.789</b>
<b>Carbon dioxide</b>	<b>7.972</b>	–

Fraction	Proximate and ultimate analysis (wt.%)					HHV (MJ/kg)
	C	H	N	O	Ash	
Biomass	47.8	5.9	0.2	44.8	1.3	19.0
Char	78.7	2.7	0.9	10.5	7.2	29.4
Coke in top catalyst	61.8	4.4	–	33.9	–	23.2
Coke in bottom catalyst	56.5	4.8	–	38.8	–	21.3
Bio-oil*	65.4	5.8	0.1	<b>28.7</b>	–	26.7

**Table A.29. Fast pyrolysis of ws-ac over BNT and H-ZSM-5 (C/B = 0.2)**

Reaction conditions		Catalyst properties		
Raw biomass	ws-ac	Catalyst bed	Top	Bottom
Top catalyst sample	BNT	Si/Al	–	39.5
Bottom catalyst sample	H-ZSM-5	$S_{\text{BET}}/S_{\text{MES+EXT}}$ (m <sup>2</sup> /g)	43/43	384/53
$T_{\text{pyrolysis}}/T_{\text{catalysis}}$ (°C)	550/450	$V_{\text{T}}$ (cm <sup>3</sup> /g)	0.126	0.360
C/B ratio (g/g)	0.2	Acidity (mmol <sub>NH3</sub> /g)	0.080	0.314
Procedure for bio-oil recovery	2	Basicity (mmol <sub>CO2</sub> /g)	0.596	0.018

Products distribution		
Solid phase	Mass yield (wt.%)	Energy yield (%)
<b>Char</b>	<b>17.8</b>	<b>27.6</b>
<b>Coke</b>	<b>5.5</b>	<b>4.8</b>
Coke in top catalyst bed	2.8	1.3
Coke in bottom catalyst bed	2.7	3.5
Liquid phase	Mass yield (wt.%)	Energy yield (%)
<b>Bio-oil*</b>	<b>30.9</b>	<b>46.3</b>
Carboxylic acids	2.6	2.3
Light oxygenates	2.9	5.0
Furans	1.9	2.3
Sugars	1.6	1.5
Oxygenated aromatics	2.1	3.5
Aromatic hydrocarbons	1.2	2.7
Non-detected compounds	18.4	29.0
<b>Water</b>	<b>25.7</b>	–
Gaseous phase	Mass yield (wt.%)	Energy yield (%)
<b>Hydrogen</b>	<b>0.024</b>	<b>0.170</b>
<b>Methane</b>	<b>0.716</b>	<b>1.952</b>
<b>Gaseous olefins</b>	<b>1.448</b>	<b>3.549</b>
Ethylene	0.615	1.527
Propylene	0.629	1.538
Butylene	0.204	0.484
<b>Gaseous paraffins</b>	<b>0.366</b>	<b>0.934</b>
Ethane	0.176	0.452
Propane	0.063	0.159
Butane	0.128	0.323
<b>Carbon oxide</b>	<b>9.353</b>	<b>4.618</b>
<b>Carbon dioxide</b>	<b>8.270</b>	–

Fraction	Proximate and ultimate analysis (wt.%)					HHV (MJ/kg)
	C	H	N	O	Ash	
Biomass	47.8	5.9	0.2	44.8	1.3	19.0
Char	78.7	2.7	0.9	10.5	7.2	29.4
Coke in top catalyst	29.7	4.6	–	65.8	–	8.9
Coke in bottom catalyst	63.6	4.5	–	31.9	–	24.2
Bio-oil*	68.1	6.2	0.1	<b>25.6</b>	–	28.5

**Table A.30. Fast pyrolysis of ws-ac over H-ZSM-5 and MgO (C/B = 0.2)**

Reaction conditions		Catalyst properties		
Raw biomass	ws-ac	Catalyst bed	Top	Bottom
Top catalyst sample	H-ZSM-5	Si/Al	39.5	–
Bottom catalyst sample	MgO	$S_{\text{BET}}/S_{\text{MES+EXT}}$ (m <sup>2</sup> /g)	384/53	82/82
$T_{\text{pyrolysis}}/T_{\text{catalysis}}$ (°C)	550/450	$V_{\text{T}}$ (cm <sup>3</sup> /g)	0.360	0.47
C/B ratio (g/g)	0.2	Acidity (mmol <sub>NH3</sub> /g)	0.314	0.040
Procedure for bio-oil recovery	2	Basicity (mmol <sub>CO2</sub> /g)	0.018	4.130

Products distribution		
Solid phase	Mass yield (wt.%)	Energy yield (%)
<b>Char</b>	<b>17.8</b>	<b>27.6</b>
<b>Coke</b>	<b>7.0</b>	<b>7.7</b>
Coke in top catalyst bed	2.7	3.4
Coke in bottom catalyst bed	4.3	3.3
Liquid phase	Mass yield (wt.%)	Energy yield (%)
<b>Bio-oil*</b>	<b>26.1</b>	<b>39.0</b>
Carboxylic acids	4.7	4.1
Light oxygenates	2.1	3.4
Furans	2.0	2.5
Sugars	3.9	3.8
Oxygenated aromatics	2.3	3.7
Aromatic hydrocarbons	0.7	1.4
Non-detected compounds	10.4	20.0
<b>Water</b>	<b>32.6</b>	<b>–</b>
Gaseous phase	Mass yield (wt.%)	Energy yield (%)
<b>Hydrogen</b>	<b>0.141</b>	<b>1.040</b>
<b>Methane</b>	<b>0.295</b>	<b>0.852</b>
<b>Gaseous olefins</b>	<b>0.527</b>	<b>1.371</b>
Ethylene	0.269	0.706
Propylene	0.230	0.595
Butylene	0.028	0.070
<b>Gaseous paraffins</b>	<b>0.168</b>	<b>0.455</b>
Ethane	0.109	0.296
Propane	0.037	0.099
Butane	0.022	0.060
<b>Carbon oxide</b>	<b>6.943</b>	<b>3.629</b>
<b>Carbon dioxide</b>	<b>8.400</b>	<b>–</b>

Fraction	Proximate and ultimate analysis (wt.%)					HHV (MJ/kg)
	C	H	N	O	Ash	
Biomass	47.8	5.9	0.2	44.8	1.3	19.0
Char	78.7	2.7	0.9	10.5	7.2	29.4
Coke in top catalyst	63.3	4.1	–	32.6	–	23.5
Coke in bottom catalyst	56.9	3.1	–	40.0	–	19.4
Bio-oil*	69.0	5.9	0.1	<b>25.0</b>	–	28.4

**Table A.31. Fast pyrolysis of ws-ac over MgO and H-ZSM-5 (C/B = 0.2)**

Reaction conditions		Catalyst properties		
Raw biomass	ws-ac	Catalyst bed	Top	Bottom
Top catalyst sample	MgO	Si/Al	–	39.5
Bottom catalyst sample	H-ZSM-5	S <sub>BET</sub> /S <sub>MES+EXT</sub> (m <sup>2</sup> /g)	82/82	384/53
T <sub>pyrolysis</sub> /T <sub>catalysis</sub> (°C)	550/450	V <sub>T</sub> (cm <sup>3</sup> /g)	0.47	0.360
C/B ratio (g/g)	0.2	Acidity (mmol <sub>NH3</sub> /g)	0.040	0.314
Procedure for bio-oil recovery	2	Basicity (mmol <sub>CO2</sub> /g)	4.130	0.018

Products distribution		
Solid phase	Mass yield (wt.%)	Energy yield (%)
<b>Char</b>	<b>17.8</b>	<b>27.6</b>
<b>Coke</b>	<b>9.6</b>	<b>8.2</b>
Coke in top catalyst bed	6.3	5.1
Coke in bottom catalyst bed	3.3	3.1
Liquid phase	Mass yield (wt.%)	Energy yield (%)
<b>Bio-oil*</b>	<b>23.1</b>	<b>37.0</b>
Carboxylic acids	1.0	0.8
Light oxygenates	2.1	3.7
Furans	1.2	1.4
Sugars	1.1	1.6
Oxygenated aromatics	2.2	3.6
Aromatic hydrocarbons	2.7	6.0
Non-detected compounds	12.9	19.9
<b>Water</b>	<b>29.2</b>	–
Gaseous phase	Mass yield (wt.%)	Energy yield (%)
<b>Hydrogen</b>	<b>0.041</b>	<b>0.289</b>
<b>Methane</b>	<b>0.875</b>	<b>2.391</b>
<b>Gaseous olefins</b>	<b>1.694</b>	<b>4.165</b>
Ethylene	0.729	1.814
Propylene	0.756	1.853
Butylene	0.209	0.498
<b>Gaseous paraffins</b>	<b>0.387</b>	<b>0.989</b>
Ethane	0.184	0.476
Propane	0.066	0.168
Butane	0.136	0.346
<b>Carbon oxide</b>	<b>8.712</b>	<b>4.313</b>
<b>Carbon dioxide</b>	<b>8.490</b>	–

Fraction	Proximate and ultimate analysis (wt.%)					HHV (MJ/kg)
	C	H	N	O	Ash	
Biomass	47.8	5.9	0.2	44.8	1.3	19.0
Char	78.7	2.7	0.9	10.5	7.2	29.4
Coke in top catalyst	50.1	2.4	–	47.5	–	15.4
Coke in bottom catalyst	52.4	3.6	–	44.0	–	18.0
Bio-oil*	69.2	7.3	0.1	<b>23.4</b>	–	30.4